UAB

DISSERTATION FOR THE DEGREE
DOCTOR OF PHILOSOPHY IN DESIGN OF TELECOMMUNICATION SYSTEMS

MULTI-BEAM SATELLITE RESOURCE ALLOCATION OPTIMIZATION FOR BEAM HOPPING TRANSMISSION

Lei Jiang

ADVISOR: Dr. María Ágeles Vázquez Castro
DEPARTMENT OF TELECOMMUNICATIONS AND SYSTEMS ENGINEERING
UNIVERSITAT AUTÒNOMA DE BARCELONA

Bellaterra, September, 2010

Abstract

Multi-beam satellite systems have been studied a lot in the last ten years. They have many promising features like power gain, interference reduction, high flexibility to adapt the asymmetric traffic distribution, and the improvement of the system capacity compared with single-beam systems. In multi-beam satellite systems, the beamforming antenna can generate a number of spot beams over the coverage area. However, each beam will compete with others for resources to achieve satisfactory communication. This is due to the fact that the traffic demand is potentially highly asymmetrical throughout the satellite coverage. Therefore, in order to achieve a good match between offered and requested traffic, the satellite requires a certain degree of flexibility in allocating power, bandwidth and time-slot resources. Current multi-beam satellite systems with regular frequency reuse and uniform power allocation can not satisfy these increasing requirements, which motivate us to investigate new transmission schemes to replace the current ones.

In this dissertation, we first propose a novel system design, flexible system, which is an extension of current multi-beam systems. It is characterized by the non-regular frequency reuse and the flexibility in bandwidth and power allocation. Then, the Beam Hopping (BH) system is proposed to evaluate the performance improvement with the flexibility in time/space and power domain. As we know, the flexible system and BH system operate in frequency and time/space domain, respectively. In order to know which domain shows the best overall performance, we propose a novel formulation of the Signal-to-Interference plus Noise Ratio (SINR) which allows us to prove the time/frequency duality of these two schemes. Furthermore, to efficiently utilize the satellite resources (e.g., power and bandwidth), we propose two capacity optimization approaches subject to per-beam SINR constraints. Moreover, due to the realistic implementation, a general methodology is formulated including the technological constraints, which prevent the two systems dual of each other (named as technological gap). The Shannon capacity (upper bound) and the state-of-art Modulation and Coding (MODCOD) are analyzed in order to quantify the gap and evaluate the performance of the two candidate schemes. Comparing with the current conventional systems, simulation results show significant improvements in terms of power gain, spectral efficiency and traffic matching ratio. They also show that the BH system is less complex design and outperforms the flexible system specially for non-real time services. This part of the Ph.D. work supported by an ESA-funded project on next generation system of “Beam Hopping Techniques for Multi-beam Satellite Systems”. This research is in close collaboration with the leading space industry (e.g. INDRA,

MDA) and space research institutions (e.g., ESA, DLR (German Space Agency)).

In addition, we extend the work to mobile environments (e.g., railway scenario). Since the current air interface standards (e.g., DVB-S2/RCS) lack of specification for mobile scenarios, a new Fade Mitigation Technique (FMT), i.e., Link Layer Forward Error Correction (LL-FEC) is introduced as a fading countermeasure for DVB-S2/RCS in mobile environments. This part of the work points out that LL-FEC can overcome the deep fading in mobile satellite scenarios (e.g. railway) by optimizing the FEC codes (e.g. Reed-Solomon and Raptor codes). We have to note that such air interface standards might need change to adapt to the new proposed systems: flexible and BH. However, the methodology presented is also applicable.

We further investigate the secure communication of multibeam satellite systems by using the system model developed in the BH project. The physical (PHY) layer security technique is investigated to protect the broadcasted data and make it impossible to be wiretapped. A novel multibeam satellite system is designed to minimize the transmit power under the constraints of the individual secrecy rate requested per user.

The main contributions of this Ph.D. dissertation can be summarized as:

a. We study the resource allocation optimization in multi-domain (frequency, time, space and power) for multi-beam satellite systems. First, we develop novel matricial-based analytical multibeam system-level models that directly allows testing different payloads technology and system assumptions. Second, we prove that the system performance can be increased by dynamically adapting the resource allocation to the characteristics of the system, e.g., traffic requested by the terminal.

b. Theoretical studies and simulations prove that the proposed novel transmission schemes perform better than the current system design in terms of power gain, spectral efficiency, etc.. In addition, BH system turns out to show a less complex design and superior performance than the flexible system.

c. Our analytical models allows us to also prove the theoretical duality between the flexible and BH systems, which work in frequency domain and time domain, respectively. Moreover, we develop a general methodology to include technological constraints due to realistic implementation, obtain the main factors that prevent the two technologies dual of each other in practice, and formulate the technological gap between them.

d. We extend the work to mobile scenarios and prove that LL-FEC is applicable for mobile satellite systems (e.g., railway) to compensate the fade due to the mobility by optimizing the FEC codes (Reed-Solomon and Raptor codes). The results show that Multiple Protocol Encapsulation Inter-burst FEC (MPE-IFEC) and extended MPE-FEC with Raptor codes - as finally specified in DVB Return Channel via Satellite for Mobile Scenario (DVB-RCS+M) - consistently perform better than other LL-FEC schemes for mobile scenarios.

e. We point out that how to change the signalling of current version of standards (e.g., DVB-S2/RCS+M) in order to allow achievable performance in the mobile scenarios. The proposal has been finally adopted by the DVB-RCS+M standard.

f. We finally make use of our developed system models to investigate whether the multibeam scenario allows the use of PHY layer security, a very valuable feature that would broaden multibeam satellite applications. We prove that our models are directly applicable for the study of PHY layer security in terms of joint optimization of power control and beamforming for the BH payload. Moreover, the proposed algorithm can ensure the minimum power consumption subject to the individual secrecy rate requested per user.

Based on the work of the Ph.D., three journal papers and eleven international conference papers have been published, and these publications systematically cover all the contributions of this doctoral thesis work.

Acknowledgments

The work presented in this thesis could not have been done without the aids and supports of many people. Therefore I have a great honor to express my sincere gratitude to all.

I would first like to thank my supervisor M. Ángeles Vázquez-Castro for everything, of which I would like to highlight all the support and help she provided me throughout the entire Ph.D. as well as encouragement in every endeavor. She was a big motivating force behind this herculean task I finished in last couple of years. Second, I would like to thank the INDRA, DLR, MDA, and NOMOR-QUALCOMM for all the collaborative work as well as the European Space Agency for all the support.

Next, I must thank Prof. Are Hjørungnes for his invitation to visit and research at UNIK, Norway. He gives me a great support during my research there. I am also thankful to Dr. Zhu Han for the help he provided during my stay in Houston, USA. We had a very good time at University of Houston discussing the research issues.

I would also like to acknowledge my debt to Fausto Vieira, David Pradas Fernández and Joan Enric Barcelo for their helps and encouragement.

Finally, I am indebted to my wife Yi Guo for her unconditional support and continuous encouragement throughout my work. I would also like to thank my parents for providing me support when I needed it.

Lei Jiang
Barcelona, September, 2010

List of Publications

This dissertation is based on the following SIX published papers, referred to in the text by letters (A-F).

A. J. Lei and M. A. Vázquez-Castro, "Joint Power and Carrier Allocation for the Multibeam Satellite Downlink with Individual SINR Constraints," in *Proc. IEEE Int. Conf. on Commun.*, Cape Town, South Africa, pp. 1 - 5, May 2010.

B. J. Lei and M. A. Vázquez-Castro, "Duality Study over Multibeam Satellite System in Frequency and Time Domain," in *Proc. IEEE Int. Conf. on Commun.*, Cape Town, South Africa, pp. 1 - 5, May 2010.

C. J. Lei, M.A. Vázquez Castro, and T. Stockhammer, "Link Layer FEC and Cross-layer Architecture for DVB-S2 Transmission with QoS in Railway Scenarios," *IEEE Trans. Veh. Technol.*, vol. 58, no. 8, pp. 4265 - 4276, Oct. 2009.

D. J. Lei, M.A. Vázquez Castro, T. Stockhammer, and F. Vieira, "Link layer FEC for Quality-of-Service Provision for Mobile Internet Services over DVB-S2," *Int. Journal of Satellite Commun. and Netw.*, vol. 28, no. 3-4, pp. 183 - 207, 2010.

E. J. Lei, G. Seco Granados, and M. A. Vázquez Castro, "MPE/ULE-FEC vs GSE-FEC Efficiency Comparison of IP Datagram Transmission over DVB-S2," in *Proc. 25th AIAA Int. Comm. Satellite Systems Conf.*, Seoul, Korea, 10-13 April, 2007.

F. J. Lei, T. Stockhammer, M. A. Vázquez Castro, and F. Vieira, "Application of Link Layer FEC to DVB-S2 for Railway Scenarios," in *Proc. 10th Int. Workshop on Signal Process. for Space Commun.*, Rhodes Island, Greece, 6 - 8 Oct. 2008.

In addition, we also include additional contributions in the process of publication, the list of papers is (G-I):

G. J. Lei, Z. Han, M. A. Vázquez-Castro, and A. Hjørungnes, "Joint Power Control and Beamforming for Multibeam Satellite Systems with Individual Secrecy Rate Constraints," *Submitted to IEEE Trans. on Info. Forensics and Security*, 2010.

H. J. Lei and M.A. Vázquez Castro, "Multibeam Satellite Frequency/Time Duality Study and Capacity Optimization," *Submitted to Journal of Commun. and Netw.*, 2010.

I. J. Lei, Z. Han, M. A. Vázquez-Castro, and A. Hjørungnes, “Multibeam Satellite Power Control with Physical Layer Security,” *Submitted to IEEE Int. Conf. on Commun.*, Kyoto, Japan, June 2011.

Contents

List of Figures

List of Tables

Notation

In the sequel, matrices are indicated by uppercase boldface letters, vectors are indicated by lowercase boldface letters, and scalars are indicated by italics letters. Other specific notation has been introduced as follows:

$\|x\|$	Absolute value of x.
$\mathrm{diag}(\mathbf{x})$	A diagonal matrix with the elements of vector $\mathbf{x}$ along its diagonal.
$\approx$	Approximately equal to.
$\mathbf{X}^*$	Complex conjugate of matrix $\mathbf{X}$.
$\mathbf{X}^H$	Conjugate transpose (Hermitian) of matrix $\mathbf{X}$.
x^+	Denotes $\max\{0, x\}$.
$\det(\mathbf{X})$	Determinant of matrix $\mathbf{X}$.
$\varepsilon(\bullet)$	Expectation operator.
$\mathbf{X}^\dagger$	Pseudo-inverse of matrix $\mathbf{X}$.
$\|\mathbf{x}\|$	Square-norm of vector $\mathbf{x}$.
$\lceil x \rceil$	The nearest integer higher than or equal to x.
$\lfloor x \rfloor$	The nearest integer lower than or equal to x.
$\upsilon_{\max}(\mathbf{X})$	The eigenvector related to the maximum eigenvalue of matrix $\mathbf{X}$.
$x_{i,j}$	The jth component of vector $\mathbf{x}_i$.
$\lambda_{\max}(\mathbf{X})$	The maximum eigenvalue of matrix $\mathbf{X}$.
$\mathbb{R}$, $\mathbb{C}$	The set of real and complex numbers, respectively.
$\mathbf{X}^T$	Transpose of matrix $\mathbf{X}$.

Abbreviations

AAA	Authentication, Authorization, and Accounting
ACM	Adaptive Coding and Modulation
ADT	Application Data Table
ADST	Application Data Sub Table
AFR	Array Feed Reflector
ARQ	Automatic Repeat Request
ATSC	Advanced Television Systems Committee
AWGN	Additive White Gaussian Noise
BBFrame	Baseband Frame
BER	Bit Error Rate
BFSK	Binary Frequency Shift Keying
BH	Beam Hopping
BPA	Binary Power Allocation
BPSK	Binary Phase Shift Keying
BS	Base Station
BW	Band-Width
CDMA	Code Division Multiple Access
CDP	Content Delivery Protocols
CRC	Cyclic Redundancy Check
CSI	Channel State Information
DPC	Dirty Paper Coding
DSM-CC	Digital Storage Media Command and Control
DVT	Digital Television
DVB-H	Digital Video Broadcasting for Handhelds
DVB-IPDC	IP Datacast over DVB-H
DVB-RCS+M	DVB Return Channel via Satellite for Mobile Scenario
DVB-S	Digital Video Broadcasting via Satellite
DVB-SH	DVB Satellite services to Handheld devices
ES	Elementary Stream
FEC	Forward Error Correction
FECFRAME	FEC Framework
FMT	Fade Mitigation Technique
FWD	Forward Downlink
GS	Generic Streams
GSE	Generic Stream Encapsulation
GSE-FEC	Generic Stream Encapsulation FEC

HSPA	High-Speed Packet Access
IBO	Input Back-Off
IFEC	Inter-Burst FEC
ISAKMP	Internet Security Association and Key Management Protocol
IP	Internet Protocol
IPDC	IP Data-Casting
IPSEC	IP Security
LDPC	Low Density Parity Check
LL	Link Layer
LLC	Logical Link Control
LL-FEC	Link Layer Forward Error Correction
LMS	Land Mobile Satellite
LMSC	Land Mobile Satellite Channel
LOS+PA	Line-of-Sight plus Power Archers
LT	Luby Transform
NOFR	Non-Orthogonal Frequency Reuse
MAC	Multiple Access Channel
MBMS	Multimedia Broadcasting/Multicast Services
MDS	Maximum Distance Separable
MIMO	Multiple Input Multiple Output
MODCOD	Modulation and Coding
MPE-FEC	Multiple Protocol Encapsulation-FEC
MPE-IFEC	MPE Inter-Burst FEC
MPEG2-TS	Moving Picture Experts Group 2-Transport Streams
MTBL	Maximum Tolerant Burst Length
nLOS	non-Line of Sight
NPA	Network Point of Attachment
OBO	Output Back-Off
OBP	On-Board Processor
PA	Power Arches
PDU	Protocol Data Unit
PER	Packet Error Rate
PHY	Physical
PL-FEC	Packet-Level Forward Error Correction
PLR	Packet Loss Ratio
PPTP	Point-to-Point Tunnelling Protocol
QEF	Quasi-Error Free
QOS	Quality of Service
QPSK	Quadrature Phase Shift Keying
RCSTs	Return Channel Satellite Terminals
RMT	Reliable Multicast Transmission
RS	Reed-Solomon
RTN	Return Link
Rx	Receiver
SCPC	Single Carrier Per Channel
SFPB	Single Feed Per Beam

SINR	Signal-to-Interference plus Noise Ratio
SNDU	Sub-Network Data Unit
SNR	Signal to Noise Ratio
SW	Sliding Window
TDMA	Time Division Multiple Access
TLS	Transport Layer Security
TS	Transport Streams
TWTA	Traveling Wave Tube Amplifiers
Tx	Transmitter
ULE	Ultra Light Encapsulation
ULE-FEC	Ultra Light Encapsulation FEC
UMTS	Universal Mobile Telecommunications System
VSAT	Very Small Aperture Terminal
ZFBF	Zero Forcing Beam Forming

Part I

Dissertation Summary

Dissertation Summary

In this chapter, a summary of this dissertation will be presented. We will briefly introduce the work during my Ph.D. study. In Section 1.1, the motivation and the objective of this Ph.D. dissertation will be discussed. Section 1.2 presents the system model of the novel systems we proposed. The satellite resource allocation optimization approaches are described in Section 1.3. In Section 1.4, we discuss the problem of how to extend the system design to the mobile scenarios. Section 1.7 summarize the main contributions of this dissertation, and the main work of the included papers is presented in Section 1.6. Finally, we list the publications in Section 1.8.

1.1 Introduction

In this section, the motivation and the objective of this Ph.D. dissertation will be presented. We will first introduce the state-of-the-art satellite systems, and point out that these systems can not satisfy the increasing requirement of the interactive and high capacity services. In order to solve these problems, we propose an alternative route to design the new multi-beam satellite systems.

1.1.1 State-of-the-art

Information can be efficiently distributed over very large geographical areas by taking advantage of satellites' capability, e.g., the large available bandwidth in the Ku/Ka band. Therefore, satellite communications can be a "natural" solution for interactive services of data communications. As we have indicated in the abstract, in the last few years, multi-beam satellite systems are widely studied to increase the overall system bandwidth and the throughput (e.g., in [1–3]). Those satellites take advantage of the idea of frequency band reuse from terrestrial cellular networks [4]. This technique can illuminate the region of coverage by several spot beams with relative small aperture. The coverage area is divided into several cells, each cell corresponds to one spot beam.

For the current multi-beam satellite systems, the total available bandwidth in the forward link, B_{tot} is divided within f_R segments, where the f_R parameter is the fre-

quency reuse factor. The bandwidth allocated to user beam i, B_i is:

$$B_i = \frac{B_{\text{tot}}}{f_R}. \tag{1.1}$$

User beams that share B_{tot} conform a beam cluster. The number of beam clusters in the total system corresponding to the frequency reuse pattern, F_R where $F_R = \lceil \frac{N_b}{f_R} \rceil$, where $\lceil \cdot \rceil$ denotes the ceiling function. Obviously, due to the implementation of frequency reuse pattern, we can see the obtained gain (e.g., Δ) by using multi-beam techniques (the gain against the single-beam systems in terms of bandwidth is bounded at $\Delta \leq F_R$). Following the nomenclature defined in [10], we indicate $\hat{R}_i$ as the traffic demand in beam i, and R_i as the user beam capacity that the system may offer. The average system throughput is provided by:

$$R_{\text{tot}} = \sum_{i=1}^{N_b} \min\left(\hat{R}_i, R_i\right). \tag{1.2}$$

Equ. (1.2) shows that there is no flexibility in terms of bandwidth allocation in the conventional systems. It means that all the user beams of the system will be allocated the same bandwidth, independently on the traffic requirements of each cell. In the realistic application, a finite number of frequency carriers will be assigned to each beam with B_c bandwidth. Thus, the total amount of bandwidth allocated per beam equals $B_i = N_i B_c$, where N_i is the number of carriers in beam i. The power allocated to a carrier (e.g., carrier j) within a user beam (e.g., beam i) represent as P_{ij}. In this conventional case, the power allocation is uniform to each carrier, and hence, we can denote as P_c for any carriers.

In summary, the system architecture of the conventional satellite systems is designed without carrying out optimization to adapt the unbalanced traffic demand. Therefore, the on-board power and bandwidth are uniformly distributed to the satellite beams. In general, the conventional satellite systems can be characterized as follows:

- The conventional satellite systems manage a large amount of beams, controlled by several gateways.
- Each gateway manages a given number of beams according to the maximum bandwidth that can be processed.
- A regular frequency reuse and uniform power/carrier allocation are assumed, which means that no optimization should be carried out to adapt the unbalanced traffic distribution.
- Co-channel interference should be considered for the assumed frequency re-use pattern.

For a specific conventional satellite system, the more spot beams will increase the performance increases in terms of bandwidth. However, the interferences will become higher due to more frequency reuse spot beams. This fact is very counterproductive in terms of throughput. Therefore, in order to overcome this situation, we propose and study different techniques during the Ph.D. study.

1.1.2 Motivation and Objective of the Dissertation

As we know that the traffic distribution is highly asymmetrical throughout the coverage. Therefore, in order to match the traffic offered and requested as close as possible, the satellite systems require a certain degree of flexibility in allocating the power, bandwidth and time-slot resources. As mentioned in the literatures [5–11], the system performance can be improved by adapting the resource allocation to the system characteristics dynamically. These characteristics could be the state of the channel, the traffic demands or the Quality of Service (QoS) that requested by the terminals. Providing flexibility definitely improves the overall performance. However, at the same time, it increases the complexity not only at the technical level but also at the optimization level. The new satellite systems payload must support higher degree of flexibility in terms of power, bandwidth, switching than the conventional satellite payloads. Efficient and complex resource allocation algorithms will be strictly needed in the new systems with large number of beams. Therefore, in this Ph.D. dissertation, we propose two new schemes, i.e., flexible system and BH system.

The objective of this dissertation is to evaluate the improvements at system level provided by the proposed schemes, we compare with the conventional one in terms of capacity, performance and flexibility. The system scenarios studied in this dissertation can be summarized as:

- Conventional multi-beam satellite system: the current regular frequency reuse and uniform power/carrier allocation scheme (referred also as “conventional” in this dissertation).
- Flexible multi-beam satellite system: the first proposed novel system design, which is an extension of the conventional multi-beam system with non-regular frequency reuse and flexibility in bandwidth and power to beam allocation (referred also as “flexible” in this dissertation).
- Beam hopping multi-beam satellite system: the second proposed novel system design with flexibility in time-slot and power allocation (referred also as “beam hopping” or “ BH” in this dissertation).

In this section, we assume that the air interface is DVB-S2/RCS as it is today. We have to note that such standards might need change to adapt to the new proposed systems: flexible and BH. However, the methodology presented in this section is also applicable.

In addition, we study the extension of current satellite system to mobile environments (e.g., railway scenario) in this dissertation. Since the current air interface standards lack of the specification for mobile scenarios, a new Fade Mitigation Technique (FMT), i.e., Link Layer Forward Error Correction (LL-FEC) is introduced for the standards of DVB-S2/RCS in mobile environments. We have to note that such air interface standards might need change to adapt to the new proposed systems: flexible and BH. However, the methodology presented is also applicable.

1.2 Proposed Multi-beam Satellite Systems

This section presents the proposed system scenarios according to the framework of the Ph.D. research line. Two novel multi-beam satellite systems, flexible and BH, will be briefly introduced.

1.2.1 Flexible System

As we indicated, flexible system can be considered as an extension of the conventional satellite systems. For this scheme, the number of carriers allocated to each beam may vary, and the system is able to adapt this allocation pattern to the traffic distribution. Regarding to the issue of the flexibility, each beam trends to allocate the amount of bandwidth to satisfy users' requirement.

We assume that all the carriers have the same granularity B_c, which is an important parameter subject to be optimized. B_c represents the step size in the bandwidth allocation algorithm, and also limits the minimum and maximum bandwidth allocated per user beam. Since each beam will be allocated at least one carrier in the realistic scenario, i.e., $N_i \in \{1, 2, \cdots, N_{\max}\}$, where $N_{\max} = N_c - (f_R - 1)$ and N_c is the number of carriers defined as $N_c = \frac{B_{\text{tot}}}{B_c}$.

The frequency reuse pattern is implemented in the flexible system, and various beams will be transmitted/received at the same time over the same frequency carrier. Thus, we have to take into account the co-channel interference and try to minimize it as small as possible. For that reason, it is important to take care of that the carriers can not be reused by the neighboring beams to limit the co-channel interference. This point will be discussed in detail in Section 1.3.

The bandwidth allocation pattern matrix (also referred as spectral mask matrix) $\mathbf{C} \in \mathbb{R}^{N_c \times N_b}$ is defined as $\mathbf{C} = [\mathbf{c}_1, \mathbf{c}_2, \cdots, \mathbf{c}_{N_b}]$, where the ith column vector $\mathbf{c}_i \in \mathbb{R}^{N_c \times 1}$ is defined as $\mathbf{c}_i = [C_{i1}, C_{i2}, \cdots, C_{iN_c}]^T$. $\mathbf{c}_i$ indicates that which TDM carriers are allocated to beam i. Therefore, the number of carriers allocated to each beam (e.g., for beam i) can be directly derived from $\mathbf{C}$ as:

$$N_i = \sum_{j=1}^{N_c} C_{ij}, \tag{1.3}$$

where $C_{ij} = \{0, 1\}$ indicates if the carrier j is allocated to beam i ($C_{ij} = 1$); or not be allocated ($C_{ij} = 0$). Then the SINR of the i-th beam can be given as

$$\gamma_{i,j} = \frac{\alpha_i^2 P_{ij}}{\sigma^2 + \sum\limits_{\substack{m=1 \\ m \neq i}}^{N_b} \alpha_m^2 C_{mj} P_{mj}}. \tag{1.4}$$

where α_i denotes the channel attenuation factor, σ^2 indicates the variance of the Gaussian noise, P_{ij} is the power allocated for beam i and carrier j. Where $\sum\limits_{\substack{m=1 \\ m \neq i}}^{N_b} \alpha_m^2 C_{mj} P_{mj}$ is the co-channel interference.

Equ. (1.4) shows that $\gamma_{i,j}$ not only depends on the spectral mask vector of beam i ($\mathbf{c}_i$), but also depends on the co-channel beams. Hence, the spectral mask vector for each beam must be optimized jointly with the others. The specific design of one beam's spectral mask vector may affect the crosstalk experienced by the other beams. Hence, it's a complicated task to jointly design the spectral mask matrix $\mathbf{C}$. In order to match the offered and requested traffic on a per-beam basis, we develop a method to jointly optimize power and carrier allocation and solve the spectral mask matrix $\mathbf{C}$ in Section 1.3.

In summary, for the flexible system, the total available bandwidth can be allocated to match the unbalanced traffic demand throughout the coverage region. Therefore, the non-regular frequency reuse pattern will be implemented in the flexible system. It means that the allocated bandwidth per beam should be optimized to maximize the system capacity. The flexible multi-beam satellite system can be characterized by the following parameters:

- The satellite system manages a large amount of beams, controlled by several gateways.
- Each gateway manages a limited amount of beams according to the maximum bandwidth that can be processed by each gateway. In this case, one downlink beam might be not fully managed by a single gateway, but by several gateways at the same time.
- On the contrary to the conventional system, the flexible system implements the non-regular frequency reuse pattern instead of regular frequency reuse and uniform power/carrier allocation.
- In the flexible system, the carriers can not be reused by the neighboring beams to limit the co-channel interference. Nevertheless, the allocation of the bandwidth (or carrier) to beam should be fully performed by the optimization algorithm.

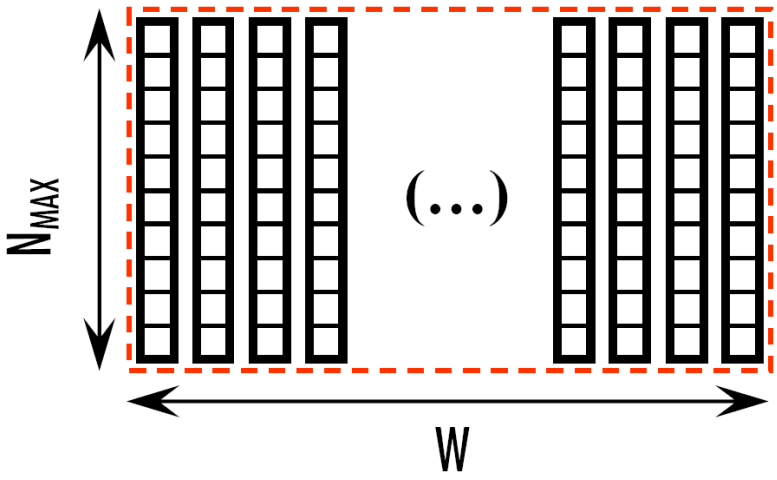

Figure 1.1: Beam Hopping Window representation with no bandwidth segmentation.

1.2.2 Beam Hopping System

The BH technique is a concept that a limited amount N_{MAX} of beams are simultaneously illuminated with a regular repetition pattern (where $N_{MAX} < N_b$). Thus, the flexible bandwidth to beam allocation (on the average) can be provided to each beam according to its capacity required.

The general concept of BH is presented in Fig. 1.1 with no bandwidth segmentation. A regular time window W is periodically applied to the BH system, and the illuminated beams are allocated with the full bandwidth B_{tot} in each window column. The maximum number of beams can be simultaneously illuminated in the system as N_{MAX}. It can be defined according to the payload design. In addition, the duration of the given illuminated beam, T_s, needs to be carefully studied. This value shall be traded off so that the amount of information carried during T_s can be optimized to satisfy the user transmission delay requirement.

In the BH technique, the data are not continuously received by the user terminals, because beams are not always illuminated. This will modifie the format of the frames. The frame format inherent to the technique as well as the traffic burst format should be carefully studied. In addition, the BH technique introduce additional delay on the transmitted traffic, which might be critical for the given class of QoS (real-time applications such as VoIP).

In the more general case where bandwidth segmentation is assumed, each beam can be illuminated with a fraction of the total available bandwidth B_{tot}. In this case, the illumination patter matrix shall have a three dimensional representation, as shown in Fig. 1.2.

As we described the flexible system, the illumination pattern of BH system can also be indicated by a matrix. The beam illumination pattern matrix $\mathbf{T} \in \mathbb{R}^{N_t \times N_b}$ can be defined as $\mathbf{T} = [\mathbf{t}_1, \mathbf{t}_2, \cdots, \mathbf{t}_{N_b}]$, where N_t is the number of time slot in each window length, and the ith column vector $\mathbf{t}_i \in \mathbb{R}^{N_t \times 1}$ is defined as $\mathbf{t}_i = [T_{i1}, T_{i2}, \cdots, T_{iN_t}]^T$. $\mathbf{t}_i$

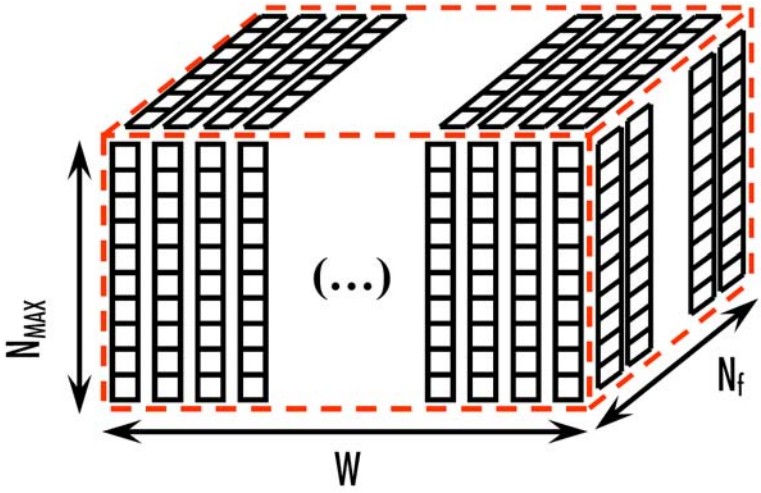

Figure 1.2: Beam Hopping Window representation with bandwidth segmentation.

indicates which time slot is allocated to beam i. Therefore, the number of time slot allocated to each beam (e.g., for beam i) can be directly derived from $\mathbf{T}$ as:

$$N_i^t = \sum_{j=1}^{N_t} T_{ij}, \tag{1.5}$$

where $T_{ij} = \{0, 1\}$ indicates if the time slot j is allocated to beam i ($T_{ij} = 1$); or not be allocated to beam ($T_{ij} = 0$).

From the Section 1.2.1 and Section 1.2.2 we can note that the flexible system and the BH system are quite similar, just change the formulation from frequency domain to time/space domain. In Section 1.3.2, we will study the duality of the flexible and BH systems and prove that they are theoretically dual of each other.

1.3 Resource Allocation Optimization

In this section, we first formulate the multi-beam system model in frequency domain (i.e., for the flexible scheme). In the subsequent section we state the conditions for duality and prove that flexible system and BH system are dual of each other and hence the formulation is also valid in time domain(i.e., for the BH scheme). This dual formulation allows us to derive a unique SINR expression, which will be used in the following section for capacity optimization.

1.3.1 Multi-beam System Model for the Proposed Schemes

First, we note that the system model in the frequency domain, we refer to the fact that the transmission to the beams should explicitly be formulated in terms of the

bandwidth carriers. We assume N_c carriers in total with a given granularity, B_c. In this section, the number of beams is referred as K (i.e., $K = N_b$) in order to formulate clearly. Following, we introduce the different sub-models.

1.3.1.1 Channel Model

We do an analysis in time and hence the channel attenuation corresponds to the free space losses and atmospheric losses (in case of frequencies above Ka band). We assume an instantaneous analysis with fixed coefficient. The channel attenuation amplitude matrix $\mathbf{A} \in \mathbb{C}^{K \times K}$ is defined as

$$\mathbf{A} = \text{diag}\left\{\alpha_1, \alpha_2, \cdots, \alpha_K\right\}, \tag{1.6}$$

where α_i denotes the channel attenuation factor over the destination user beam i.

1.3.1.2 Antenna Model

An Array Feed Reflector (AFR) based Antenna system is assumed in this paper, it can generate a regular beam grid array consisting of a very high number of highly overlapping, narrow beam width, composite user beams. Each beam is synthesized by adding array elements whose phases and amplitudes are adjustable, and hence we can provide flexible power allocation by controlling the On-Board Processor (OBP). Therefore, we can suppose that the antenna gain matrix $\mathbf{G} \in \mathbb{C}^{K \times K}$ is given as

$$\mathbf{G} = \begin{bmatrix} g_{11} & g_{12} & \cdots & g_{1K} \\ g_{21} & g_{22} & \cdots & g_{2K} \\ \vdots & \vdots & \ddots & \vdots \\ g_{K1} & g_{K2} & \cdots & g_{KK} \end{bmatrix}, \tag{1.7}$$

where $|g_{ij}|^2 \in \mathbb{R}^{1 \times 1}$ is the antenna gain of the on-board antenna feeds for jth beam towards the ith user beam.

1.3.1.3 Received Signal Model

In frequency domain, the transmitted symbols over N_c carriers to beam $i (i = 1, 2, \cdots, K)$ is defined as $\mathbf{x}_i = [x_{i1}, x_{i2}, \cdots, x_{iN_c}]^T$. Let the spectral mask matrix $\mathbf{C} \in \mathbb{R}^{N_c \times K}$ be defined as $\mathbf{C} = [\mathbf{c}_1, \mathbf{c}_2, \cdots, \mathbf{c}_K]$, and the ith column vector $\mathbf{c}_i \in \mathbb{R}^{N_c \times 1}$ be defined as $\mathbf{c}_i = [C_{i1}, C_{i2}, \cdots, C_{iN_c}]^T$, which is the spectral mask vector for beam i and indicates which TDM carriers and how much power is allocated to beam i.

Let $\mathbf{H} = \mathbf{AG}$ be the overall channel matrix, and $\mathbf{C}_i = \text{diag}\{\mathbf{c}_i\}$. Then the received signal by all the N_c carriers for ith user beam, $\mathbf{y}_i \in \mathbb{C}^{N_c \times 1}$, can be expressed as desired

signal and interference as

$$\mathbf{y}_i = h_{ii}\tilde{\mathbf{x}}_i + \sum_{\substack{k=1 \\ k\neq i}}^{K} h_{ik}\tilde{\mathbf{x}}_k + \mathbf{n}_i, \tag{1.8}$$

where $\tilde{\mathbf{x}}_i$ is the spectral masked symbols for beam i, defined as $\tilde{\mathbf{x}}_i = \mathbf{C}_i\mathbf{x}_i$. The term $h_{ii}\tilde{\mathbf{x}}_i$ corresponds to the desired signals coming from the ith on-board antenna. The term $\sum_{\substack{k=1 \\ k\neq i}}^{K} h_{ik}\tilde{\mathbf{x}}_k$ is the sum of interference signals from the other on-board antennas. $\mathbf{n}_i \in \mathbb{C}^{N_c\times 1}$ is a column vector of zero-mean complex circular Gaussian noise with variance σ^2 at beam i.

1.3.1.4 Signal-to-Interference plus Noise Ratio

In the frequency domain, the whole bandwidth is segmented into N_c carriers. The spectral mask matrix can be reformulated as $\mathbf{C} = [\tilde{\mathbf{c}}_1^T, \tilde{\mathbf{c}}_2^T, \cdots, \tilde{\mathbf{c}}_{N_c}^T]^T$, where $\tilde{\mathbf{c}}_j = [C_{1j}, C_{2j}, \cdots, C_{Kj}]$, indicates which beams are allocated carrier j. Let the ith row of $\mathbf{H}$ be defined as $\mathbf{h}_i = [h_{i1}, h_{i2}, \cdots, h_{iK}]$ and $\tilde{\mathbf{h}}_i = \mathbf{h}_i|_{(h_{ii}=0)}$ is the channel of interference contribution. We assume that the amplitude of the transmitted symbols is normalized (i.e., $|x_{ij}|^2 = 1, \forall i = 1, \cdots, K; \forall j = 1, \cdots, N_c$).

Then, the transmitted signal power of all the carriers for beam i can be given by the diagonal elements of the matrix $\mathbf{U}_i^f \in \mathbb{R}^{N_c\times N_c}$ as (note that the superscript f and t in this paper indicate the expression in frequency and time domain, respectively)

$$\mathbf{U}_i^f = |h_{ii}|^2\mathbf{C}_i\mathbf{C}_i^H. \tag{1.9}$$

And the co-channel interference power of all the carriers for beam i can also be given by the diagonal elements of the matrix $\mathbf{V}_i^f \in \mathbb{R}^{N_c\times N_c}$ as

$$\mathbf{V}_i^f = \mathrm{diag}\left\{\left[\tilde{\mathbf{h}}_i\tilde{\mathbf{c}}_j^H\tilde{\mathbf{c}}_j\tilde{\mathbf{h}}_i^H\right]_{j=1,2,\cdots,N_c}\right\}. \tag{1.10}$$

Thus the interference power plus the noise matrix, $\mathbf{R}_i^f$, will be given as

$$\mathbf{R}_i^f \;=\; \mathbf{V}_i^f + \sigma^2\mathbf{I}_{N_c}. \tag{1.11}$$

Consequently, the SINR for ith beam, defined as $\mathbf{\Gamma}_i^f \in \mathbb{R}^{N_c\times N_c}$, can be expressed as

$$\mathbf{\Gamma}_i^f = \mathbf{U}_i^f(\mathbf{R}_i^f)^{-1}. \tag{1.12}$$

Obviously, $\mathbf{\Gamma}_i^f$ is a diagonal matrix, because both $\mathbf{U}_i^f$ and $\mathbf{R}_i^f$ are diagonal matrix. Thus, the SINR for jth carrier used by beam i will be the jth diagonal element of the

matrix $\mathbf{\Gamma}_i^f$. This means that for each carrier j of beam i, the SINR can be formulated as

$$\gamma_{ij}^f = \frac{|h_{ii}C_{ij}|^2}{\sum\limits_{\substack{k=1 \\ k\neq i}}^{K} |h_{ik}C_{kj}|^2 + \sigma^2}. \tag{1.13}$$

1.3.2 Frequency/Time Duality

In the previous section, expression (1.13) gives the signal-to-interference plus noise ratio in terms of the spectral mask vector, i.e., the unknown power and carrier allocation vector in the frequency domain.

In this section, we propose the frequency/time duality of (1.13). For doing so, we first state the dual expression of (1.13) in time domain. After that, we find the conditions for the duality.

1.3.2.1 Dual System Model

In the time domain, the time window is segmented into N_t time-slots. The time-slot mask matrix can be formulated as $\mathbf{T} = [\tilde{\mathbf{t}}_1^T, \tilde{\mathbf{t}}_2^T, \cdots, \tilde{\mathbf{t}}_{N_t}^T]^T$, where $\tilde{\mathbf{t}}_j = [T_{1j}, T_{2j}, \cdots, T_{Kj}]$, indicates which beams are allocated time-slot j. Then, the transmitted signal power matrix $\mathbf{U}_i^t$, the co-channel interference power matrix $\mathbf{V}_i^t$, the interference power plus the noise matrix $\mathbf{R}_i^t$ and the SINR matrix $\mathbf{\Gamma}_i^t$ in time domain can be formulated as follows

$$\mathbf{U}_i^t = |h_{ii}|^2 \mathbf{T}_i \mathbf{T}_i^H, \tag{1.14}$$

$$\mathbf{V}_i^t = \mathrm{diag}\left\{ \left[\tilde{\mathbf{h}}_i \tilde{\mathbf{t}}_j^H \tilde{\mathbf{t}}_j \tilde{\mathbf{h}}_i^H \right]_{j=1,2,\cdots,N_t} \right\}, \tag{1.15}$$

$$\mathbf{R}_i^t = \mathbf{V}_i^t + \sigma^2 \mathbf{I}_{N_t}, \tag{1.16}$$

$$\mathbf{\Gamma}_i^t = \mathbf{U}_i^t (\mathbf{R}_i^t)^{-1}. \tag{1.17}$$

Then the SINR for jth time-slot allocated to ith beam will be the jth diagonal element of the matrix $\mathbf{\Gamma}_i^t$. Hence, the SINR for jth time-slot of beam i can be formulated

as

$$\gamma_{ij}^{t} = \frac{|h_{ii}T_{ij}|^2}{\sum\limits_{\substack{k=1 \\ k\neq i}}^{K} |h_{ik}T_{kj}|^2 + \sigma^2}. \tag{1.18}$$

From the point of view of duality definition in [14], (1.13) and (1.18) are dual of each other from a theoretical point of view. However, for a practical system, we derive the duality conditions in the next section.

1.3.2.2 Duality Conditions

From (1.13) and (1.18) we can extract the duality conditions. In order to do so, we first express the beam-level sum-rate throughput as follows

$$R_i^f = \sum_{j=1}^{N_c} \frac{B_{\text{tot}}}{N_c} \eta_{ij}^f, \tag{1.19}$$

and the dual is

$$R_i^t = \sum_{j=1}^{N_t} \frac{B_{\text{tot}}}{N_t} \eta_{ij}^t, \tag{1.20}$$

where $\eta_{ij} = f(\gamma_{ij})$ is the spectral efficiency, and $f(\gamma_{ij})$ is a function that relates the SINR with a corresponding spectral efficiency (as shown in Table 1.1). This function can be $\log_2(1+\gamma_{ij})$ for Shannon limit with Gaussian coding, or can be a quasi-linear function in DVB-S2 [16] with respect to SINR .

Hence in order to obtain

$$R_i^f = R_i^t. \tag{1.21}$$

The following conditions should be fulfilled for systems to be dual in practice:

- Granularity in frequency and time domains should be the same:

$$N_c = N_t, \tag{1.22}$$

- The entries of Resource Allocation Matrix should be the same in frequency and time domains:

$$C_{ij} = T_{ij}, \tag{1.23}$$

- The spectral efficiency function $f(\cdot)$ should be the same for flexible and BH systems in frequency and time domains, respectively.

$$f(\eta_{ij}^f) = f(\eta_{ij}^t). \tag{1.24}$$

For a practical flexible system, it is not acceptable to have a very fine carrier band-

width, i.e., N_c can not be very large. However, N_t can be much finer than bandwidth. Hence, it can be concluded that BH implementation allows higher flexibility. In paper B, we assume that granularity can be the same for both technologies and we focus on the actual limitation which is given by the levels of interference that each technology can achieve. The difference in the interference levels achieved will be a direct consequence in the technological implementation. The results show that, in the realistic implementation, the BH system performs slightly better than the flexible one, due to the payload constraints, e.g. different OBO.

1.3.3 Capacity Optimization

In this section, we propose a capacity optimization problem subject to the traffic request per-beam and the power constraints. It is a non-convex optimization problem, since the co-channel interference is taken into account. Therefore, an iterative algorithm is proposed.

Obviously, γ_{ij}^{f} in formula (1.13) not only depends on the spectral mask vector of beam i ($\mathbf{c}_i$), but also depends on that of the co-channel beams. And hence, the spectral mask vector for each beam must be optimized jointly with the others. The specific design of one beam's spectral mask vector may affect the crosstalk experienced by other beams. Hence it's a complicated task to design the spectral mask matrix $\mathbf{C}$ jointly. In order to best match offered and requested traffic on a per-beam basis, we develop a methodology to solve the spectral mask matrix $\mathbf{C}$ in this section and to jointly optimize power and carrier allocation. Note that we only discuss the capacity optimization for flexible system because BH is dual with flexible, thus the formulation is also applicable for BH system by changing the duality parameters in Table 1.1.

Existing results in the references [32–34] on similar problems assume power limitation and the optimization is exclusively over the power allocation. However, we assume an additional degree of freedom: carrier allocation (bandwidth granularity). We propose to use Binary Power Allocation (BPA), thus, the power allocation status can also be indicated by the resource allocation matrix (i.e., $\mathbf{C}$ or $\mathbf{T}$). In order to formulate simply and decrease the complexity, we let ($|C_{ij}|^2 = \{0, P_{\max}\}, i = 1, 2, \cdots, K; j = 1, 2, \cdots, N_c$) and quantized bandwidth allocation, where $P_{\max}$ is the TWTA saturation power per carrier.

1.3.3.1 Optimization Problem Formulation

In this dissertation, we focus on the capacity per-beam optimizing based on the BPA and quantized bandwidth allocation with given bandwidth granularity and SINR con-

Table 1.1: Frequency-Time Duality

	Frequency Domain	Time Domain
Granularity	B_c	T_s
Total Number of carriers / time-slot	N_c	N_t
Resource Allocation Matrix	C_{ij}	T_{ij}
SINR (γ_{ij})	$\gamma_{ij}^f = \frac{\frac{\|h_{ii}C_{ij}\|^2}{\sum_{\substack{k=1 \\ k\neq i}}^{K} \|h_{ik}C_{kj}\|^2 + \sigma^2}}{}$	$\gamma_{ij}^t = \frac{\frac{\|h_{ii}T_{ij}\|^2}{\sum_{\substack{k=1 \\ k\neq i}}^{K} \|h_{ik}T_{kj}\|^2 + \sigma^2}}{}$
Spectral Efficiency (η_{ij})	$\eta_{ij}^f = f(\gamma_{ij}^f)$	$\eta_{ij}^t = f(\gamma_{ij}^t)$
Throughput (R_i) for Beam i	$R_i^f = \sum_{j=1}^{N_c} \frac{B_{\text{tot}}}{N_c}\eta_{ij}^f$	$R_i^t = \sum_{j=1}^{N_t} \frac{B_{\text{tot}}}{N_t}\eta_{ij}^t$

straint. The optimization problem can be formulated as

$$\begin{aligned} &\max_{\mathbf{C}} \sum_{i=1}^{K} \frac{R_i(\mathbf{C})}{\hat{R}_i} \\ &\text{subject to } R_i \leq \hat{R}_i \\ &\sum_{i=1}^{K} \mathbf{c}_i^H \mathbf{c}_i \leq P_{\text{tot}}; \text{and } |C_{ij}|^2 = \{0, P_{\max}\}, \forall i, j. \end{aligned} \tag{1.25}$$

where $\hat{R}_i$ is the traffic requested by beam i, $R_i(\mathbf{C})$ is defined in Table 1.1. P_{tot} is total available satellite power, $P_{\max}$ is saturation power per carrier, which is the constraint of satellite amplifier.

1.3.3.2 Iterative Algorithm Solution

The general analytical solution of (1.25) is a complex problem due not only to the clear non-convexity but also to the need of preserving the geometry of the optimization model (i.e., the structure of matrix $\mathbf{C}$). Therefore, we propose an iterative algorithm solution, which is summarized in Table 1.2. The beam set $\mathcal{A}_s$ is constituted by all the beams, in which the traffic request is not achieved (i.e., $\frac{R_k}{\hat{R}_k} < 1$). Quantities associated with the nth iteration are denoted by n_{it}. Each iteration is based on a two-step process.

Firstly, we optimize subspace-by-subspace and obtain an analytical solution to the sub-problem of allocating the carrier on a per-beam basis (as shown in step 4 of

Table 1.2: Algorithm Solution for flexible system

1: Initialize: $R_k \Leftarrow 0, \forall k$; $n_{\text{it}} \Leftarrow 0$; $\mathbf{C} \Leftarrow \mathbf{0}$

2: $i \Leftarrow 0$;

Generating beam set $\mathcal{A}_s$:

$\mathcal{A}_s = \left\{ i_1, i_2, \cdots, i_N | 0 \leq \frac{R_{i_n}}{\hat{R}_{i_n}} \leq \frac{R_{i_{n-1}}}{\hat{R}_{i_{n-1}}} < 1 \right\}$;

where $i_n \in \{1, 2, \cdots, K\}, n = 1, 2, \cdots, N$;

3: $n_{\text{it}} \Leftarrow n_{\text{it}} + 1$

Repeat: $i \Leftarrow i + 1$; $k \Leftarrow \mathcal{A}_s(i)$

4: Solve the Rayleigh quotient problem:

$$\arg\max \frac{\mathbf{e}_j^H \mathbf{U}_k^f \mathbf{e}_j}{\mathbf{e}_j^H \mathbf{R}_k^f \mathbf{e}_j}$$

5: $C_{kj} \Leftarrow \mathbf{e}_j^H \mathbf{e}_j (P_{\max})^{1/2}$

6: Update $\mathbf{U}_k^f$, $\mathbf{V}_k^f$; $\mathbf{R}_k^f \Leftarrow \mathbf{V}_k^f + \sigma^2 \mathbf{I}$

7: go to step 3,

until $k > i_N$;

8: Update $\gamma_{kj}^f, \forall k, j$; $R_k \Leftarrow \sum_{j=1}^{N_c} \frac{B_{\text{tot}}}{N_c} \eta_{ij}^f, \forall k$;

9: go to step 2, until $\mathcal{A}_s$ is empty or $\sum_{i=1}^{K} \mathbf{c}_i^H \mathbf{c}_i \leq P_{\text{tot}}$;

Table 1.2). The optimal carrier allocation per-beam can be formulated as a Rayleigh quotient, e.g. for beam i, the problem can be formulated as:

$$\begin{aligned} &\arg\max_j \frac{\mathbf{e}_j^H \mathbf{U}_i^f \mathbf{e}_j}{\mathbf{e}_j^H \mathbf{R}_i^f \mathbf{e}_j} \\ &\text{subject to} \sum_{i=1}^{K} \mathbf{c}_i^H \mathbf{c}_i \leq P_{\text{tot}}, \end{aligned} \tag{1.26}$$

where $\mathbf{e}_j \in \mathbb{R}^{N_c \times 1}$ is standard basis vector, which denotes the vector with a 1 in the jth coordinate and 0's elsewhere.

The solution of Rayleigh quotient problem shown in (1.26) is given as

$$\mathbf{e}_j = \upsilon_{\max}(\mathbf{U}_i^f (\mathbf{R}_i^f)^{-1}) = \upsilon_{\max}(\mathbf{\Gamma}_i^f), \tag{1.27}$$

where $\upsilon_{\max}(\mathbf{\Gamma}_i^f)$ (as expressed in 1.12) indicates the eigenvector related to the maximum eigenvalue of matrix $\mathbf{\Gamma}_i^f$.

Secondly, we obtain the power allocated to the selected carriers from the power constraint (as shown in step 5 of Table 1.2). C_{ij} for jth carrier of beam k can be

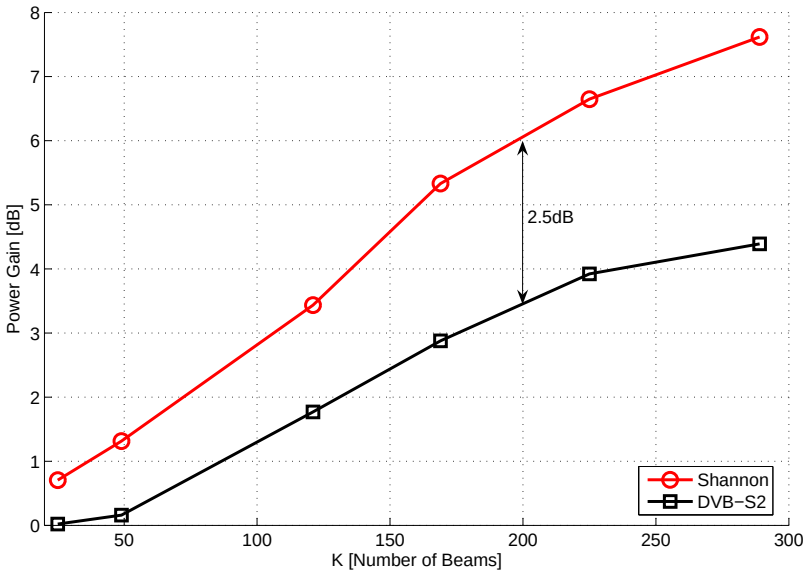

Figure 1.3: Power Gain (g_p) vs. Number of beams (K).

obtained with the solution of $\mathbf{e}_j$ as

$$C_{ij} = \mathbf{e}_j^H \mathbf{e}_j (P_{\max})^{1/2}, \tag{1.28}$$

After each iteration, we update matrix $\mathbf{U}_i^f$ and $\mathbf{R}_i^f$ according to the updated spectral mask matrix $\mathbf{C}$.

1.3.4 Main Results

The objective of this section is to present a summary of the performances of the proposed novel system designs. In addition, we compare the proposed system designs with the conventional system designs. Finally, we obtain the technological gap between flexible and BH systems. The detailed simulation results can be found in Paper A and B.

The power gain respect to the number of beams is shown in Fig. 1.3. We can see that about 6dB and 3.5dB power gain can be achieved by capacity optimizing with Gaussian coding and DVB-S2 ModCods, respectively (when $K = 200$). By optimizing the capacity achieved per-beam, we do not only reduce power and bandwidth consumption of small traffic request beams, but also achieve reasonable proportional fairness from the viewpoint of user beams. In Fig.A.5, the result shows that the spectral efficiency decreases with the number of beams increasing, especially when $K > 200$. The reason is that co-channel interference will increase with the beamwidth decreasing. In order to evaluate the technology gap, we define the difference of OBO between flexible and BH systems as $\Delta_{\text{OBO}} = x_1 - x_2$. Fig. 1.5 shows Δ_{OBO} respect to

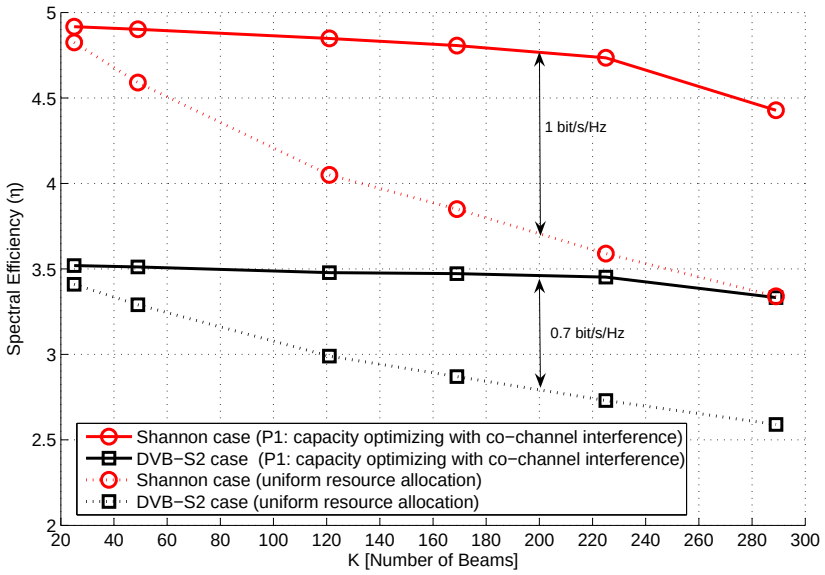

Figure 1.4: Spectral Efficiency (η) vs. Number of beams (K).

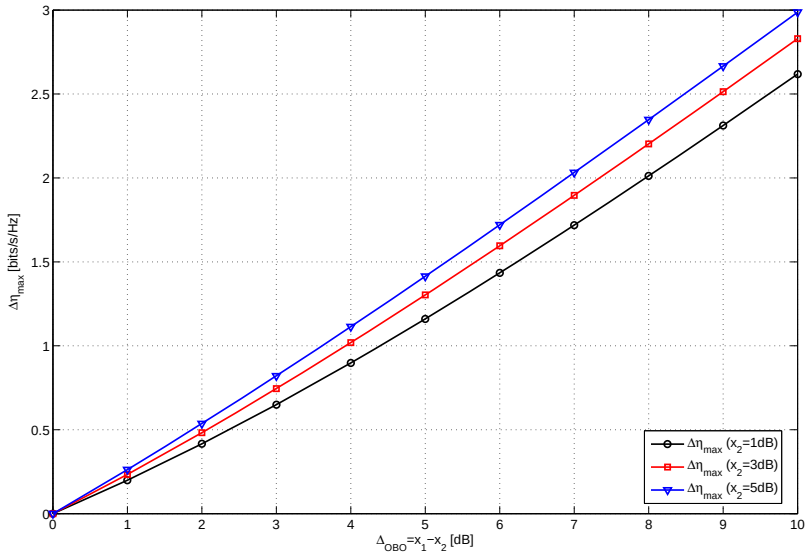

Figure 1.5: Δ_{OBO} vs. $\Delta\eta_{\mathrm{max}}$.

$\Delta\eta_{\mathrm{max}}$, which is defined in Paper B. We can see that $\Delta\eta_{\mathrm{max}}$ is almost linear with Δ_{OBO}, and the slope is increasing with BH system OBO (x_2) increasing. This result is very useful to predict the technological gap between flexible and BH systems.

The new transmission schemes (i.e., flexible and BH) for the multi-beam satellite system we proposed are for the fixed terminals. However, recently market study have shown that more and more mobile terminals are installed in the mobile platform, such

as a train, ship, or aircraft, are exposed to challenging environments that will impact the system performance since the current standard lacks any specific provision for mobile scenarios. Especially in Europe, due to the success of DVB-S [15], DVB-S2 [16], and the Return Channel via Satellite (DVB-RCS) [17] standards. As is well known, neither DVB-S2 nor DVB-RCS has been designed for mobile users, hence, new techniques have to be introduced to compensate the fading due to the mobility. In this thesis, we propose to apply FEC technique at the link layer (i.e., LL-FEC).

1.4 Extension to Mobile Scenarios

In this section, we assume that the air interface is DVB-S2/RCS as it is today. We have to note that such standards might need change to adapt to the new proposed systems: flexible and BH. However, the methodology presented in this section is also applicable. This part of Ph.D. work focuses on the specific mobile scenario with collective terminals, such as ships, trains, and planes. The characteristics of the mobile scenarios will be studied. Since the current standards are lack of specific provision for mobile scenarios, LL-FEC is introduced as a fading countermeasure for DVB-S2/RCS in mobile environments. We will dissert the selected solution after a critical analysis of the existing LL-FEC frameworks, e.g., MPE-FEC, ULE-FEC, and GSE-FEC.

1.4.1 Reference Scenario

In general, mobile terminals experience critical signal impairments in the synchronization acquisition and maintenance since the mobile channel undergoes shadowing and fading due to mobility, as well as deep fading due to blockage. Terminals installed in mobile platforms, such as trains, ships, aircraft, trucks or other vehicles are exposed to challenging environments that will impact the system performance since these baseline standards lack any specific provision for mobile scenarios. The Land Mobile Satellite Channel (LMSC) has been widely studied in the literature [18]. Several measurement campaigns have been carried out and a number of narrow and wideband models have been proposed for a wide range of frequencies, including Ku [19] and Ka [20] bands. Nevertheless, for the specific case of railway environment, only few results are available in [21] as a consequence of a limited trial campaign using a narrowband test signal at 1.5 GHz, performed more than 10 years ago in the north of Spain. These results represent a very interesting reference, although no specific channel model has been extracted from the collected data. After an initial qualitative analysis, the railway environment appears to differ substantially with respect to the scenarios normally considered when modelling the LMSC. Excluding railway tunnels and areas in the proximity of large railway stations, one has to consider the frequent presence of several metallic obstacles like Power Arches (PAs), posts with horizontal brackets, and catenaries, i.e. electrical cables are frequent obstacles to Line of Sight (LOS) reception. Results of direct measurements performed along the Italian railway aiming to characterize these peculiar obstacles are reported in [22]. In summary, the

attenuation introduced by the catenaries (less than 2 dB) and by posts with brackets (2-3 dB) is relatively low and can be easily compensated by an adequate link margin. However, the attenuation introduced by the power arches increases to values as high as 10 dB and beyond, depending on the geometry, the antenna radiation pattern and the carrier frequency. Typically, due to reflections and scattering multipath, signals are received that result in typical correlated Rayleigh fading, the directivity is taken into account by shaping the spectrum. Therefore, in this work we focus on railway channel models that have, for example, been introduced in [22; 23] and the Land Mobile Satellite channel models have been discussed in [20; 24; 25]. Based on these preliminaries, the two introduced channel models can be further simplified as follows.

LOS+PA channel: For the sake of simplicity, the presence of PAs in the railway environment can be medelled as erasures with different duty cycle, therefore an ON/OFF model assumed, during the "ON State", the Packet Error Rate (PER) of the signal received equals to 0. During the "OFF State", the PER received equals to 100%. The duty cycle of PAs can be computed as

$$\text{Duty Cycle} = \frac{l_{\text{PA}}}{l_{\text{PA}} + d_{\text{PA}}}, \tag{1.29}$$

where l_{PA} is the width of PA, and d_{PA} is the distance between two consecutive PAs. Therefore, for the LOS+PA case depending on the velocity of the train v_{train}, the number of lost DVB-S2 Baseband Frames (BB-Frames) $N_{\text{BB\_PA}}$ during the PA obstructions can be easily obtained. Assume $T_{\text{PA}} = l_{\text{PA}}/v_{\text{train}}$ the obstruction duration for the transmitted signal, B_s is the symbol rate, M is modulation constellation, r_{phy} the physical coding rate and S_{BBFrame} the size of a BB-Frame. Then $R_{\text{BB}} = B_s M r_{\text{phy}}/S_{\text{BBFrame}}$ is the rate at which BB-Frames are transmitted (e.g. $S_{\text{BBFrame}} = 32208$ bits for 64k FECframe with LDPC coding rate=1/2 and S_{BBFrame}=48408 bits for coding rate=3/4) and the number of lost BB-Frames lost during the PA is $N_{\text{BB\_PA}} = \lceil T_{\text{PA}} R_{\text{BB}} \rceil$. In terms of performance criteria for this scenario, we are interested in the Maximum Tolerant Burst Length (MTBL), which corresponds to the maximum duty cycle that can be overcome by the link layer.

nLOS channel: In certain circumstances, LOS to the satellite is heavily obstructed, for example if the receiver moves in some urban areas. Typically, due to reflections and scattering multipath signals are received that result in typical correlated Rayleigh fading, the directivity is take into account by shaping the spectrum. In this thesis we model the nLOS Rayleigh channel at link layer. We use time series of 0s and 1s representing received BB-Frames of DVB-S2, which are either fully received or lost. Such time series of 0s and 1s are used as the input of the link layer module of the simulator presented herein below. In terms of performance evaluation we assess the residual packet loss rate that generally needs to be below some threshold for sufficient quality.

In order to compensate the deep fading in the mobile satellite scenarios, an excellent fading countermeasure for erasure channels is the application of FEC on the link layer, i.e., LL-FEC, which will be discussed in detail in the next section.

1.4.2 Proposed Solution: Link-Layer Forward Error Correction

As already indicated, an excellent fading countermeasure for erasure channels is the application of FEC on the link layer. DVB has applied this principle already in several systems, such as DVB-H [26] or DVB-SH [27]. FEC may be applied at Application or Transport Layer as for example done in 3GPP's Multimedia Broadcasting/Multicast Services (MBMS) or IP Data-Casting (IPDC) file delivery over DVB-H based on the Raptor codes. However, this type of FEC is service specific and is not generic and applicable to any packet flow. Traditionally, the FEC is applied at the PHY Layer/bit-level, nowadays usually either based on the Turbo codes or Low Density Parity Check (LDPC) codes. However, such codes are usually limited in the amount of interleaving due to hardware restrictions. Therefore, in the DVB family of standards, e.g. DVB-T/H, link layer FEC is considered for protecting data packets/symbol-level, rather than bit/byte-level. The FEC on the link layer can be integrated on top of existing physical layer. Other codes than those applied on the physical layer are more suitable for a variety of applications and contexts at higher layers as typically erasure correction needs to be applied. In DVB, RS and Raptor codes are applied for this purpose.

Generally, it should be distinguished between link layer FEC codes itself and the framework or specific design defining how the code is applied in a specific system. The framework involves both architectural and signalling considerations. The first link layer FEC codes proposed in DVB were the RS codes as currently applied in the first generation of DVB family of standards, i.e. DVB-C, DVB-S, or DVB-H. Raptor Codes have been invented lately and introduced into DVB standards: in contrast to RS codes they provide more flexibility, large code dimensions, and lower decoding complexity. Raptor codes have therefore been adopted in latest DVB standards, e.g. within DVB-H for file delivery or DVB-IPTV. Therefore, RS codes and Raptor codes have been chosen for performance testing for the LL-FEC in the railway scenarios in this work. For both codes we use maximum likelihood decoding algorithms. Whereas the complexity of RS code decoding is know to be rather high, for Raptor codes a low-complexity maximum-likelihood decoding is for example introduced in [29], Annex E. Different frameworks are possible that allow integrating LL-FEC into DVB-S2/RCS systems.

1.4.2.1 MPE-FEC Framework

DVB has adopted a LL-FEC in DVB-H at the data link layer (MPE Layer) referred to as MPE-FEC. At the time when DVB-H was specified, only RS codes were available, and therefore, the MPE-FEC is based on RS codes. FEC operations are performed in the DVB-H link layer as illustrated in Fig. 1.6. For MPE-FEC the repair data is generated based on an Application Data Table (ADT) with size of at most 191 KBytes, such that for 200ms latency data rates of at most 7.8 Mbit/s can support, and for 10 seconds delay, only up to 156 Kbit/s are supported. The processes are fully defined and standardized in [30].

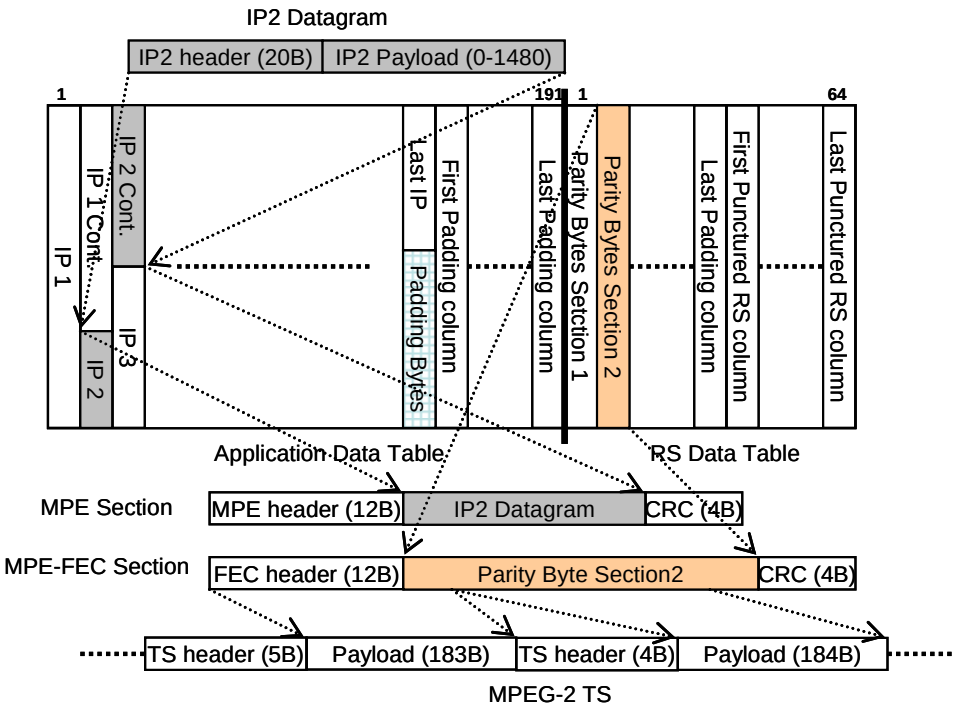

Figure 1.6: MPE-FEC Frame and the MPE encapsulation process (from DVB-H Standard [30]).

The MPE sections containing the original data packets within one ADT as well as the corresponding MPE-FEC sections containing are transmitted in a single burst. For example, for file delivery services over DVB-H, one major drawback of LL-FEC in DVB-H is that each of the unique bursts where the file is partitioned must be successfully decoded to recover the file. Note also that if one burst is completely received (i.e., all source and parity data), it cannot be used to correct errors in other bursts. In particular, when using this framework for DVB-S2 another drawback is the size of the MPE-FEC frame, which is not big enough to protect against long burst errors since the number of address signalling bits for the ADT and RS data table is only 18-bit [30]. Therefore, in order to protect longer bursts, more bits to signal the address of ADT table must be allocated along with the corresponding signalling structure to address this issue. This is addressed in the extended MPE-FEC.

1.4.2.2 Sliding encoding MPE-FEC Framework

The protection of MPE-FEC in DVB-H spans over only a single burst. In DVB-SH, the fade event durations may be much larger due to the land-mobile satellite channel. Thus Sliding Encoding is proposed for multi-burst protection [35]. The principle of MPE-FEC Sliding Encoding with RS Codes is shown in Fig. 1.7.

The principle of MPE-FEC Sliding Encoding is derived from the MPE-FEC, the difference being that MPE-FEC Sliding Encoding scheme implements interleaving among

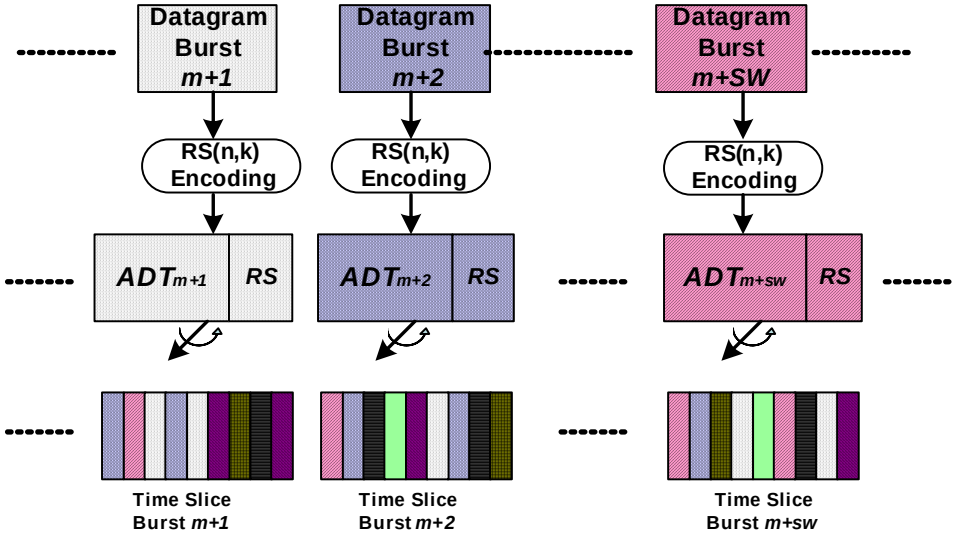

Figure 1.7: The MPE-FEC Sliding Encoding with RS Codes.

several continuous MPE-FEC Frame after the RS encoding. Thus, each transmitted time slice burst is composed of MPE sections and MPE-FEC sections coming from different MPE-FEC Frames. Thus, at the receiver, the RS decoding will be implemented after the de-interleaving when Sliding Window (SW) MPE-FEC frames are received. Hence, additional delay will be introduced in order to collect enough MPE-FEC frames to do the de-interleaving.

An MPE-FEC encoder ($RS(n,k)$) implementing sliding encoding will select the k data sections from an SW of MPE-FEC Frames and will spread the $n-k$ parity sections over the same frame window (show in the Fig. 1.7). Basically, the same effect could be obtained by first normally encoding SW frames and then interleaving sections among the encoded SW frames. Here SW represents the interleaver depth. After the de-interleaving process (before the FEC decoding), an error burst greater than one frame will be spread among the SW frames. Therefore, the continuous multiple error bursts (e.g. power archers) can be recovered with proper SW value. The drawback of MPE-FEC Sliding Encoding scheme extension to DVB-S2 in mobile environment is long delay, which degrades the performance of interactive services, as well as the fact that the SW method is not MPE-FEC compatible.

1.4.2.3 MPE-IFEC Framework

During the DVB-SH standardization activities, it was recognized that for satellite-to-handheld services, the MPE-FEC is not sufficient. Therefore, it was decided to specify a multi-burst link layer FEC framework referred to as Inter-Burst FEC (IFEC) [36]. The MPE-IFEC was introduced to support reception in situations of long erasures at the MPE section level spanning several consecutive time-slice bursts due to the characteristics of the Land-Mobile Satellite (LMS) channel. Obstacles may hinder direct satellite reception and induce losses of several successive bursts. MPE-FEC

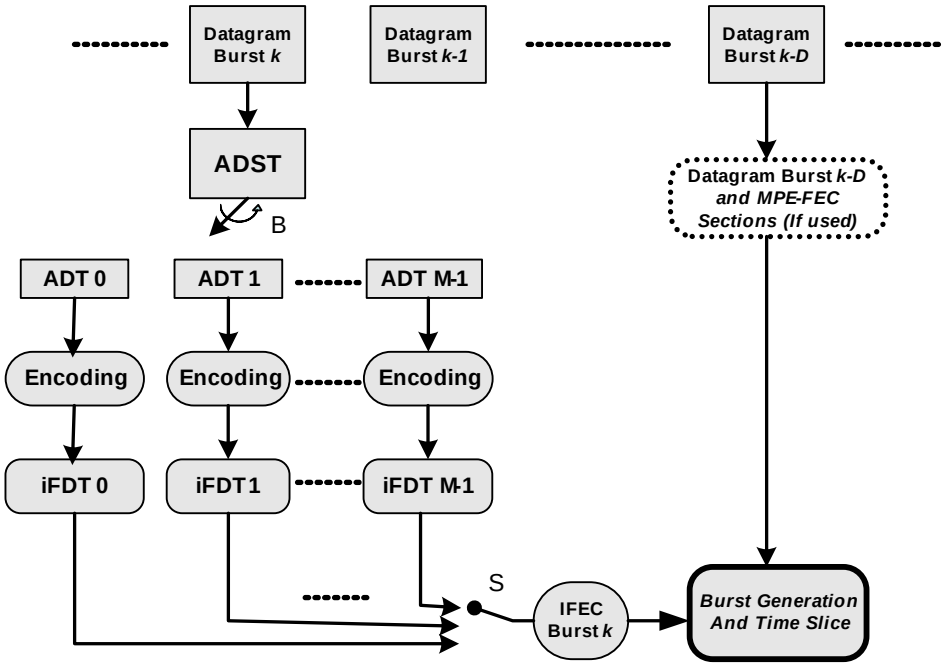

Figure 1.8: MPE-IFEC encoding process (from MPE-IFEC Standard [36]).

Sliding Encoding [35] had been proposed initially to enable multi-burst protection based on RS codes, but with the availability of more powerful and low-complexity Raptor erasure codes, the MPE-IFEC has been generalized.

Therefore, the MPE-IFEC is specified as a generic framework that presents enough flexibility for a variety of applications. For a usage in DVB-SH, its parameters are restricted to some specific values via the "framework mapping". Two of such "mappings" are presented in this thesis work. One is based on MPE-FEC RS code [30]. The other mapping is based on Raptor code as specified in the Content Delivery Protocols (CDP) specification of IP Datacast over DVB-H (DVB-IPDC) [37]. For more details on Raptor codes please refer to [38] and the specification in 3GPP [29], DVB and IETF.

The MPE-IFEC is defined by the parameters encoding period EP, which reflects the ADT size in compared to the burst size, data burst spread B, i.e. over how many bursts an ADT is spread, FEC spread S, i.e., over how many multiple of EP bursts the FEC is spread, the sending delay D, i.e. how long the sending of data is delayed at sender in units of time-slice bursts, the code rate r_{ll} as well as code being used, namely Raptor or RS codes. Note that whereas Raptor codes allow very flexible parameters, for RS codes due to restricted code parameters only EP=1 can be used.

The MPE-IFEC protection is computed over several successive datagram bursts, as opposed to MPE-FEC and sliding encoding where the computation is performed on a single datagram burst. This multi-burst protection is enabled by an enlargement of the encoding matrix to sizes greater than one burst (an iFEC matrix shown in Fig. 1.8 is filled not by one burst as in MPE-FEC but by several successive bursts), by a parallelization of the encoding mechanism (instead of using only one matrix, the

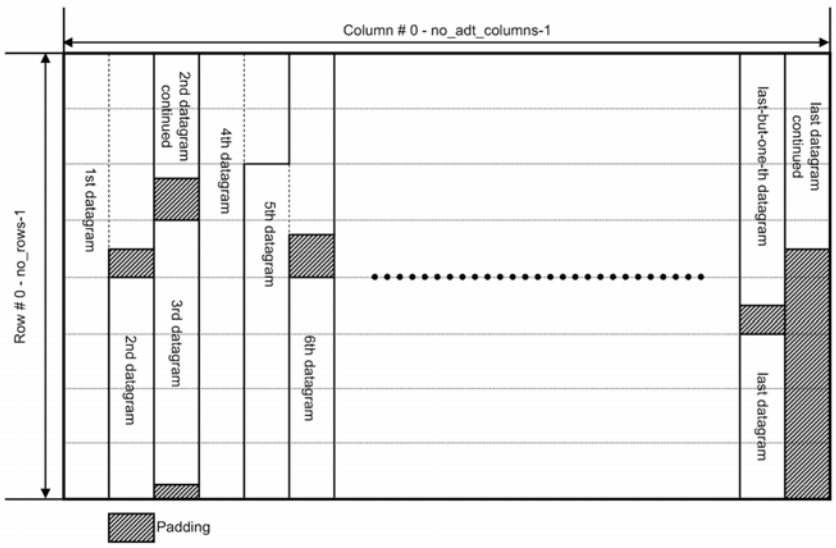

Figure 1.9: Generalized DVB-RCS+M LL-FEC mapping of datagrams to ADT (from DVB-RCS Guidelines [17]).

data are distributed to a number of parallel matrices equal to B) or by a combination of both principles. The datagrams themselves are sent in MPE sections without any modification compared to the section 9.6 of [30]. The resulting parity may also be spread over several bursts instead of one single burst in the MPE-FEC case: each burst contains parity coming from S matrices.

Note that for MPE-IFEC the mapping of MPE-IFEC sections to MPEG-2 TS packets is identical as for the MPE-FEC. At the receiver the decoding matrix (combination of ADT + iFDT) is generated and decoding each of the decoding matrix with frequency EP eliminates the unreliable columns of the decoding matrix. The ADT of the decoding matrix is then mapped back to Application Data Sub Table (ADST) to reconstruct the datagrams in each ADST.

1.4.2.4 Extended MPE-FEC Framework

Despite its flexibility, the MPE-IFEC is mainly designed for the purpose of multicasting live video over time-slice bursts. The FEC is designed for the purpose to minimize tune-in and channel switching delays over burst-based transmission, but not to minimize end-to-end delay, which is essential for bidirectional data delivery services. Therefore, a new Link layer FEC (LL-FEC) has been defined in DVB Return Channel Satellite (RCS) for mobile extension in [17] “Interaction Channel for Satellite Distribution Systems“, section 6.4.5, as a countermeasure for nLOS conditions due to obstruction, blockage, or other situations in which the line of sight is interrupted. With this LL-FEC, transmissions of multicast and unicast traffic data can be protected against channel impairments such as short interruptions and shadowing. Return Channel Satellite Terminals (RCSTs) that declare support for nLOS countermeasures shall be able to receive and process a forward link signal transmit-

ted in accordance with these provisions. This technique can also be applied to the optional continuous return link carrier transmissions defined in Section 10 of [17]. Transmissions employing LL-FEC use the same basic data structures as other MPE transmissions. However, due to the restricted signalling space of the address, datagrams may not be directly concatenated in the ADT, but some padding may be added such that a new datagram always starts at an address being multiples of some value referred to as *address granularity* (see Fig. 1.9). The address granularity is inherently configured in the setup with the specification of the frame size coding. The use of LL-FEC is defined separately for each elementary stream in the transport stream. Each elementary stream may configure different code parameters, resulting in different delays, levels of protection and FEC overheads. LL-FEC can use the Raptor code for LL-FEC frame ADT sizes up to 12 MBytes or the MPE-FEC Reed-Solomon code for any LL-FEC frame ADT sizes up to 191 KBytes. The chosen code is identified in the forward link signalling. We will analyse the performance of an extension of MPE-FEC towards larger ADT sizes for DVB-S2 railway scenarios. Such extensions require larger dimensions for the block code and are therefore most suitable provided by Raptor codes.

1.4.3 Main Results

In this section, we present a selected result of the LL-FEC performance in nLOS channel (detailed results can be found in Paper C, D, E and F). The time series of the nLOS channel dumps are generated from the Rayleigh channel. The parameter settings of the simulation refer to Paper D. The FEC coding parameters of MPE-FEC, MPE-IFEC and extended MPE-FEC can be derived based on the guidelines in Paper C and D.

Fig. 1.10 shows the performance of PER over the E_s/N_0 for different link layer schemes with v_{train} =100km/h, compared to the performance without link layer FEC. Note that for MPE-FEC with RS codes, the transmission parameters did not allow suitable parameter settings (discussed in Paper D). But here we increase the size column up to 4096 Bytes for RS codes in order to compare the performance under the same target delay assumption.

Generally, a residual packet loss rate of about 10^{-4} (or even lower) needs to be achieved for data services. The uncoded performance is completely unsatisfying. With the use of LL-FEC, the target performance can be achieved. The MPE-IFEC may solve the problem and the performance of Raptor based MPE-IFEC outperforms RS by about 1.5 dB and the extended MPE-FEC with Raptor codes outperforms MPE-FEC with RS by about 0.5dB. This is due to the fact that the extended MPE-FEC does not have any restrictions in terms of time-slice bursts. For lower speeds at around 30km/h as well as for larger delays the extended MPE-FEC shows consistently better results than the any MPE-IFEC.

It can be concluded that the codes analyzed here can be used for both purposes, to protect against LOS+PA scenarios as well as Rayleigh environments. Especially

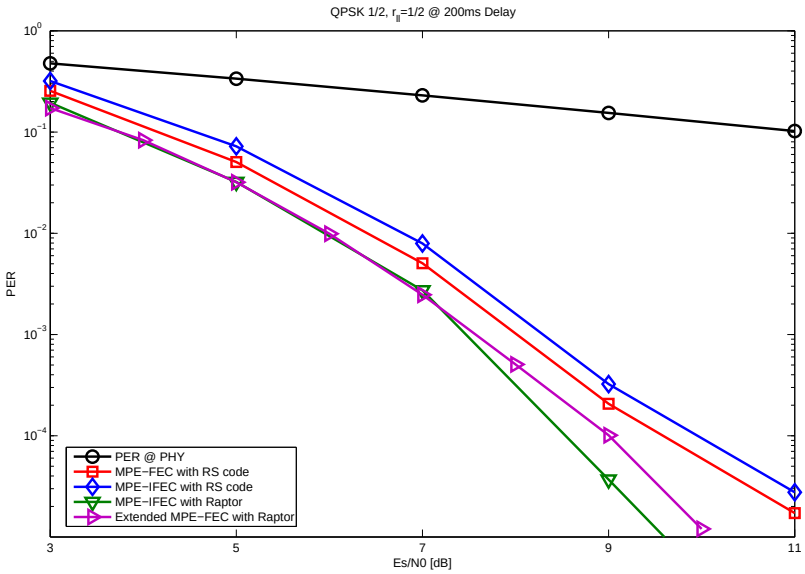

Figure 1.10: Performance of different LL-FEC schemes with $v_{\text{train}} = 100\text{km/h}$).

by the use of the extended MPE-FEC with Raptor codes as finally specified in DVB-RCS+M consistently shows superior results than with other link layer FEC for railway scenarios.

1.5 Additional Contribution in the Process of Publication

Using the system model developed in the BH project, we investigate the secure communication of multibeam satellite systems with PHY layer security technique, which can protect the broadcasted data and make it impossible to be wiretapped. A joint power control and beamforming problem has been studied by minimizing the satellite transmit power subject to the individual secrecy rate requested per user.

1.5.1 PHY Layer Security

Although there exits a significant amount of work on security in satellite networks. However, most of it only focus on the upper layer and realize the security communication through packet-level protocols. The PHY layer security approach can be an alternative approach for satellite networks applications.

The basic idea of physical layer security is to exploit the physical characteristics of the wireless channel to provide secure communications. This line of work was pioneered by Aaron Wyner, who introduced the wiretap channel and established fundamental results of creating perfectly secure communications without relying on private keys [43]. Wyner showed that when an eavesdropper's channel is a degraded version

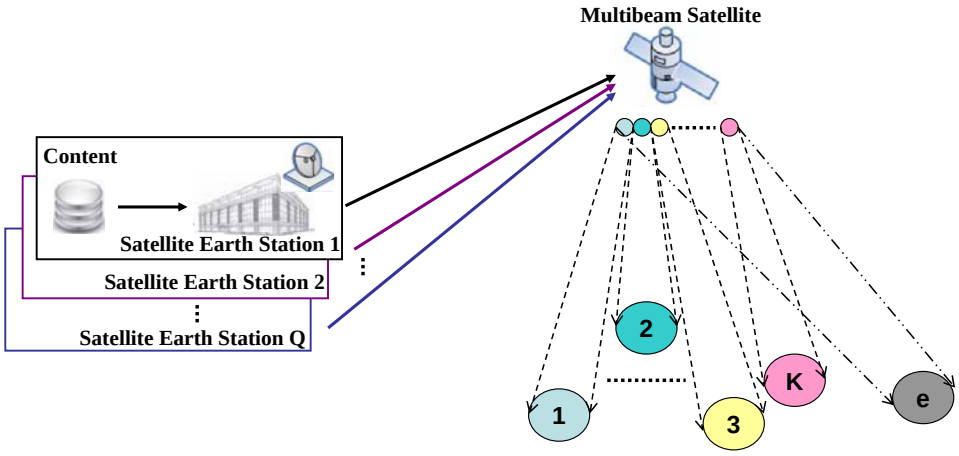

Figure 1.11: Multibeam satellite scenario.

of the main source-destination channel, the source and destination can exchange perfectly secure messages at a non-zero rate, while the eavesdropper can learn almost nothing about the messages from its observations. A rate at which information can be transmitted secretly from the source to its intended destination is termed an achievable secrecy rate, and the maximal achievable secrecy rate is named the *secrecy capacity*.

In this section, we make use of the system model developed in the BH project to investigate whether the multibeam scenario allows the use of PHY layer security, a very valuable feature that would broaden multibeam satellite applications. We prove that our models are directly applicable for the study of PHY layer security in terms of joint optimization of power control and beamforming for the BH payload. Moreover, the proposed algorithm can ensure the minimum power consumption subject to the individual secrecy rate requested per user.

1.5.2 System Model

In the multibeam satellite scenario (as shown in Fig. 1.11), without loss of generality, we focus on a single gateway and assume that the multi-antenna satellite system is equipped with M transmitting antennas. By coherently processing (e.g., beamforming), M antennas can generate K beams to serve K decentralized legitimate users at the same frequency band. One eavesdropper, denoted e, is located outside/inside the satellite coverage. Both legitimate users and eavesdropper are assumed equipped with a single antenna. Therefore, for each of the specific users, the system can be seen as a MISO wiretap channel, which is different from the work in [54; 55], since we focus on the beam-level and co-channel interference is studied. Our aim is to minimize the transmit power under the secrecy rate constraints. Next, we introduce the secrecy rate model.

There have been several precedents that investigate the MIMO wiretap channel

([49–53]). Certainly, these results also cover the special case of the MISO channel. For the case of one eavesdropper ([47; 52]), an achievable secrecy rate for a specific user (e.g., for the kth user) is given as

$$R_s^k = \max\{R_k - R_e^k\}, \tag{1.30}$$

where the achievable of the maximum was shown in [53; 54] with Gaussian inputs, R_k is the achievable rate of the link between the satellite and the kth user, R_e^k is the achievable rate of the link between the satellite and the eavesdropper. Note that the secrecy rate in (1.30) is achievable unless the maximum value is negative, in which case, the achieved secrecy rate is zero [42]. Note that we only focus on the practical scenario in which the secrecy rate is non-zero.

In fact, Gaussian signalling only maximizes the terms of R_k and R_e^k, but does not necessarily maximize the difference. In [54; 55], the authors discuss how to maximize the difference by adaptively adjust the power allocation. Conversely, we restrict ourselves to the difference between R_k and R_e^k. Our aim is to characterize the best power allocation scheme over multibeam satellite systems subject to the individual secrecy rate constraints.

By assuming Gaussian inputs, the difference between R_k and R_e^k can be written as

$$\begin{aligned} R_k - R_e^k &= \log\left(1+\Gamma_k\right) - \log\left(1+\Gamma_e^k\right) \\ &= \log\frac{1+\Gamma_k}{1+\Gamma_e^k} \\ &= \log\left(1+\frac{\Gamma_k-\Gamma_e^k}{1+\Gamma_e^k}\right) \\ &= \log\left(1+\Gamma_s^k\right), \end{aligned} \tag{1.31}$$

where Γ_k and Γ_e^k are the SINR of the destination and eavesdropper for the kth user, respectively. Γ_s^k is defined as the secrecy SINR, which is the updated SINR after introducing the eavesdropping, and it is given by

$$\Gamma_s^k \triangleq \frac{\Gamma_k - \Gamma_e^k}{1+\Gamma_e^k}. \tag{1.32}$$

In the next sections we will discuss how to minimize the overall power consumption under the individual secrecy SINR constraint per user. From (1.31), we can see that the optimization problem with the secrecy SINR constraint is the same with the secrecy rate constraint. If we consider that the secrecy rate required by the kth user is $\hat{R}_s^k$, the secrecy SINR requirement can be derived as $\gamma_k = 2^{\hat{R}_s^k} - 1$. Therefore, in the following section, we focus on the power control problem with the secrecy SINR constraint per user.

1.5.3 Power Control Problem with Fixed Beamforming

In this section, we assume that the beamforming matrix $\widetilde{\mathbf{W}} = [\widetilde{\mathbf{w}}_1, \widetilde{\mathbf{w}}_2, \ldots, \widetilde{\mathbf{w}}_K]$ is optimized, with $\|\widetilde{\mathbf{w}}_k\| = 1$ for $k = 1, 2, \ldots, K$. We focus on the secrecy SINR constraints per user after introducing the eavesdropping, and a more general solution based on [56] is proposed to solve the power control problem.

By doing the multibeam satellite power control, the overall transmit power of each beam is optimized, so that the received secrecy rate of each user has $R_s^k \geq \hat{R}_s^k$ for $k = 1, 2, \ldots, K$, i.e., the secrecy SINR has $\Gamma_s^k \geq \gamma_k$ for $k = 1, 2, \ldots, K$, (where γ_k is the predefined targeted SINR threshold in order to realize the required secrecy rate), while the overall transmitted power used by all beams is minimized. Hence, the power control problem can be defined as

$$\begin{aligned} &\min_{\mathbf{p}} \ \sum_k P_k, \\ &\text{subject to } \Gamma_s^k(\widetilde{\mathbf{W}}, \mathbf{p}) \geq \gamma_k, \ \ k = 1, 2, \ldots, K. \end{aligned} \tag{1.33}$$

The minimum power is achieved when the SINR is equal to the target value, i.e., $\Gamma_s^k = \gamma_k$ for $k = 1, 2, \ldots, K$. The problem in (1.33) is a Nondeterministic Polynomial (NP) hard problem [44]. Therefore, we will present an iteration algorithm to achieve the optimized solution. Many iteration algorithms (e.g., in [56–59]) have been proposed in order to decrease the complexity. However, the algorithm that we propose is different from [56–59], since the eavesdropping problem is introduced.

For each beam, we first construct the interference function $I_k(\mathbf{p})$, which is the power-update equation in the iteration algorithm. Then the power allocated to each beam can be iteratively updated until converge with the individual secrecy SINR constraints. The algorithm steps at the $(n+1)$th iteration are as follows:

Iteration Algorithm:

$$P_k^{n+1} = \frac{\gamma_k}{\mu_k^n - (1+\gamma_k)\mu_e^{k,n}} \triangleq I_k(\mathbf{p}^n), \tag{1.34}$$

where $\mathbf{p}^n = [P_1^n, P_2^n, \ldots, P_K^n]$ is the power vector for all the K beams at the nth iteration step, μ_k^n and $\mu_e^{k,n}$ are defined as

$$\mu_k^n = \frac{\Gamma_k^n}{P_k^n} = \frac{\Theta_{kk}}{\sigma^2 + \sum_{j \neq k} P_j^n \Theta_{kj}}, \tag{1.35}$$

and

$$\mu_e^{k,n} = \frac{\Gamma_e^{k,n}}{P_k^n} = \frac{\Theta_{ek}}{\sigma^2 + \sum_{j \neq k} P_j^n \Theta_{ej}}, \tag{1.36}$$

respectively, where Γ_k^n and $\Gamma_e^{k,n}$ are the updated SINR of the legitimate user k and eavesdropper at the nth iteration step,

$$\Theta_{kk} = \widetilde{\mathbf{w}}_k^H \mathbf{R}_k \widetilde{\mathbf{w}}_k, \text{ and } \Theta_{kj} = \widetilde{\mathbf{w}}_j^H \mathbf{R}_k \widetilde{\mathbf{w}}_j,$$

and

$$\Theta_e^k = \widetilde{\mathbf{w}}_k^H \mathbf{R}_e \widetilde{\mathbf{w}}_k, \text{ and } \Theta_e^j = \widetilde{\mathbf{w}}_j^H \mathbf{R}_e \widetilde{\mathbf{w}}_j.$$

In [56], the author has proved that if the interference function is *standard*, the algorithm will achieve the optimal solution if there exists at least one feasible solution. The interference function $I_k(\mathbf{p})$ is *standard* if for all $\mathbf{p} \geq 0$ the following three properties are satisfied [56]:

- Positivity: $I_k(\mathbf{p}) \geq 0$.
- Monotonicity: If $\mathbf{p} \geq \mathbf{p}'$, then $I_k(\mathbf{p}) \geq I_k(\mathbf{p}')$, or $I_k(\mathbf{p}) \leq I_k(\mathbf{p}')$. [1]
- Scalability: For all $\rho > 1$, $\rho I_k(\mathbf{p}) \geq I_k(\rho \mathbf{p})$.

For the proposed interference function (1.34), we obtain the following theorem:

Theorem 1 *The interference function $I_k(\mathbf{p}^n)$ in (*1.34*) is a* standard *function under the following three conditions:*

- *Condition 1:* $b \geq c$.
- *Condition 2:* $b\tilde{\mathbf{h}}_k \geq c\tilde{\mathbf{h}}_e$ *and* $b\tilde{\mathbf{h}}_e \geq c\tilde{\mathbf{h}}_k$, *for* $\forall k$.
- *Condition 3:* $b[\tilde{\mathbf{h}}_k]_j \tilde{\mathbf{h}}_e^T \tilde{\mathbf{h}}_e \geq c[\tilde{\mathbf{h}}_e]_j \tilde{\mathbf{h}}_k^T \tilde{\mathbf{h}}_k$, *for* $\forall k, j \neq k$.

Where $b = \Theta_{kk}$, $c = (1+\gamma_k)\Theta_e^j$, *and* $\tilde{\mathbf{h}}_k$ *denotes the channel gain vector* $(1 \times K)$ *of the interference contribution to the desired user, defined as*

$$[\tilde{\mathbf{h}}_k]_j = \begin{cases} \Theta_{kj}, & \text{if } j \neq k, \\ 0, & \text{otherwise.} \end{cases}$$

$\tilde{\mathbf{h}}_e$ *denotes the channel gain vector* $(1 \times K)$ *of the interference contribution to the eavesdropper, defined as*

$$[\tilde{\mathbf{h}}_e]_j = \begin{cases} \Theta_e^j, & \text{if } j \neq k, \\ 0, & \text{otherwise.} \end{cases}$$

[1] The inequality between two vectors, e.g., $\mathbf{a} \geq \mathbf{b}$, means that $a_i \geq b_i$ for $i = 1, \ldots, K$, where $\mathbf{a} = [a_1, a_2, \ldots, a_K]$, $\mathbf{b} = [b_1, b_2, \ldots, b_K]$.

In a practical scenario: the overall channel gain of the link "satellite - desired user" is larger than that of the link "satellite - co-channel users", i.e., $\Theta_{kk} \gg \Theta_{kj}$ for $\forall j \neq k$, the overall channel gain of the link "satellite - desired user" is larger than that of the link "satellite - eavesdropper", i.e., $\Theta_{kk} \gg \Theta_e^j$ for $\forall j$. The magnitudes of Θ_{kk}, Θ_{kj} and Θ_e^j are roughly equal. Therefore, with low secrecy SINR request γ_k, the above three conditions are indeed available. In the case of very high SINR requirement, we can introduce optimization of the satellite antenna beamformer in order to decrease or eliminate the co-channel interference and the eavesdropper interference, and thereby the above conditions can still be satisfied.

1.5.4 Joint Power Control and Beamforming

The level of co-channel interference and wiretapped signal for each user depends both on the gain between interfering transmitters and user, as well as on the level of transmitter powers, i.e., the beamforming weight vector may vary for different power allocation policy. Hence, beamforming and power control should be considered jointly. In this section, we will discuss how to optimize the beamforming vector and power allocation jointly.

In the joint power control and beamforming problem, the objective is to find the optimized weight vector and power allocations such that the secrecy SINR threshold is achieved by all the users, while minimize the transmission power. Therefore, the joint power control and beamforming problem can be formulated as

$$\begin{aligned} &\min_{\mathbf{W},\mathbf{p}} \ \sum_k P_k, \\ &\text{subject to } \Gamma_s^k(\mathbf{W},\mathbf{p}) \geq \gamma_k, \ \ k = 1,2,\ldots,K. \end{aligned} \tag{1.37}$$

The problem in (1.37) can be solved in two steps. In order to minimize the overall power consumption, we can first obtain the beamforming weight vector of each beam by joint ZFBF and eavesdropper signal nulling, in which all the co-channel signal and eavesdropper signal are completely eliminated. In the second step, the optimal power allocation solution can be easily obtained by solving $\Gamma_s^k = \gamma_k$ for $k = 1,2,\ldots,K$ under the beamforming weight vector obtained in the first step.

In the Zero-Forcing Beamforming, ZFBF (e.g., in [60–62]), weights are selected so as the co-channel interference is canceled (zero-interference condition), i.e., for desired user k, $\mathbf{h}_k\mathbf{w}_j = 0$ for $j \neq k$. Similarly, the eavesdropping interference can also be completely nulled by beamforming (e.g., in [47; 63; 64]), i.e., for desired user k, $\mathbf{h}_e\mathbf{w}_k = 0$ for $k = 1,2,\ldots,K$.

Let us introduce an additional constraint to completely eliminate the co-channel interference and null the signals at eavesdropper. Note that the condition $M > K$ is needed here. In case of $M \leq K$, we cannot completely eliminate the interference from the co-channel users and nulling the signals at the eavesdropper; appropriate system design for the case of $M \leq K$ would be an interesting future research direction. By

ZFBF, the co-channel interference to the desired user becomes zero; By nulling the signal at eavesdropper, the Shannon capacity to the eavesdropper becomes to zero too. Hence, the secrecy SINR can be reformulated as

$$\Gamma_s^k(\mathbf{W}, \mathbf{p}) = \frac{P_k \mathbf{w}_k^H \mathbf{R}_k \mathbf{w}_k}{\sigma^2} = \frac{P_k |\mathbf{h}_k \mathbf{w}_k|^2}{\sigma^2}, \tag{1.38}$$

Therefore, in order to minimize the transmitted power P_k for $k = 1, 2, \ldots, K$ under the secrecy SINR constraint γ_k, we have to maximize the gain between the satellite antenna and the kth user, i.e., $\max |\mathbf{h}_k \mathbf{w}_k|^2$, for $k = 1, 2, \ldots, K$. It means that we have to solve K maximize problems jointly. The kth optimization problem can be formulated as

$$\begin{aligned} &\arg\max_{\mathbf{w}_k} \ |\mathbf{h}_k \mathbf{w}_k|^2, \\ &\text{subject to} \begin{cases} \mathbf{h}_k \mathbf{w}_j = 0, \ \text{for } j \neq k, \\ \mathbf{h}_e \mathbf{w}_k = 0, \\ \mathbf{w}_k^H \mathbf{w}_k = 1. \end{cases} \end{aligned} \tag{1.39}$$

Note that the overall optimization problem is composed of K optimization problems as expressed in (1.39) (for $k = 1, 2, \ldots, K$). We can re-formulate the K *jointly* maximize problems as K *independent* maximize problem, e.g., the problem to solve the kth beamforming weight vector can be formulated as

$$\begin{aligned} &\arg\max_{\mathbf{w}_k} \ |\mathbf{h}_k \mathbf{w}_k|^2, \\ &\text{subject to} \begin{cases} \mathbf{H}_e^k \mathbf{w}_k = \mathbf{0}_{K \times 1}, \\ \mathbf{w}_k^H \mathbf{w}_k = 1. \end{cases} \end{aligned} \tag{1.40}$$

where $\mathbf{H}_e^k$ is defined as

$$[\mathbf{H}_e^k]_{ij} = \begin{cases} [\mathbf{H}]_{ij}, & \text{if } i \neq k, \\ [\mathbf{h}_e]_j, & \text{if } i = k. \end{cases} \tag{1.41}$$

The solution of the beamforming weight problem in (1.40) is given by [60] as

$$\mathbf{w}_k = \frac{(\mathbf{I}_M - \mathbf{F}_e)\, \mathbf{h}_k^H}{\| (\mathbf{I}_M - \mathbf{F}_e)\, \mathbf{h}_k^H \|}, \ \text{for } k = 1, 2, \ldots, K. \tag{1.42}$$

where

$$\mathbf{F}_e = (\mathbf{H}_e^k)^\dagger \mathbf{H}_e^k,$$

where $(\mathbf{H}_e^k)^\dagger = (\mathbf{H}_e^k)^H \left(\mathbf{H}_e^k (\mathbf{H}_e^k)^H \right)^{-1}$.

As we discussed in Section 1.5.3, the minimum power is achieved when the SINR

is equal to the target value, i.e., $\Gamma_s^k = \gamma_k$ for $k = 1, 2, \ldots, K$. Therefore, we can obtain the solution from (1.38) as

$$P_k = \frac{\gamma_k \sigma^2}{|\mathbf{h}_k \mathbf{w}_k|^2}, \text{ for } k = 1, 2, \ldots, K. \tag{1.43}$$

where $\mathbf{w}_k$ is the optimized beamforming weight vector for the kth beam.

1.5.5 Impact on CSI of Eavesdropper

The channels between the satellite antenna elements and the desired users can be estimated accurately, since they are legitimate. However, in practice, the channels between the satellite antenna elements and the eavesdropper can only be estimated with some certain errors. In this section, we will investigate the system design with unknown and imperfect CSI of eavesdropper.

1.5.5.1 Unknown Eavesdropper CSI

In this case, we assume that the entries of $\mathbf{h}_e$ are random variables, and $\widehat{\mathbf{R}}_e = \mathbb{E}\left\{\hat{\mathbf{h}}_e^H \hat{\mathbf{h}}_e\right\}$ is known a priori. Therefore, in order to minimize the power consumption subject to given target secrecy SINR, the best option is to cancel the co-channel interference, i.e., ZFBF. Therefore, we can formulate the kth beamforming weight vector optimization problem as

$$\begin{aligned} &\arg\max_{\mathbf{w}_k} \quad |\mathbf{h}_k \mathbf{w}_k|^2, \\ &\text{subject to} \begin{cases} \mathbf{h}_k \mathbf{w}_j = 0, \text{ for } j \neq k, \\ \mathbf{w}_k^H \mathbf{w}_k = 1. \end{cases} \end{aligned} \tag{1.44}$$

This problem is similar to the problem formulated in (1.39), thus, we can obtain the solution as

$$\mathbf{w}_k = \frac{(\mathbf{I}_M - \mathbf{F})\, \mathbf{h}_k^H}{\| (\mathbf{I}_M - \mathbf{F})\, \mathbf{h}_k^H \|}, \text{ for } k = 1, 2, \ldots, K. \tag{1.45}$$

where

$$\mathbf{F} = (\mathbf{H}_k)^\dagger \mathbf{H}_k,$$

where $(\mathbf{H}_k)^\dagger = (\mathbf{H}_k)^H \left(\mathbf{H}_k (\mathbf{H}_k)^H\right)^{-1}$, where $\mathbf{H}_k$ is the co-channel contribution matrix $((K-1) \times M)$ be defined as

$$\mathbf{H}_k = [\mathbf{h}_1^T, \ldots, \mathbf{h}_{k-1}^T, \mathbf{h}_{k+1}^T, \ldots, \mathbf{h}_K^T]^T. \tag{1.46}$$

where $\mathbf{h}_i$ $(i \neq k)$ is the ith row of the channel matrix $\mathbf{H}$.

After obtain the beamforming weight vector for each beam, the optimal power allocation can also be obtained by the iteration algorithm that we propose in (1.34), i.e.,

$$P_k^{n+1} = \frac{\gamma_k}{\mu_k^n - (1+\gamma_k)\mu_e^{k,n}}, \tag{1.47}$$

where μ_k^n and $\mu_e^{k,n}$ are re-defined in *Theorem* 2.

Theorem 2 *The interference function in (*1.47*) is a* standard *function under the condition: $b \geq c$, where $b = \mathbf{w}_k^H \mathbf{R}_k \mathbf{w}_k$, $c = (1+\gamma_k)\mathbf{w}_k^H \widehat{\mathbf{R}}_e \mathbf{w}_k$. μ_k and μ_e^k are defined as*

$$\mu_k^n = \frac{\mathbf{w}_k^H \mathbf{R}_k \mathbf{w}_k}{\sigma^2}, \tag{1.48}$$

and

$$\mu_e^{k,n} = \frac{\mathbf{w}_k^H \widehat{\mathbf{R}}_e \mathbf{w}_k}{\sum_{j \neq k} P_j^n \mathbf{w}_j^H \widehat{\mathbf{R}}_e \mathbf{w}_j + \sigma^2}. \tag{1.49}$$

1.5.5.2 Imperfect Eavesdropper CSI

The perfect channel gain between the satellite antenna elements and eavesdropper is modeled as

$$\mathbf{h}_e = \hat{\mathbf{h}}_e + \mathbf{\Delta}_e, \tag{1.50}$$

where $\hat{\mathbf{h}}_e$ is the imperfect eavesdropper channel estimation, and $\mathbf{\Delta}_e$ corresponds to the channel estimation error. We assume that the entries of $\mathbf{\Delta}_e$ are random variables, and $\mathbf{R}_\Delta \triangleq \mathbb{E}\left\{\mathbf{\Delta}_e^H \mathbf{\Delta}_e\right\}$ is known a priori. Thus,

$$\mathbf{R}_e = \mathbb{E}\left\{\mathbf{h}_e^H \mathbf{h}_e\right\} = \widehat{\mathbf{R}}_e + \mathbf{R}_\Delta, \tag{1.51}$$

where $\widehat{\mathbf{R}}_e = \hat{\mathbf{h}}_e^H \hat{\mathbf{h}}_e$.

By joint ZFBF and nulling eavesdropper's signal, we can obtain the beamforming weight vector, e.g., for kth beam, as expressed in function (1.42). But $\mathbf{H}_e^k$ is replaced with $\widehat{\mathbf{H}}_e^k$, which is defined as

$$[\widehat{\mathbf{H}}_e^k]_{ij} = \begin{cases} [\mathbf{H}]_{ij}, & \text{if } i \neq k, \\ [\hat{\mathbf{h}}_e]_j, & \text{if } i = k. \end{cases} \tag{1.52}$$

Then we can solve the power control problem with the iteration algorithm in func-

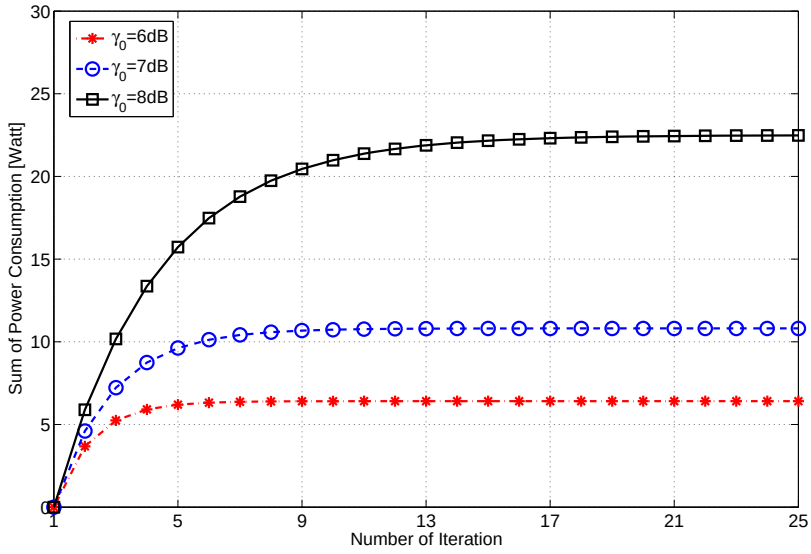

Figure 1.12: Total transmitted power versus the iteration number.

tion (1.47), but μ_e^k is re-defined as

$$\mu_e^{k,n} = \frac{\mathbf{w}_k^H \mathbf{R}_\Delta \mathbf{w}_k}{\sum_{j \neq k} P_j^n \mathbf{w}_j^H \mathbf{R}_\Delta \mathbf{w}_j + \sigma^2}. \tag{1.53}$$

As expressed in *Theorem* 2, the interference function in (1.47) is *standard* with given μ_k and μ_e^k expressed in (1.48) and (1.53), respectively.

1.5.6 Main Results

In order to evaluate the performance of the proposed system design, we perform Monte carlo experiments consisting of 1000 independent trials to obtain the average results. We define the satellite system payload parameters the same as in [12]. For simplicity, we assume that the secrecy SINR request for all the beams is the same, i.e., $\gamma_k = \gamma_0$ for $k = 1, 2, \ldots, K$. The channel for each link is modeled as a product of an attenuation factor and a random phase. For example, the channel between the legitimate user k and the antenna element m is defined as $h_{km} = \alpha_k e^{j\varsigma}$ for $k = 1, 2, \ldots, K$ and $m = 1, 2, \ldots, M$, where ς is a random phase uniformly distributed within $[0, 2\pi)$. The channel between the antenna elements and the eavesdropper is modeled in the same way as $h_{em} = \alpha_e e^{j\varsigma}$ for $m = 1, 2, \ldots, M$. The noise power σ^2 is assumed as -10 dBm.

We first fix the number of antenna elements as $M = 8$, the number of beams as $K = 5$, the channel attenuation factor $\alpha_k = \alpha_e = 0.8$ for $k = 1, 2, \ldots, K$ to investigate the convergence of the iteration algorithm. In Fig. 1.12, the curves show the total power

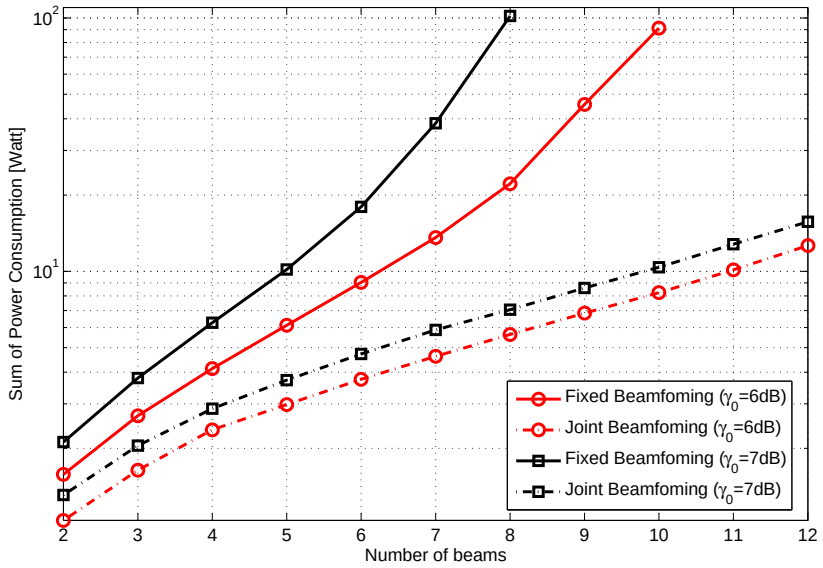

Figure 1.13: Total transmitted power versus the number of beams.

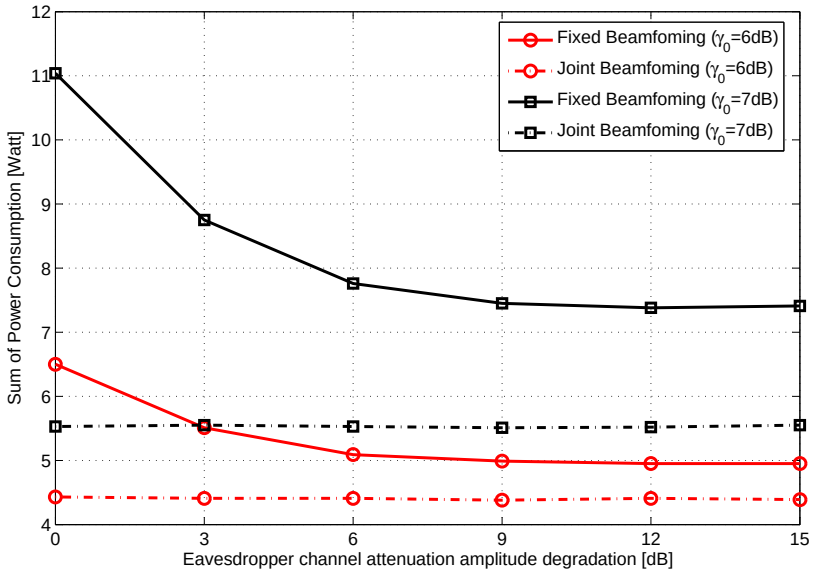

Figure 1.14: Total power consumption versus the channel attenuation amplitude to the eavesdropper.

consumption at each iteration for different target secrecy SINR. The results show that the algorithm is always convergent. We can also notice from the figure that the black curve with higher target SINR ($\gamma_0 = 8$ dB) converges slower than that of the red curve with lower target SINR ($\gamma_0 = 6$ dB).

In Fig. 1.13, we evaluate the transmitted power according to different number of

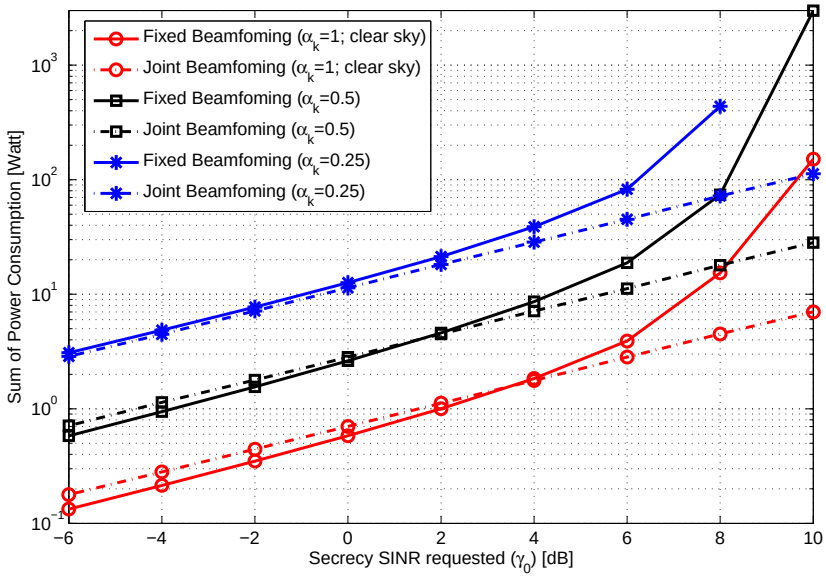

Figure 1.15: Total transmitted power versus the target secrecy SINR.

beams on the satellite. We fix the number of antenna elements as $M = 15$ and increase the number of beams K from 2 to 12. As expected, the power consumption increases as the number of beams and secrecy request increase for both schemes. Especially, the transmitted power increases very quickly in the case of large number of beams. In Fig. 1.14, we simulate the power allocation according to the channel attenuation amplitude of the eavesdropper, the horizontal axis in the figure indicates the channel attenuation amplitude degradation in dB, e.g., 0 dB means the clear sky scenario. From the figure we can see that the joint beamforming scheme is almost independent of the eavesdropper's channel condition, it means that the satellite can adapt the channel degradation by optimizing the beamformer design. For the case of the fixed beamforming scheme, the transmitted power will decrease as the eavesdropper's channel condition deteriorates.

The performance of transmitted power as a function of the secrecy SINR request is shown in Fig. 1.15. For simplicity, we assume that the channel attenuation amplitude for all the users is the same, and the channel attenuation amplitude of the eavesdropper is assumed as $\alpha_e = 1$, clear sky. All other parameters are the same as previous figures. For both fixed beamforming and joint beamforming schemes, the curves in Fig. 1.15 show that, as the channel condition deteriorates, more power will be consumed in order to compensate the signal attenuation. We can also conclude from this figure that the joint beamforming scheme is more favorable than fixed beamforming scheme in the case of a higher secrecy SINR request, since the power allocation is more sensitive to the higher secrecy SINR request (e.g., when $\gamma_0 > 6$ dB).

The performance of a single legitimate user (e.g., User 1) is evaluated in Fig. 1.16. We assume that the secrecy SINR request for all the users is $\gamma_0 = 8$, 6, and 4 dB, the channel attenuation amplitude of User 1 (α_1) is changed from 1 (i.e., clear sky) to 0.2,

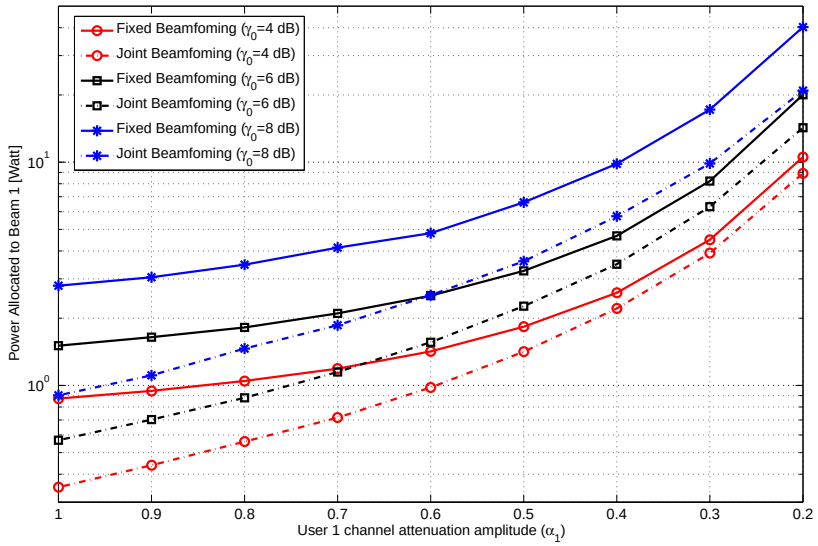

Figure 1.16: Transmitted power for a specific beam (e.g., beam 1) versus the channel condition.

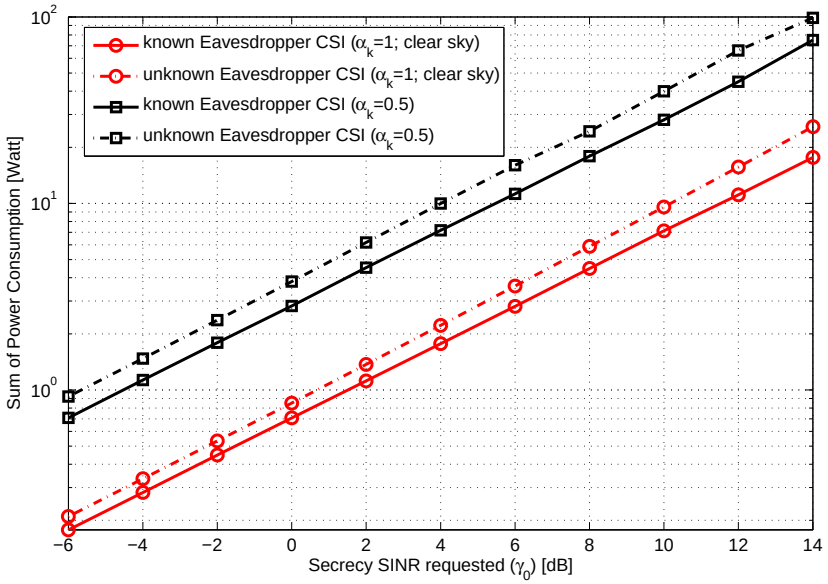

Figure 1.17: Power allocation with or without the available the eavesdropper CSI.

and all other parameters are the same in Fig. 1.12. As expected, the power allocated to Beam 1 will increase as channel condition of User 1 deteriorates, especially in the case of a worse channel condition. In Fig. 1.17, we compare the power allocation with and without the available of the eavesdropper's CSI. The value of the parameters is the same in Fig. 1.15. Under the given total power limitation (e.g., 100 Watts), the achieved secrecy SINR per user with known eavesdropper's CSI outperforms about

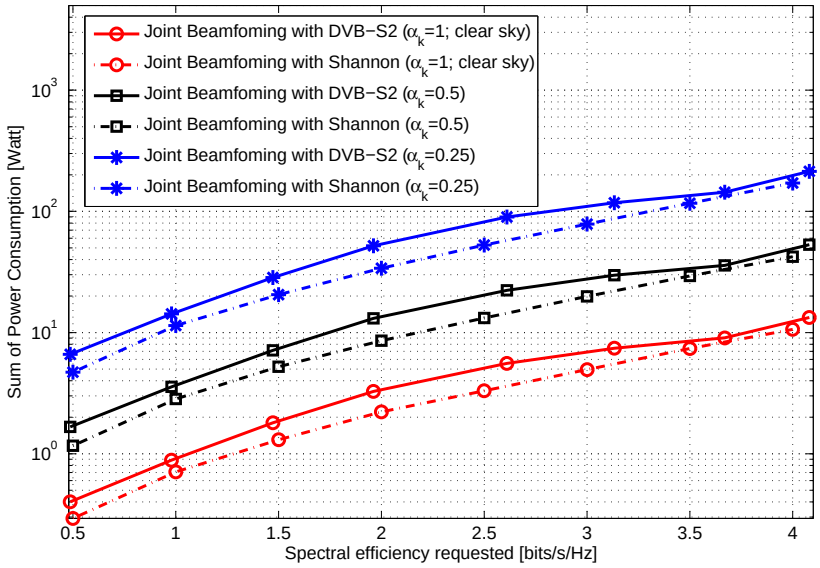

Figure 1.18: Total transmitted power comparison for the DVB-S2 air-interface and Gaussian inputs.

2 dB than the case of without CSI available. In addition, this gap increases as the available total power increases.

In Fig. 1.18, we compare the results with Gaussian inputs and with the current air-interface in DVB-S2. The value of the parameters is assumed the same in Fig. 1.15. For the case of the joint beamforming scheme, the sum of power consumption increases as the spectral efficiency requirement increases for both Gaussian inputs and DVB-S2 cases. The power consumption of the DVB-S2 case is always larger than the Gaussian inputs case, and the gap between them tends to decrease as the spectral efficiency increases.

1.6 Brief Summary of Published Papers

This dissertation consists of SIX published papers numbered with letters (A-F). In this section, we present a brief summary of these papers.

1.6.1 Paper A

J. Lei and M. A. Vázquez-Castro, "Joint Power and Carrier Allocation for the Multi-beam Satellite Downlink with Individual SINR Constraints," in *Proc. IEEE Int. Conf. on Commun.*, Cape Town, South Africa, PP. 1 - 5, May 2010.

In Paper A, we propose a novel system design for the downlink of multi-beam satel-

lite based on jointly optimizing power and carrier allocation to best match individual SINR constraints. Although the optimization problem has been addressed in terrestrial networks e.g., in [5; 6], it is new in satellite communications, which requires a different channel model and system formulation. A mathematical formulation is proposed for our problem based on SINR balancing theory, but introducing one more degree of freedom, since we do not only optimize the power vector but also the carrier allocation. An iterative algorithm is proposed to solve this problem. In the algorithm, each iteration solves a Rayleigh quotation over the beams subspace.

The current state-of-the-art PHY layer technology: DVB-S2 and Shannon are implemented in order to obtain the gap between them. The results show significant improvements in terms of power gain, spectral efficiency and traffic matching ratio compared to the conventional system. For a DVB-S2 and $K = 200$ (number of users) case, we can achieve up to 3 dB power gain, 0.7 bit/s/Hz spectral efficiency gain by our jointly resource optimization allocation, and we can also improve 10% traffic matching ratio with this approach. We also prove the primary goal of the study, that the joint optimization of power and carrier allocation can match much better than the conventional design in the realistic case of asymmetric traffic request (SINR constraints).

1.6.2 Paper B

J. Lei and M. A. Vázquez-Castro, "Duality Study over Multibeam Satellite System in Frequency and Time Domain," in *Proc. IEEE Int. Conf. on Commun.*, Cape Town, South Africa, PP. 1 - 5, May 2010.

In this paper, two new technologies, Non-Orthogonal Frequency Reuse (NOFR) and BH, over multi-beam satellite system are studied. The two technologies operate in different domains (frequency and time/space), and we want to know which domain shows best performance. We prove the theoretical duality between them. Moreover, we also develop a general methodology to conclude the technological constraints due to realistic implementation, obtain the main factors that prevent the two technologies and formulate the technological gap between NOFR and BH systems. The results show that the technological gap is only related to the OBO of NOFR and BH, and the gap is almost linear with Δ_{OBO}. Further, we solve the frequency/time-slot resource optimization problem with different cost functions. Fairness cost function is more favorable for low traffic request cells while n-order cost function distribute more resource to high traffic request beam. The study of the resource optimization shows that the BH system performs only slightly better than NOFR.

1.6.3 Paper C

J. Lei, M. A. Vázquez Castro, and T. Stockhammer, "Link Layer FEC and Cross-layer Architecture for DVB-S2 Transmission with QoS in Railway Scenarios," *IEEE Trans.*

Veh. Technol., vol. 58, no. 8, pp. 4265 - 4276, Oct. 2009.

In Paper C, we introduce the application of FEC at the link layer LL-FEC for the purpose of adapting DVB-S2 for mobile receptions. In addition, we analyse the performance that can be achieved when applying these schemes with particular focus on two typical railway scenarios: Line-of-Sight together with the effect of railway power archers (LOS+PA) and non-Line of Sight (nLOS). Both theoretical and simulation analysis reveal that LL-FEC can overcome typical fading effects in the railway scenario by selecting appropriate FEC codes and by optimizing the coding parameters. Two typical FEC codes, Reed-Solomon and Raptor, are applied and analyzed within different encapsulation schemes, e.g., MPE-FEC and MPE-IFEC. We show that MPE-IFEC and extended MPE-FEC with Raptor codes -as finally specified in DVB-RCS+M- consistently show superior results than other link layer FEC for railway scenarios. We also indicate signaling update in order to allow achievable performance. As for practical implementation, we propose two possible novel cross-layer architectures for unicast DVB-S2 in order to provide QoS. The architectures allow the migration from traditional packet encapsulation based on Moving Picture Experts Group 2-Transport Streams (MPEG2-TS) to new schemes such as the GSE [31].

1.6.4 Paper D

J. Lei, M. A. Vázquez Castro, T. Stockhammer, and F. Vieira, "Link layer FEC for Quality-of-Service Provision for Mobile Internet Services over DVB-S2," *Int. Journal of Satellite Commun. and Netw.*, vol. 28, no. 3-4, pp. 183 - 207, 2010.

This paper presents the performance that can be achieved when applying FEC at the link layer for DVB-S2-based transmission to attain reliable reception in mobile environments. Our scenario of interest is the interactive mobile scenario with burst erasure channel. We analyze the performance and compatibility of the different LL-FEC schemes already available in the DVB family of standards: MPE-FEC, sliding encoding MPE-FEC, MPE-IFEC, and extend MPE-IFEC. We compare their performance when adopting RS or Raptor FEC Codes. Both theoretical and simulation analysis reveal that LL-FEC can overcome the fade in the mobile scenario by selecting appropriate FEC codes. The solution finally adopted by the DVB-RCS+M standard is also discussed.

1.6.5 Paper E

J. Lei, G. Seco Granados, and M. A. Vázquez Castro, "MPE/ULE-FEC vs GSE-FEC Efficiency Comparison of IP Datagram Transmission over DVB-S2," in *Proc. 25th AIAA Int. Comm. Satellite Systems Conf.*, Seoul, Korea, 10-13 April, 2007.

The encapsulation of DVB-S2, unlike DVB-S, allows for several input stream formats. In addition to MPEG Transport Streams (TS), Generic Streams (GS) are encompassed by the standard. The DVB-S2 standard introduces generic stream transport method not only for providing digital TV services, but also as technology for building IP networks and dedicated data streaming.

In this paper, the efficiency of MPE, ULE and GSE is compared for typical IP packet sizes. Moreover, we also analyze the aggregated efficiency when applying Packet-Level Forward Error Correction (PL-FEC) at MPE, ULE and GSE. The efficiency of DiffServ is also analyzed using GSE-FEC over DVB-S2 network. The intention of this paper is to compare the transport efficiency of MPE-FEC, ULE-FEC and GSE-FEC for IP transmission and to present the characteristics of GSE-FEC used in IP traffic and DiffServ classes over DVB-S2 networks.

A layered efficiency calculation model is presented in order to simplify the computation. The results show that the total efficiency of DVB-S2 network has a low relation with ModCods and can be approximated as a function only with the distribution of IP packet size and puncturing efficiency. The theoretical analysis and comparison of the simulation results revealed that GSE-FEC is more efficient than MPE-FEC and ULE-FEC for DVB-S2 networks. The efficiency of GSE-FEC can be also improved by puncturing RS columns. The results show that the efficiency is improved about 5% with puncturing 16 RS columns and 25% with puncturing 64 RS columns. But the number of punctured RS columns should be designed precisely because it will deteriorate the performance of the receive systems.

1.6.6 Paper F

J. Lei, T. Stockhammer, M. A. Vázquez Castro, and F. Vieira, “Application of Link Layer FEC to DVB-S2 for Railway Scenarios,” in *Proc. 10th Int. Workshop on Signal Process. for Space Commun.*, Rhodes Island, Greece, 6 - 8 Oct. 2008.

The application of LL-FEC based on RS and Raptor codes is discussed and analyzed in Paper E. Theoretical analysis and simulation revealed that LL-FEC can overcome the fade in the railway scenarios by adjusting the FEC Codes parameters and the extended MPE-FEC with Raptor Codes is the best scheme to counteract the railway fade.

In particular, we have shown in this paper that MPE-FEC completely removes the effect of PAs for high speeds only, due to the fact that the target protection delay is limited in the current version of the standard. On the other hand, we have shown that MPE-FEC with sliding encoding can also completely remove the effect of PAs while in this case there is no limitation on the target delay that can be protected. Moreover we have obtained the optimal windows for the selected system parameters (10 for a target delay of 200ms for QPSK 1/2).

1.7 Main Contributions of the Dissertation

The main contributions of this dissertation can be summarized as follows:

a. We study the resource allocation optimization in multi-domain (frequency, time, space and power) for multi-beam satellite systems. First, we develop novel matricial-based analytical multibeam system-level models that directly allows testing different payloads technology and system assumptions. Second, we prove that the system performance can be increased by dynamically adapting the resource allocation to the characteristics of the system, e.g., traffic requested by the terminal.

b. Theoretical studies and simulations prove that the proposed novel transmission schemes perform better than the current system design in terms of power gain, spectral efficiency, etc.. In addition, BH system turns out to show a less complex design and superior performance than the flexible system.

c. Our analytical models allows us to also prove the theoretical duality between the flexible and BH systems, which work in frequency domain and time domain, respectively. Moreover, we develop a general methodology to include technological constraints due to realistic implementation, obtain the main factors that prevent the two technologies dual of each other in practice, and formulate the technological gap between them.

d. We extend the work to mobile scenarios and prove that LL-FEC is applicable for mobile satellite systems (e.g., railway) to compensate the fade due to the mobility by optimizing the FEC codes (Reed-Solomon and Raptor codes). The results show that Multiple Protocol Encapsulation Inter-burst FEC (MPE-IFEC) and extended MPE-FEC with Raptor codes - as finally specified in DVB Return Channel via Satellite for Mobile Scenario (DVB-RCS+M) - consistently perform better than other LL-FEC schemes for mobile scenarios.

e. We point out that how to change the signalling of current version of standards (e.g., DVB-S2/RCS+M) in order to allow achievable performance in the mobile scenarios. The proposal has been finally adopted by the DVB-RCS+M standard.

f. We finally make use of our developed system models to investigate whether the multibeam scenario allows the use of PHY layer security, a very valuable feature that would broaden multibeam satellite applications. We prove that our models are directly applicable for the study of PHY layer security in terms of joint optimization of power control and beamforming for the BH payload. Moreover, the proposed algorithm can ensure the minimum power consumption subject to the individual secrecy rate requested per user.

1.8 Journal and Conference Contributions during Ph.D. Studies

During the Ph.D. studies, the author has contributed to the following journals and conference publications:

List of journal publications during Ph.D.:

- J. Lei, Z. Han, M. A. Vázquez-Castro, and A. Hjørungnes, "Joint Power Control and Beamforming for Multibeam Satellite Systems with Individual Secrecy Rate Constraints," *Submitted to IEEE Trans. on Inf. Forensics and Security*, 2010.
- J. Lei and M. A. Vázquez Castro, "Multibeam Satellite Frequency/Time Duality Study and Capacity Optimization," *Submitted to Journal of Commun. and Netw.*, 2010.
- J. Lei, M. A. Vázquez Castro, T. Stockhammer, and F. Vieira, "Link Layer FEC for Quality-of-Service Provision for Mobile Internet Services over DVB-S2," *Int. Journal of Satellite Commun. and Netw.*, vol. 28, no. 3-4, pp. 183 - 207, 2010.
- J. Lei, M. A. Vázquez Castro, and T. Stockhammer, "Link Layer FEC and Cross-layer Architecture for DVB-S2 Transmission with QoS in Railway Scenarios," *IEEE Trans. Veh. Technol.*, vol. 58, no. 8, Oct. 2009.

List of conference publications during Ph.D.:

- J. Lei, Z. Han, M. A. Vázquez-Castro, and A. Hjørungnes, "Multibeam Satellite Power Control with Physical Layer Security," *Submitted to IEEE Int. Conf. on Commun.*, Kyoto, Japan, June 2011.
- X. Alberti, J. M. Cebrian, A. Del Bianco, Z. Katona, J. Lei, M. A. Vázquez-Castro, A. Zanus, L. Gilbert, N. Alagha, "System Capacity Optimization in Time and Frequency for Multibeam Multi-media Satellite Systems," in *Proc. 5th Advanced Satellite Multimedia Systems Conf. and the 11th Signal Process. for Space Commun. Workshop*, Cagliari, Italy, Sep. 2010.
- J. Lei and M. A. Vázquez-Castro, "Joint Power and Carrier Allocation for the Multibeam Satellite Downlink with Individual SINR Constraints," in *Proc. IEEE Int. Conf. on Commun.*, Cape Town, South Africa, pp. 1 - 5, May 2010.
- J. Lei and M. A. Vázquez-Castro, "Duality Study over Multibeam Satellite System in Frequency and Time Domain," in *Proc. IEEE Int. Conf. on Commun.*, Cape Town, South Africa, pp. 1 - 5, May 2010.

- D. Pradas, P. Barsocchi, J. Lei, F. Potortì, and M. A. Vázquez-Castro, "Satellite PHY-layer Selector Design for Video Applications in Tropical Areas," in *Proc. Int. Workshop on Satellite and Space Commun.*, Siena-Tuscany, Italy, pp. 407 - 411, April 2009.

- J. E. Barcelo, M. A. Vázquez Castro, J. Lei, and A. Hjørungnes, "Distributed Power and Carrier Allocation in Multibeam Satellite Uplink with individual SINR constraints," in *Proc. IEEE Global Commun. Conf.*, Honolulu, USA, pp. 1 - 6, Nov. 2009.

- D. Pradas, P. Barsocchi, J. Lei, F. Potortì, and M. A. Vázquez-Castro, "Cost-Efficient Design of Hybrid Network for Video Transmission in Tropical Areas," in *Proc. IEEE Veh. Technol. Conf. - Spring*, Barcelona, Spain, Apr. 2009.

- J. Lei, T. Stockhammer, M. A. Vázquez Castro, and F. Vieira, "Application of Link Layer FEC to DVB-S2 for Railway Scenarios," in *Proc. 10th Int. Workshop on Signal Process. for Space Commun.*, Rhodes Island, Greece, 6 - 8 Oct. 2008.

- F. Vieira, M. A. Vázquez Castro, and J. Lei, "Datacast Transmission Architecture for DVB-S2 Systems in Railway Scenarios," in *Proc. 10th Int. Workshop on Signal Process. for Space Commun.*, Rhodes Island, Greece, 6 - 8 Oct. 2008.

- A. Mayer, F. Vieira, J. Lei, B. Collini-Nocker, and M. A. Vázquez Castro, "Analytical and Experimental IP Encapsulation Efficiency Comparison of GSE, MPE, and ULE over DVB-S2," in *Proc. Third Int. Workshop on Satellite and Space Commun.*, Paris-Lodron University of Salzburg, Austria, 13-14 Sep, 2007. (**This paper won the Best Paper Award**)

- J. Lei, G. Seco Granados, and M. A. Vázquez Castro, "MPE/ULE-FEC vs GSE-FEC Efficiency Comparison of IP Datagram Transmission over DVB-S2," in *Proc. 25th AIAA Int. Commun. Satellite Systems Conf.*, Seoul, Korea, 10-13 April, 2007.

List of Intellectual Property during Ph.D.:

- F. Vieira, M. A. Vázquez Castro, and Jiang Lei,"DVB-RCS+M normative text", Intellectual Property request no. B-0906-08, Barcelona, 20th February 2008.

Bibliography

[1] N. Letzepis and A. J. Grant, “Capacity of the Multiple Spot Beam Satellite Channel With Rician Fading,” *IEEE Trans. on Inf. Theory*, vol. 54, no. 11, pp. 5210 - 5222, Nov. 2008.

[2] Yingjie Li, Martin J. Feuerstein, and Douglas O. Reudink, “Performance Evaluation of a Cellular Base Station Multibeam Antenna,” *IEEE Trans. Veh. Technol.*, vol. 46, no. 1, pp. 1 - 9, Aug. 1997.

[3] A. Paraboni, M. Buti, C. Capsoni, D. Ferraro, C. Riva, A. Martellucci, and P. Gabellini, “Meteorology-Driven Optimum Control of a Multibeam Antenna in Satellite Telecommunications,” *IEEE Trans. on Antennas and Propagation*, vol. 57, no. 2, pp. 508 - 519, Feb. 2009.

[4] Andrea Goldsmith, *Wireless Communications*, Cambridge University Press, 2005.

[5] M. Schubert and H. Boche, “QoS-Based Resource Allocation and Transceiver Optimization,” *Foundations and Trends in Commun. and Inform. Theory*, vol. 2, no. 6, pp. 383 - 529, 2005.

[6] M. Schubert and H. Boche, “Solution of the Multiuser Fownlink Beamforming Problem with Individual sinr Constraints,” *IEEE Trans. Veh. Technol.*, vol. 53, no. 1, pp. 18 - 28, Jan. 2004.

[7] M. J. Neely, E. Modiano and C. E. Rohrs, “Power Allocation and Routing in Multibeam Satellites with Time-Varying Channels,” *IEEE/ACM Trans. Netw.*, vol. 11, no. 1, pp. 138 - 152, Feb. 2003.

[8] J. P. Choi, V. W. S. Chan, “Optimum Multi-Beam Satellite Downlink Power Allocation based on Traffic Demands,” in *Proc. IEEE Globecom Commun. Conf.*, pp. 2875 - 2881, 2002.

[9] J. P. Choi and V. W. S. Chan, “Optimum Power and Beam Allocation Based on Traffic Demands and Channel Conditions over Satellite Downlinks,” *IEEE Trans. on Wireless Commun.*, vol. 4, no. 6, pp. 2983 - 2993, Nov. 2005.

[10] J. E. Barcelo, M. A. Vázquez-Castro, J. Lei, and A. Hjøungnes, “Distributed Power and Carrier Allocation in Multibeam Satellite Uplink with individual SINR constraints,” in Proc. *IEEE Global Commun. Conf.*, Honolulu, USA, pp. 1 - 6, Nov. 2009.

[11] X. Alberti, J.M. Cebrian, A. Del Bianco, Z. Katona, J. Lei, M. A. Vázquez-Castro, A. Zanus, L. Gilbert, and N. Alagha, "System Capacity Optimization in Time and Frequency for Multibeam Multi-media Satellite Systems," in *Proc. 5th Advanced Satellite Multimedia Systems Conf. and the 11th Signal Process. for Space Commun. Workshop*, Cagliari, Italy, Sep. 2010.

[12] J. Lei and M. A. Vázquez-Castro, "Joint Power and Carrier Allocation for the Multibeam Satellite Downlink with Individual SINR Constraints," accepted by *IEEE Int. Conf. on Commun.*, Cape Town, South Africa, pp. 1 - 5, May 2010.

[13] J. Lei, M. A. Vázquez-Castro, "Frequency and Time-Space Duality Study for Multibeam Satellite Communications," accepted by *IEEE Int. Conf. on Commun.*, Cape Town, South Africa, pp. 1 - 5, May 2010.

[14] Bello, P., "Time-Frequency Duality," *IEEE Trans. on Inf. Theory*, vol. 10, no. 1, pp. 18 - 33, Jan. 1964.

[15] ETSI EN 300 421 v1.1.2, Digital Video Broadcasting (DVB): Framing structure, channel coding and modulation for 11/12 GHz satellite services, Aug. 1997.

[16] ETSI EN 302 307 v1.1.1, Digital Video Broadcasting (DVB): Second generation framing structure, channel coding and modulation system for Broadcasting, Interactive Services, News Gathering and other broadband satellite applications, Jun. 2004.

[17] ETSI EN 301 790 V1.5.1, Digital Video Broadcasting (DVB): Interaction channel for satellite distribution systems, Jan. 2009.

[18] E. Lutz, M. Werner, and A. Jahn, *Satellite Systems for Personal and Broadband Communications*. Springer, New York, NY, USA, 2000.

[19] A. D. Panagopoulos, P. D. M. Arapoglou, and P. G. Cottis, "Satellite Communications at Ku, Ka, and V Bands: Propagation Impairments and Mitigation Techniques," *IEEE Commun. Surveys and Tutorials*, vol. 6, no.3, pp. 2 - 14, 2004.

[20] E. Kubista, F. P. Fontan, M. A. V. Castro, S. Buonomo, B. R. Arbesser-Rastburg, and J. P. V. Polares Baptista, "Ka Band Propagation Measurements and Statistics for Land Mobile Satellite Applications," *IEEE Trans. on Veh. Technol.*, vol. 49, no. 3, pp. 973 - 983, 2000.

[21] A. Benarroch and L.Mercader, "Signal Statistics obtained form a LMSS Experiment in Europe with the MARECS Satellite," *IEEE Trans. on Commun.*, vol. 42, no. 2-4, pp. 1264 - 1269, 1994.

[22] S. Scalise, R.Mura, and V.Mignone, "Air Interfaces for Satellite based Digital TV Broadcasting in the Railway Environment," *IEEE Trans. on Broadcast*, vol. 52, no. 2, pp. 158 - 166, 2006.

[23] S. Cioni, A. Vanelli-Coralli, C.P. Niebla, S. Scalise, G.S. Granados and M. A. Vázquez Castro, "Antenna Diversity and GSE-based Packet Level FEC for DVB-S2

Systems in Railway Scenarios", in *Proc. 25th AIAA Int. Commun. Satellite Systems Conf.*, Seoul, South Korea, Apr. 2007.

[24] F.P. Fontan, M. A. Vázquez Castro, C.E. Cabado, J. P. Garcia, E. Kubista, "Statistical Modeling of the LMS Channel", *IEEE Trans. on Veh. Technol.*, vol. 50, no. 6, pp. 1549 - 1567, Nov. 2001.

[25] Pérez-Fontán, F. Gonzalez, J. P., Ferreiro, M. J. S., M. A. Vázquez Castro, Buonomo, S., and Baptista J. P., "Complex Envelope Threestate Markov Model based Simulator for the Narrow-band LMS Channel", *Int. Journal on Satellite Commun.*, vol. 15, no. 1, pp. 1 - 15, Dec. 1998.

[26] ETSI EN 302 304 v1.1.1, Digital Video Broadcasting (DVB): Transmission System for Handheld Terminals (DVB-H), Nov. 2004.

[27] ETSI TS 102 585 v1.1.1, Digital Video Broadcasting (DVB): System Specifications for Satellite services to Handheld devices (SH) below 3 GHz, July, 2007.

[28] ETSI TS 102 034 v1.3.1, Digital Video Broadcasting (DVB): Transport of MPEG 2 Transport Stream (TS) Based DVB Services over IP Based Networks, Mar. 2005.

[29] 3GPP TS26.346, "Multimedia Broadcast/Multicast Service (MBMS): Protocols and Codecs (release 8)," Sep. 2008.

[30] ETSI EN 301 192 v1.4.1, Digital Video Broadcasting (DVB): DVB Specification for Data Broadcasting, Nov. 2004.

[31] ETSI TS 102 606 v1.1.1, Digital Video Broadcasting (DVB): Generic Stream Encapsulation (GSE) Protocol, Oct.2007.

[32] Weidong Yang and Guanghan Xu, "Optimal Downlink Power Assignment for Smart Antenna Systems," in *Proc. IEEE Int. Conf. on Acoustics, Speech and Signal Process.*, vol. 6, pp. 3337 - 3340, May 1998.

[33] R. Rinaldo, X. Maufroid and R. Casaleiz Garcia, "Non-Uniform Bandwidth and Power Allocation in Multi-Beam Broadband Satellite Systems," European Space Agency ESTEC, Keplerlaan1, 2200 AG Noordwijk, The Netherlands, Aug. 2, 2005.

[34] M. A. Vázquez-Castro and G. Seco, "Cross-layer Packet Scheduler Design of a Multibeam Broadband Satellite System with Adaptive Coding and Modulation", *IEEE Wireless Trans.*, vol. 6, no. 1, pp. 248-258, Jan. 2007.

[35] P. Marco, F. Rosario, C. Giovanni, and E. V. C. Alessandro, "On The Application of MPE-FEC to Mobile DVB-S2: Performance Evaluation in Deep Fading Conditions," in *Proc. Int. Workshop on Satellite and Space Commun.*, Salzburg, Austria, pp. 223 - 227, Sep. 2007.

[36] DVB Bluebook DVB A131, MPE IFEC, November 2008.

[37] ETSI TS 102 472 v1.2.1, IP Datacast over DVB-H: Content Delivery Protocols (CDP), Jun. 2006.

[38] A. Shokrollahi, "Raptor Codes," *IEEE Trans. on Inf. Theory.*, vol. 52, no. 6, pp. 2551 - 2567, Jun. 2006.

[39] F. Vieira, M. A. Váquez Castro, J. Lei, "Datacast Transmission Architecture for DVB-S2 Systems in Railway Scenarios," in *Proc. 10th Int. Workshop on Signal Process. for Space Commun.*, Rhode Island, Greece, 6-8 Oct. 2008.

[40] J. Lei, G. S. Granados, and M. A. Váquez Castro, "MPE/ULE-FEC vs GSE-FEC Efficiency Comparison of IP Datagram Transmission over DVB-S2," in *Proc. 25th AIAA Int. Commun. Satellite Systems Conf.*, Seoul, South Korea, Apr. 2007.

[41] A. Mayer, F. Vieira, J. Lei, B. Collini-Nocker, M. A. Váquez Castro, "Analytical and Experimental IP Encapsulation Efficiency Comparison of GSE, MPE, and ULE over DVB-S2", in *Proc. Int. Workshop on Satellite and Space Commun.*, Salzburg, Austria, pp. 114-118, Sep. 2007.

[42] I. Csiszár and J. Körner, "Broadcast Channels with Confidential Messages," *IEEE Trans. Inf. Theory*, vol. 24, no. 3, pp. 339 - 348, May 1978.

[43] A. D. Wyner, "The Wire-tap Channel," *Bell Syst. Tech. Journal*, vol. 54, no. 8, pp. 1355 - 1387, Oct. 1975.

[44] M. R. Garey and D. S. Johnson, *Computers and Intractability: A Guide to the Theory of NP-Completeness*. W. H. Freeman, 1979.

[45] L. Liang, S. Iyengar, H. Cruickshank, and Z. Sun, "Security for FLUTE over Satellite Networks," in *Proc. Int. Conf. on Commun. and Mobile Computing*, Kunming, China, pp. 485 - 491, Jan. 2009.

[46] M. S. B. Mahmoud, N. Larrieu, and A. Pirovano, "An Aeronautical Data Link Security Overview," in *Proc. 28th IEEE/AIAA Digital Avionics Systems Conf., 2009*, Orlando, USA, pp. 4.A.4-1 - 4.A.4-14, Oct. 2009.

[47] L. Dong, Z. Han, A. Petropulu, and H. V. Poor, "Improving Wireless Physical Layer Security via Cooperating Relays," *IEEE Trans. Signal Process.*, vol. 58, no. 3, pp. 1875 - 1888, Mar. 2010.

[48] Y. Liang, H. V. Poor, and S. Shamai (Shitz), "Secure Communication over Fading Channels," *IEEE Trans. Inf. Theory*, vol. 54, no. 6, pp. 2470 - 2492, Jun. 2008.

[49] E. Ekrem and S. Ulukus, "Gaussian MIMO Multi-Receiver Wiretap Channel," in *Proc. IEEE Global Commun. Conf.*, Honolulu, USA, pp. 1 - 6, Nov. 2009.

[50] S. Shafiee, N. Liu, and S. Ulukus, "Secrecy Capacity of the 2-2-1 Gaussian MIMO Wire-tap Channel," in *Proc. 3rd Int. Symp. on Commun., Control and Signal Process.*, Malta, pp. 207 - 212, Mar. 2008.

[51] Z. Li, W. Trappe, and R. Yates, "Secret Communication via Multi-antenna Transmission," in *Proc. 41st Conf. Inf. Sciences Systems*, Baltimore, MD, pp. 905 - 910, Mar. 2007.

[52] F. Oggier and B. Hassibi, "The Secrecy Capacity of the MIMO Wiretap Channel," in *Proc. IEEE Int. Symp. Inf. Theory*, Toronto, Ontario, Canada, pp. 524 - 528, Jul. 2008.

[53] T. Liu and S. Shamai, "A Note on the Secrecy Capacity of the Multiple-Antenna Wiretap Channel," *IEEE Trans. Inf. Theory*, vol. 55, no. 6, pp. 2547 - 2553 , Jun. 2009.

[54] S. Shafiee and S. Ulukus, "Achievable Rates in Gaussian MISO Channels with Secrecy Constraints," in *Proc. IEEE Int. Symp. Inf. Theory*, Nice, France, pp. 2466 - 2470, Jun. 2007.

[55] A. Khisti and G. W. Wornell, "Secure Transmission with Multiple Antennas I: The MISOME Wiretap Channel," *IEEE Trans. Inf. Theory*, vol. 56, no. 7, pp. 3088 - 3104, Jul. 2010.

[56] R. Yates, "A Framework for Uplink Power Control in Cellular Radio Systems," *IEEE J. Sel. Areas Commun.*, vol. 13, no. 7, pp. 1341 - 1348, Sept. 1995.

[57] Z. Han and K. J. R. Liu, "Joint Link Quality and Power Management with Fairness Constraint over Wireless Networks," *IEEE Trans. Veh. Technol.*, vol. 53, no. 4, pp. 1138 - 1148, Jul. 2004.

[58] F. Rashid-Farrokhi, L. Tassiulas, and K. J. R. Liu, "Joint Optimal Power Control and Beamforming in Wireless Network using Antenna Arrays," *IEEE Trans. Commun.*, vol. 46, pp. 1313 - 1323, Oct. 1998.

[59] F. Rashid-Farrokhi, K. J. R. Liu, and L. Tassiulas, "Transmit Beamforming and Power Control for Cellular Wireless Systems," *IEEE J. Select. Areas Commun.*, vol. 16, no. 8, pp. 1437 - 1449, Oct. 1998.

[60] Q. Spencer, A. Swindlehurst, and M. Haardt, "Zero-Forcing Methods for Downlink Spatial Multiplexing in Multiuser MIMO Channels," *IEEE Trans. Signal Process.*, vol. 52, no. 2, pp. 461 - 471, Feb. 2004.

[61] T. Yoo and A. Goldsmith, "On the Optimality of Multi-Antenna Broadcast Scheduling using Zero Forcing Beam Forming," *IEEE J. Sel. Areas Commun.*, vol. 24, no. 3, pp. 528 - 541, Mar. 2006.

[62] O. Somekh, O. Simeone, Y. Bar-Ness, A. M. Haimovich, and S. Shamai (Shitz), "Cooperative Multicell Zero-Forcing Beamforming in Cellular Downlink Channels," *IEEE Trans. Inf. Theory*, vol. 55, no. 7, pp. 3206 - 3219, Jul. 2009.

[63] L. Dong, Z. Han, A. Petropulu, and H. V. Poor, "Secure Wireless Communications via Cooperation," in *Proc. 46th Annu. Allerton Conf. Commun., Control, Computing*, Monticello, IL, Sep. - Oct. 2008.

[64] L. Dong, Z. Han, A. Petropulu, and H. V. Poor, "Amplify-and-Forward based Cooperation for Secure Wireless Communications," in *Proc. IEEE Int. Conf. Acoust., Speech, Signal Process.*, Taipei, Taiwan, Apr. 2009.

[65] G. Maral and M. Bousquet, *Satellite Communications Systems: Systems, Techniques and Technology (5th Edition)*, New York: Wiley, 2009.

Part II

Included Papers

Paper A

Joint Power and Carrier Allocation for the Multi-beam Satellite Downlink with Individual SINR Constraints

J. Lei, M. A. Vázquez Castro

IEEE International Conference on Communication (ICC 2010), Cape Town, South Africa, May 2010.

Abstract

A novel multibeam satellite system design is proposed in this paper based on jointly optimizing power and carrier allocation in order to best match the asymmetric traffic requests. This design introduces higher and asymmetric interference levels throughout the coverage. However, both power and bandwidth will be used more efficiently. Even though the problem of power and bandwidth allocation has been addressed in terrestrial wireless communications, it is new in satellite systems and since architecture and channel are different, available results and algorithms are not applicable to satellite payload systems. In this paper we formulate the resource allocation problem as max-min SINR balancing based on the recently introduced axiomatic-based interference model, but in addition, we also optimize the carrier allocation when performing the SINR balancing problem. An analytical solution for the optimal carrier allocation is proposed and we iteratively find the optimal power allocation for each beam. The Shannon (upper bound) and current state-of-the art PHY layer technology: DVB-S2 are proposed to be implemented in order to obtain the gap between them. Simulation results show significant improvements in terms of power gain, spectral efficiency and traffic matching ratio comparing with conventional system, which is designed based on uniform bandwidth and power allocation.

A.1 Introduction

The efficient management of satellite resources, e.g. power and bandwidth, is crucial for economic competitiveness. In modern satellite networks, each satellite uses multiple beams, each of which illuminates a cell on the earth to serve a coverage area. Multibeam antenna technology is used because it can increase the total system capacity significantly, which has been studied in [1]. However, each beam will compete with others for resources such as power and bandwidth to achieve satisfactory communication. This is due to the fact that the traffic demand among the beams of the coverage is potentially highly asymmetrical. Therefore, the satellite requires a certain degree of flexibility in allocating the power and bandwidth resources to achieve a good match between offered and requested traffic.

Most of current satellite payloads are designed to allocate a fixed bandwidth segment to each beam according to regular frequency re-use scheme and constant equal power. This approach leads to a waste of resources in beams which the traffic demand is relatively low. On the contrary, it does not satisfy traffic demand in the "hot" beams, where the traffic request is high. There are serval precedents of resources allocation in multibeam satellite systems. In [2], a power allocation policy is suggested to stabilize the system based on the amount of unfinished work in the queue and the channel state, and a routing decision is made for the maximum total throughput. In [3], the authors make an effort to design a tradeoff strategy between different objectives and system optimization. The power and beam allocation over satellite downlinks are optimized based on traffic distribution and channel condition, as well as achieving reasonable fairness among beams. However, the co-channel interference does not taking into account and only a convex optimization problem is solved. In [4], an axiomatic-based interference model for SINR balancing problem is proposed with individual target SINR per user, but it focused on the terrestrial wireless communications. The authors in [5] discussed power and carrier allocation problem, but it only focused on the uplink. Even though the problem of power and carrier allocation has been addressed in terrestrial wireless communications (e.g. [4], [6]), the problem we tackle in this paper is different. We do not only balance the power allocation for each beam in order to mach the SINR request, but also optimize the strategy of carrier allocation in order to minimize the co-channel interference.

This paper is organized as follows: In Section A.2, the problem statement is presented. In Section A.3, we model the multibeam downlink system to obtain a mathematical expression of SINR. In Section A.4, the joint power and carrier allocation problem is formulated and solved. And the simulation is presented in Section A.5. In Section A.6, we conclude the paper.

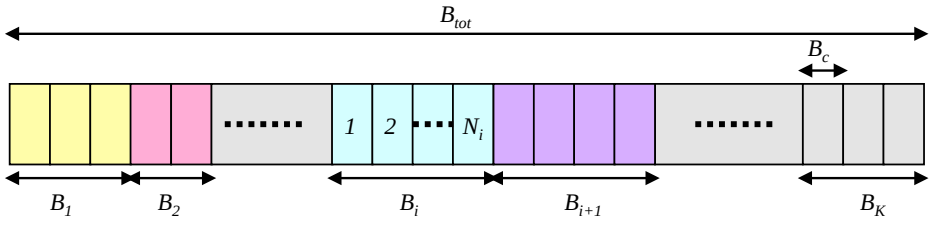

Fig. A.1: Bandwidth segmentation.

A.2 Problem Statement

In multibeam systems, the beamforming antenna generating K beams over the coverage area. The total available downlink bandwidth, B_{tot}, is divided in Q frequency carriers providing carrier granularity of $B_c = B_{\text{tot}}/Q$ as shown in Fig.A.1. Each beam can be allocated a variable number of carriers depending on the traffic request. Let N_k be the number of carriers assigned to beam k, the allocated bandwidth will be $B_k = B_c N_k$ (Herein $0 \leq N_k \leq Q$, therefore $0 \leq B_k \leq B_{\text{tot}}$). The carriers assigned to each beam do not need to be contiguous. The total satellite available power, P_{tot}, will be shared by all beams.

The problem tackled in this paper is to find the optimal allocation of power and carrier for all the beams in order to meet the per-beam SINR requests. The novelty of this paper is that we do not only optimize the power and bandwidth allocation (e.g. SINR balancing problem discussed in [4]), but also optimize the structure of spectral mask matrix $\mathbf{W}$, which indicates which carriers allocated per-beam in order to minimize co-channel interference. Although the power and carrier optimization problem has been addressed in terrestrial networks, it is new in satellite communications, which requires a different channel model and system formulation.

A.3 System Model

Let the symbols transmitted to beam k be defined as $\mathbf{x}_k = [x_{k1}, x_{k2}, \cdots, x_{kQ}]^T \in \mathbb{C}^{Q\times 1}$, which is modelled with a spectral mask vector $\mathbf{w}_k \in \mathbb{R}^{Q\times 1}$. Let the spectral mask matrix $\mathbf{W} \in \mathbb{R}^{Q\times K}$ be defined as $\mathbf{W} = [\mathbf{w}_1, \mathbf{w}_2, \cdots, \mathbf{w}_K]$, and the kth column vector $\mathbf{w}_k \in \mathbb{R}^{Q\times 1}$ be defined as $\mathbf{w}_k = [w_{k1}, w_{k2}, \cdots, w_{kQ}]^T$, which is the spectral mask vector for beam k and indicates which TDM carriers and how much power allocated to beam k.

Let the channel attenuation amplitude matrix $\mathbf{A} \in \mathbb{C}^{K\times K}$ be defined as $\mathbf{A} = \text{diag}\{\alpha_1, \alpha_2, \cdots, \alpha_K\}$, where α_k denotes the channel attenuation factor over the des-

tination user beam k. Let the antenna gain matrix $\mathbf{G} \in \mathbb{C}^{K\times K}$ be defined as

$$\mathbf{G} = \begin{bmatrix} g_{11} & g_{12} & \cdots & g_{1K} \\ g_{21} & g_{22} & \cdots & g_{2K} \\ \vdots & \vdots & \ddots & \vdots \\ g_{K1} & g_{K2} & \cdots & g_{KK} \end{bmatrix}. \tag{A.1}$$

Let $\mathbf{H} = \mathbf{AG}$, $\mathbf{W}_k = \operatorname{diag}\{\mathbf{w}_k\}$, and assuming instantaneous analysis, the received signal by all the Q carriers for kth user beam, $\mathbf{y}_k \in \mathbb{C}^{Q\times 1}$, can be expressed as desired signal and interference as

$$\mathbf{y}_k = h_{kk}\tilde{\mathbf{x}}_k + \sum_{\substack{i=1 \\ i\neq k}}^{K} h_{ki}\tilde{\mathbf{x}}_i + \mathbf{n}_k, \tag{A.2}$$

where $\tilde{\mathbf{x}}_k$ is the spectral masked symbols for beam k, defined as $\tilde{\mathbf{x}}_k = \mathbf{W}_k\mathbf{x}_k$. The term $h_{kk}\tilde{\mathbf{x}}_k$ corresponds to the desired signals coming from the kth on-board antenna. And $\sum_{\substack{i=1 \\ i\neq k}}^{K} h_{ki}\tilde{\mathbf{x}}_i$ is the sum of interference signals from the other on-board antennas. $\mathbf{n}_k \in \mathbb{C}^{Q\times 1}$ is a column vector of zero-mean complex circular Gaussian noise with covariance σ^2 at beam k.

The spectral mask matrix $\mathbf{W}$ can be reformulated as $\mathbf{W} = [\tilde{\mathbf{w}}_1^T, \tilde{\mathbf{w}}_2^T, \cdots, \tilde{\mathbf{w}}_Q^T]^T$, where $\tilde{\mathbf{w}}_j = [w_{1j}, w_{2j}, \cdots, w_{Kj}]$, indicates which beams are allocated carrier j. Let the kth row of $\mathbf{H}$ be defined as $\mathbf{h}_k = [h_{k1}, h_{k2}, \cdots, h_{kK}]$ and $\mathbf{g}_k = \mathbf{h}_k|_{(h_{kk}=0)}$. We assume that the amplitude of transmitted symbols is normalized (i.e. $|x_{ij}|^2 = 1, \forall i = 1, \cdots, K; \forall j = 1, \cdots, Q$). Then, the transmitted signal power of all the carriers for beam k can be given by the diagonal elements in matrix $\mathbf{U}_k \in \mathbb{R}^{Q\times Q}$ as

$$\mathbf{U}_k = |h_{kk}|^2\mathbf{W}_k\mathbf{W}_k^H. \tag{A.3}$$

And the co-channel interference power at all Q carriers of beam k can also be given by the diagonal elements in matrix $\mathbf{R}_k^{\text{int}} \in \mathbb{R}^{Q\times Q}$ as

$$\mathbf{R}_k^{\text{int}} = \operatorname{diag}\left\{\left[\mathbf{g}_k\tilde{\mathbf{w}}_j^H\tilde{\mathbf{w}}_j\mathbf{g}_k^H\right]_{j=1,2,\cdots,Q}\right\}. \tag{A.4}$$

Thus the interference plus the noise $\mathbf{R}_k \in \mathbb{R}^{Q\times Q}$ will be given as

$$\begin{aligned} \mathbf{R}_k &= \mathbf{R}_k^{\text{int}} + \sigma^2\mathbf{I} \\ &= \operatorname{diag}\left\{\left[\mathbf{g}_k\tilde{\mathbf{w}}_j^H\tilde{\mathbf{w}}_j\mathbf{g}_k^H + \sigma^2\right]_{j=1,2,\cdots,Q}\right\}. \end{aligned}$$

Consequently, the SINR for beam k, defined as $\mathbf{\Gamma}_k \in \mathbb{R}^{Q\times Q}$, can be expressed as

$$\mathbf{\Gamma}_k = \mathbf{U}_k \mathbf{R}_k^{-1}. \tag{A.5}$$

Obviously, $\mathbf{\Gamma}_k$ is a diagonal matrix, because both $\mathbf{U}_k$ and $\mathbf{R}_k$ are diagonal matrix.

Note that the jth diagonal element of $\mathbf{\Gamma}_k$ indicates the SINR of carrier j at beam k. Assuming perfect CSI (Channel State Information) at the transmitter, then $\mathbf{\Gamma}_k$, $\mathbf{U}_k$ and $\mathbf{R}_k$ will be a function only with $\mathbf{W}$, which is the parameter we need to optimized.

Assuming a lossless MMSE receiver, the Shannon capacity of beam k can be given as

$$R_k(\mathbf{W}) \quad = \quad B_c \log\det\left(\mathbf{I} + \mathbf{\Gamma}_k\right). \tag{A.6}$$

Let γ_{kj} be the SINR of beam k on carrier j, with any practical implementation, e.g. DVB-S2, and given carrier bandwidth B_c, the allocated traffic has a finite set of values given as

$$R_k(\mathbf{W}) = B_c \sum_{j=1}^{Q} \eta_{\text{DVB-S2}}\left(\gamma_{kj}\right), \tag{A.7}$$

where $\eta_{\text{DVB-S2}}(\cdot)$ is a function that relates SINR with a corresponding spectral efficiency, which is quasi-linear in DVB-S2 standard [7] respect to SINR.

A.4 Joint Power and Carrier Allocation

In order to best match offered and requested throughput on a per-beam basis, we develop a methodology to jointly optimize power and carrier allocation in this section. Existing results on the references [2; 3; 6] on similar problems assume power limitation and the optimization is exclusively over the power allocation. However, we assume an additional degree of freedom: carrier allocation (bandwidth granularity). We propose to use binary power allocation (BPA) ($|w_{ij}|^2 = \{0, P_{\text{max}}\}, i = 1, 2, \cdots, K; j = 1, 2, \cdots, Q$) and quantized bandwidth allocation in order to decrease the complexity, where P_{max} is the saturation power per carrier.

A.4.1 Optimization Problem Formulation

The problem we need to solve is both SINR a balancing problem (as in [4]) and a problem of allocating the carriers. The resource allocation problem in the framework of the axiomatic-based SINR balancing model proposed in [4] is expressed as

$$\mathcal{C} = \inf_{\mathbf{p}>0} \left(\max_{1\le k\le K} \frac{\hat{\gamma_k}}{\gamma_k(\mathbf{p})} \right), \tag{A.8}$$

where $\hat{\gamma_k}$ is SINR request, $\gamma_k(\mathbf{p})$ is SINR model. Note that $\gamma_k(\mathbf{p})$ is a function of power allocation vector $\mathbf{p}$, but in our problem, the expression of SINR is a function of spectral mask matrix $\mathbf{W}$. Because we do not only balance the power allocation, but also optimize the strategy of carrier allocation (i.e. the structure of matrix $\mathbf{W}$). Therefore, the theory of SINR balancing is not applicable straightforwardly in this paper.

In this paper, we focus on the joint power and carrier allocation based on the BPA and quantized bandwidth allocation with given bandwidth granularity. The optimization problem can be formulated as

$$\begin{aligned} &\max_{\mathbf{W}} \left(\min_{1\leq i\leq K} \frac{\gamma_i(\mathbf{W})}{\hat{\gamma}_i} \right) \\ &\text{subject to} \sum_{i=1}^{K} \mathbf{w}_i^H \mathbf{w}_i \leq P_{\text{tot}} \\ &|w_{ij}|^2 = \{0, P_{\max}\}, i = 1, 2, \cdots, K; j = 1, 2, \cdots, Q. \end{aligned} \tag{A.9}$$

where P_{tot} is total available satellite power, $P_{\max}$ is saturation power per carrier, which is the constraint of satellite amplifier.

The general analytical solution of (A.9) is a complex problem due not only to the clear non-convexity but also to the need of preserving the geometry of the optimization model (i.e. the structure of matrix $\mathbf{W}$). However, we propose an iterative solution where each iteration is based on a two-step process as follows. First, we optimize subspace-by-subspace and obtain an analytical solution to the sub-problem of allocating the carrier on a per-beam basis. Second, we obtain the power allocated to the selected carriers from the power constraint.

A.4.1.1 First-step of each iteration

carrier allocation The first step of each iteration will consist of obtaining the optimal carrier allocation on a per-beam basis. In order to do so, we first sort the beams according to SINR demand, which actually corresponds to an iterative approach to the minimization in (A.9). Therefore, the sorted beam set $\mathcal{A}_s$ can be given as

$$\mathcal{A}_s = \left\{ i_1, i_2, \cdots, i_N | 0 \leq \frac{R_{i_n}(\mathbf{W})}{\hat{R}_{i_n}} \leq \frac{R_{i_n-1}(\mathbf{W})}{\hat{R}_{i_n-1}} < 1 \right\}, \tag{A.10}$$

where $i_n \in \{1, 2, \cdots, K\}, n = 1, 2, \cdots, N$, and $\hat{R}_k$ is traffic request of beam k.

Let $\hat{\gamma_k}$ and γ_k be the SINR request and SINR allocated for beam k, the formula (A.10) can be reformulate as

$$\mathcal{A}_s = \left\{ i_1, i_2, \cdots, i_N | 0 \leq \frac{\gamma_{i_n}(\mathbf{W})}{\hat{\gamma}_{i_n}} \leq \frac{\gamma_{i_n-1}(\mathbf{W})}{\hat{\gamma}_{i_n-1}} < 1 \right\}. \tag{A.11}$$

In the following, we will allocate a optimal carrier to each beam in set $\mathcal{A}_s$ from i_1 to

i_N. Note that only one carrier allocated per-beam during each iteration.

As mentioned in formula (A.5), $\mathbf{\Gamma}_k \in \mathbb{R}^{Q\times Q}$ is a diagonal SINR matrix for beam k. Therefore, a Rayleigh quotient problem is proposed here in order to select the optimum carrier on a per-beam basis. The carrier selection problem for beam k can be formulated as

$$\begin{aligned} \text{maximize} \quad & \frac{\mathbf{e}_j^H \mathbf{\Gamma}_k \mathbf{e}_j}{\mathbf{e}_j^H \mathbf{e}_j} \\ \text{subject to} \quad & ||\mathbf{e}_j||_2 = 1, \forall j \in \{1, 2, \cdots, Q\}, \end{aligned} \tag{A.12}$$

where $\mathbf{e}_j \in \mathbb{R}^{Q\times 1}$ is a unity column vector with only the jth element non-zero. Here $\mathbf{e}_j$ is introduced to indicate which carrier is allocated. The solution of Rayleigh quotient problem shown in (A.12) is given as

$$\mathbf{e}_j = v_{\max}(\mathbf{\Gamma}_k), \tag{A.13}$$

where $v_{\max}(\mathbf{\Gamma}_k)$ indicates the eigenvector related to the maximum eigenvalue of matrix $\mathbf{\Gamma}_k$. Hence, w_{kj} for jth carrier of beam k can be obtained with the solution of $\mathbf{e}_j$ as

$$w_{kj} = \mathbf{e}_j^H \mathbf{e}_j (P_{\max})^{1/2}. \tag{A.14}$$

A.4.1.2 Second-step of each iteration

power allocation Using the above analytical solution of optimal carrier, the power allocation is straightforward since we are assuming a BPA power allocation policy.

The Rayleigh quotient problem will be solved for all the beams from i_1 to i_N in beam set $\mathcal{A}_s$ during each iteration. Then, a new beam set $\mathcal{A}_s$ will be generated and run the iteration again until $\mathcal{A}_s$ is empty or $\sum_{i=1}^{K} \mathbf{w}_i^H \mathbf{w}_i > P\text{tot}$. Simulation results presented in section A.5 show that the algorithm converges fast.

A.4.2 Realistic Payload Constraints

Aside from the typical constraints discussed in section A.2, e.g. $0 \leq N_k \leq Q$, and $0 \leq B_k \leq B_{\text{tot}}$, there are still two additional constraints that should be considered.

A.4.2.1 Cluster Constraint

In a realistic satellite payload structure, all the beams are partitioned into geometric frequency re-use clusters. The beams in the same cluster sharing the whole bandwidth. In this way, no co-channel interference introduced within the cluster because the vector $\mathbf{w}_k$ is orthogonal for all the beams insider the same cluster. Thus, the total

available bandwidth for each cluster is constrained as $\sum_{i \in \Psi_m} B_i \leq B_{\text{tot}}$, where Ψ_m is the set of beams in the cluster m.

A.4.2.2 Total Power Constraint

The total available power constraint in the realistic payload is already shown in (A.9), where the total allocated power can not exceed P_{tot}.

A.5 Simulation Results Analysis

The objective of the simulation is: Firstly, to evaluate the performance of our proposed system design, joint power and carrier allocation. Secondly, to compare our novel system design with the conventional design, which is regular frequency reuse ($f_R = 7$) and uniform power allocation.

In order to fairly compare the performance with different number of beams in the same coverage (e.g. the European countries), we assume that the total traffic request is the same for all the cases. The linear traffic requested distribution is defined as $\hat{R}_i = i\beta; i = 1, 2, \cdots, K$, β is the slope of the linear function. Thus, the slope β decreases with the number of beams K decreasing. The following parameters are assumed in the simulations: $P_{\text{max}} = 4$Watt; $B_{\text{tot}} = 500$MHz; $Q = 112$; each cluster (hexagonal layout contains 7 beams as shown in Fig.A.2); $\beta = 8 \times 10^6$bps for $K = 121$. Therefore, $B_c = B_{\text{tot}}/Q = 4.4643$MHz and total traffic request is about 59Gbps.

The parameters of power gain (g), spectral efficiency (η) and traffic matching ratio (MR) (ρ) are studied in the simulation, which are defined as the following.

A.5.1 Performance Parameters Definition

A.5.1.1 Power Gain

We compare the amount of total power consumption for joint power and bandwidth optimized allocation with that for uniform power and bandwidth allocation when both achieve the same useful throughput using the same total bandwidth. We define the power gain g as

$$g = \frac{KP_{\text{uni}}}{\sum_{i=1}^{K} \mathbf{w}_i^H \mathbf{w}_i}, \tag{A.15}$$

where P_{uni} denotes the power per-beam in the case of uniform allocation.

A.5.1.2 Spectral Efficiency

The spectral efficiency is defined based on the total allocated traffic and total allocated bandwidth

$$\eta = \frac{\sum_{i=1}^{K} R_i(\mathbf{W})}{\sum_{i=1}^{K} B_i}. \tag{A.16}$$

A.5.1.3 Traffic MR

In order to describe the satisfaction degree of the allocated traffic respect to the total request traffic, the traffic matching ratio is defined here as

$$\rho = \frac{\sum_{i=1}^{K} R_i(\mathbf{W})}{\sum_{i=1}^{K} \hat{R}_i}. \tag{A.17}$$

A.5.2 Beam Layout and Antenna Model

In order to evaluate the performance of joint power and carrier allocation, we assume a general beam layout model (shown in Fig.A.2). A fixed-size space is used to generate different number of beams, thus, the beamwidth is decreasing as the number of beams increases. It means that the larger the number of beams, the narrower the beamwidth. The antenna gain model we used is a tapered aperture antenna model with 50 dBi maximum antenna gain. Then SINR will be calculated in each iteration of the algorithm with a given link budget of a typical Ka-Band (19.95 GHz) satellite payload.

A.5.3 Simulation Results

In order to evaluate the relevance of our iterative algorithm, we perform a study of convergence. It can be observed from Fig.A.3 that the algorithm is always convergent for different number of beams, and the convergence is faster with the number of beams increasing, e.g. our algorithm runs 24 and 33 iterations for number of 225 and 49 beams respectively. The reason is that our algorithm allocates resources to all unsatisfied beams in each iteration, thus the more traffic will be allocated with larger number of beams. Consequently, all the beams will reach the traffic request faster.

Fig.A.4 shows the power gain respect to the number of beams. We can see that, when $K = 200$, more than 6dB power gain can be achieved by Shannon case; and

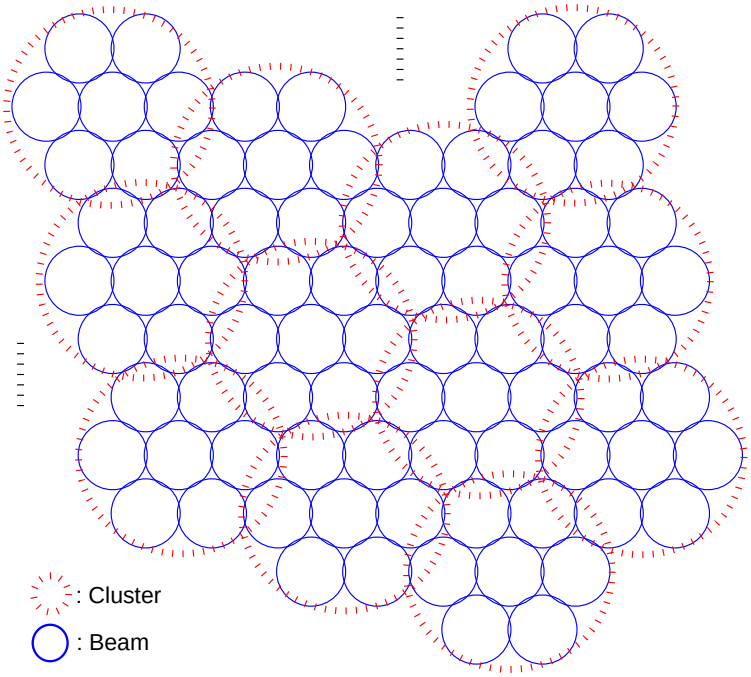

Fig. A.2: Beam layout model.

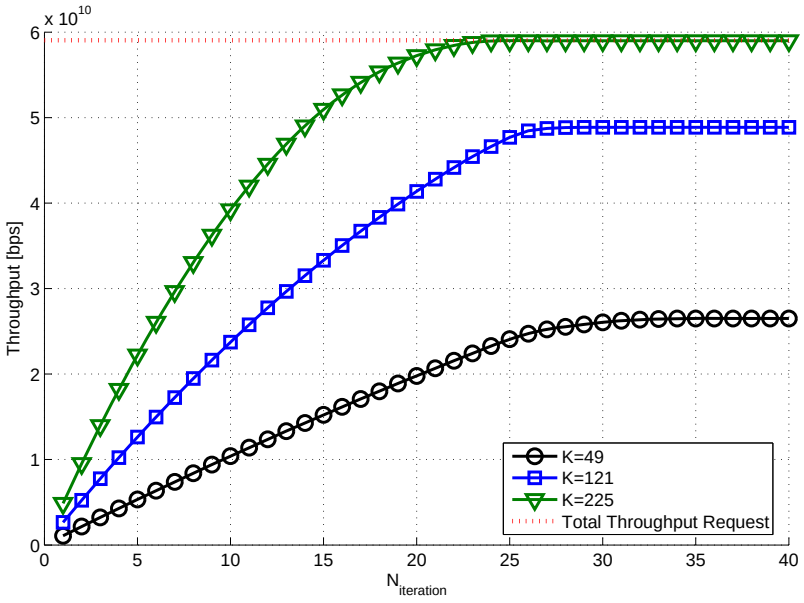

Fig. A.3: Convergence speed.

2.5dB gap between Shannon and DVB-S2 cases. By jointly allocate power and bandwidth, we do not only reduce power and bandwidth consumption of small traffic request beams, but also achieve reasonable proportional fairness from the viewpoint of user beams.

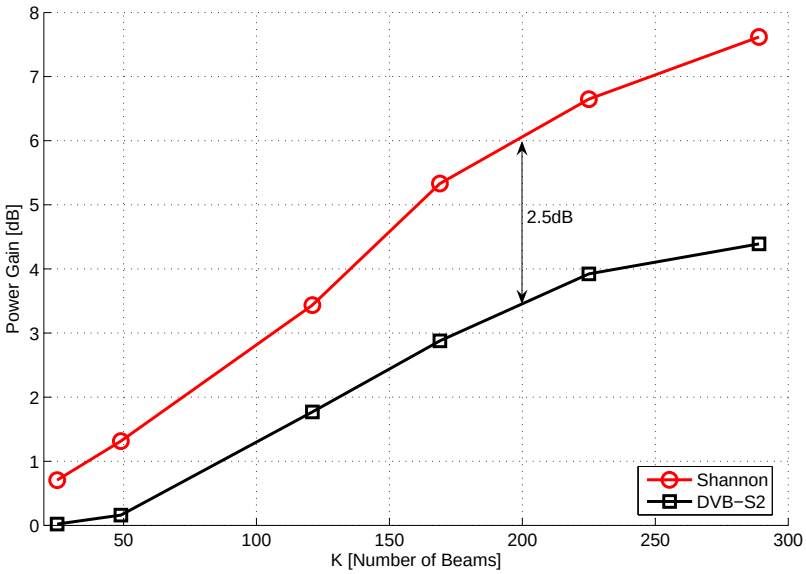

Fig. A.4: Power gain Vs. K.

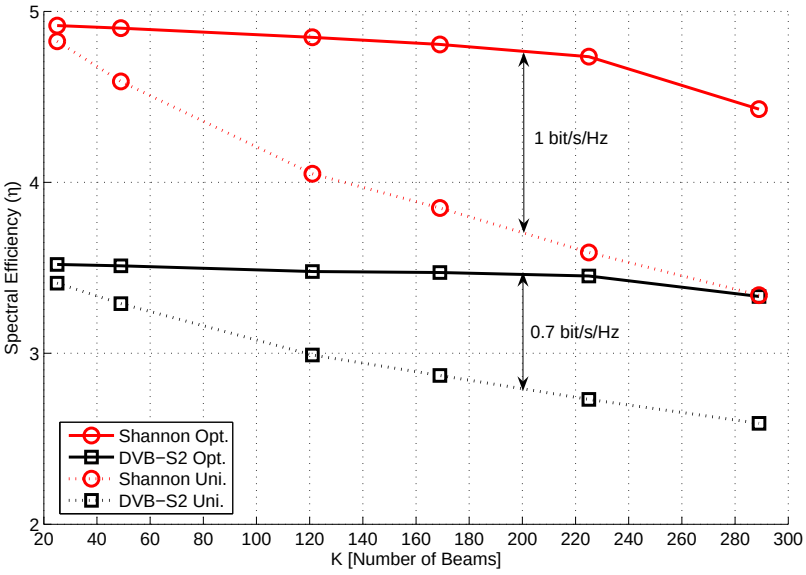

Fig. A.5: Spectral efficiency Vs. K.

Fig.A.5 shows the spectral efficiency respect to the number of beams. We can observe that the spectral efficiency decreases with the number of beams increasing, especially when $K > 200$. The reason is that co-channel interference will increase with the beamwidth decreasing.

Fig.A.6 shows the traffic MR respect to the number of beams. It can be observed that more throughput will be obtained in case of larger number of beams. How-

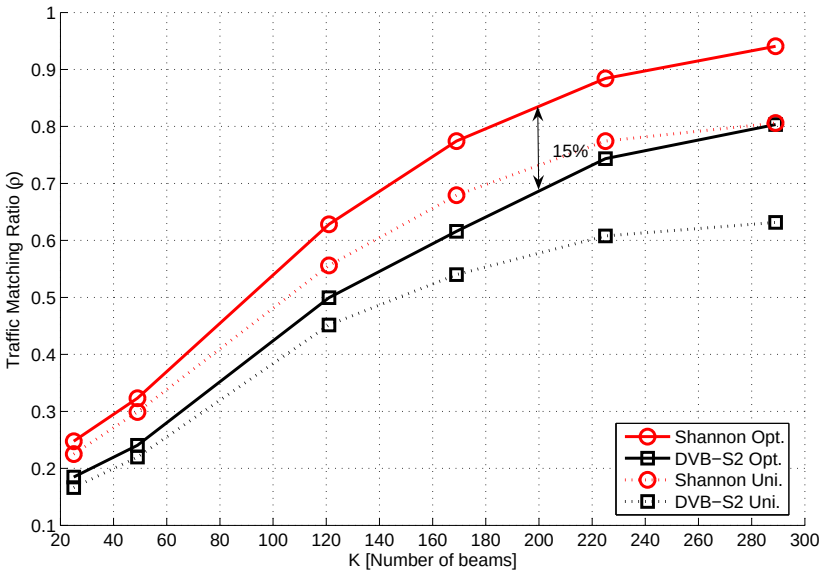

Fig. A.6: Traffic MR Vs. K.

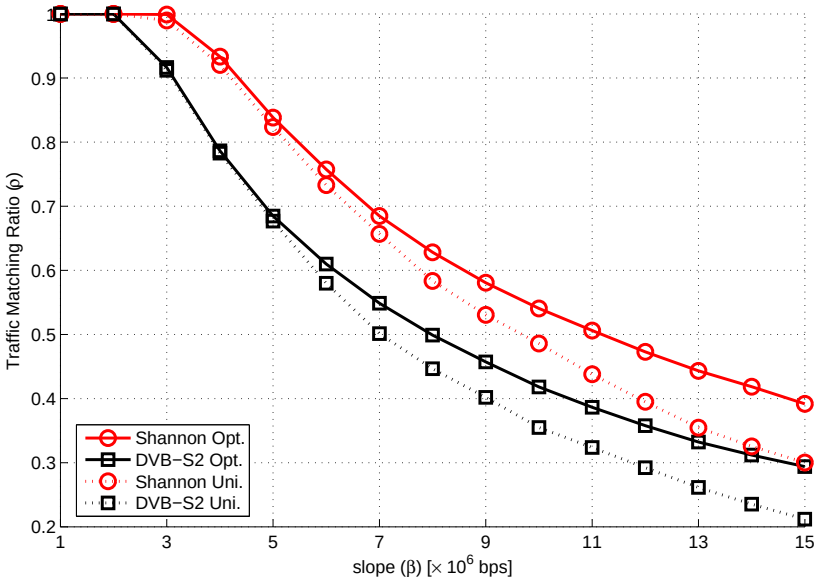

Fig. A.7: Traffic MR Vs. slope β.

ever, the power consumption and the complexity will increase with larger number of beams. Therefore, we should balance the total achieved throughput with respect to both power consumption and complexity. The result shows that, in the case $K = 200$, the traffic MR of Shannon case can improve about 15% compared to DVB-S2 case, and our jointly resource allocation approach can improve 10% compared to the conventional uniform resource allocation.

Fig.A.7 shows the traffic MR respect to different traffic distribution slope. Obviously, the satisfaction factor drops down with the slope increasing. Because the traffic distribution is more asymmetric with larger slope. However, our approach can achieve larger satisfaction factor gain compared to the conventional design for both Shannon and DVB-S2 cases.

A.6 Conclusions

Current designs of broadband satellite systems are based on regular frequency reuse pattern, thus lack of the necessary flexibility to match realistic asymmetric traffic requests. In this paper, we proposed a novel system design for the downlink of multibeam satellite based on jointly optimizing power and carrier allocation to best match individual SINR constraints. Although the optimization problem has been addressed in terrestrial networks, it is new in satellite communications, which requires a different channel model and system formulation. A mathematical formulation is proposed for our problem based on SINR balancing theory, but introducing one more degree of freedom, since we do not only optimize the power vector but also the carrier allocation. An iterative algorithm is proposed to solve this problem. In the algorithm, each iteration solves a Rayleigh quotation over the beams subspace. The current state-of-the art PHY layer technology: DVB-S2 and Shannon are implemented in order to obtain the gap between them. The results show significant improvements in terms of power gain, spectral efficiency and traffic MR compared to the conventional system. For a DVB-S2 and $K = 200$ case, we can achieve up to 3 dB power gain, 0.7 bit/s/Hz spectral efficiency gain by our jointly resource optimization allocation, and we can also improve 10% traffic MR with this approach. We also prove the primary goal of the study, that the joint optimization of power and carrier allocation can match much better than the conventional design in the realistic case of asymmetric traffic request (SINR constraints).

Acknowledgment

This work has been partly funded by the European Space Agency (ESA) under the project of “Study of Beam Hopping Techniques in Multi-Beam Satellite Systems”.

Bibliography

[1] N. Letzepis and A. J. Grant, “Capacity of the Multiple Spot Beam Satellite Channel With Rician Fading,” *IEEE Trans. on Inf. Theory*, vol. 54, no. 11, pp. 5210 - 5222, Nov. 2008.

[2] M. J. Neely, E. Modiano, and C. E. Rohrs, “Power Allocation and Routing in Multibeam Satellites with Time-Varying Channels,” *IEEE/ACM Trans. Netw.*, vol. 11, no. 1, pp. 138 - 152, Feb. 2003.

[3] J. P. Choi and V. W. S. Chan, “Optimum Power and Beam Allocation Based on Traffic Demands and Channel Conditions over Satellite Downlinks,” *IEEE Trans. on Wireless Commun.*, vol. 4, no. 6, pp. 2983 - 2993, Nov. 2005.

[4] M. Schubert and H. Boche, “QoS-Based Resource Allocation and Transceiver Optimization,” *Foundations and Trends in Commun. and Inf. Theory*, vol. 2, no. 6, pp. 383 - 529, 2005.

[5] J. E. Barcelo, M. A. Vázquez-Castro, J. Lei, and A. Hjøungnes, “Distributed Power and Carrier Allocation in Multibeam Satellite Uplink with individual SINR constraints,” accepted by *IEEE Global Commun. Conf.*, 2009.

[6] M. Schubert and H. Boche, “Solution of the Multiuser Downlink Beamforming Problem with Individual sinr Constraints,” *IEEE Trans. Veh. Technol.*, vol. 53, no. 1, pp. 18 - 28, Jan. 2004.

[7] ETSI EN 302 307 v1.1.1, Digital Video Broadcasting (DVB): Second generation framing structure, channel coding and modulation system for Broadcasting, Interactive Services, News Gathering and other broadband satellite applications.

Paper B

Duality Study over Multibeam Satellite System in Frequency and Time Domain

J. Lei, M. A. Vázquez Castro

IEEE International Conference on Communication (ICC 2010), Cape Town, South Africa, May 2010.

Abstract

In this paper, we investigate two new candidate transmission schemes to replace current ones in satellite communication systems. They operate in different domains (frequency and time-space), and we want to know which domain shows overall best performance. The two new transmission schemes are: Non-Orthogonal Frequency Reuse (NOFR) and Beam-Hoping (BH). We propose a novel formulation of the Signal-to-Interference-plus-Noise Ratio (SINR) and spectral efficiency of these two schemes and prove the theoretical duality between them. Further, we also develop a general methodology to include the technological constraints due to realistic implementation, which is common for the two domains and obtain the main factors that prevent the two technologies be in practice dual of each other (what we have called the technological gap). Moreover, we solve the frequency/time-space resource optimization problem with two different cost functions for an asymmetric traffic distribution. Both Gaussian codes and current state-of-the-art adaptive coding and modulation transmission over time division multiplexing (DVB-S2) are assumed in the simulation. It is shown that the Beam Hopping system turns out to show a less complex design and performs better specially for non-real time services.

B.1 Introduction

In electrical engineering, a number of concepts are related through some type of duality (e.g. current and voltage or time and frequency domains [1]) which gives rise to many interesting properties. For example, space/time duality [2], Gaussian multiple-access/broadcast channel duality [3], uplink/downlink duality [4], are also very useful to simplify system models.

In this paper, we investigate two new transmission schemes which have been chosen as candidates to replace current transmission schemes in multibeam satellite communications systems. Current schemes are basically time-division based with uniform frequency and power allocation while the new ones are: Non-Orthogonal Frequency Reuse (NOFR) technique and Beam-Hopping (BH). The first one is based on the frequency division over a flexible payload design which allows managing interference as an alternative to a complete orthogonal frequency reuse. The second one is based on time and space division, the so-called beam-hopping scheme. Both techniques have been selected as they can potentially cope with per-beam asymmetric traffic requests since current satellite resources (e.g. bandwidth and time-slot) allocation techniques are designed to allocate fixed power and bandwidth to each ground cell according to a regular frequency reuse scheme. This technique leads to a waste of resources in beams in which the traffic demand is relatively low. On the contrary, it does not satisfy traffic demand in the hot ground cells, where the traffic request is high. There are serval precedents of resources allocation in multibeam satellite systems. In [5–7], the authors discussed the power allocation policy and beam allocation, as well as achieving reasonable fairness among beams. The authors in [8] discussed power and carrier allocation problem, but it only focused on the uplink. Even though the problem of power and carrier allocation has been addressed in terrestrial wireless communications (e.g. [7]), the problem we tackle in this paper is different. We want to solve the frequency/time-space resource optimization problem with different cost functions for an asymmetric traffic demand distribution and obtain the capacity that each scheme is able to offer, so they can be compared with current systems.

The duality of NOFR and BH techniques, i.e. frequency/time-space duality, is discussed in this paper. We develop a general methodology to study the duality of the two schemes that also considers the technological constraints due to realistic implementation, which is common for the two domains and obtain the main factors that prevent the two schemes be in practise dual of each other.

The rest of this paper is organized as: In Section B.2, the problem statement is presented. In Section B.3, the study of the duality is formulated and the main factors that prevent NOFR and BH technologies be dual are identified. In Section B.4, the technological gap is obtained with a realistic system payload model. In section B.5, the frequency/time-space optimization with different cost functions for NOFR and BH

is analytically formulated and the solution is presented in Section B.6. In Section B.7, we draw the conclusions of the paper.

B.2 Problem Statement

We assume a multibeam satellite system where the satellite antenna generates K beams over the coverage area.

In the case of a NOFR system, the total available bandwidth, B_{tot}, is divided in N_c frequency carriers providing carrier granularity of $B_c = B_{\text{tot}}/N_c$. Each ground cell can be allocated a variable number of carriers depending on the traffic request. Carriers can be re-used throughout the coverage, but we do not impose any restrictions on the frequency reuse, it will be given by the resource optimization (i.e. interference minimization for a given traffic demand pattern) and therefore will be non-orthogonal.

In the case of a BH system, the total bandwidth is simultaneously used in specific ground cells during a time slot (dwelling time). We assume the resource allocation takes place during a given time window divided into N_t time-slots. Each ground cell can be allocated a variable number of time-slots.

Note that both techniques allow a number of ground cells to use the same frequency band or time slot, resulting in co-channel interference.

The problem tackled in this paper is to understand the duality of these techniques by developing a formulation that allows including technological constraints. Further, we want to solve the frequency/time-space resource optimization problem with different cost functions for an asymmetric traffic demand distribution and obtain the capacity that each scheme is able to offer, so they can be compared with current systems.

B.3 Duality Formulation

B.3.1 Payload Parameters Definition

In order to formulate the duality between NOFR and BH, we firstly introduce some important parameters (shown in Table B.I).

B.3.1.1 Granularity

B_c is the carrier granularity defined as $B_c = B_{\text{tot}}/N_c$ in NOFR system. It means that the allocated bandwidth per ground cell should be an integral multiple of B_c. We use T_s, with the same meaning but in BH system, i.e. the minimum unit of time duration that can be allocated per cell.

Table B.I: Payload Parameters

	Frequency Domain	Time Domain
Granularity	B_c	T_s
Total Number of arriers/time-slot	N_c	N_t
Resource Allocation Matrix	$C_{i,j} = \{0,1\}$ $i = 1,2,\cdots,K;$ $j = 1,2,\cdots,N_c$	$T_{i,j} = \{0,1\}$ $i = 1,2,\cdots,K;$ $j = 1,2,\cdots,N_T$
Number of carrier/time-slot allocated per cell	$N_i^c = \sum_{j=1}^{N_c} C_{i,j}$	$N_i^t = \sum_{j=1}^{N_t} T_{i,j}$

B.3.1.2 Resource Allocation Matrix

$C_{i,j}$ and $T_{i,j}$ are the resource allocation matrix for the NOFR and BH systems, respectively. The matrix indicates which carrier/time-slot j allocated to ground cell i. Note that BH can direct the satellite beams to specific ground cells, i.e. it is a space allocation too.

B.3.1.3 Number of carrier/Time-slot Allocated per cell

N_i^c and N_i^t indicates how many carrier/time-slot are allocated to ground cell i for NOFR and BH systems, respectively. These two parameters are to be optimized in order to meet the asymmetric traffic requested per cell. The optimization is presented in section B.5.

B.3.2 Duality Function Formulation

From the point of view of duality definition in [1], the following set of functions are dual in our scenario:

B.3.2.1 SINR

$$\gamma_{i,j}^{\text{NOFR}} = \frac{\alpha_i^2 P_{i,j}}{N_0 + \sum\limits_{\substack{m=1 \\ m \neq i}}^{N_b} \alpha_m^2 C_{m,j} P_{m,j}}. \tag{B.1}$$

The SINR for BH, $\gamma_{i,j}^{\text{BH}}$, can also be formulated as (B.1) by replacing $C_{m,j}$ with $T_{m,j}$. In (B.1), α_i denotes the channel attenuation factor, $P_{i,j}$ is power allocated for ground

cell i and carrier j for NOFR or time-slot j for BH system. $\sum_{\substack{m=1 \\ m\neq i}}^{N_b} \alpha_m^2 C_{m,j} P_{m,j}$ is the co-channel interference for NOFR system. We can see that the difference of function $\gamma_{i,j}^{\text{NOFR}}$ and $\gamma_{i,j}^{\text{BH}}$ is only the resource allocation matrix $C_{i,j}$ and $T_{i,j}$.

B.3.2.2 Spectral Efficiency

$$\eta_{i,j}^{\text{NOFR}} = f(\gamma_{i,j}^{\text{NOFR}}), \tag{B.2}$$

where $f(\gamma_{i,j})$ is a function that relates the SINR with a corresponding spectral efficiency. This function can be $\log_2(1+\gamma_{i,j})$ for Shannon limit with Gaussian coding, or can be a quasi-linear function in DVB-S2 [9] with respect to SINR. The spectral efficiency for BH system can be defined as: $\eta_{i,j}^{\text{BH}} = f(\gamma_{i,j}^{\text{BH}})$.

B.3.2.3 System Throughput

$$R_i^{\text{NOFR}} = \sum_{j=1}^{N_c} B_c C_{i,j} \eta_{i,j}^{\text{NOFR}} = \sum_{j=1}^{N_c} \frac{B_{\text{tot}}}{N_c} C_{i,j} \eta_{i,j}^{\text{NOFR}}. \tag{B.3}$$

Given the spectral efficiency defined in (B.2), we can formulate the throughput, which is the summary of all the allocated carriers capacity as shown in (B.3) for NOFR system. Accordingly, the throughput of BH system is: $R_i^{\text{BH}} = \sum_{j=1}^{N_t} \frac{B_{\text{tot}}}{N_t} T_{i,j} \eta_{i,j}^{\text{BH}}$.

B.3.3 Technological Constraints

The duality conditions of NOFR and BH system can be derived when:

$$R_i^{\text{NOFR}} = R_i^{\text{BH}}. \tag{B.4}$$

From (B.3), we obtain the following conditions:

B.3.3.1 Granularity

$$N_c = N_t, \tag{B.5}$$

B.3.3.2 Resource Allocation Matrix

$$C_{i,j} = T_{i,j}, \tag{B.6}$$

B.3.3.3 Spectral Efficiency

$$\eta_{i,j}^{\text{NOFR}} = \eta_{i,j}^{\text{BH}}. \tag{B.7}$$

For a practical NOFR system, it is not acceptable to have a very fine carrier bandwidth, i.e. N_c can not be very large. However, N_t can be much finer than bandwidth. Hence, it can be concluded that BH implementation allows higher flexibility. However, in this paper, we assume that granularity can be the same for both technologies and we focus on the actual limitation which is given by the levels of interference that each technology can achieve. The difference in the interference levels achieved will be a direct consequence in the technological implementation and this is discussed in the next section.

B.4 Technological Gap Upper Bound

From section B.3.3 we can see that the spectral efficiency that each technology can provide makes the real difference. Therefore, NOFR and BH systems are not completely dual of each other. In this section, we will demonstrate the technological gap between NOFR and BH. Note that we only consider the FWD (forward) downlink, because the uplink is not a big issue since power at the gateway can be greatly increased to compensate the attenuation.

Equivalent isotropically radiated power (EIRP) is defined as (in dB)

$$EIRP = P_{\text{sat}} - OBO - L_{\text{repeater}} - L_{\text{antenna}} + G_{\text{tx}}, \tag{B.8}$$

where Output BackOff (OBO) is the ratio of maximum output (saturation) power to actual output power, and the other parameters are defined in Table B.II. With known EIRP, we can obtain FWD downlink C/N_0 (in dBHz) and SNR (in dB) as

$$C/N_0 = EIRP - L_{\text{propagation}} + (G/T)_{\text{gt}} - 10\log(k_B), \tag{B.9}$$

$$SNR = C/N_0 - 10\log_{10}(B_c). \tag{B.10}$$

Let $a = P_{\text{sat}} - L_{\text{repeater}} - L_{\text{antenna}} + G_{\text{tx}} - L_{\text{propagation}} + (G/T)_{\text{gt}} - 10\log(k_B) - 10\log_{10}(B_c)$, and let x_1 and x_2 be the OBO for NOFR and BH system, respectively. Therefore, (B.10)

can be reformulated as

$$SNR_{\text{NOFR}} = a - x_1, \tag{B.11}$$

$$SNR_{\text{BH}} = a - x_2. \tag{B.12}$$

Let the FWD downlink signal to co-channel interference SIR be given as y (in linear), Therefore, the FWD downlink SINR can be formulated as (in linear)

$$\begin{aligned} SINR_{\text{down}}^{-1} &= SIR^{-1} + SNR^{-1} \\ &= y^{-1} + 10^{-(\frac{a-x}{10})}, \end{aligned} \tag{B.13}$$

where x can be x_1 or x_2 and SNR can be SNR_{NOFR} or SNR_{BH} for NOFR or BH system.

Let the FWD uplink SINR be z (in linear), then the FWD whole link SINR is given as (in linear)

$$\begin{aligned} SINR_{\text{tot}}^{-1} &= SINR_{\text{up}}^{-1} + SINR_{\text{down}}^{-1} \\ &= z^{-1} + y^{-1} + 10^{-(\frac{a-x}{10})}. \end{aligned} \tag{B.14}$$

Let the whole FWD link SINR be $\gamma = SINR_{\text{tot}}$, the spectral efficiency in the case of Shannon limit with Gaussian coding can be given as

$$\begin{aligned} \eta &= \log_2(1+\gamma) \simeq \log_2(\gamma) \\ &= -\log_2(z^{-1} + y^{-1} + 10^{\frac{x-a}{10}}), \end{aligned} \tag{B.15}$$

where we make a high SINR approx given as, $\log_2(1+\gamma) \simeq \log_2(\gamma)$. Therefore, the spectral efficiency for NOFR and BH system are

$$\eta_{\text{NOFR}} = -\log_2(z^{-1} + y^{-1} + 10^{\frac{x_1-a}{10}}), \tag{B.16}$$

$$\eta_{\text{BH}} = -\log_2(z^{-1} + y^{-1} + 10^{\frac{x_2-a}{10}}). \tag{B.17}$$

Let the technological gap of spectral efficiency between BH and NOFR system $\Delta\eta$ be given as

$$\begin{aligned} \Delta\eta &= \eta_{\text{BH}} - \eta_{\text{NOFR}} \\ &= \log_2 \frac{z^{-1} + y^{-1} + 10^{\frac{x_1-a}{10}}}{z^{-1} + y^{-1} + 10^{\frac{x_2-a}{10}}}. \end{aligned} \tag{B.18}$$

Let z, x_1 and x_2 be constant and $x_1 > x_2$, $\Delta\eta$ will be a monotonically increasing function of y. Therefore, the upper bound (maximum) of the technological gap $\Delta\eta$ will

be

$$\begin{aligned}\Delta\eta_{\max} &= \Delta\eta|_{y\to+\infty} \\ &= \log_2 \frac{1+z10^{-(\frac{a-x_1}{10})}}{1+z10^{-(\frac{a-x_2}{10})}}.\end{aligned} \tag{B.19}$$

As we indicated before, the uplink is not relevant. Thus we can suppose that the uplink SINR z is constant. We have demonstrated the result of (B.19) in Fig.B.1 and Fig.B.2, it is meaningful for us to evaluate the performance of NOFR and BH and very useful to predict the technological gap between NOFR and BH systems. In the next section, we discuss the optimization approach for NOFR and BH in order to obtain the technological gap influence on the resource optimization results.

B.5 Resource Optimization for NOFR and BH

In order to best match offered and requested throughput on a per-cell basis, we develop a methodology for NOFR and BH systems to optimize the carriers and time-slot/space allocation. Existing results on references [5–8] on similar problems assume power limitation and the optimization is over the power allocation only.

Two type of cost functions are proposed to solve the frequency/time-space resource optimization problem. In this section, we only discuss the optimization problem for BH system because NOFR is dual with BH (see section B.3), thus we only need to change the related parameters (e.g. $T_s \to B_c$, $N_t \to N_c$), the formulation is also applicable for NOFR system.

B.5.1 n-th Order Difference Cost Function

Here we want to match allocated bit rate R_i to requested bit rate $\hat{R}_i$ as closely as possible, i.e., we want to minimize a general function of the difference between $\{R_i\}$ and $\{\hat{R}_i\}$ across all the ground cells.

If an n-th order deviation cost function is used, the problem can be formulated as

$$\begin{aligned}\text{minimize} \quad & \sum_{i=1}^{K} \left| R_i - \hat{R}_i \right|^n \\ \text{subject to} \quad & R_i \le \hat{R}_i \\ & \sum_{i=1}^{K} N_i^t \le N_{\max}^{\text{re}} N_t,\end{aligned} \tag{B.20}$$

where N_t is the total number of time-slot. $N_{\max}^{\text{re}}$ is the number of cells illuminated simultaneously. K is the total number of ground cells, N_i^t is the number of time-slot allocated to ground cell i.

If we assume Gaussian codes, the bit rate per-cell, R_i, can be given as (B.3) with $\eta_{i,j} = \log_2(1+\gamma_{i,j})$. We also assume that the co-channel interference is negligible (i.e. $y \to +\infty$ as shown in (B.19)), because the simultaneously illuminated ground cells are separated far from each other. In practice, we do not allow adjacent cells illuminated at the same time slot. The power allocated to each time-slot is assumed constant. Thus R_i can be simplified as:

$$R_i = \frac{N_i^t}{N_t} B_{\text{tot}} \log_2(1+\gamma_i). \tag{B.21}$$

Therefore, the optimization problem shown in (B.20) is convex. The lagrangian function is given as

$$J(N_i^t) = \sum_{i=1}^{K} \left| R_i - \hat{R}_i \right|^n + \lambda \left(\sum_{i=1}^{K} N_i^t - N_{\text{max}}^{\text{re}} N_t \right). \tag{B.22}$$

Let $\frac{\partial J(N_i^t)}{\partial N_i^t} = 0$, we can obtain

$$N_i^t = \frac{\hat{R}_i N_t}{B_{\text{tot}} \log_2(1+\gamma_i)} - \left(\frac{\lambda}{n}\right)^{\frac{1}{n-1}} \left(\frac{N_t}{B_{\text{tot}} \log_2(1+\gamma_i)} \right)^{\frac{n}{n-1}}, \tag{B.23}$$

where λ is the lagrange multiplier and determined from the total available time slot constraint, which can be obtained by solving the following equation

$$\sum_{i=1}^{K} N_i^t \quad = \quad N_{\text{max}}^{\text{re}} N_t. \tag{B.24}$$

From (B.23) and (B.24) we can obtain

$$\lambda = n \left(\frac{\sum_{i=1}^{K} \frac{\hat{R}_i N_t}{B_{\text{tot}} \log_2(1+\gamma_i)} - N_{\text{max}}^{\text{re}} N_t}{\sum_{i=1}^{K} \left(\frac{N_t}{B_{\text{tot}} \log_2(1+\gamma_i)} \right)^{\frac{n}{n-1}}} \right)^{n-1}. \tag{B.25}$$

If we replace λ in (B.23) with (B.25), the solution will be

$$N_i^t = \frac{\hat{R}_i N_t}{B_{\text{tot}} \log_2(1+\gamma_i)} - \frac{\sum_{k=1}^{K} \left(\frac{\hat{R}_k N_t}{B_{\text{tot}} \log_2(1+\gamma_k)} \right) - N_{\text{max}}^{\text{re}} N_t}{\sum_{k=1}^{K} \left(\frac{\log_2(1+\gamma_i)}{\log_2(1+\gamma_k)} \right)^{\frac{n}{n-1}}}. \tag{B.26}$$

With the the number of time-slot allocated to each ground cell (N_i^t), the throughput allocated to each cell (R_i) can be calculated with (B.21).

B.5.2 Fairness Cost Function

Another way to match allocated capacity R_i to requested capacity $\hat{R}_i$ is to maximize the ratio of them as close as to 1.

$$\begin{aligned} \text{maximize} \quad & \prod_{i=1}^{K} \left(\frac{R_i}{\hat{R}_i} \right)^{\omega_i} \\ \text{subject to} \quad & R_i \leq \hat{R}_i \\ & \sum_{i=1}^{K} N_i^t \leq N_{\text{max}}^{\text{re}} N_t, \end{aligned} \tag{B.27}$$

where ω_i is the weighting factor that represents the priority of each beam. The problem (B.27) can be easily converted to a convex problem by introducing the logarithm in the objective function. Thus, the optimization problem is converted to

$$\text{maximize} \quad \sum_{i=1}^{K} \omega_i \log \left(\frac{R_i}{\hat{R}_i} \right). \tag{B.28}$$

Thus, the lagrangian function is given as

$$J(N_i^t) = -\sum_{i=1}^{K} \omega_i \log \left(\frac{R_i}{\hat{R}_i} \right) + \lambda \left(\sum_{i=1}^{K} N_i^t - N_{\text{max}}^{\text{re}} N_t \right). \tag{B.29}$$

Let $\frac{\partial J(N_i^t)}{\partial N_i^t} = 0$, then

$$N_i^t = \frac{\omega_i \hat{R}_i N_t}{\lambda \ln 2 B_{\text{tot}} \log_2(1+\gamma_i)}. \tag{B.30}$$

With given constraint $\sum_{i=1}^{K} N_i^t = N_{\text{max}}^{\text{re}} N_t$, the lagrange multiplier can be solved as

$$\lambda = \frac{\sum_{i=1}^{K} \frac{\omega_i \hat{R}_i N_t}{B_{\text{tot}} \log_2(1+\gamma_i)}}{N_{\text{max}}^{\text{re}} N_t \ln 2}. \tag{B.31}$$

The solution will be (replace λ in (B.30) with (B.31))

$$N_i^t = \frac{\omega_i \hat{R}_i N_t}{\log_2(1+\gamma_i)} \frac{N_{\text{max}}^{\text{re}} N_t}{\sum_{k=1}^{K} \frac{\omega_k \hat{R}_k N_t}{\log_2(1+\gamma_k)}}. \tag{B.32}$$

Therefore, the throughput allocated to each ground cell (R_i) can be calculated with (B.21).

Table B.II: NOFR and BH satellite system Payload Comparison (FWD downlink)

	Frequency Domain (NOFR syatem)	Time Domain (BH system)
Carrier Bandwith (B_c)	250Mhz	
OBO	4.5dB	1.05dB
Repeater Loss (L_{repeater})	2.55dB	
Antenna Feed Loss (L_{antenna})	1.17dB	
Satellite Tx. antenna gain (G_{tx})	47.14dB	
RF saturation power per carrier (P_{sat})	22.8dB	
EIRP per carrier (in dBW)	61.72dBW	65.17dBW
Propagation loss ($L_{\text{propagation}}$)	211.10dB	
Ground Terminal G/T $(G/T)_{gt}$	18.70 dB/K	
Boltzmann Constant (k_B)	$1.3806503 \times 10^{-23} m^2 kgs^{-2} K^{-1}$	
C/N_0 (in dBHz)	97.92dBHz	101.37dBHz
SNR (in dB)	13.94dB	17.39dB

As we indicated before, the optimization problem for BH system formulated above is also applicable to NOFR system because of duality. However, the optimized results of BH and NOFR systems will be different because of the technological gap (i.e. OBO difference) as we discussed in section B.4. In the next section, the simulation results will show that the BH system performs slightly better than NOFR system.

B.6 Simulation Results Analysis

The results shown in this section are based on the realistic parameters provided by MDA (Canada), which are presented in Table B.II). In order to evaluate the performance of NOFR and BH techniques and obtain the technological gap for a realistic implementation. The traffic requested distribution is defined as linear given as $\hat{R}_i = i\beta; i = 1, 2, \cdots, K$ and β is the slope of linear function. Assuming $B_{\text{tot}} = 500$ MHz, $K = 50$ and SINR of FWD uplink $\gamma_{\text{up}}^{\text{lin}} = 20$dB, the spectral efficiency requested per-cell will be $\hat{\eta}_i = i\beta/B_c$.

Figure B.1 shows the spectral efficiency (η) of NOFR and BH systems respect to SIR for Shannon and DVB-S2. We can see that the technological gap is about 0.496bits/s/Hz and 0.75bits/s/Hz in the case of DVB-S2 and Shannon, respectively.

Let the difference of OBO between NOFR and BH systems be defined as $\Delta_{\text{OBO}} = x_1 - x_2$. Fig.B.2 shows Δ_{OBO} respect to $\Delta\eta_{\text{max}}$, which is defined in (B.19). We can see that $\Delta\eta_{\text{max}}$ is almost linear with Δ_{OBO}, and the slope is increasing with BH system OBO (x_{BH}) increasing. This result is very useful to predict the technological gap between

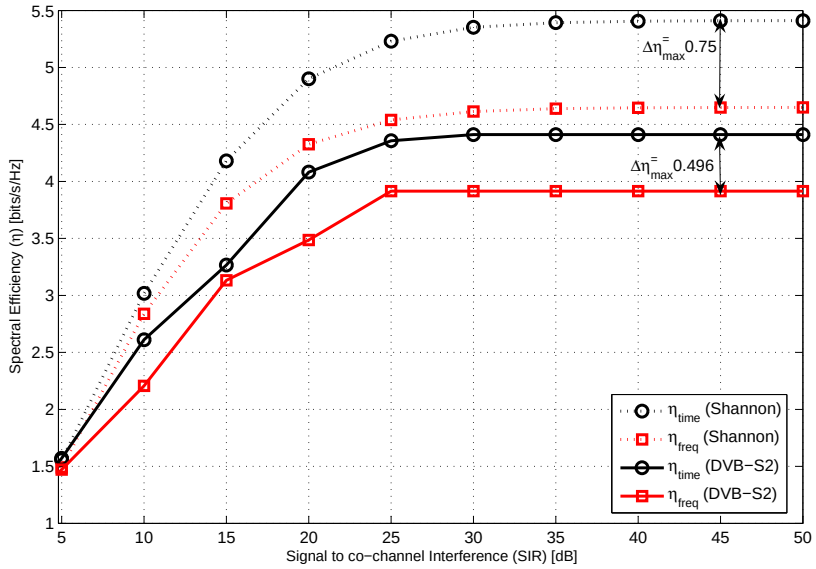

Fig. B.1: Spectral efficiency (η and $\Delta\eta$.) Vs. SIR

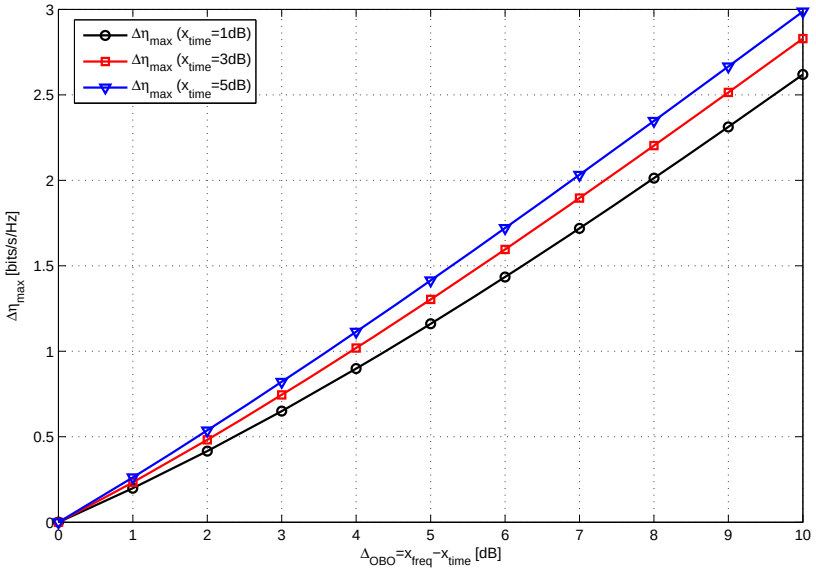

Fig. B.2: Δ_{OBO} Vs. $\Delta\eta_{\text{max}}$.

NOFR and BH systems.

Figure B.3 shows the distribution of throughput for n-order difference cost function and fairness cost function along 50 beams that have a linear distribution traffic demand. In this simulation, we assume that $\beta = 3\times10^7$; $n = 2$ (second order function); $N_t = 32$; $N_{\text{max}}^{\text{re}} = 8$; the SINR γ_i and the weighting factor ω_i are constant for all the cells in order to simplify. The result shows that two different cost functions distribute the

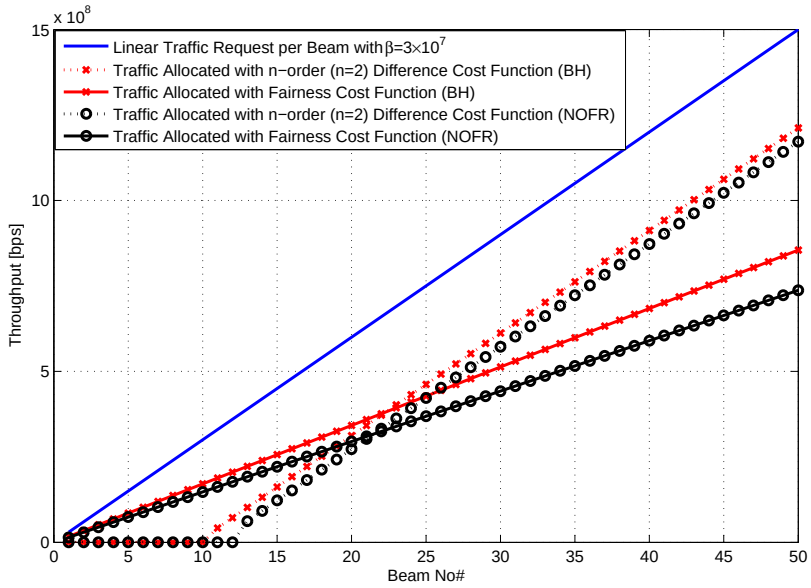

Fig. B.3: Comparison of cost functions in terms of throughput.

total available resource (carriers or time/space) to all the ground cells with different pattern. Fairness cost function is more favorable for low traffic request cells while n-order cost function distribute more resource to high traffic request beam. We can also see that the performance of BH is slightly better than NOFR, especially for the low traffic request beams. Further, the n-order simply neglect too low-loaded beams. This is relevant result since it is already considered in satcom design.

B.7 Conclusions

Two new technologies, NOFR and BH, over multibeam satellite system are studied in this paper. The two technologies operate in different domains (frequency and time/space), and we want to know which domain shows best performance. We prove the theoretical duality between them. Moreover, we also develop a general methodology to conclude the technological constraints due to realistic implementation, obtain the main factors that prevent the two technologies and formulate the technological gap between NOFR and BH systems. The results show that the technological gap is only related to the OBO of NOFR and BH, and the gap is almost linear with Δ_{OBO}. Further, we solve the frequency/time-slot resource optimization problem with different cost functions. Fairness cost function is more favorable for low traffic request cells while n-order cost function distribute more resource to high traffic request beam. The study of the resource optimization shows that the BH system performs only slightly better than NOFR.

Acknowledgment

This work has been partly funded by the European Space Agency (ESA) under the project of “Study of Beam Hopping Techniques in Multi-Beam Satellite Systems”.

Bibliography

[1] P. Bello, “Time-Frequency Duality,” *IEEE Trans. on Inf. Theory*, vol. 10, no. 1, pp. 18 - 33, Jan. 1964

[2] B. H. Kolner, “Space-Time Duality and the Theory of Temporal Imaging,” *IEEE Journal of Quantum Electronics*, vol. 30, no. 8, pp. 1951 - 1963, Aug. 1994

[3] N. Jindal, S. Vishwanath, and A. J. Goldsmith, “On the Duality of Gaussian Multiple-Access and Broadcast Channels,”*IEEE Trans. Inf. Theory*, vol. 50, pp. 768-783, May 2004.

[4] Minhua Ding and S. D. Blostein, “Uplink-Downlink Duality in Normalized MSE or SINR Under Imperfect Channel Knowledge,” in *Proc. IEEE Global Telecommunications Conf.*, pp. 3786 - 3790, Nov. 2007.

[5] M. J. Neely, E. Modiano and C. E. Rohrs, “Power Allocation and Routing in Multibeam Satellites with Time-Varying Channels,” *IEEE/ACM Trans. Netw.*, vol. 11, no. 1, pp. 138 - 152, Feb. 2003.

[6] J. P. Choi and V. W. S. Chan, “Optimum Power and Beam Allocation Based on Traffic Demands and Channel Conditions over Satellite Downlinks,” *IEEE Trans. on Wireless Commun.*, vol. 4, no. 6, pp. 2983 - 2993, Nov. 2005.

[7] M. Schubert and H. Boche, “QoS-Based Resource Allocation and Transceiver Optimization,” *Foundations and Trends in Commun. and Inform. Theory*, vol.2, no.6, pp. 383 - 529, 2005.

[8] J. E. Barcelo, M. A. Vázquez-Castro, J. Lei, and A. Hjøungnes, “Distributed Power and Carrier Allocation in Multibeam Satellite Uplink with individual SINR constraints,” in *Proc. IEEE Global Commun. Conf.*, Honolulu, USA, pp. 1 - 6, Nov. 2009.

[9] ETSI EN 302 307 v1.1.1, Digital Video Broadcasting (DVB): Second generation framing structure, channel coding and modulation system for Broadcasting, Interactive Services, News Gathering and other broadband satellite applications.

Paper C

Link Layer FEC and Cross-layer Architecture for DVB-S2 Transmission with QoS in Railway Scenarios

J. Lei, M. A. Vázquez Castro, and T. Stockhammer

IEEE Trans. Vehicular Technology, vol. 58, no. 8, pp. 4265 - 4276, Oct. 2009.

Abstract

DVB-S2 was originally designed for fixed terminals, but it has been recently adopted by the DVB Return Channel via Satellite for Mobile scenario (DVB-RCS+M) under Single Carrier Per Channel (SCPC) mode. For the purpose of adapting DVB-S2 for mobile reception, it has been agreed that among others Forward Error Correction (FEC) at the Link Layer (LL) is a suitable means to achieve reliable reception in mobile environments. Prime candidates for LL-FEC had been already available schemes in the DVB family of standards: Multiple Protocol Encapsulation-FEC (MPE-FEC) and MPE Inter-Burst FEC (MPE-IFEC). Furthermore, different FEC codes may be applied within these schemes, namely Reed-Solomon (RS) or Raptor FEC Codes. This paper introduces the integration of such schemes and codes on top of DVB-S2. In addition, we analyse the performance that can be achieved when applying these schemes with particular focus on two typical railway scenarios: Line-of-Sight together with the effect of railway Power Archers (LOS+PA) and non-Line of Sight (nLOS). Both theoretical and simulation analysis reveal that LL-FEC can overcome typical fading effects in the railway scenario by selecting appropriate FEC codes and by optimizing the coding parameters. We show that MPE-IFEC and extended MPE-FEC with Raptor codes -as finally specified in DVB-RCS+M-consistently show superior results than other link layer FEC for railway scenarios. We also indicate signaling update in order to allow achievable performance. As for practical implementation, we propose two possible novel cross-layer architectures for unicast DVB-S2 in order to provide Quality of Service (QoS). The architectures allow the migration from traditional packet encapsulation based on Moving Picture Experts Group 2-Transport Streams (MPEG2-TS) to new schemes such as the Generic Stream Encapsulation (GSE).

C.1 Introduction

Interactivity is a general trend for telecommunication services today. Satellite communications can be a ”natural” solution for extending interactive services for point-to-point data communication, by taking advantage of satellites' capability to efficiently distribute information over very large geographical areas and given the large available bandwidth in the Ku/Ka band. Particularly in Europe, due to the success of Digital Video Broadcasting via Satellite (DVB-S) [1], an important technical foundation has been laid for the evolution of satellite communications into this new market by using the second generation of DVB-S [2], commonly referred to as DVB-S2, as well as the Return Channel via Satellite (DVB-RCS) [3] standards.

Complementary to satellite services for fixed terminals is the ever increasing demand for broadband communications on mobile terminals. Higher data rates for mobile devices are provided by new standards such as Universal Mobile Telecommunications System (UMTS), High-Speed Packet Access (HSPA), mobile WiMAX (IEEE 802.16e), Digital Video Broadcasting for Handhelds (DVB-H) [4] and the emerging DVB specification for Satellite services to Handheld devices (DVB-SH) [5]. However, most of those systems have significant coverage restrictions and can generally not provide a universal data connectivity. Therefore, complementary satellite-based systems, in particular DVB-S2/RCS appears to be an ideal candidate for universal data connectivity, also as it can ideally combine digital TV broadcast reception in mobile environments and IP multimedia services. Furthermore, if remote vehicles such as trains or ships can be easily equipped with IP connectivity through satellite backhauls, mobile GSM base stations may be created providing connectivity to standard terminals. However, DVB-S2 and DVB-RCS have not been designed for mobile use. Terminals installed in a mobile platform, such as train, ship, or aircraft, are exposed to challenging environments that will impact the system performance since the current standard lacks any specific provision for mobile scenarios. An attractive solution is to adopt the DVB-S2 with Single Carrier Per Channel (SCPC) mode to support the Mobile services of DVB-RCS (DVB-RCS+M) by extending the system such that legacy DVB-S2 hardware can be reused and modifications are only applied on the link layer.

In general, mobile terminals will have to cope with stringent frequency regulations (especially in Ku band), Doppler effects, frequent handovers and impairments in the synchronization acquisition and maintenance. Furthermore, the railway scenario is affected by shadowing and fast fading due to mobility, as well as deep and frequent fades. According to [6], this mainly results from the presence of metallic obstacles along electrified lines and long blockages, for example, due to the presence of tunnels and large train stations.

In this paper, Link Layer Forward Error Correction (LL-FEC) will be introduced as fading countermeasure to compensate the impact of the railway scenarios, in par-

ticular shadowing, fast fading and power arches (PA). Specifically, we analyze various LL-FEC frameworks, namely Multiple Protocol Encapsulation/Generic Stream Encapsulation-Forward Error Correction (MPE/GSE-FEC) and MPE Inter-Burst FEC (MPE-IFEC). Moreover, different codes, namely Reed-Solomon (RS) codes and Raptor codes [7] (also specified in 3GPP [8], DVB and IETF) are applied within the different LL-FEC frameworks. Two typical railway scenarios, line-of-sight plus PA (LOS+PA) and non-LOS (nLOS), are used to analyze the performance of FEC. We focus on train speeds of around 100 km/h as they serve as the lower bound of the speeds of interest. Lower speeds are not investigated as they only apply in the proximity of stations where generally some terrestrial infrastructure is available.

The rest of this paper is organized as follows. Section C.2 introduces the requirements for extending DVB-S2 to railway scenarios and discusses the modelling of the railway channel. Section C.3 identifies the available link layer FEC codes and frameworks in the DVB family standards. Section C.4 analyses the impact of including link layer FEC for DVB-S2 standards and proposes two novel cross-layer architectures for DVB-S2 datacasting. Section C.5 presents our proposed evaluation and simulation framework of MPE-FEC and MPE-IFEC. Section C.6 discusses how to optimize the code parameters for different FEC schemes and provides selected simulation results and section C.7 discusses the migration LL-FEC to Generic Stream Encapsulation (GSE). Finally, the summarizing conclusions are presented in section C.8.

C.2 Requirements for DVB-S2 Extension to Railway Scenarios

The Land Mobile Satellite Channel (LMSC) has been widely studied in the literature [9]. Several measurement campaigns have been carried out and a number of narrow and wideband models have been proposed for a wide range of frequencies, including Ku [10] and Ka [11] bands. Nevertheless, for the specific case of railway environment, only few results are available in [12] as a consequence of a limited trial campaign using a narrowband test signal at 1.5 GHz, performed more than 10 years ago in the north of Spain. These results represent a very interesting reference, although no specific channel model has been extracted from the collected data. After an initial qualitative analysis, the railway environment appears to differ substantially with respect to the scenarios normally considered when modelling the LMSC. Excluding railway tunnels and areas in the proximity of large railway stations, one has to consider the frequent presence of several metallic obstacles like power arches, posts with horizontal brackets, and catenaries, i.e. electrical cables are frequent obstacles to LOS reception. Results of direct measurements performed along the Italian railway aiming to characterize these peculiar obstacles are reported in [6]. In summary, the attenuation introduced by the catenaries (less than 2 dB) and by posts with brackets (2-3 dB) is relatively low and can be easily compensated by an adequate link margin. However, the attenuation introduced by the power arches increases to values as high as 10 dB and beyond, depending on the geometry, the antenna radiation pattern and

Table C.I: Effect of power arches on transmitted packets (BB-Frames and Transport Streams)

Duty Cycle	l_{PA}	d_{PA}	MODCOD (QPSK 1/2 / 8PSK 3/4)			
1%	0.5	49.5	16/24	1522/2278	336/768	31962/72896
2%	1	49	31/47	1507/2255	651/1504	31647/72160
4%	2	48	62/93	1476/2209	1302/2976	30996/70688
5%	2.5	47.5	77/116	1461/2186	1617/3712	30681/69952
6%	3	47	93/139	1445/2163	1953/4448	30345/69216
7%	3.5	46.5	108/162	1430/2140	2268/5184	30030/68480
8%	4	46	123/185	1415/2117	2583/5920	29694/67744
9%	4.5	45.5	139/208	1399/2094	2919/6656	29379/67008
10%	5	45	154/231	1384/2071	3234/7392	29064/66272
20%	10	40	308/461	1230/1841	6468/14752	25830/58912

the carrier frequency. Therefore, advanced fading countermeasures are needed to compensate such attenuation phenomena.

A number of Railway channel models have also been introduced in [6; 13] and Land Mobile Satellite channel models have been discussed in [11; 14; 15].

C.2.1 LOS+PA channel

For the sake of simplicity, the presence of PAs in the Railway environment can be medelled as erasures with different duty cycle, therefore an ON/OFF model assumed; during the "ON State", the Packet Error Rate (PER) of the signal received equals to 0. During the "OFF State", the PER received equals to 100%. The duty cycle of PAs can be computed as

$$\text{Duty Cycle} = \frac{l_{\text{PA}}}{l_{\text{PA}} + d_{\text{PA}}}, \tag{C.1}$$

where l_{PA} is the width of PA, and d_{PA} is the distance between two consecutive PAs. Therefore, for the LOS+PA case depending on the velocity of the train v_{train}, the number of lost DVB-S2 Baseband Frames (BB-Frames) $N_{\text{BB\_PA}}$ during the PA obstructions can be easily obtained. Assume $T_{\text{PA}} = l_{\text{PA}}/v_{\text{train}}$ the obstruction duration for the transmitted signal, B_s is the symbol rate, M is modulation constellation, r_{phy} the physical coding rate and S_{BBFrame} the size of a BB-Frame. Then $R_{\text{BB}} = B_s M r_{\text{phy}}/S_{\text{BBFrame}}$ is the rate at which BB-Frames are transmitted (e.g. $S_{\text{BBFrame}} = 32208$ bits for 64k FECframe with LDPC coding rate=1/2 and S_{BBFrame}=48408 bits for coding rate=3/4) and the number of lost BB-Frames lost during the PA is $N_{\text{BB\_PA}} = \lceil T_{\text{PA}} R_{\text{BB}} \rceil$. The duty cycle selected in the simulation and corresponding PA parameters are presented in Table C.I with v_{train}=100 km/h, B_s=27.5 Mbaud/s, M=2, r_{phy}=1/2 for QPSK and M=3, r_{phy}=3/4 for 8PSK. In terms of performance criteria for this scenario, we are interested in the Maximum Tolerant Burst Length (MTBL), which corresponds to the

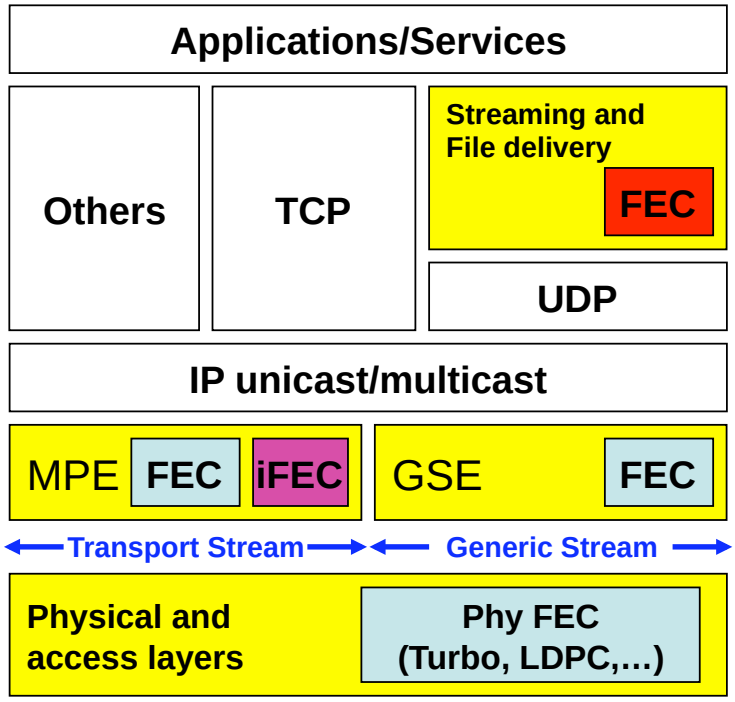

Fig. C.1: FEC location in the DVB protocol stack.

maximum duty cycle that can be overcome by the link layer.

C.2.2 nLOS channel

In certain circumstances, LOS to the satellite is heavily obstructed, for example if the receiver moves in some urban areas. Typically, due to reflections and scattering multipath signals are received that result in typical correlated Rayleigh fading, the directivity is take into account by shaping the spectrum. In this paper we model the nLOS Rayleigh channel at link layer. We use time series of 0s and 1s representing received BB-Frames of DVB-S2, which are either fully received or lost. Such time series of 0s and 1s are used as the input of the Link Layer module of the simulator presented herein below. In terms of performance evaluation we assess the residual packet loss rate that generally needs to be below some threshold for sufficient quality.

C.3 Available Link-Layer FEC Codes and Frameworks in the DVB Family Standards

As already indicated, an excellent fading countermeasure for erasure channels is the application of FEC on the link layer. DVB has applied this principle already in several systems, such as DVB-H or DVB-SH. Figure C.1 shows a high-level protocol stack highlighting the usage of FEC codes for DVB services over IP-based networks [16].

The top layer of this stack represents the service offering intended by the Service Provider. This consists of programs, information about programs, multicast and/or unicast data; in short, the essential items needed to enable a DVB service over an IP network. FEC may be applied at Application or Transport Layer as for example done in 3GPP's Multimedia Broadcasting/Multicast Services (MBMS) or IPDC file delivery over DVB-H based on the Raptor codes. However, this type of FEC is service specific and is not generic and applicable to any packet flow. Traditionally, the FEC is applied at the PHY Layer/bit-level, nowadays usually either based on the Turbo codes or Low Density Parity Check (LDPC) codes. However, such codes are usually limited in the amount of interleaving due to hardware restrictions. Therefore, in the DVB family of standards, e.g. DVB-T/H, link layer FEC is considered for protecting data packets/symbol-level, rather than bit/byte-level. The FEC on the link layer can be integrated on top of existing physical layer. Other codes than those applied on the physical layer are more suitable for a variety of applications and contexts at higher layers as typically erasure correction needs to be applied. In DVB, RS and Raptor codes are applied for this purpose.

Generally, it should be distinguished between link layer FEC codes itself and the framework or specific design defining how the code is applied in a specific system. The framework involves both architectural and signalling considerations. The first link layer FEC codes proposed in DVB were the RS codes as currently applied in the first generation of DVB family of standards, i.e. DVB-C, DVB-S, or DVB-H. Raptor Codes have been invented lately and introduced into DVB standards: in contrast to RS codes they provide more flexibility, large code dimensions, and lower decoding complexity. Raptor codes have therefore been adopted in latest DVB standards, e.g. within DVB-H for file delivery or DVB-IPTV. Therefore, RS codes and Raptor codes have been chosen for performance testing for the LL-FEC in the railway scenarios in this paper. For both codes we use maximum likelihood decoding algorithms. Whereas the complexity of RS code decoding is know to be rather high, for Raptor codes a low-complexity maximum-likelihood decoding is for example introduced in [8], Annex E. Different frameworks are possible that allow integrating LL-FEC into DVB-S2/RCS systems. In Section C.6 below we present a performance comparison for each of these frameworks.

C.3.1 MPE-FEC Framework of DVB-H and Applicability to DVB-S2

DVB has adopted a LL-FEC in DVB-H at the data link layer (MPE Layer) referred to as MPE-FEC. At the time when DVB-H was specified, only RS codes were available, and therefore, the MPE-FEC is based on RS codes. FEC operations are performed in the DVB-H link layer as illustrated in Fig. C.2. For MPE-FEC the repair data is generated based on an Application Data Table (ADT) with size of at most 191 KBytes, such that for 200ms latency data rates of at most 7.8 Mbit/s can support, and for 10 seconds delay, only up to 156 Kbit/s are supported. The processes are fully defined and standardized in [17]. For an ideal memory-less erasure channel with symbol

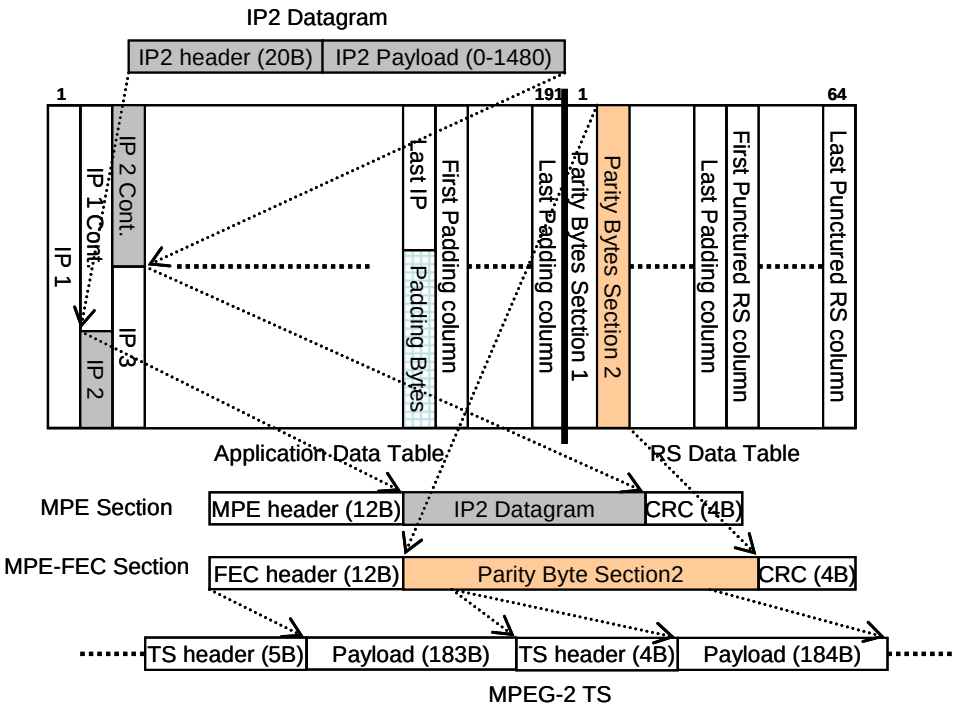

Fig. C.2: MPE-FEC Frame and the MPE encapsulation process.

erasure probability ε, the residual PER of RS(n, k) code over an can be computed as

$$P_e \cong \varepsilon \left(1 - \sum_{i=1}^{n-k} \binom{n}{i} \varepsilon^i (1-\varepsilon)^{n-i} \right). \tag{C.2}$$

For RS(255,191) in DVB-H, n=255 and k=191. However, the code can also be punctured and shortened such that any k with $0 < k < 191$ and any n with $k < n < \min(k + 64, 255)$.

The MPE sections containing the original data packets within one ADT as well as the corresponding MPE-FEC sections containing are transmitted in a single burst. For example, for file delivery services over DVB-H, one major drawback of LL-FEC in DVB-H is that each of the unique bursts where the file is partitioned must be successfully decoded to recover the file. Note also that if one burst is completely received (i.e., all source and parity data), it cannot be used to correct errors in other bursts. In particular, when using this framework for DVB-S2 another drawback is the size of the MPE-FEC frame, which is not big enough to protect against long burst errors since the number of address signalling bits for the ADT and RS data table is only 18-bit [17]. Therefore, in order to protect longer bursts, more bits to signal the address of ADT table must be allocated along with the corresponding signalling structure to address this issue. This is addressed in the extended MPE-FEC as introduced in section C.3.3.

C.3.2 MPE-IFEC Framework and Applicability to DVB-S2

During the DVB-SH standardization activities, it was recognized that for satellite-to-handheld services, the MPE-FEC is not sufficient. Therefore, it was decided to specify a multi-burst link layer FEC framework referred to as Inter-Burst FEC (IFEC) [18]. The MPE-IFEC was introduced to support reception in situations of long erasures at the MPE section level spanning several consecutive time-slice bursts due to the characteristics of the land-mobile satellite (LMS) channel. Obstacles may hinder direct satellite reception and induce losses of several successive bursts. MPE-FEC Sliding Encoding [19] had been proposed initially to enable multi-burst protection based on RS codes, but with the availability of more powerful and low-complexity Raptor erasure codes, the MPE-IFEC has been generalized.

Therefore, the MPE-IFEC is specified as a generic framework that presents enough flexibility for a variety of applications. For a usage in DVB-SH, its parameters are restricted to some specific values via the ”framework mapping”. Two of such ”mappings” are presented in this paper. One is based on MPE-FEC RS code [17]. The other mapping is based on Raptor code as specified in the Content Delivery Protocols (CDP) specification of IP Datacast over DVB-H (DVB-IPDC) [20]. For more details on Raptor codes please refer to [7] and the specification in 3GPP [8], DVB and IETF.

The MPE-IFEC is defined by the parameters encoding period EP, which reflects the ADT size in compared to the burst size, data burst spread B, i.e. over how many bursts an ADT is spread, FEC spread S, i.e., over how many multiple of EP bursts the FEC is spread, the sending delay D, i.e. how long the sending of data is delayed at sender in units of time-slice bursts, the code rate r_{ll} as well as code being used, namely Raptor or RS codes. Note that whereas Raptor codes allow very flexible parameters, for RS codes due to restricted code parameters only EP=1 can be used.

Note that for MPE-IFEC the mapping of MPE-IFEC sections to MPEG-2 TS packets is identical as for the MPE-FEC. At the receiver the decoding matrix (combination of ADT + iFDT) is generated and decoding each of the decoding matrix with frequency EP eliminates the unreliable columns of the decoding matrix. The ADT of the decoding matrix is then mapped back to Application Data Sub Table (ADST) to reconstruct the datagrams in each ADST.

C.3.3 Extended MPE-FEC Framework for DVB-S2 - DVB-RCS+M Link-Layer FEC

Despite its flexibility, the MPE-IFEC is mainly designed for the purpose of multicasting live video over time-slice bursts. The FEC is designed for the purpose to minimize tune-in and channel switching delays over burst-based transmission, but not to minimize end-to-end delay, which is essential for bidirectional data delivery services. Therefore, a new Link layer FEC (LL-FEC) has been defined in DVB Return Channel Satellite (RCS) for mobile extension in [3] “Interaction Channel for Satellite Distribution Systems”, section 6.4.5, as a countermeasure for Non-Line-of-Sight (nLOS)

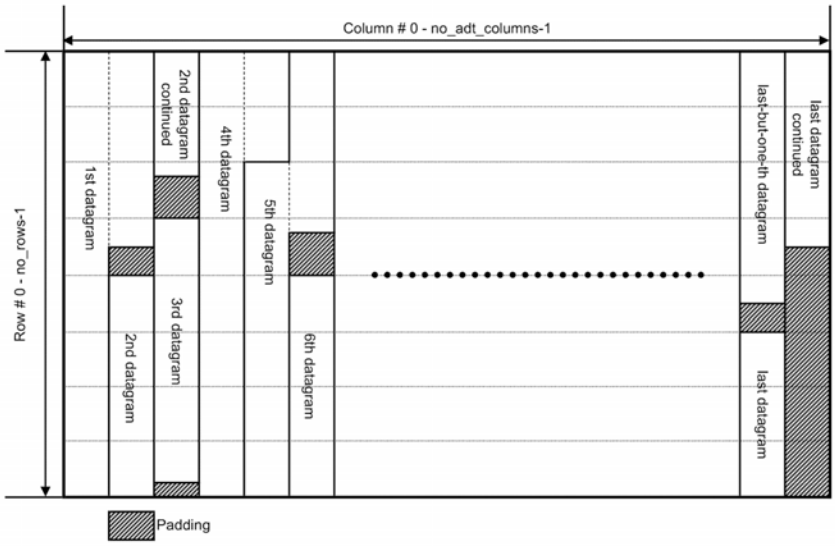

Fig. C.3: Generalized DVB-RCS+M LL-FEC mapping of datagrams to ADT.

conditions due to obstruction, blockage, or other situations in which the line of sight is interrupted. With this LL-FEC, transmissions of multicast and unicast traffic data can be protected against channel impairments such as short interruptions and shadowing. Return Channel Satellite Terminals (RCSTs) that declare support for nLOS countermeasures shall be able to receive and process a forward link signal transmitted in accordance with these provisions. This technique can also be applied to the optional continuous return link carrier transmissions defined in section 10 of [3]. Transmissions employing LL-FEC use the same basic data structures as other MPE transmissions. However, due to the restricted signalling space of the address, datagrams may not be directly concatenated in the ADT, but some padding may be added such that a new datagram always starts at an address being multiples of some value referred to as *address granularity* (see Fig. C.3). The address granularity is inherently configured in the setup with the specification of the frame size coding. The use of LL-FEC is defined separately for each elementary stream in the transport stream. Each elementary stream may configure different code parameters, resulting in different delays, levels of protection and FEC overheads. LL-FEC can use the Raptor code for LL-FEC frame ADT sizes up to 12 MBytes or the MPE-FEC Reed-Solomon code for any LL-FEC frame ADT sizes up to 191 KBytes. The chosen code is identified in the forward link signalling. We will analyse the performance of an extension of MPE-FEC towards larger ADT sizes for DVB-S2 railway scenarios. Such extensions require larger dimensions for the block code and are therefore most suitable provided by Raptor codes.

C.4 Cross-Layer Link-Layer FEC Architectures for DVB-S2

The datacast term used within the scope of DVB-H and DVB-T refers to broadcast distribution using IP multicast. In fact, in general DVB bearers do not define any

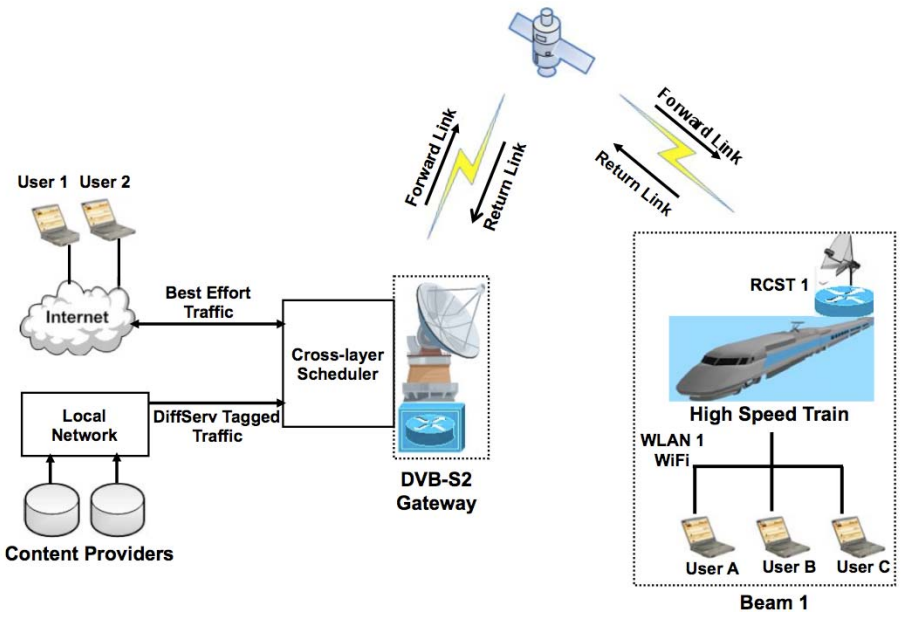

Fig. C.4: Unicast services to trains over a DVB-S2/RCS system architecture.

return channel and therefore do not inherently support bi-directional transmission capabilities (unless connected to GSM/GPRS/3G networks). However, by the use of DVB-RCS satellite systems such as DVB-S2 can be extended with a return link and provide bi-directional communication including IP unicast. An overview of a system architecture to transmit unicast traffic over DVB-S2/RCS is shown in Fig. C.4. The traffic sources are assumed to be coming from both the public Internet and local servers. The latter are assumed to implement Quality of Service (QoS) according to a Diffserv model. The unicast IP traffic is scheduled by a cross-layer scheduler before entering the DVB-S2 modem. In this paper we propose two cross-layer architectures for unicast services in order to allow the use of LL-FEC for QoS provision for unicast traffic transmission.

MPE-FEC and extender MPE-FEC are designed for multicast distribution of real-time services. Therefore, those frameworks only take into account transport of IP datagrams distributed over IP multicast. The signalling is only defined for the broadcast/multicast transmission architecture. In order to define backward-compatible FEC signalling also for unicast traffic, the cross-layer architectures are proposed and designed in line with DVB-S2 nomenclature. Detailed discussion of the signalling problem is also presented in [21].

C.4.1 LL-FEC per-Mobile Terminal

The datacast (multicast/broadcast and unicast) transmission cross-layer architecture with either MPE-FEC over transport streams or GSE over Generic Streams (GS) is shown in Fig. C.5. This architecture aggregates traffic and creates an Elementary Stream (ES) per-mobile terminal. This means that one PID (Packet IDentifier) is

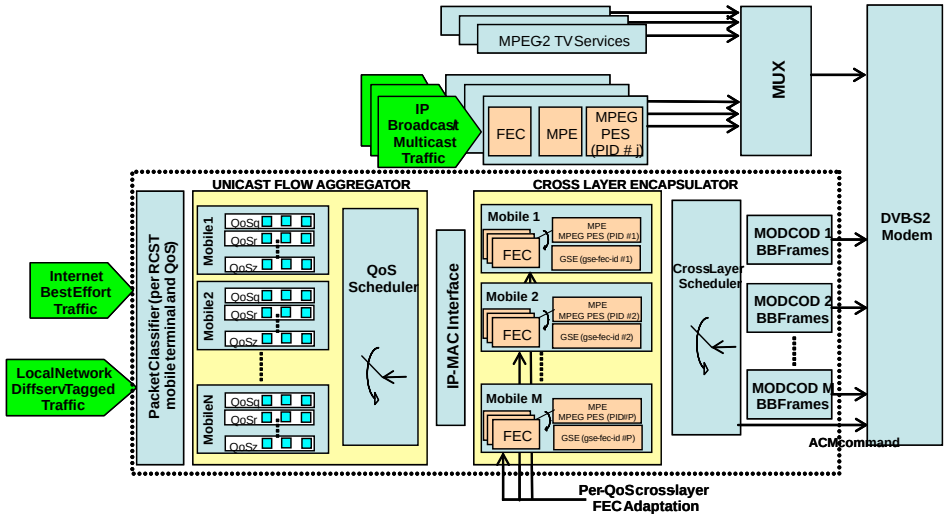

Fig. C.5: Datacast Transmission over DVB-S2/RCS: Per-Mobile terminal architecture.

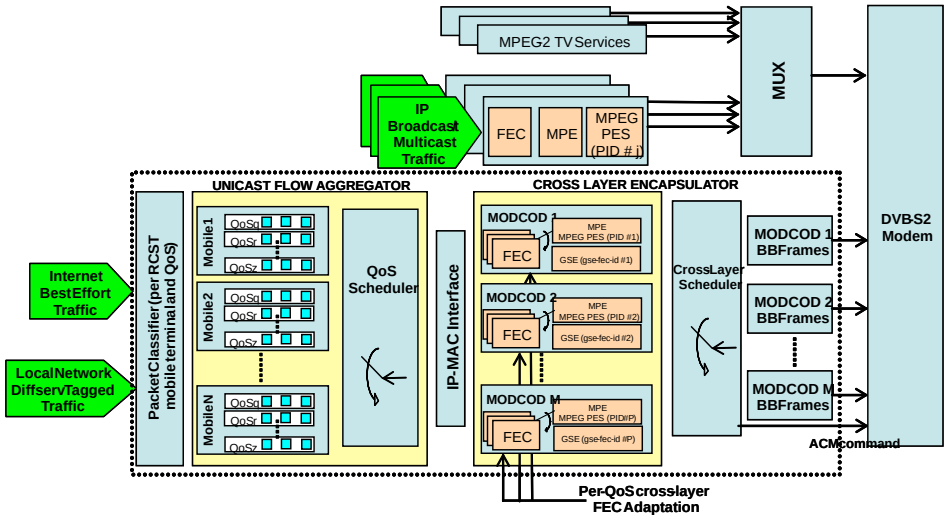

Fig. C.6: Datacast Transmission over DVB-S2/RCS: Per-MODCOD architecture.

needed per mobile terminal. The packets are then aggregated according to the physical layer parameters (MODCOD). This architecture allows QoS scalability, i.e. it is possible to assign different FEC levels per terminal. This is possible by introducing parallel FEC processes each with different FEC protection levels. The drawback of this option is the scalability with the number of terminals since there is a limited number of PIDs and therefore a small address range could be provided. Furthermore, the level of traffic aggregation achieved when using one PID per terminal is low. This not only increases delay and jitter but also it may decrease FEC efficiency by having to use padding to fill up the FEC Frame.

C.4.2 LL-FEC per-MODCOD

An alternative architecture solution for both MPE and GSE scenarios is shown in Fig. C.6. The underlying mechanism for providing scalability is the implementation of just one LL-FEC process per MODCOD, instead of per mobile terminal. Note that in DVB-S2 systems a few MODCODs carry most of the traffic. The limitations in data rates when employing LL-FEC require the use of load balancing within high data rate MODCODs. The architecture of LL-FEC per-MODCOD aggregates traffic per MODCOD creating an Elementary Stream per MODCOD. This means that one PID is needed per MODCOD. This architecture is highly scalable and it maintains backwards compatibility since FEC is signalled per ES and low overhead by aggregating traffic per MODCOD. However, the implementation will be more complex due to the cross-layer interface between layer 2 and the DVB-S2 mode adaptation. Furthermore, it may require signalling all FEC parameters to every terminal and enhancements to the signalling structure for GSE support. Finally, in contrast to the architecture according to Figure 5, each terminal needs to decode the whole MODCOD to extract the data being assigned to it.

C.5 Simulation Framework

A LL-FEC simulation platform has been developed in order to assess the performance of different parameter configurations without repeating the time-consuming physical layer simulations (see Fig. C.7). Given that this performance assessment entails many layers, in particular, from the physical to the network layers of the protocol stack, a modular approach has been considered. The Physical-Layer module, which generates the time series of channel dumps, interfaces with the Link Layer simulator. The rightmost module in Fig. C.7 is the simulator framework for LL-FEC. Note that we use the generic term LL-FEC and LL-FEC section in the remainder. This refers to the different frameworks, namely MPE-FEC, MPE-IFEC as well as extended MPE-FEC as specified for LL-FEC in DVB-RCS as well as GSE-FEC and GSE-FEC packets. It takes a stream of IP packets as input and applies an LL-FEC encoding technique, generating BB-frames either directly as in case of GSE or in case of MPE by first encapsulating the sections into an MPEG-2 TS and then mapping the resulting MPEG-TS packets into BB-frames. At this point, the output of the physical-layer simulator is used to mark the BB-Frames as well as all MPEG-2 TS packets within one BB-frame as correctly received or being erroneous. Next, the LL-FEC decoding process is applied by reconstructing columns of the FEC matrix applying the correction capabilities of different FEC codes. Finally, the sequence of IP packets affected by the unreliable columns (an IP packet is considered wrong if any part of it falls inside an unreliable column which cannot be corrected) is obtained and the PER at IP level is computed.

By making use of MPEG-2 TS loss patterns the LL-FEC simulator is extremely powerful to quickly assess the performance of different parameter configurations without repeating the tedious physical layer simulations.

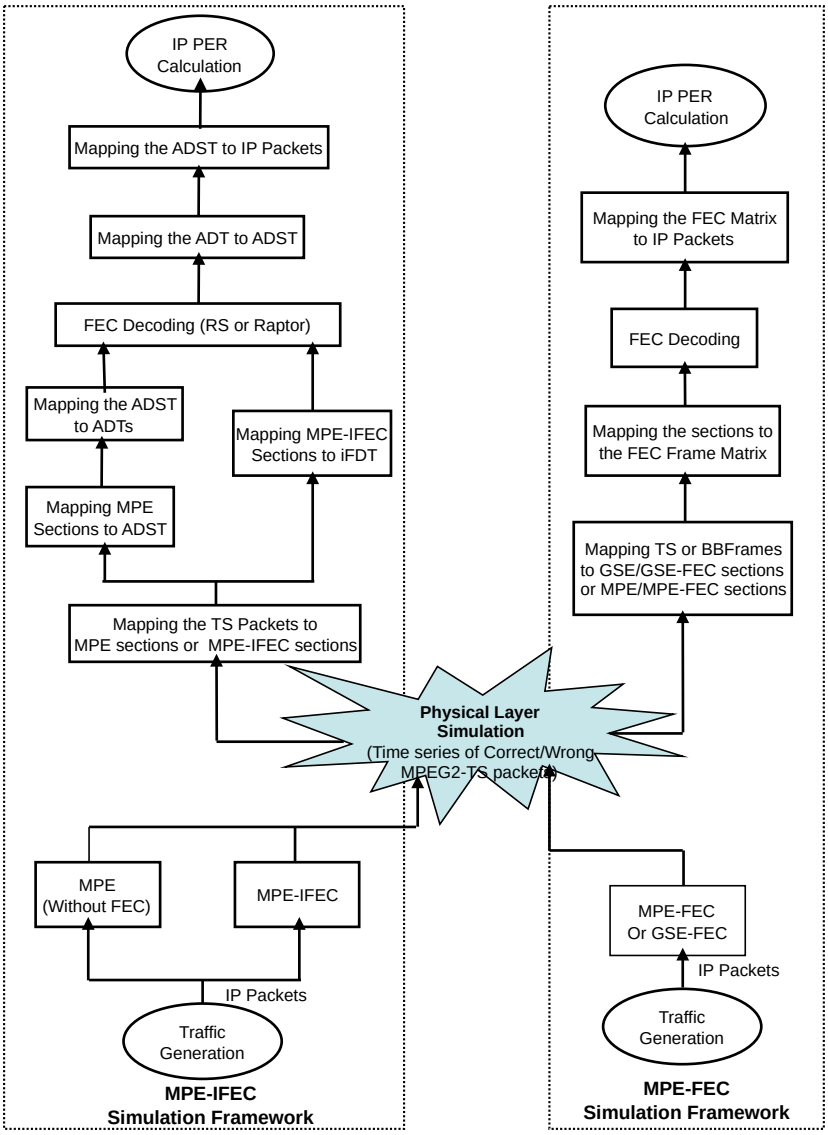

Fig. C.7: Simulation flow diagram.

C.6 Parameters Optimization and Simulation Results Analyses

Table C.II summarizes the description of the parameters, for details on other parameters such D, EP, G, B, S, R and T we refer to the MPE-IFEC specification [18]. Before conducting the simulation, we first propose some optimizations on the parameters for MPE-FEC, MPE-IFEC and extended MPE-FEC based on the specific scenario as introduced in Table C.III.

Table C.II: System and Simulation Parameters

Parameters	Description
B_s	Symbol rate
S_{ip}	Size of IP Packet
τ	Target Delay
M	Size of signal constellation (QPSK M=2, 16QAM M=4)
r_{phy}	The PHY Layer coding rate
S_{protect}	Amount of the data bit to be protected during the target delay
S_{burst}	Amount of data in each time slice burst
S_{adt}	Size of the ADT
N_{burst}	Number of bursts protected during the target Delay
r_{ll}	Link Layer coding rate
v_{train}	Vehicle velocity
N_{rows}	Number of rows of MPE-FEC Frame
l_{PA}	The duration/length of Power Arches
d_{PA}	The distance between Power Arches

Table C.III: System parameters numerical values for the LOS+PA scenario

Parameters	Value
B_s	27.5M baud/s
S_{ip}	1500 Bytes
τ	200 ms
M	2 (For QPSK); 3 (For 8PSK)
r_{phy}	1/2 (For QPSK); 3/4 (For 8PSK)
S_{burst}	512K Bytes
S_{adt}	256K Bytes
N_{burst}	10
r_{ll}	1/2 (For QPSK); 2/9 (For 8PSK)
v_{train}	100 km/h

C.6.1 Parameters Optimization

The introduced LL-FEC frameworks allow a significant variability in terms of parameter settings. The amount of data (bits) that can be protected within target delay τ can be computed as $S_{\text{protect}} = \tau B_s M r_{\text{phy}} r_{\text{ll}}$, and the size of ADT (for MPE-FEC) in the time slice burst can be derived as $S_{\text{adt}} = S_{\text{burst}} r_{\text{ll}}$. Thus, the number of ADTs that can be

protected within target delay τ is given as

$$N_{\text{burst}} = \left\lfloor \frac{S_{\text{protect}}}{S_{\text{adt}}} \right\rfloor = \lfloor \tau R_{\text{burst}} \rfloor , \tag{C.3}$$

where $R_{\text{burst}} = B_s M r_{\text{phy}} / S_{\text{burst}}$ is the rate at which bursts are transmitted. Note that for the MPE-FEC, the amount of data in each time slice burst S_{burst} cannot exceed 2 Mbits due to the addressing field being only 18-bit [17]. For the Raptor in case of LL-FEC, S_{burst} can be as large as 255 Mbits.

C.6.1.1 MPE/GSE-FEC Parameters Selection

For an RS code referred as $\text{RS}(n, k)$, n denotes the number of columns of FEC frame matrix, k is the number of columns of ADT, N_{rows} is the number of rows of FEC Frame. Optimal values of n, k and N_{rows} can be calculated with the given desired protection. E.g. $n = \lfloor S_{\text{burst}} / (N_{\text{rows}} 8) \rfloor$. The available number of FEC matrix rows for MPE-FEC is $N_{\text{rows}} \in \{256, 512, 768, 1024\}$. Then for a given k the link layer coding rate can be computed from $r_{\text{ll}} = k/n$ with known n. In addition, for the LL-FEC in DVB-RCS+M N_{rows} can be extended to 2048 and 4080 in order to be tolerant to long burst errors in the mobile scenario. In addition, one smaller value of $N_{\text{rows}} = 64$ is supported in RCS LL-FEC.

C.6.1.2 Parameters Optimization of the MPE-IFEC with RS Code

For the MPE-IFEC with RS code, $D = 0$, $EP = 1$ and $G = 1$ are assumed in order to simplify. Then $T = N_{\text{rows}} \in \{256, 512, 768, 1024\}$. n can be calculated as $n = \lfloor S_{\text{burst}} / (N_{\text{rows}} 8) \rfloor$, then k can be derived from $k = n r_{\text{ll}}$ with known n. Optimized parameters for B and S can be calculated as

$$\begin{cases} B + S = \frac{N_{\text{burst}}}{EP} = N_{\text{burst}}, \\ S = \lceil (1 - r_{\text{ll}})(B + S) \rceil = \lceil (1 - r_{\text{ll}}) N_{\text{burst}} \rceil , \\ B = N_{\text{burst}} - \lceil (1 - r_{\text{ll}}) N_{\text{burst}} \rceil . \end{cases} \tag{C.4}$$

C.6.1.3 Parameters Optimization of the MPE-IFEC with Raptor Code

Let us represent Raptor codes as $\text{Raptor}(n, k, T)$ with n and k the code parameters and with the symbols size T. For the MPE-IFEC with Raptor code, $D = 0$ and $G = 1$ are selected for minimum delay and lowest decoding complexity. Then T corresponds to the row size and can also be calculated as $T = N_{\text{rows}} \in \{256, 512, 768, 1024\}$. Furthermore, n can be derived as $n = \lfloor S_{\text{burst}} / (N_{\text{rows}} 8) \rfloor EP$. Here EP is an integer and k can be derived

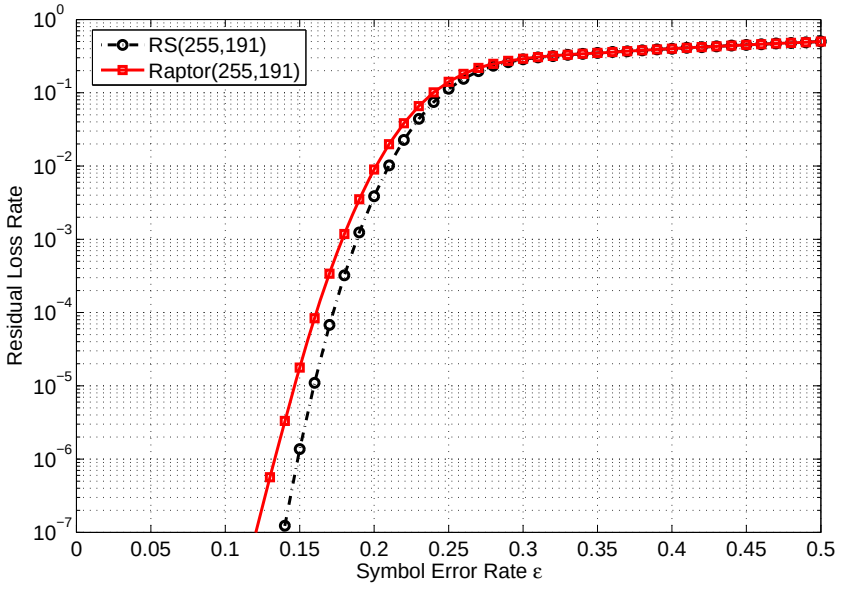

Fig. C.8: Ideal correction capability comparison of RS and Raptor code.

from $k = nr_{\mathrm{ll}}$ with known n. Then B and S can be calculated as

$$\begin{cases} B + S = \frac{N_{\mathrm{burst}}}{EP}, \\ S = \lceil (1 - r_{\mathrm{ll}})(B + S) \rceil, \\ B = (B + S) - \lceil (1 - r_{\mathrm{ll}})(B + S) \rceil. \end{cases} \tag{C.5}$$

C.6.1.4 Parameters Optimization of the Extended MPE-FEC with Raptor Code

For a $\mathrm{Raptor}(n, k, T)$, the code parameters may be $4 \leq k \leq 8192$, $k \leq n \leq 65536$, and T any power-of-two integer that divides N_{rows}. Preferably k is chosen at least as great as 1000 to keep the inefficiency of the Raptor code to below 0.2%. Therefore, for a given amount of data bit to be protected, S_{protect}, k should be selected as the smallest value larger than 1000 such that $kT \geq S_{\mathrm{protect}}$ and T any power-of-two integer that divides Nrows such that $N_{\mathrm{rows}} = GT$. Then, for a given link layer code rate r_{ll}, n is selected as k/r_{ll}. Furthermore N_{rows} may be selected appropriately to ensure $k \geq 1000$. However, obviously also values $k < 1000$ can be selected without harming the performance significantly.

C.6.2 Simulation Results Analyses

The optimized RS and Raptor code parameters in the simulation can be calculated through the approach presented above based on the specific scenario shown in Table C.III. For the target delay τ=200 ms and different MODCODs, the optimal code parameters are shown in Table C.V.

Table C.IV: Supported Code Rates (in green) for different bitrates and latency in ms for RS codes (MPE-FEC) and Raptor Codes (Extended MPE-FEC)

RS Code	Latency in ms													
Bitrate in kbit/s	10	20	40	80	160	320	640	1280	2560	5120	10240	20480	40960	81920
32	0.02	0.02	0.02	0.02	0.02	0.03	0.04	0.07	0.14	0.24	0.38	na	na	na
64	0.02	0.02	0.02	0.02	0.03	0.04	0.07	0.14	0.24	0.38	na	na	na	na
128	0.02	0.02	0.02	0.03	0.04	0.07	0.14	0.24	0.38	na	na	na	na	na
256	0.02	0.02	0.03	0.04	0.07	0.14	0.24	0.38	na	na	na	na	na	na
512	0.02	0.03	0.04	0.07	0.14	0.24	0.38	na	na	na	na	na	na	na
1024	0.03	0.04	0.07	0.14	0.24	0.38	na	na	na	na	na	na	na	na
2048	0.04	0.07	0.14	0.24	0.38	na	na	na	na	na	na	na	na	na
4096	0.07	0.14	0.24	0.38	na	na	na	na	na	na	na	na	na	na
8192	0.14	0.24	0.38	na	na	na	na	na	na	na	na	na	na	na
16384	0.24	0.38	na	na	na	na	na	na	na	na	na	na	na	na
32768	0.38	na	na	na	na	na	na	na	na	na	na	na	na	na
65536	na	na	na	na	na	na	na	na	na	na	na	na	na	na
131072	na	na	na	na	na	na	na	na	na	na	na	na	na	na
262144	na	na	na	na	na	na	na	na	na	na	na	na	na	na
524288	na	na	na	na	na	na	na	na	na	na	na	na	na	na
1048576	na	na	na	na	na	na	na	na	na	na	na	na	na	na

Raptor Code	Latency in ms													
Bitrate in kbit/s	10	20	40	80	160	320	640	1280	2560	5120	10240	20480	40960	81920
32	0.00	0.00	0.00	0.00	0.00	0.00	0.00	0.00	0.00	0.00	0.00	0.00	0.00	0.00
64	0.00	0.00	0.00	0.00	0.00	0.00	0.00	0.00	0.00	0.00	0.00	0.00	0.00	0.00
128	0.00	0.00	0.00	0.00	0.00	0.00	0.00	0.00	0.00	0.00	0.00	0.00	0.00	0.00
256	0.00	0.00	0.00	0.00	0.00	0.00	0.00	0.00	0.00	0.00	0.00	0.00	0.00	0.01
512	0.00	0.00	0.00	0.00	0.00	0.00	0.00	0.00	0.00	0.00	0.00	0.00	0.01	0.02
1024	0.00	0.00	0.00	0.00	0.00	0.00	0.00	0.00	0.00	0.00	0.00	0.01	0.02	0.04
2048	0.00	0.00	0.00	0.00	0.00	0.00	0.00	0.00	0.00	0.00	0.01	0.02	0.04	0.08
4096	0.00	0.00	0.00	0.00	0.00	0.00	0.00	0.00	0.00	0.01	0.02	0.04	0.08	na
8192	0.00	0.00	0.00	0.00	0.00	0.00	0.00	0.00	0.01	0.02	0.04	0.08	na	na
16384	0.00	0.00	0.00	0.00	0.00	0.00	0.00	0.01	0.02	0.04	0.08	na	na	na
32768	0.00	0.00	0.00	0.00	0.00	0.00	0.01	0.02	0.04	0.08	na	na	na	na
65536	0.00	0.00	0.00	0.00	0.00	0.01	0.02	0.04	0.08	na	na	na	na	na
131072	0.00	0.00	0.00	0.00	0.01	0.02	0.04	0.08	na	na	na	na	na	na
262144	0.00	0.00	0.00	0.01	0.02	0.04	0.08	na	na	na	na	na	na	na
524288	0.00	0.00	0.01	0.02	0.04	0.08	na	na	na	na	na	na	na	na
1048576	0.00	0.01	0.02	0.04	0.08	na	na	na	na	na	na	na	na	na

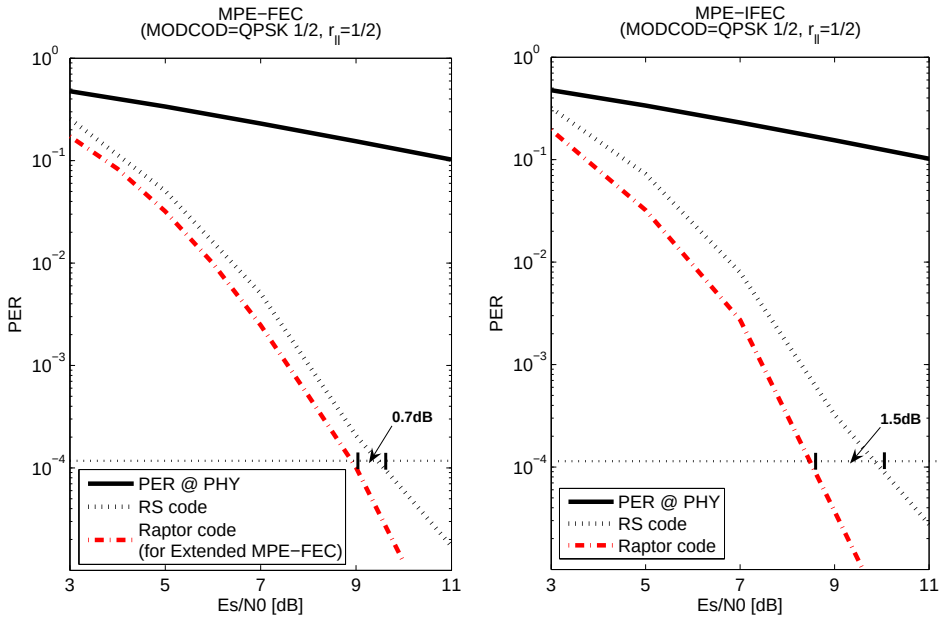

Fig. C.9: Performance comparison of RS and Raptor code for MPE-FEC and MPE-IFEC for Rayleigh channel (MODCOD=QPSK 1/2, r_{ll}=1/2).

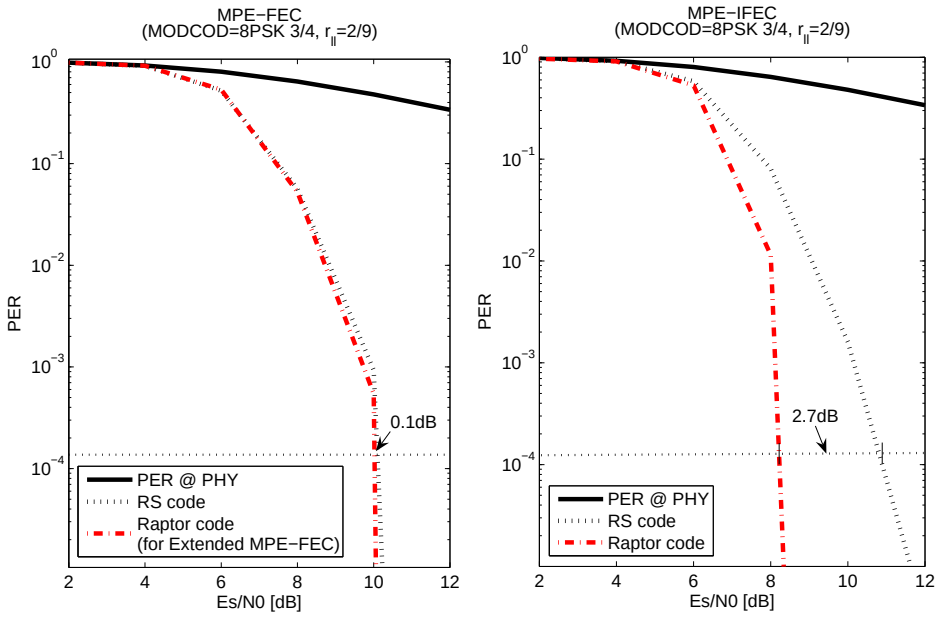

Fig. C.10: Performance comparison of RS and Raptor code for MPE-FEC and MPE-IFEC for Rayleigh channel (MODCOD=8PSK 3/4, r_{ll}=2/9).

Table C.V: Theoretical values of MTBL for the LOS+PA scenario

LL-FEC Scheme	MODCOD	FEC Codes	MTBL	
			30km/h	100km/h
MPE-FEC	QPSK 1/2	RS(128,64) N_{rows}=4096	0.65m	2.18m
	8PSK 3/4	RS(704,152) N_{rows}=2048	1.25m	4.15m
MPE-IFEC	QPSK 1/2	RS(128,64) N_{rows}=512, EP=1, B=S=5 Or Raptor(640,320) N_{rows}=512, EP=5, B=S=1	0.82m	2.73m
	8PSK 3/4	RS(81,18) N_{rows}=1024, EP=1, B=4, S=14 Or Raptor(486,108,512) N_{rows}=512, G=1, EP=3, B=1,S=5	1.28m	4.28m
Extended MPE-FEC	QPSK 1/2	Raptor(2560, 1280, 256), N_{rows}=1024, G=4	0.82m	2.73m
	8PSK 3/4	Raptor(5760, 1280, 256), N_{rows}=1024, G=4	1.26m	4.22m
GSE-FEC	QPSK 1/2	RS(128,64) N_{rows}=4096	0.33m	1.09m
	8PSK 3/4	RS(704,152) N_{rows}=2048	0.63m	2.08m

C.6.2.1 Performance Comparison of RS code and Raptor Code

It is well known that RS codes are Maximum distance separable (MDS) codes and the coding rate can be adjusted by puncturing and shorting [17]. However the decoding

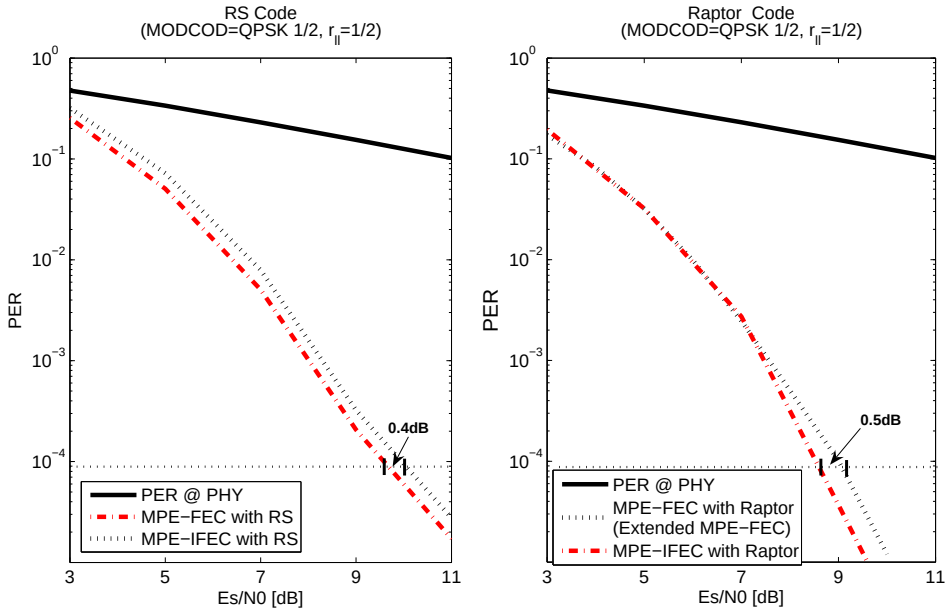

Fig. C.11: Performance comparison of MPE-FEC and MPE-IFEC for Rayleigh channel (MODCOD=QPSK $1/2$, r_{ll}=$1/2$).

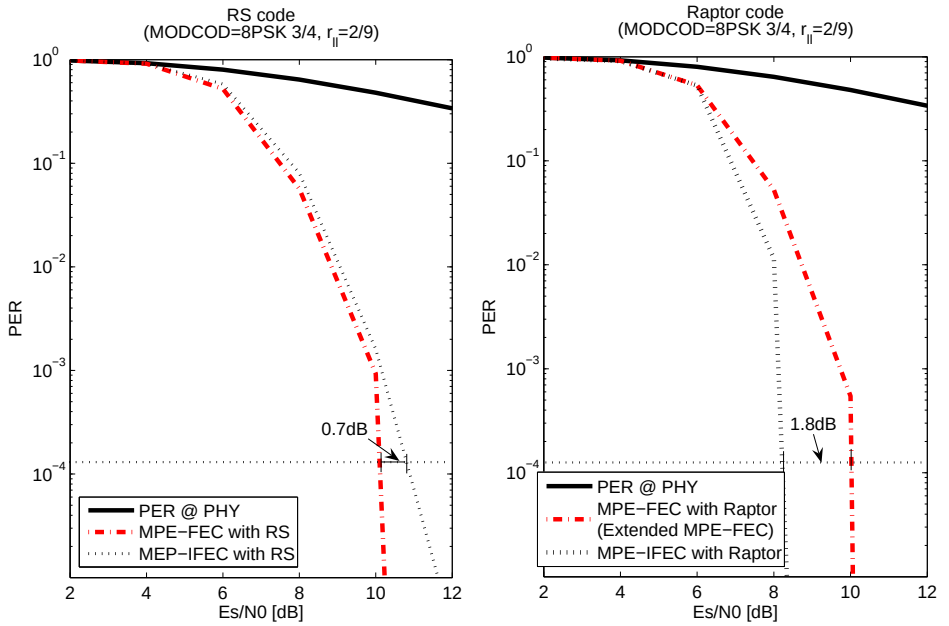

Fig. C.12: Performance comparison of MPE-FEC and MPE-IFEC for Rayleigh channel (MODCOD=8PSK $3/4$, r_{ll}=$2/9$).

complexity is very high, and generally the decoder is implemented in hardware. The Raptor codes are almost MDS codes, and the performance is very close to the ideal MDS code as shown in Fig. C.8. Moreover, Raptor code is more flexible than RS because the coding rate can be adjusted without puncturing or shorting, and the decoding can be implemented with software.

Table C.IV shows the supported code rates for different bitrates and latencies for RS codes (MPE-FEC) and Raptor codes (extended MPE-FEC). Note that the value provides the lowest code rate, any higher code rates are also supported at this latency/bitrate combination. The extended MPE-FEC supports higher bit-rates as well as latencies in much larger dimensions and is therefore significantly more suitable for the considered scenarios.

The performance of Raptor code is slightly worse than RS code as shown in Fig. C.8, because Raptor code is not ideal MDS code. But when applying to the specific environments (here we consider MPE-FEC and MPE-IFEC under Rayleigh scenario), the performance of Raptor code is better than RS code. Figure C.9 shows the performance of LL-FEC with RS code and Raptor code under $v = 100$ km/h and MODCOD=QPSK 1/2. For the target $\mathrm{PER} = 10^{-4}$, Raptor code outperforms RS code by about 0.7 dB and 1.5 dB for MPE-FEC and MPE-IFEC respectively. Figure C.10 is the same as Fig. C.9 except the MODCOD=8PSK 3/4, 0.1dB and 2.7 dB gain can be obtained by Raptor code for MPE-FEC and MPE-IFEC respectively. The reason is that Raptor code is more flexible than RS, thus it can support larger ADT and higher bit-rates. From the Table V we can see that the size ADT supported by Raptor code is larger than RS code, thus the Raptor code performs better than the RS code.

C.6.2.2 Performance Comparison of LL-FEC Frameworks

The results of this section are also based on the Rayleigh (nLOS) scenario and the system parameters are defined in Table III. Figure C.11 and Fig .C.12 show the performance of PER over the E_s/N_0 for MPE-FEC and MPE-IFEC schemes with $v = 100$ km/h and MODCOD=QPSK 1/2, 8PSK 3/4, compared to the performance without FEC. Note that for MPE-FEC with RS codes, the transmission parameters did not allow suitable parameter settings (shown in Table IV). But here we increase the column size up to 4080 Bytes for RS codes in order to compare the performance under the same target delay assumption.

Generally, a residual packet loss rate of about 10^{-4} (or even lower) needs to be achieved for data services. The uncoded performance is completely unacceptable. With the use of MPE-FEC and MPE-IFEC, the target performance can be achieved. When applying Raptor code, the MPE-IFEC outperforms MPE-FEC by about 0.5 dB and 1.8 dB for QPSK 1/2 and 8PSK 3/4 respectively, but MPE-FEC outperforms MPE-IFEC by about 0.4 dB and 0.7 dB if using RS code. Because RS is the native code for MPE-FEC, thus compatible better than MPE-IFEC.

C.6.2.3 MTBL Performance Analyses

The Performance of MTBL is analyzed for the LOS+PA scenario. The theoretical value of MTBL following the approach presented above is straightforward. We have obtained the theoretical ideal values of MTBL of 2.86 m and 4.43 m for QPSK 1/2 and 8PSk 3/4 respectively. And Table V presents the MTBL of various LL-FEC schemes showing

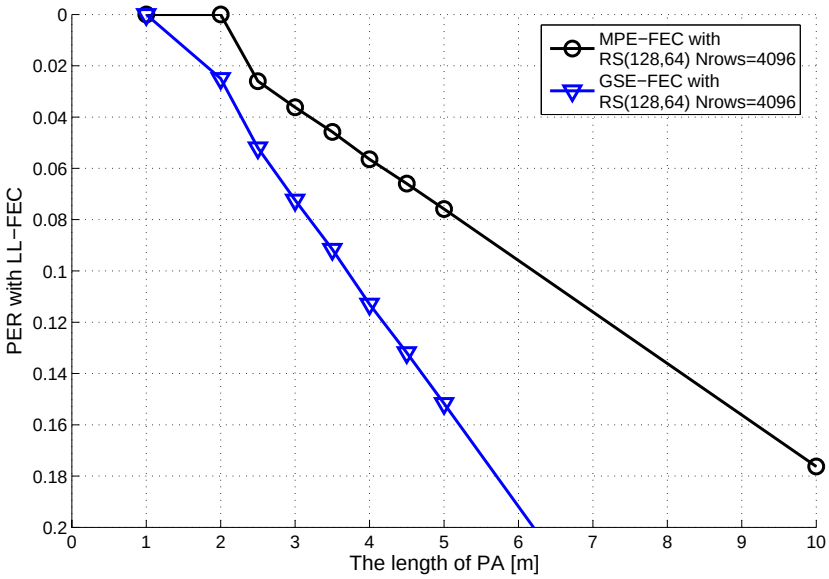

Fig. C.13: Performance comparison of MPE-FEC and GSE-FEC (PER Vs. l_{PA}).

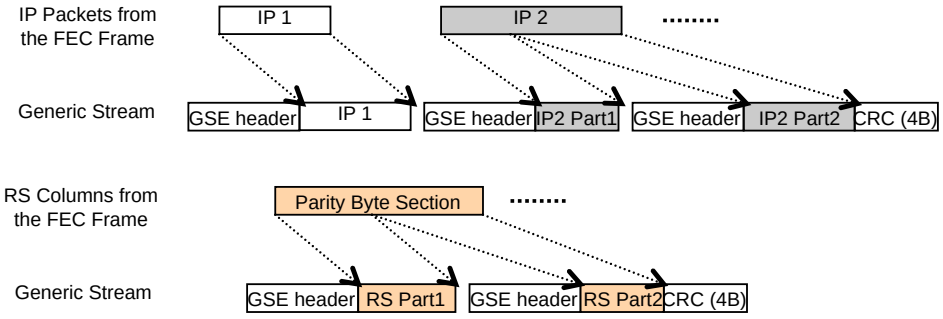

Fig. C.14: GSE encapsulation process.

a slight degradation respect to the ideal MTBL. Typical length of PAs in Europe are in the range of 0.5 m to 3 m [6; 9] and therefore the theoretical results already show that the FEC codes shown in Table V can overcome the effect of the PAs for high speeds. This is an acceptable result since the current time of the train is at speeds below 100 km/h is almost negligible.

We can also observe the performance of PER over length of PA for MPE-FEC and GSE-FEC from Fig. C.13 (only MODCOD: QPSK 1/2 is considered). The result shows that the performance of GSE-FEC is about half of the MPE-FEC because CRC is absent in some cases (see Fig. C.2 and Fig. C.14). This results in a worse decoding capability of the RS code because the positions of the erroneous bytes are unknown. Thus the performance of GSE is significant difference with respect to MPE.

It can be concluded that the codes analyzed here can be used for both protection against PA as well as Rayleigh fading. Especially by the use of the MPE-IFEC and

extended MPE-FEC with Raptor codes as finally specified in DVB-RCS+M consistently show superior results than with other link layer FEC for railway scenarios.

C.7 The Impact of Migration LL-FEC to GSE

The FEC Frame of GSE is the same with MPE. However, the encapsulation of Sub-Network Data Unit (SNDU) sections is different (shown in Fig. C.14). GSE protocol [22] allows for direct encapsulation of IP and other network-layer packets over DVB-S2 physical layer frames. The IP datagrams and RS columns are encapsulated in one or more GS units. Each GS unit is constructed of a GS header and a Data Field. The CRC part is only added at the end of the last fragmented GS unit, as opposed to MPE sections as shown in figure 2 where the CRCs are added at the end of every SNDU sections.

In [23; 24], the authors discussed the application of GSE-FEC in DVB-S2 systems and give the results of the encapsulation efficiency comparison between GSE-FEC, MPE-FEC and Ultra Light Encapsulation-FEC (ULE-FEC). The results show that GSE-FEC is more efficient than MPE/ULE-FEC for the encapsulation of IP datagrams. However, the results of the performance comparison in section C.6 show that GSE-FEC is bad due to the fact that there is no CRC for unfragmented GS units, as shown in Fig. C.14. Thus, the receiver cannot detect all the erroneous GS units except the ones protected by the CRC. This results in a worse decoding capability of the RS code because the position of the erroneous bytes is unknown. Note that GSE was designed with DVB-S2 in mind, which is considered as a Quasi-Error Free (QEF) environment. Hence, GSE only requires a CRC when a datagram fragmented.

In order to implement GSE-FEC in DVB-S2 and DVB-RCS standards without decreasing the performance, the necessary modifications of GS units' format are indispensable. Therefore we propose to use the extension header to introduce the CRC and also to signal in the real-time parameters field in the section header.

C.8 Conclusion

The performance of the LL-FEC codes and frameworks available in the DVB family has been analyzed by means of a simulation framework for LL-FEC over DVB-S2 that allows to optimize the FEC parameters. Two typical railway scenarios have been analyzed: LOS+PA and nLOS. Both theoretical and simulation analysis reveal that LL-FEC can overcome the fade in the railway scenario by selecting appropriate FEC codes. In particular, we have shown that MPE-FEC completely removes the effect of PAs for high speeds only, due to the fact that the target protection delay is limited in the current version of the standard. Finally, we have proved that the analyzed DVB LL-FEC and frameworks are more suitable for the LOS+PA scenario than for the Rayleigh scenario, which needs a relatively high Es/No to achieve a good perfor-

mance. This is due to the important fact that the Rayleigh channel is not an erasure channel. Further, we show that the best performance combination is MPE-IFEC with Raptor codes. We also show that achievable performance may not be actually reached in some cases due to current signaling settings. As for practical implementation, we propose two possible novel cross-layer architectures for unicast DVB-S2 in order to provide QoS. The architectures allow the migration from traditional packet encapsulation based on MPEG2-TS to new schemes such as the Generic Stream Encapsulation, GSE and the impact of the migration on LL-FEC is discussed at the end of the paper and indicates that necessary modifications should be studied for the header of the GS units and the corresponding signaling tables.

Acknowledgment

The authors would like to express their gratitude to the University of Bologna (UoB) for providing the physical layer time series of the nLOS scenario, allowing us to achieve the results presented in this paper. Also the collaboration with the experts in the DVB TM-RCS group, led by Dr. Harald Skinnemon, was a great pleasure and significantly inspired this work. The authors also would like to thank the anonymous reviewers for their constructive comments and suggestions that greatly helped improve the final quality of this paper.

Bibliography

[1] ETSI EN 300 421 v1.1.2, Digital Video Broadcasting (DVB): Framing structure, channel coding and modulation for 11/12 GHz satellite services, Aug. 1997.

[2] ETSI EN 302 307 v1.1.1, Digital Video Broadcasting (DVB): Second generation framing structure, channel coding and modulation system for Broadcasting, Interactive Services, News Gathering and other broadband satellite applications, June 2004.

[3] DVB BlueBook A054r4.1, Digital Video Broadcasting (DVB): Interaction channel for satellite distribution systems (draft EN 301 790 V1.5.1 - DVB-RCS+M), Jan. 2009.

[4] ETSI EN 302 304 v1.1.1, Digital Video Broadcasting (DVB): Transmission System for Handheld Terminals (DVB-H), Nov. 2004.

[5] ETSI TS 102 585 v1.1.1, Digital Video Broadcasting (DVB): System Specifications for Satellite services to Handheld devices (SH) below 3 GHz, July, 2007.

[6] S. Scalise, R.Mura, and V.Mignone, "Air Interfaces for Satellite based Digital TV Broadcasting in the Railway Environment," *IEEE Trans. on Broadcast,* vol. 52, no. 2, pp. 158 - 166, 2006.

[7] A. Shokrollahi, "Raptor Codes," *IEEE Trans. on Inform. Theory.,* vol. 52, no. 6., pp. 2551 - 2567, Jun. 2006.

[8] 3GPP TS26.346, "Multimedia Broadcast/Multicast Service (MBMS): Protocols and Codecs (release 8)," Sep. 2008.

[9] E. Lutz, M. Werner, and A. Jahn, *Satellite Systems for Personal and Broadband Communications.* Springer, New York, NY, USA, 2000.

[10] A. D. Panagopoulos, P. D. M. Arapoglou, and P. G. Cottis, "Satellite Communications at Ku, Ka, and V Bands: Propagation Impairments and Mitigation Techniques," *IEEE Commun. Surveys and Tutorials,* vol. 6, no. 3, pp. 2 - 14, 2004.

[11] E. Kubista, F. P. Fontan, M. A. V. Castro, S. Buonomo, B. R. Arbesser-Rastburg, and J. P. V. Polares Baptista, "Ka Band Propagation Measurements and Statistics for Land Mobile Satellite Applications," *IEEE Trans. on Veh. Technol.,* vol. 49, no. 3, pp. 973 - 983, 2000.

[12] A. Benarroch and L. Mercader, "Signal Statistics obtained form a LMSS Experiment in Europe with the MARECS Satellite," *IEEE Trans. on Commun.*, vol. 42, no. 2-4, pp. 1264 - 1269, 1994.

[13] S. Cioni, A. Vanelli-Coralli, C. P. Niebla, S. Scalise, G. S. Granados and M. A. Vázquez Castro, "Antenna Diversity and GSE-based packet level FEC for DVB-S2 systems in Railway scenarios", in *Proc. 25th AIAA Int. Commun. Satellite Systems Conf.,* Seoul, South Korea, Apr. 2007.

[14] F.P. Fontan, M. A. Vázquez Castro, C.E. Cabado, J.P. Garcia, and E. Kubista, "Statistical Modeling of the LMS Channel", *IEEE Trans. on Veh. Technol.,* vol. 50, no .6, pp. 1549 - 1567, Nov. 2001.

[15] Pérez-Fontán, F., Gonzalez, J. P., Ferreiro, M. J. S., M. A. Vázquez Castro, Buonomo, S., and Baptista J. P., "Complex Envelope Threestate Markov Model based Simulator for the Narrow-band LMS Channel", *Int. Journal on Satellite Commun.*, vol. 15, no. 1, pp. 1 - 15, Dec. 1998.

[16] ETSI TS 102 034 v1.3.1, Digital Video Broadcasting (DVB): Transport of MPEG 2 Transport Stream (TS) Based DVB Services over IP Based Networks, Mar. 2005.

[17] ETSI EN 301 192 v1.4.1, Digital Video Broadcasting (DVB): DVB Specification for Data Broadcasting, Nov. 2004.

[18] DVB Bluebook DVB A131, MPE IFEC, November 2008.

[19] P. Marco F. Rosario C. Giovanni and E. V. C. Alessandro, "On The Application of MPE-FEC to Mobile DVB-S2: Performance Evaluation in Deep Fading Conditions" in *Proc. Int. Workshop on Satellite and Space Commun.,* Salzburg, Austria, pp. 223 - 227, Sep. 2007.

[20] ETSI TS 102 472 v1.2.1, IP Datacast over DVB-H: Content Delivery Protocols (CDP), June 2006.

[21] F. Vieira, M. A. Váquez Castro, and J. Lei, "Datacast Transmission Architecture for DVB-S2 Systems in Railway Scenarios," in *Proc. 10th Int. Workshop on Signal Process. for Space Commun.,* Rhode Island, Greece, Oct. 2008

[22] ETSI TS 102 606 v1.1.1, Digital Video Broadcasting (DVB): Generic Stream Encapsulation (GSE) Protocol, Oct.2007.

[23] J. Lei, G. S. Granados, and M. A. Váquez Castro, "MPE/ULE-FEC vs GSE-FEC Efficiency Comparison of IP Datagram Transmission over DVB-S2," in *Proc. 25th AIAA International Communications Satellite Systems Conference*, Seoul, South Korea, Apr. 2007.

[24] A. Mayer, F. Vieira, J. Lei, B. Collini-Nocker, and M. A. Váquez Castro, "Analytical and Experimental IP Encapsulation Efficiency Comparison of GSE, MPE, and ULE over DVB-S2", in *Proc. Int. Workshop on Satellite and Space Commun.,* Salzburg, Austria, pp. 114 - 118, Sep. 2007.

Paper D

Link layer FEC for quality-of-service provision for Mobile Internet Services over DVB-S2

J. Lei, M. A. Vázquez Castro, T. Stockhammer, and F. Vieira

International Journal of Satellite Communications and Networking, vol. 28, no. 3-4, pp. 183 - 207, 2010.

Abstract

This paper presents the performance that can be achieved when applying forward error correction (FEC) at the link layer (LL) level for Digital Video Broadcasting (DVB)-S2-based transmission to attain reliable reception in mobile environments. Our scenario of interest is the interactive railway scenario with two different channel assumptions: Line-of-Sight together with the effect of railway Power Archers (LOS+PA) and non-Line-of-Sight (nLOS). We analyze the performance and compatibility of the different LL-FEC schemes already available in the DVB family of standards: Multiple Protocol Encapsulation-FEC (MPE-FEC) and MPE Inter-Burst FEC (MPE-IFEC). We compare their performance when adopting Reed-Solomon (RS) or Raptor FEC Codes. Both theoretical and simulation analysis reveal that LL-FEC can overcome the fade in the railway scenario by selecting appropriate FEC codes. The solution finally adopted by the DVB-RCS+M standard is discussed and two cross-layer transmission architectures are presented that allow adaptive Quality-of-Service provision over generic LL encapsulation.

D.1 Introduction

The growing demands for higher data rates for mobile devices are satisfied by new standards for mobile services such as Universal Mobile Telecommunications System (UMTS), High-Speed Packet Access (HSPA), mobile WiMAX (IEEE 802.16e), Digital Video Broadcasting for handhelds (DVB-H and DVB-H2) [1] and the DVB specification for satellite services to handheld devices (DVB-SH) [2]. However, most of these systems have significant coverage restrictions and generally cannot provide a universal data connectivity. Therefore, complementary satellite-based systems, in particular DVB-S2/RCS+M appears to be an ideal candidate for universal data connectivity, also as it can ideally combine digital TV broadcast reception in mobile environments and IP multimedia services. Furthermore, if remote vehicles such as trains or ships can be easily equipped with IP connectivity through satellite backhauls, mobile GSM base stations may be created providing connectivity to standard terminals. However, DVB-S2 and DVB-RCS+M have not been designed for mobile use. Terminals installed in a mobile platform, such as train, ship, or aircraft, are exposed to challenging environments that will impact the system performance since the current standard lacks any specific provision for mobile scenarios. An attractive solution is to adopt the DVB-S2 with Single Carrier Per Channel (SCPC) mode to support the mobile services of DVB-RCS+M by extending the system such that legacy DVB-S2 hardware can be reused and modifications are only applied on the LL.

In general, mobile terminals experience critical signal impairments in the synchronization acquisition and maintenance since the mobile channel undergoes shadowing and fading due to mobility, as well as deep fading due to blockage.

In this paper, we focus on the specific mobile scenario with collective terminals, such as ships, trains, and plains. link layer forward error correction (LL-FEC) will be introduced as a fading countermeasure for DVB-S2/RCS in mobile environments. We describe the selected solution after a critical analysis of the various existing LL-FEC frameworks, namely Multiple Protocol Encapsulation/Generic Stream Encapsulation-FEC (MPE/GSE-FEC) and MPE Inter-Burst FEC (MPE-IFEC). Moreover, the performance of different codes, namely Reed-Solomon (RS) codes and Raptor codes [3] (also specified in 3GPP [4], DVB and IETF) are investigated within the different LL-FEC frameworks. Typical railway scenario, burst erasure channel, is used to analyze the performance of FEC.

The rest of this paper is organized as follows. Section D.2 introduces the system and application framework of DVB-RCS. Section D.3 identifies the available LL-FEC codes and frameworks in the DVB family standards. Section D.4 proposes two novel QoS cross-layer architectures for DVB-S2 datacasting. Section D.5 discusses how to optimize the code parameters for different FEC schemes and Section D.6 presents the selected experimental results. Finally, the summarizing conclusions are presented in

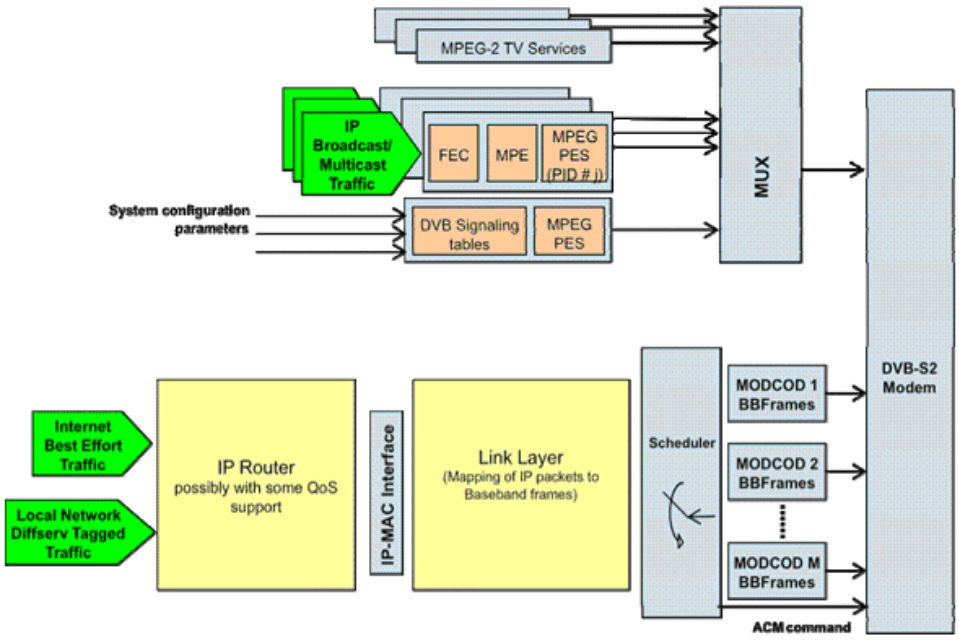

Fig. D.1: DVB RCS Architecture for mobile applications

Section D.7.

D.2 System and Application Framework

D.2.1 Architecture

DVB-S2/RCS is a technical standard that is designed by the DVB Project and defines a complete air interface specification for two-way satellite broadband very small aperture terminal (VSAT) systems. DVB-S2/RCS provides users with the equivalent of an ADSL or cable Internet connection, without the need for local terrestrial infrastructure. The mobile extension, referred to DVB-RCS+M specifications [5], provides support for mobile and nomadic terminals as well as enhanced support for direct terminal-to-terminal (mesh) connectivity. DVB-RCS+M includes the features such as live handovers between satellite spot-beams, spread-spectrum features to meet regulatory constraints for mobile terminals, and continuous carrier transmission for terminals with high traffic aggregation. It also includes link-layer FEC based on Raptor or RS codes, used as a countermeasure against shadowing and blocking of the satellite link as will be discussed in this work.

We focus on DVB-S2 extension to mobile as generally most of the data are transmitted to the terminals. However, it should be noted that the solutions described here are applicable for both the forward and the return link, since DVB-S2 can be used in the return when used in an SCPC mode. The forward link is shared among a population of terminals using either DVB-S [6] or the highly efficient DVB-S2 standard

Table D.I: QoS Categories: Error Tolerance, Typical Bitrate and Delay Requirements

	Conversational video and voice (e.g. VolP, Video conference)	Voice/video messaging	Streaming audio and video	Fax
Error tolerant	32 kbit/s-1 Mbits	32 kbit/s-1 Mbits	16 kbit/s-2 Mbit/s	16-128 kbit/s
Error intolerant	Command/control	Transaction (e.g. web browsing)	Messaging download (e.g. file download, e-mail)	Background (p2p traffic, etc.)
	4-64 kbit/s	16 kbit/s-2 Mbit/s	16kbit/s-2 Mbit/s	16kbit/s-2 Mbit/s
	Interactive (delay $\ll$ 1s)	Responsive (delay=2s)	Timely (delay=10s)	Non-critical (delay$\gg$10s)

[7] as shown in Fig. D.1. In this work we concentrate on DVB-S2 as this standard is state-of-the-art and already widely deployed. By the use of DVB-S2 features, adaptive transmission by the use of different modulation and coding schemes (MODCOD) to overcome variations in channel characteristics can be implemented. The QoS can even be selected in parallel by the use of different pipes, each one with a different MODCOD scheme. The LL in DVB-RCS maps IP packets to DVB-S2 baseband frames. DVB-RCS entry gateways can be viewed as IP routers, whereby the IP routers themselves provide the support of QoS by the use of appropriate LL technologies and the selection of a MODCOD scheme. DVB-S2 typically provides bitrates as high as several tens of Mbit/s. However, as DVB-S2 is not designed to cope with fading resulting from mobility, the LL is required to contain methods not only to support high QoS, but also to flexibly assign QoS to different IP traffic classes, depending on their requirements. To understand these requirements we will introduce some typical applications along with their QoS requirements.

D.2.2 Services and application requirements

The key to successful services is a high quality of experience from the perspective of the enduser. By considering a range of applications involving the media of voice, video, image and text, and the parameters that govern end-user satisfaction for these applications, a broad classification of end-user QoS categories can be determined. These categories can be used as the basis for deriving realistic QoS classes and associated QoS control mechanisms for the underlying transport networks. A major challenge for emerging wireline and wireless IP-based networks is to provide adequate Quality of Service (QoS) for different services. This requires a detailed knowledge of the performance requirements for particular services and applications.

Key parameters that influence the user perception are among others, the *delay*, *delay variations*, *information loss rates*, and the *available bitrates*. Delay has a direct impact on user satisfaction depending on the application, and includes delays in the terminal, network, and any servers. Delay variation is very important due to

the inherent variability in the arrival times of individual packets and the resulting consequences, in particular, for low-delay applications. Information loss has a very direct effect on the quality of the information finally presented to the user, whether it is voice, image, video, or data. Finally, the available bitrate is crucial for the service quality.

Table D.I provides an overview on typical QoS categories in terms of error tolerance, bit rate requirements and permitted delay according to [8]. It can be observed that for a system that offers a large variety of services, it is important to also provide a wide variety of QoS classes. It is also obvious that by understanding the QoS requirements (e.g. error tolerance, delay tolerance), these tolerances should be taken into account to provide the most efficient transport to support as many users with as many services as possible. Therefore, even for mobile DVB-S2/RCS systems, it is desirable to support this large variety of QoS parameters. In particular, it needs to be taken into account that though low loss rates and low delays are necessary on the one hand, larger delays up to several seconds or even tenth of seconds can also be permitted. Furthermore, typical service bitrates are between several kbit/s up to several Mbit/s.

D.2.3 Channel characteristics for mobile reception

Neither DVB-S2 nor RCS has been designed for mobile use. Terminals installed in mobile platforms, such as trains, ships, aircraft, trucks or other vehicles are exposed to challenging environments that will impact the system performance since these baseline standards lack any specific provision for mobile scenarios. The land mobile satellite channel (LMSC) has been widely studied in the literature [9]. Several measurement campaigns have been carried out and a number of narrow and wideband models have been proposed for a wide range of frequencies, including Ku [10] and Ka [11] bands. Nevertheless, for the specific case of railway environment, only a few results are available in [12] as a consequence of a limited trial campaign using a narrowband test signal at 1.5 GHz.

For LMSC channels typically it is observed that the signal-to-noise ratio at the receiver varies significantly. This may result from different reasons such as shadowing and fast fading due to mobility, as well as deep and frequent fades, for example, resulting from the presence of metallic obstacles along electrified lines and long blockages in railway environments. For example, results of direct measurements performed along the Italian railway aiming to characterize these peculiar obstacles [13] showed that, the attenuation introduced by the power arches (PA) increases to values as high as 10 dB and beyond when compared with Line-of-Sight (LOS) receptions, depending on the geometry, the antenna radiation pattern and the carrier frequency. Furthermore, in certain circumstances, LOS to the satellite is heavily obstructed, for example, if the receiver moves in some urban areas. Typically, due to reflections and scattering multipath, signals are received that result in typical correlated Rayleigh fading, the directivity is taken into account by shaping the spectrum. Therefore, in this work we focus on railway channel models that have, for example, been introduced in [13; 14]

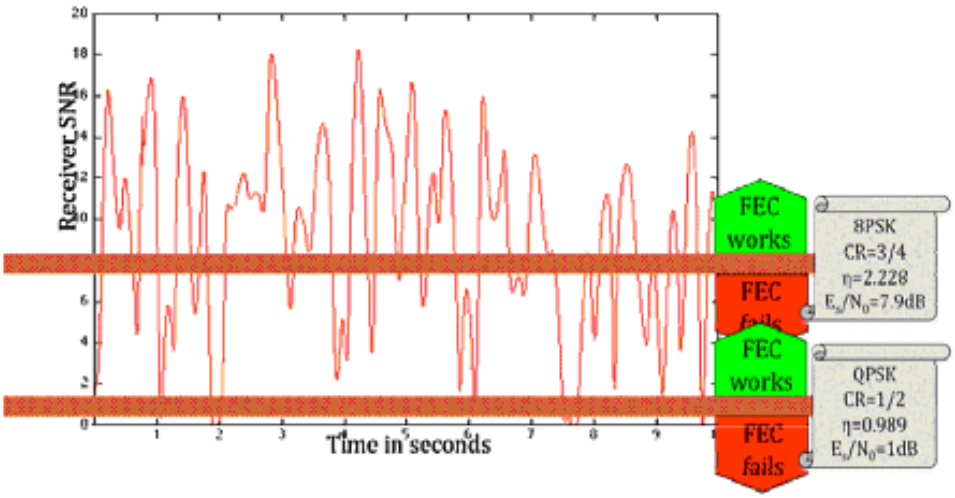

Fig. D.2: Example receiver SNR in dB in mobile satellite environments and effects of using DVB-S2 channel coding with different coding and modulation schemes.

and the Land Mobile Satellite channel models have been discussed in [11; 15; 16].

- LOS+PA channel. The presence of PAs in the railway environment is modelled as a significant drop in receiver SNR by at least dB. The duration t_{Burst} and periodicity P_{Burst} of these outages depend on the geometric width of the power arches l_{PA}, the distance between two consecutive PAs d_{PA} and the speed of the receiver v_{train} as $t_{\text{Burst}} = l_{\text{PA}}/v_{\text{train}}$ and $P_{\text{Burst}} = (l_{\text{PA}} + d_{\text{PA}})/v_{\text{train}}$.

- nLOS channel. The non-LOS reception conditions typically result in correlated Rayleigh fading due to Doppler effects. The Doppler frequency f_{Doppler} of the fading depends on the carrier frequency f_{carrier} and the receiver speed as $f_{\text{Doppler}} = f_{\text{carrier}} v_{\text{train}}/c$ with c the speed of light. Such correlated fading can typically be simulated by using Jakes [17]. Owing to the expected short echos in the LMSC channel, typically only a single delay component is considered, nor tap-delay line. For modelling such a channel we refer to [17]. For simulation purposes, an extensive amount of time series on the receiver SNR has been produced from such a radio simulation tool that can be used for the simulations for our purposes. The nLOS channel model is fully characterized by the average receiver SNR and the Doppler frequency f_{Doppler}.

D.2.4 Modulation and channel coding for mobile channels

As shown in Fig. D.1 by the application of channel coding and modulation the base band frames are mapped to the DVB-S2 modem. The application of a certain coding and modulation scheme results that receivers that experience a certain receiver SNR at a specific point of time can either decode the encapsulated baseband frame or fail to do so. Note that over short observation intervals corresponding to the length of a

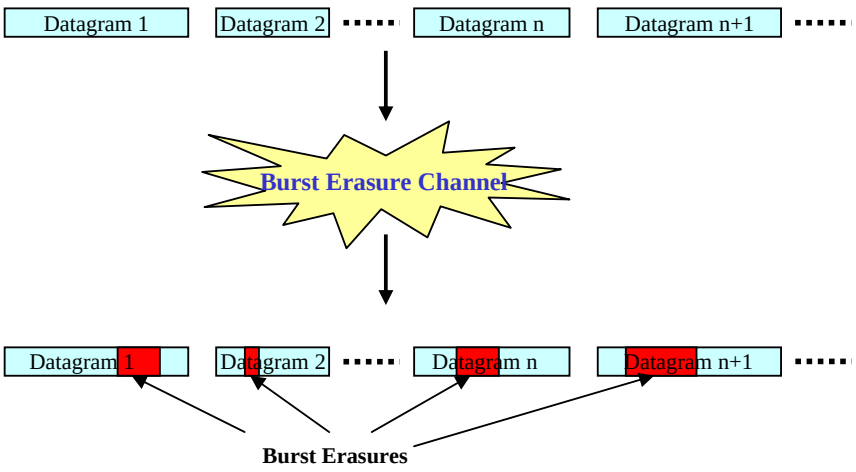

Fig. D.3: Burst erasure channel.

baseband frame, the channel can be assumed as an additive white Gaussian noise (AWGN) channel.

Therefore, due to the brick wall properties of the applied LDPC codes that for an AWGN channel it works almost perfectly above a certain signal-to-noise ratio and that it completely fails below, the effects of the application of a certain coding and modulation scheme to a time series of receiver SNRs can be quite easily modelled. The conversion from receiver SNR series to baseband loss series is performed by considering 'wrong' frames for all of the frames that experience a receiver SNR lower than equal to a decoding threshold E_S/N_0 (in dB) and 'correct' frames for a receiver SNR greater than equal to a decoding threshold E_S/N_0. The decoding threshold E_S/N_0 depends on the coding and modulation parameters defined by the input parameters. Table 13 in [7] summarizes this decoding threshold E_S/N_0 for many different coding and modulation schemes and also provides the spectral efficiency η per unit symbol rate of the individual coding schemes. For details refer to [7].

Fig. D.2 illustrates this process: First of all it shows a typical receiver SNR in dB in mobile satellite environment over time in this case for 10 s. It is obvious that the dynamic range of the receiver signal is quite high over a short period of time and this results in significant challenges in the system design. By the application of a specific coding scheme and by the use of a cyclic redundancy check (CRC) code, the receiver SNR series is converted to a series of base band frame losses. The figure shows the application of two schemes, namely QPSK code rate 1/2 and 8PSK with code rate 3/4. The corresponding decoding thresholds and the spectral efficiencies of both schemes are provided. It is obvious that the remaining baseband frame loss rates for lower spectral efficiencies is significantly lower at the expense of lower supported bitrates, whereas for higher spectral efficiencies loss rates and also supported bit rates are higher.

For a DVB-S2 system with symbol rate B_s, the use of a modulation constellation with modulation order M in bit/symbol and the application of a normal FEC frame

with $S_{\text{FECFrame}} = 64800$ bit for the LDPC code word, the baseband rate R_{BB} is given as $R_{\text{BB}} = B_s M / S_{\text{FECFrame}}$. The size of the base band frame S_{BBFrame} depends on the applied physical layer code rate r_{phy} according to [7]. For our cases with code rate $r_{\text{phy}} = 1/2$ and $r_{\text{phy}} = 3/4$, the resulting baseband frames have size $S_{\text{BBFrame}} = 32208$ bit and $S_{\text{BBFrame}} = 48408$ bit, respectively.

Note that the service bitrate R_{service} is directly obtained as $R_{\text{service}} = S_{\text{BBFrame}} R_{\text{BB}}$. A typical symbol rate for DVB-S2 is B_s = 527.5Mbaud/s, but other symbol rates are supported by different transponders.

By the application of these principles the DVB-S2 physical layer with a specific coding and modulation scheme can be converted to a baseband frame erasure channel with baseband rate R_{BB} and baseband frame size S_{BBFrame} depending on the code rate r_{phy}, for details refer to [7].

Based on these preliminaries, the two introduced channel models can be further simplified as follows.

- For the LOS+PA channel the presence of PAs in the railway environment resulting in signal drops of at least 10 dB and with duration tBurst can be modelled as a sequence of baseband frame erasures as it is expected that under PA, the baseband frame is lost and under LOS the signal is received. Therefore, an ON/OFF model can be assumed: during the 'ON State', the baseband frame loss rate of the signal equals to 0. During the 'OFF State', the baseband frame loss rate equals to 100%. The number of baseband frames lost during the PA is $N_{\text{BB PA}} = \lceil t_{\text{Burst}} R_{\text{BB}} \rceil$ which alternates with $P_{\text{Burst}}\ R_{\text{BB}} - N_{\text{BB PA}}$ correct baseband frames. Note that if this number is not an integer then ceil and the floor of this number is selected with an appropriate distribution.
- For the nLOS channel the time series of fading patterns can be converted to a sequence of received and lost baseband frames as shown in Fig. D.2. The loss/reception can be detected by the use of CRC such that the time series are as simple as 0 and 1 s.

Based on these preliminaries, we model the mobile channel for collective terminals as a *burst erasure channel* (as shown in Fig. D.3 for the power arch case), in which each transmitted baseband frame is either received correctly or is corrupted so badly as to be considered erased. As the erasures are generally clustered together and not statistically independent, we refer to the channel as Burst Erasure Channel.

D.2.5 Fading countermeasures

To counteract the fading from mobile transmission, additional measures need to be introduced such that the QoS requirements according to Table can be fulfilled. The countermeasures need to ensure that service constraints are fulfilled and at the same time that the integration of such measures is as efficient as possible. Four different countermeasures are briefly discussed in the following.

D.2.5.1 Physical layer FEC interleaving

Typically, QoS measures reside on the physical layer, in particular FEC techniques. To compensate signal variations in combination with FEC, typically interleaving is applied, such that a code word is spread over multiple milliseconds or even seconds. By interleaving and the use of good physical layer codes such as LDPC codes in S2, such signal variations can be overcome as long as the interleaver depth is long enough to 'average out' the signal drops. This is a very efficient means to address these types of variations. However, typically the signal drops are in the range of several 10 or even 100 ms such that the interleaver depth should be in the range of seconds. The memory requirements at the receiver are at least in the order of the product of the service bitrate (27.5 Mbaud/s), the symbol constellation, the interleaver depth and the resolution of the soft values in the receiver, so several 100MBit per second interleaver depth are necessary. Such a modification would require a new design of DVB-S2 receiver chips and would also require a modification of the DVB-S2 specifications and hard sending and receiving equipment. Therefore, such solutions are generally considered far too cost intensive to be economically viable. Alternative solutions are therefore required.

D.2.5.2 LL retransmission

A common solution to address the losses of radio frames in mobile communication is the application of Automatic Repeat request (ARQ) protocols to request the retransmission of lost radio frames. In the context of our envisaged system, such a solution may be attractive as well. However, obviously for retransmission in any case a back-channel is needed. In case of a multicast/broadcast service, such a back channel is generally not available due to scalability reasons. In case of unicast transmission, such back-channels generally exist and may be employed. However, due to the long transmission delays on the satellite, an ARQ scheme causes significant delays due to the extensive round trip delays of several 100 ms up to one second, which is incompatible with many of the QoS requirements as discussed earlier. Therefore, retransmission solutions have limited applicability in the context of DVB-RCS+M systems.

D.2.6 Application layer reliability

IP protocol stacks typically also include the means for reliable distribution of data. TCP incorporates retransmission features, and other protocols as defined in the IETF Reliable Multicast Transmission (RMT) working group or IETF FEC Framework (FECFRAME) can also be used to support reliability above the IP layer. The advantage in this case is that the solutions are integrated in the IP protocol stack. However, such solutions are specific to each application and typically not considered in QoS frameworks for which the transport layer shall support the QoS means. Also, some of the features such as TCP retransmissions are not suitable for protecting against radio frame

losses. Overall, the use of the application layer reliability generally requires a tight coupling between the applications and the transport and is not suitable for generic QoS supported frameworks.

D.2.6.1 Link-layer forward error correction

Instead of applying retransmission, another method to address the loss of radio frames is the application of FEC on the LL, usually referring to an erasure correction scheme. In this case, some portion of the baseband frames are proactively filled with repair symbols that can be reused by the receivers to overcome baseband frame losses. The advantage in this case compared with physical layer interleaving is that the memory and processing requirements are generally significantly reduced (at the expense of slightly lower efficiency) and the tools can be implemented on top legacy hardware and specifications. Such methods can be used for unicast and multicast distribution and no back-channels are required. As this scheme has many advantages compared with physical layer interleaving, retransmission and application layer reliability, it has been integrated in DVB-RCS+M and we will discuss such schemes in more detail in the following.

D.3 Link-Layer FEC in DVB RCS+M

D.3.1 Requirements

As already indicated, an excellent fading countermeasure is the application of FEC on the LL. Following our discussion, we will investigate the integration of link-layer FEC into DVB RCS+M. To motivate the choices, we will summarize the requirements for such a solution taking into account the application requirements as well as QoS frameworks. According to the application portfolio that should be supported bitrates range up to several MBit/s. In addition, as in several QoS frameworks multiple applications may be combined in a single service class, bitrates as large as the multiplex need to be supported, that is, up to 30 MBit/s and even beyond. The latencies that are permitted to range over several seconds and for exploiting full time diversity, time interleaving of at least 10 s should be supported. It is required that the LL-FEC permits to guarantee quasi-free packet loss rates in the range of 10¨C4 and below. This requires that some potentially low code rates need to be applied. Furthermore, the LL-FEC needs to be integrated into existing unicast and multicast protocol environments based on MPE and GSE. Based on this summary, LL-FEC codes are required that permit large block sizes, typically defined by the product of the bitrate and the protection period, a wide range of parameter in terms of protection periods and code rates as well as the flexibility to integrate them into different protocol environments.

D.3.2 Available LL-FEC codes In DVB

RS and Raptor codes are applied for this purpose. DVB RCS+M has decided to support both codes, RS codes and Raptor codes. We will briefly summarize their properties in the following.

D.3.2.1 RS codes

The first LL-FEC codes integrated in DVB were RS codes as currently applied in the first generation of DVB family of standards, that is, DVB-C, DVB-S and DVB-H. RS codes are block codes, that is, a fixed block of input data is processed into a fixed block of output data. RS codes are based on algebraic methods using finite fields and they are the ideal maximum distance separable (MDS) codes. Traditionally, the RS FEC Codes can be described as: $RS(n,k)$-code is defined as a FEC code that converts k source data packets / symbols into n encoded symbols ($n > k$). Therefore, any k thereof received correctly allows the original data to be reconstructed. However, in practice, the values of k and n must be small (for example, below 256) for such FEC codes as large values make encoding and decoding prohibitively expensive with hardware implementation. For example, RS codes are restricted to $k = 191$, $n = 255$ in DVB-H, thus the receiver system can tolerate up to 64 error bytes per row of the FEC matrix.

D.3.2.2 Raptor codes

Raptor codes [3] have been invented in 2001 and introduced into DVB standards for the DVB-H file delivery: in contrast to RS codes they provide more flexibility, large code dimensions and lower decoding complexity. Raptor codes have therefore been adopted in latest DVB standards, for example, in the content delivery protocols (CDP) specification of IP Datacast over DVB-H (DVB-IPDC) [18]. For more details on Raptor codes please refer to [3] and the specification in 3GPP [4], DVB and IETF. The complexity of RS decoding is known to be rather high, for Raptor codes a low-complexity maximum-likelihood decoding is, for example, introduced in [4], Annex E.

Raptor codes are an example of rateless codes with a small reception overhead based on Luby transform (LT) [19] codes. The encoder can be seen as a fountain that produces an endless supply of encoded packets so that anyone who wishes to receive the encoded file holds a bucket under the fountain and collects packets until their number in the bucket is equal to $k^{'}$ ($k^{'}$ slightly larger than the source symbols / packets k). A Raptor encoder uses randomization to generate each encoding symbol randomly and independently of all other encoding symbols. The number of source symbols k may be as large as $k = 8192$ for Raptor codes. A Raptor encoder can generate as few or as many encoding symbols as required on demand.

In summary, RS codes are MDS codes and the coding rate can be adjusted by puncturing and shorting [20]. But the decoding complexity is very high, and generally

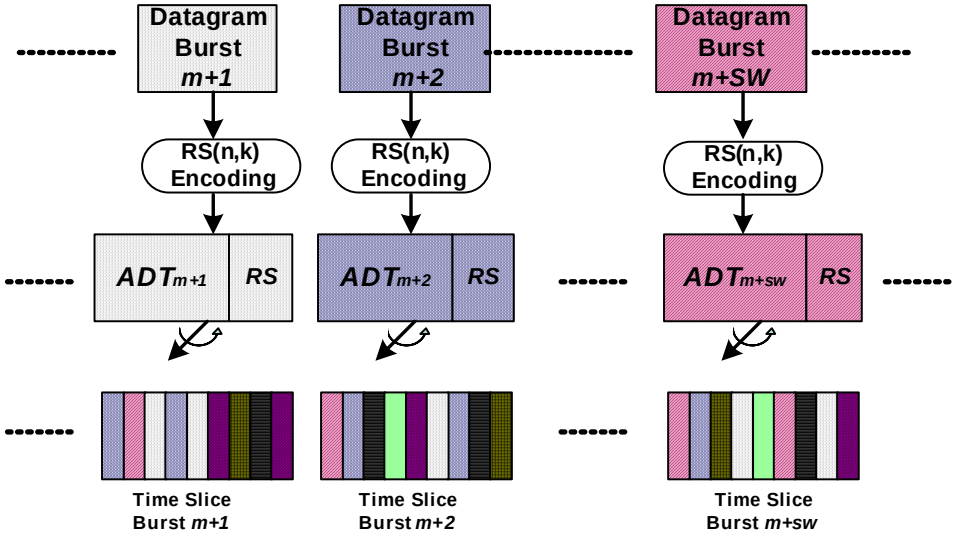

Fig. D.4: The MPE-FEC Sliding encoding with RS codes.

the decoder needs to be implemented in hardware. The Raptor codes are almost MDS code, and the performance is very close to the ideal MDS code. Moreover, Raptor code is more flexible than RS because the coding rate can be adjusted without puncturing or shorting, and the decoding can be implemented with software.

D.3.3 Framework

D.3.3.1 RS codes-based LL-FEC design

DVB has adopted an LL-FEC in DVB-H at the data LL (MPE Layer) referred to as MPE-FEC. At the time when DVB-H was specified, only RS codes were available, and therefore, the MPE-FEC is based on RS codes. For MPE-FEC the repair data are generated based on an application data table (ADT) with a size of at most 191 kbyte, such that for 200 ms latency data rates of at most 7.8Mbit/s can support, and for 10 s delay, only up to 156 kbit/s are supported. The processes are fully defined and standardized in [20]. The MPE sections containing the original data packets within one ADT as well as the corresponding MPE-FEC sections are transmitted in a single burst. For example, for file delivery services over DVB-H, one major drawback of LL-FEC in DVB-H is that each of the unique bursts where the file is partitioned must be successfully decoded to recover the file. Note also that if one burst is completely received (i.e. all source and parity data), it cannot be used to correct errors in other bursts. In particular, when using this framework to DVB-S2 another drawback is the size of the MPE-FEC frame, which is not big enough to protect against long burst errors since the number of address signalling bits for the ADT and RS data table is only 18-bit [20]. Therefore, in order to protect longer bursts, more bits to signal the address of ADT table must be allocated along with the corresponding signalling structure to address this issue. This is addressed in the extended MPE-FEC based on

Raptor codes.

The protection of MPE-FEC in DVB-H spans over only a single burst. In DVB-SH, the fade event durations may be much larger due to the land-mobile satellite channel. Thus Sliding Encoding is proposed for multi-burst protection [21]. The principle of MPE-FEC Sliding Encoding with RS Codes is shown in Fig. D.4.

The principle of MPE-FEC Sliding Encoding is derived from the MPE-FEC, the difference being that MPE-FEC Sliding Encoding scheme implements interleaving among several continuous MPE-FEC Frame after the RS encoding. Thus, each transmitted time slice burst is composed of MPE sections and MPE-FEC sections coming from different MPE-FEC Frames. Thus, at the receiver, the RS decoding will be implemented after the de-interleaving when Sliding Window (SW) MPE-FEC frames are received. Hence, additional delay will be introduced in order to collect enough MPE-FEC frames to do the de-interleaving.

An MPE-FEC encoder ($RS(n,k)$) implementing sliding encoding will select the k data sections from an SW of MPE-FEC Frames and will spread the $n-k$ parity sections over the same frame window (show in the Fig. D.4). Basically, the same effect could be obtained by first normally encoding SW frames and then interleaving sections among the encoded SW frames. Here SW represents the interleaver depth. After the de-interleaving process (before the FEC decoding), an error burst greater than one frame will be spread among the SW frames. Therefore, the continuous multiple error bursts (e.g. power archers) can be recovered with proper SW value. The drawback of MPE-FEC Sliding Encoding scheme extension to DVB-S2 in mobile environment is long delay, which degrades the performance of interactive services, as well as the fact that the SW method is not MPE-FEC compatible.

D.3.3.2 Raptor codes-based LL-FEC design

During the DVB-SH standardization activities, it was recognized that for satellite-to-handheld services, theMPE-FEC is not sufficient. Therefore, it was decided to specify a multi-burst LL-FEC framework referred to as Inter-Burst FEC (IFEC) [22]. The MPE-IFEC was introduced to support reception in situations of long erasures at the MPE section level spanning several consecutive time-slice bursts due to the characteristics of the LMS channel. Obstacles may hinder direct satellite reception and induce losses of several successive bursts. MPE-FEC Sliding Encoding had been proposed initially to enable multi-burst protection based on RS codes, but with the availability of more powerful and low-complexity Raptor erasure codes, the MPE-IFEC has been generalized.

The MPE-IFEC is defined by the parameters encoding period EP, which reflects the ADT size comparison with the burst size, data burst spread B, that is, over how many bursts an ADT is spread, FEC spread S, that is, over how many multiple of EP bursts the FEC is spread, the sending delay D, that is, how long the sending of data is delayed at sender in units of time-slice bursts, the code rate r_{ll} as well as code being used, namely Raptor or RS codes. Note that whereas Raptor codes allow

very flexible parameters, for RS codes due to restricted code only parameters $EP = 1$ can be used. Note that for MPE-IFEC the mapping of MPE-IFEC sections to MPEG-2 TS packets is identical as for the MPE-FEC. At the receiver, the decoding matrix (combination of ADT+iFDT) is generated and decoding each of the decoding matrices with frequency EP eliminates the unreliable columns of the decoding matrix. The ADT of the decoding matrix is then mapped back to ADST to reconstruct the datagrams in each ADST.

D.3.3.3 LL-FEC framework in DVB-RCS

Despite its flexibility, the MPE-IFEC is mainly designed for the purpose of multicasting live video over time-slice bursts. The FEC is designed for the purpose to minimize tune-in and channel switching delays over burst-based transmission, but not to minimize end-to-end delay, which is essential for bidirectional data delivery services. Therefore, a new LL-FEC framework has been defined in DVB-RCS for mobile extension in [5], Section 6.4.5, as a countermeasure for nLOS conditions due to obstruction, blockage or other situations in which the line-of-sight is interrupted. With this LL-FEC, transmissions of multicast and unicast traffic data can be protected against channel impairments such as short interruptions and shadowing. Return Channel Satellite Terminals (RCSTs) that declare support for nLOS countermeasures shall be able to receive and process a forward link signal transmitted in accordance with these provisions. This technique can also be applied to the optional continuous return link carrier transmissions defined in Section 10 of [5].

Transmissions employing LL-FEC in DVB-RCS use the same basic data structures as other MPE transmissions. However, due to the restricted signalling space of the address, datagrams may not be directly concatenated in the ADT, but some padding may be added such that a new datagram always starts at an address being multiples of some value referred to as address granularity. The address granularity is inherently configured in the setup with the specification of the frame size coding. The use of LL-FEC is defined separately for each elementary stream in the transport stream. Each elementary stream may configure different code parameters for different QoS classes, resulting in different delays, levels of protection and FEC overheads. LLFEC can use the Raptor codes for LL-FEC frame ADT sizes up to 12 Mbytes or the MPE-FEC RS codes for any LL-FEC frame ADT sizes up to 191 KBytes. The chosen code is identified in the forward link signalling. The LL-FEC frame is a conceptual construction used to generate LL-FEC parity sections from a sequence of layer 3 datagrams. It is composed of the ADT and the FDT (shown in Fig. D.5). The LL-FEC frame shall conceptually be arranged as a matrix with a flexible number of columns for both the ADT and FDT. The maximum number for $no_adt_columns$ and $no_fdt_columns$ depends on the type of code used. The $no_adt_columns$ is signalled in each parity section/packet transmitted along with this LL-FEC frame. The $no_fdt_columns$ is not explicitly signalled for Raptor, but is signalled for the RS code. The matrix has a flexible number of rows with a maximum that depends on the type of code used. Fig. D.5 shows the conceptual organization of the frame. The number of rows is signalled in the LL-FEC identifier descriptor. Each

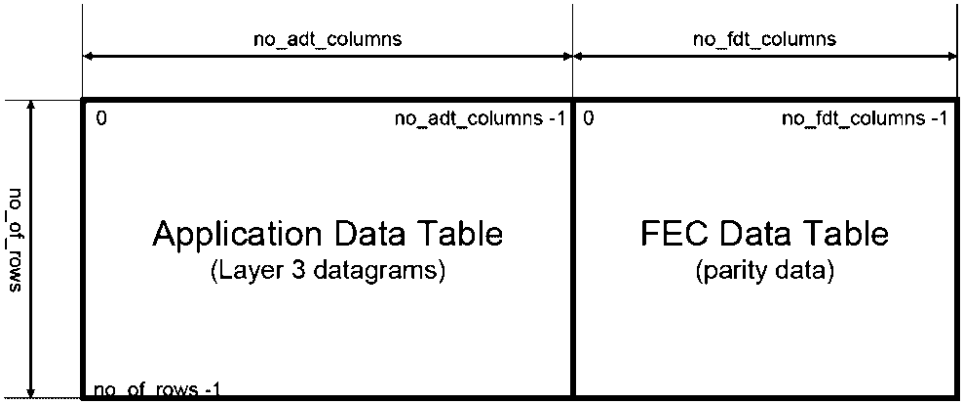

Fig. D.5: DVB-RCS+M LL-FEC frame.

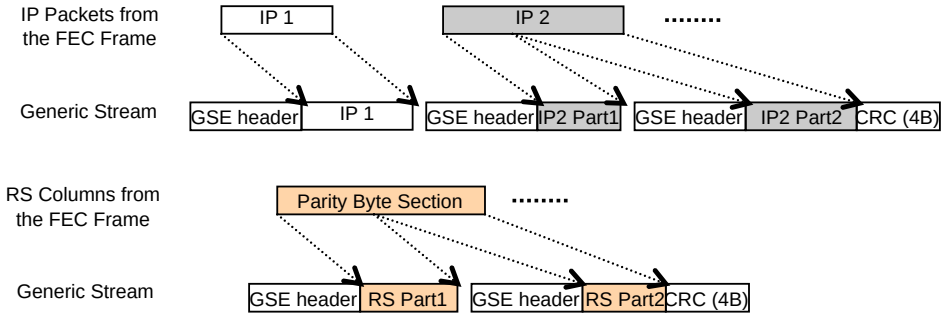

Fig. D.6: GSE encapsulation process.

position in the matrix can hold an information byte. The left part of the LL-FEC Frame is used for OSI layer 3 (Network layer) datagrams (e.g. IP datagrams) and possible padding, and is called the application data table. The right part of the LL-FEC Frame is dedicated for the parity information of the FEC code and is called the FEC data table (FDT). The number of columns in the ADT and FDT can vary frame-by-frame.

D.3.4 Support of FEC for generic stream encapsulation

The FEC Frame of GSE is the same as MPE. However, the encapsulation of sub-network data unit (SNDU) sections is different (shown in Fig. D.6). GSE protocol [23] allows for direct encapsulation of IP and other network-layer packets over DVB-S2 physical layer frames. The IP datagrams and RS columns are encapsulated in one or more GS units. Each GS unit is constructed of a GS header and a Data Field. The CRC part is only added at the end of the last fragmented GS unit, as opposed to MPE sections (see Section 9.3 of [20]) where the CRCs are added at the end of every SNDU sections.

In [24; 25], the authors discussed the application of GSE-FEC in DVB-S2 systems and give the results of the encapsulation efficiency comparison between GSE-FEC, MPE-FEC and ultra light encapsulation-FEC (ULE-FEC). The results show that GSE-

FEC is more efficient than MPE/ULE-FEC for the encapsulation of IP datagrams. However, the results of the performance comparison in Section D.7 show that GSE-FEC is bad due to the fact that there is no CRC for unfragmented GS units, as shown in Fig. D.6. Thus, the receiver cannot detect all the erroneous GS units except the ones protected by the CRC. This results in a reduced decoding performance of the RS code because the position of the erroneous bytes is unknown. Note that GSE was designed with DVB-S2 in mind, which is considered as a quasi-error free (QEF) environment. Hence, GSE only requires a CRC when a datagram fragmented.

In order to implement GSE-FEC in DVB-S2 and DVB-RCS standards without decreasing the performance, some necessary modifications of GS units¡¯ format are indispensable. Therefore, the use of extension headers is proposed in [26] to introduce the CRC and also to signal in the LL-FEC real-time parameters field in the section header.

D.4 QoS Architectures

To fully optimize wireless broadband networks, both the challenges from the physical medium and the QoS-demands from the applications have to be taken into account. Rate, power and coding at the physical layer can be adapted to meet the requirements of the applications given the current channel and network conditions. Knowledge has to be shared between (all) layers to obtain the highest possible adaptivity. Therefore, cross-layer design is proposed for adapting all the layers. In paper [27], the authors proposed a cross-layer design for the packet scheduling on a forward link that implements ACM. A cross-layer approach is considered whereby the physical and MAC layers share knowledge of the channel dynamics in presence of ACM. In this paper, we would like to use cross-layer design to provide QoS for DVB-S2/RCS+M.

MPE-FEC and MPE-IFEC are designed for multicast distribution of real-time services. Therefore, those frameworks only take into account transport of IP datagrams distributed over IP multicast. The signalling is only defined for the broadcast/multicast transmission architecture. In order to define backwards-compatible FEC signalling also for unicast traffic, the proposed cross-layer architectures are designed in line with DVB-S2 nomenclature. Two possible architectures with different signalling implications have been identified as following.

D.4.1 LL-FEC per-mobile terminal

The datacast (multicast/broadcast and unicast) transmission cross-layer architecture with either MPE-FEC over transport streams or GSE over Generic Streams (GS) is shown in Fig. D.7. This architecture aggregates traffic and creates an Elementary Stream (ES) per-mobile terminal. This means that one PID (Packet IDentifier) is needed for each mobile terminal. A similar concept to PIDs is also introduced for the LL-FEC support in GSE, namely the gse-fec-id. This identifier bounds the LL-FEC

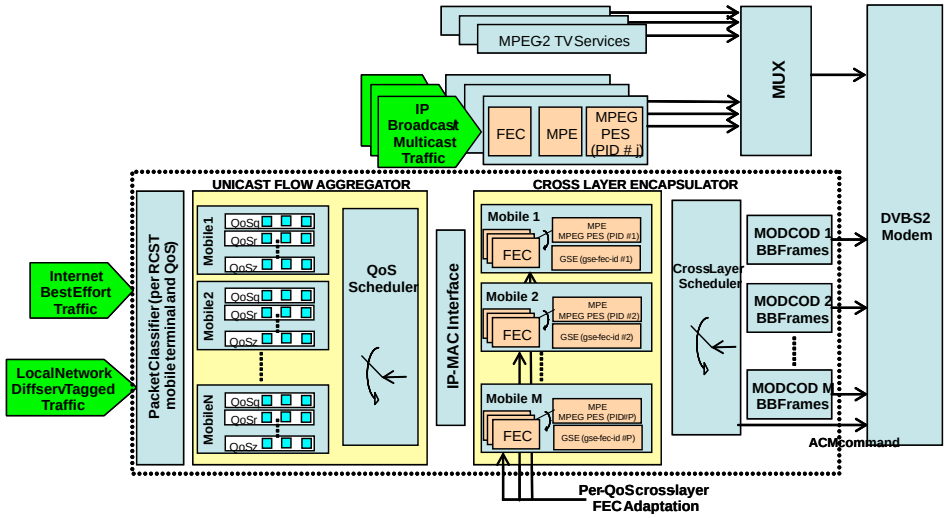

Fig. D.7: Datacast Transmission over DVB-S2/RCS: Per-mobile terminal architecture.

context and the out-of-band LL-FEC signalling parameters use it as a reference. The packets are then aggregated according to the physical layer parameters (MODCOD). This architecture allows QoS scalability, that is, it is possible to assign different FEC levels per terminal. This is possible by introducing parallel FEC processes each with different FEC protection levels. The drawback of this option is the scalability for large number of terminals since there is a limited number of PIDs and therefore only a small address space can be provided. Furthermore, the level of traffic aggregation achieved when using one PID per terminal is low. This not only increases delay and jitter but it may also decrease the FEC efficiency by having to use padding to fill up the FEC Frame.

D.4.2 LL-FEC Per-MODCOD

An alternative architecture for both MPE and GSE scenarios is shown in Fig. D.8. The underlying mechanism for providing scalability is the implementation of just one LL-FEC process per MODCOD, instead of per mobile terminal. Note that in DVB-S2 systems a few MODCODs carry most of the traffic. The limitations in data rates when employing LL-FEC require the use of load balancing within high data rate MODCODs, which can be achieved by adding parallel LL-FEC processes to these MODCODs. The architecture of LL-FEC per- MODCOD aggregates traffic per MODCOD creating an Elementary Stream per MODCOD. This means that one PID is needed per MODCOD. Moreover, the different FEC levels for QoS support are also on per-MODCOD basis. This architecture is highly scalable and it maintains backwards compatibility since FEC is still signalled per ES and low overhead by aggregating traffic per MODCOD. However, the implementation will be more complex due to the crosslayer interface between layer 2 and the DVB-S2 mode adaptation. Furthermore, it may require signalling all FEC parameters to every terminal and enhancements to the DVB signalling structure for GSE support. Finally, in contrast to the architecture according to Fig.

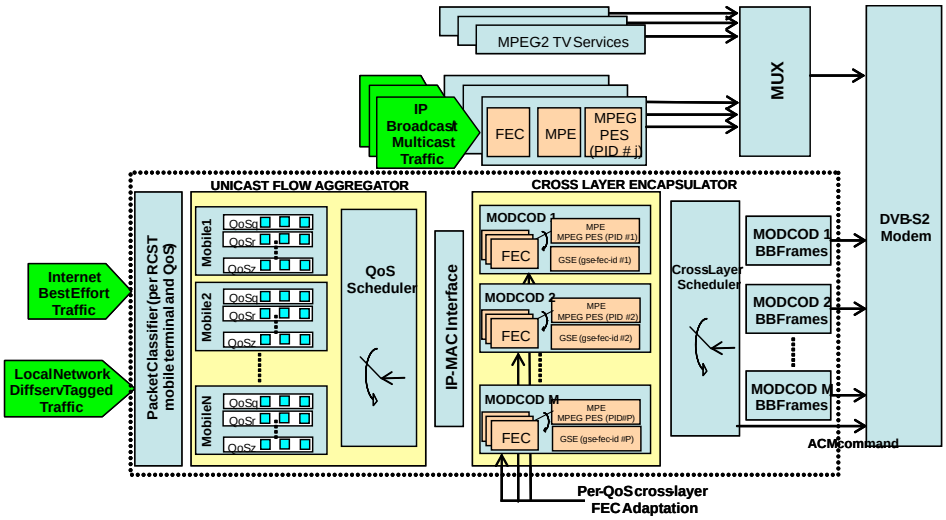

Fig. D.8: Datacast Transmission over DVB-S2/RCS: Per-ModCod architecture.

D.7, each terminal needs to decode the whole MODCOD to extract the data being assigned to it. Note that the gse-fec-id is present in both architectures and it was designed to replicate in GSE the concept of ES, thus allowing LL-FEC to be implemented both in MPE and GSE using the same algorithms, concepts and methods.

D.5 System Configuration Options and Optimization

The introduced LL-FEC frameworks shown in Section D.3 allow a significant variability in terms of parameter settings: Table D.II summarizes the description of some main parameters, for details on other parameters such as D, EP, G, B, S, R and T we refer to the MPE-IFEC specification [22]. Given target QoS, the target delay τ can de derived from Table D.I, and then the amount data (bits) protected with target delay will be computed as

$$S_{\text{protect}} = \tau B_s M r_{\text{phy}} r_{\text{ll}}, \tag{D.1}$$

and the size of ADT (for MPE-FEC) or ADST (for MPE-IFEC) in the time slice burst can be derived as:

$$S_{\text{ADT}} = S_{\text{protect}} r_{\text{ll}}. \tag{D.2}$$

Thus, the number of time slice bursts that can be protected within target delay τ is given as

$$N_{\text{burst}} = \lfloor \frac{S_{\text{protect}}}{S_{\text{ADT}}} \rfloor = \lfloor \tau v_{\text{burst}} \rfloor, \tag{D.3}$$

Table D.II: System and Simulation Parameters

Parameters	Description
B_s	Symbol rate
S_{ip}	Size of IP packet
τ	Target delay
M	Size of signal constellation (QPSK $M = 2$, 16QAM $M = 4$)
r_{phy}	The PHY layer coding rate
S_{protect}	Amount of data bit to be protected during the target delay
S_{burst}	Amount of data bit in each time slice burst
S_{adt}	Size of the ADT
N_{burst}	Number of bursts protected during the target delay
r_{ll}	Link layer coding rate
v_{train}	vehicle velocity
N_{rows}	Number of rows of MPE-FEC frame
l_{PA}	The duration/length of power arches
d_{PA}	The distance between power arches

where $v_{\text{burst}} = B_s M r_{\text{phy}}/S_{\text{burst}}$ is the rate at which bursts are transmitted. The amount of data in each time slice burst S_{burst} cannot exceed 2 Mbit for the MPE-FEC framework with RS codes due to the address field being only 18 bit [20]. But for the MPE-FEC with Raptor codes, the size of ADT can be up to 12 Mbytes (hence, more data can be protected in DVB-RCS).

D.5.1 Optimization for RS codes-based LL-FEC frameworks

For an RS referred to as $RS(n, k)$, where n denotes the number of columns of the FEC frame matrix, k the number of columns of the ADT and N_{rows} the number of rows of the typical MPE-FEC frame used in DVB-H. Optimal values of n, k and N_{rows} can be calculated with the following formulas for a given desired protection:

$$k = \lfloor \frac{S_{\text{protect}}}{8N_{\text{rows}}} \rfloor. \tag{D.4}$$

That available number of FEC matrix rows in the standard [20] is $N_{\text{rows}} \in \{256, 512, 768, 1024\}$. Then, for a given n the LL code rate can be computed as:

$$r_{\text{ll}} = \frac{k}{n}. \tag{D.5}$$

We will extend N_{rows} to be larger (e.g. 2048 or 4096) in order to be tolerant to long

burst errors in the mobile scenario.

For MPE-FEC Sliding Encoding, with the availability of the size of the burst, S_{burst}, n can be computed as

$$n = \lfloor \frac{S_{\text{burst}}}{8N_{\text{rows}}} \rfloor, \tag{D.6}$$

where N_{rows} is defined as for the MPE-FEC. Then k can be calculated from (F.5). The size of the sliding windows SW yields:

$$SW = \lfloor \frac{S_{\text{protect}}}{8kN_{\text{rows}}} \rfloor. \tag{D.7}$$

D.5.2 Optimization for Raptor codes-based LL-FEC Frameworks

Let us present Raptor codes as $Raptor(n, k, T)$ with n and k the code parameters and with the symbol size T. For the MPE-IFEC with Raptor code, $D = 0$ is selected for minimum delay and lowest decoding complexity. Then T corresponds to the row size and can also be calculated as:

$$T = \frac{N_{\text{rows}}}{G} \text{ with } N_{\text{rows}} \in \{256, 512, 768, 1024\}. \tag{D.8}$$

Furthermore, n can be derived as

$$n = \left\lfloor \frac{S_{\text{burst}}}{8N_{\text{rows}}} \right\rfloor EP, \tag{D.9}$$

where EP is an integer. k can be derived from the (F.5) with known n. Then B and S can be calculated from (F.11) as:

$$\begin{cases} B + S = \frac{N_{\text{burst}}}{EP}, \\ S = \lceil (1 - r_{\text{ll}})(B + S) \rceil, \\ B = (B + S) - \lceil (1 - r_{\text{ll}})(B + S) \rceil. \end{cases} \tag{D.10}$$

D.5.3 Optimization for the LL-FEC frameworks in DVB-RCS

For an $RS(n, k)$-based MPE-FEC applied in DVB-RCS, the optimization of parameters n and k is the same as presented in Section D.5.1. For a $Raptor(n, k, T)$, the code parameters may be $4 \leq k \leq 8192$, $k \leq n \leq 65536$ and T any power-of-two integer that divides N_{rows}. Preferably k is chosen at least as great as 1000 to keep the inefficiency of the Raptor code to below 0.2%. Therefore, for a given amount of data bit to be protected, S_{protect}, k should be selected as the smallest value larger than 1000 such

Table D.III: System parameters numerical values for the LOS+PA scenario

Parameters	Description
B_s	27.5 M baud/s
S_{ip}	1500 bytes
τ	200 ms
M	2 for QPSK; 3 for 8PSK
r_{phy}	1/2 for QPSK; 3/4 for 8PSK
S_{burst}	512 K bytes
S_{adt}	256 K bytes
N_{burst}	10
r_{ll}	1/2 for QPSK; 2/9 for 8PSK
v_{train}	100 km/h

that $kT \geq S_{\text{protect}}$ and T any power-of-two integer that divides N_{rows} such that $N_{\text{rows}} = GT$. Then, for a given LL code rate r_{ll}, n is selected as k/r_{ll}. Furthermore N_{rows} may be selected appropriately to ensure $k \geq 1000$. However, obviously values $k < 1000$ can also be selected without harming the performance significantly.

D.6 Selected Experimental Results

Table D.III shows the parameter settings for the conducted simulations. The parameters for MPE-FEC, MPE-IFEC and extended MPE-FEC can be derived based on the guidelines in Section D.5.

D.6.1 Simulation results for LOS+PA scenario

Before presenting the simulation results, we compute the theoretical values of Maximum Tolerant Burst Length (MTBL) following the approach presented in Section D.5.

The theoretical MTBL can be calculated as

$$l_{\text{PA}}\left(N_{\text{BB-p}}\right) = \frac{N_{\text{BB-p}} v_{\text{phy}}}{v_{\text{BB}}}, \tag{D.11}$$

where $v_{\text{BB}} = B_s M r_{\text{phy}}/S_{\text{BBFrame}}$ is the rate at which BB-Frames are transmitted and the $N_{\text{BB-p}}$ is the number of BB-Frames protected by the target delay τ, (e.g. 200 ms in this paper) with various LL-FEC schemes.

The appropriate number of BB-Frames included in one protection period can be

Table D.IV: Theoretical values of MTBL for the LOS+PA scenario

LL-FEC scheme	MODCOD	FEC codes	MTBL	
			30 km/h	100 km/h
MPE-FEC	QPSK 1/2	RS(128,64), N_{rows} =4096	0.65m	2.18m
	8PSK 3/4	RS(704,152), N_{rows} =2048	1.25m	4.15m
MPE-IFEC	QPSK 1/2	RS(128,64), N_{rows} =512 EP =1, $B = S$ =5 or Raptor(640,320),N_{rows} =512 EP =5, $B = S$ =1	0.82m	2.73m
	8PSK 3/4	RS(81,18), N_{rows} =1024 EP =1, B = 4,S =14 or Raptor(486,108,512),N_{rows} =512 G =1, EP =3, B = 1,S =5	1.28m	4.28m
Extend MPE-FEC	QPSK 1/2	Raptor(2560, 1280, 256) N_{rows} =1024,G =4	0.82m	2.73m
	8PSK 3/4	Raptor(5760, 1280, 256) N_{rows} =1024,G =4	1.26m	4.22m
GSE-FEC	QPSK 1/2	RS(128,64), N_{rows} =4096	0.33m	1.09m
	8PSK 3/4	RS(704,152), N_{rows} =2048	0.63m	2.08m

computed as

$$N_{\text{ideal}-\text{BB}-\text{p}} = \left\lfloor \frac{\tau v_{\text{TS}} (1 - r_{\text{ll}})}{N_{\text{TS}-\text{BB}}} \right\rfloor, \tag{D.12}$$

where $v_{\text{TS}} = B_s M r_{\text{phy}}/S_{\text{TS}}$ is the rate at which TS Packets are transmitted (here S_{TS} =188 bytes) and $N_{\text{TS}-\text{BB}} = [(S_{\text{BBFrame}} - 10 \times 8)/(8S_{\text{TS}})]$ is the number of TS packets encapsulated in one BBFrame. The actual number of BB-Frames that can be protected for the different LL-FEC schemes can be computed as:

$$N_{\text{BB}-\text{p}} = \left\lfloor \frac{(n-k) N_{\text{rows}} SW}{184 N_{\text{TS}-\text{BB}}} \right\rfloor. \tag{D.13}$$

We obtain theoretical ideal values of MTBL of 2.86m for QPSK 1/2. However, Table D.IV shows the theoretical MTBL of various LL-FEC schemes showing a slight degradation with respect to the ideal.

Typical length of PAs in Europe are in the range of 0.5 to 3m [9; 13] and therefore the theoretical results already show that the FEC codes shown in Table D.IV can

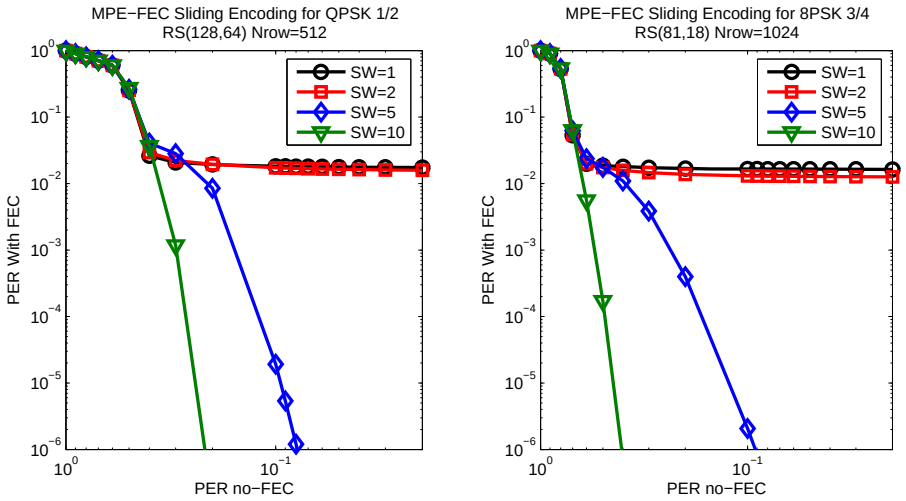

Fig. D.9: Performance of MPE-FEC sliding encoding with different SW.

overcome the effect of the PAs for high speeds. This is an acceptable result since the time of the train is at speeds below 100 km/h is almost negligible.

Fig. D.9 shows the results of the MPE-FEC sliding encoding with different values of SW. The system parameters for this simulation are $l_{\text{PA}} = 1$m, $d_{\text{PA}} = 49$ m, v_{train} =100 km/h and B_s =27.5 Mbaud.

The results show that the MPE-FEC sliding encoding cannot overcome the effect of PA with $SW \leq 2$ and there will be an error floor around 10^{-2}. The error floor disappears when $SW \geq 5$ for both ModCod QPSK 1/2 and 8PSK 3/4.

We can conclude that MPE-FEC completely removes the effect of PAs for high speeds only, due to the fact that the target protection delay is limited due to the restrictions in the standard. On the other hand, MPE with sliding encoding can also completely remove the effect of PAs while there is no limitation on the target delay that can be protected.

D.6.2 Simulation results for nLOS scenario

The system parameters of nLOS Scenario are the same as in the LOS+PA Scenario except for the channel model. The time series of channel dumps were generated from the Rayleigh Channel, which corresponds to the nLOS channel model.

D.6.2.1 RS and Raptor codes based LL-FEC Performance

Fig. D.10 shows the performance of RS codes based MPE-FEC for two ModCods, QPSK 1/2 and 8PSK 3/4. In order compare the performance fairly for different ModCods, we suppose that the total system spectral efficiency is 1/2. Therefore the link layer coding rate rll will be 1/2 and 2/9 for QPSK 1/2 and 8PSK 3/4 respectively.

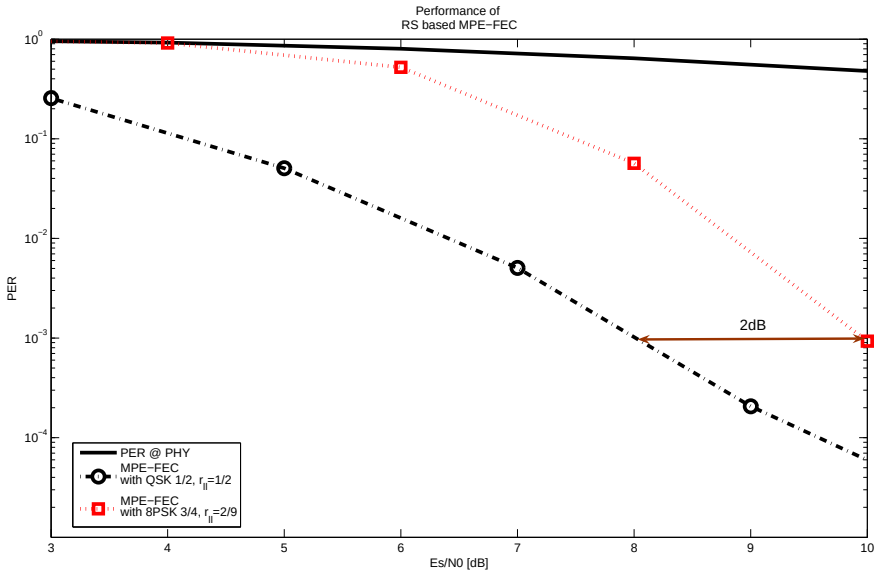

Fig. D.10: Performance of RS codes based MPE-FEC.

From the results we can see that QPSK 1/2 outperforms 8PSK 3/4 about 2dB at PER= 10^{-3}. It means that the lower ModCod the better performance for a given system spectral efficiency. It also means that physical layer protection is better than the link layer. However, the physical layer protection has some shortcomings as shown in section II-E.

For the Raptor codes based MPE-FEC, the performance is shown in Fig. D.11. QPSK 1/2 outperforms 8PSK 3/4 about 2.3dB at PER= 10^{-3}.

D.6.2.2 LL-FEC Frameworks comparison

Fig. D.12 shows the performance of PER over the E_s/N_0 for different link layer schemes with v_{train} =100km/h, compared to the performance without link layer FEC. Note that for MPE-FEC with RS codes, the transmission parameters did not allow suitable parameter settings (discussed in Section D.3.3.1). But here we increase the size column up to 4096 Bytes for RS codes in order to compare the performance under the same target delay assumption.

Generally, a residual packet loss rate of about 10^{-4} (or even lower) needs to be achieved for data services. The uncoded performance is completely unsatisfying. With the use of LL-FEC, the target performance can be achieved. The MPE-IFEC may solve the problem and the performance of Raptor based MPE-IFEC outperforms RS by about 1.5 dB and the extended MPE-FEC with Raptor codes outperforms MPE-FEC with RS by about 0.5dB. This is due to the fact that the extended MPE-FEC does not have any restrictions in terms of time-slice bursts. For lower speeds at around 30km/h as well as for larger delays the extended MPE-FEC shows consistently better

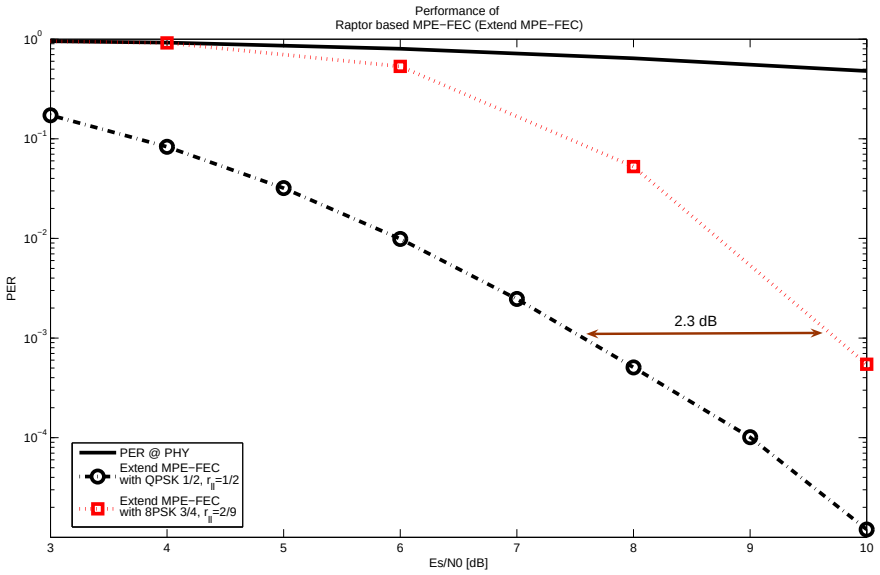

Fig. D.11: Performance of Raptor codes based MPE-FEC (Extend MPE-FEC).

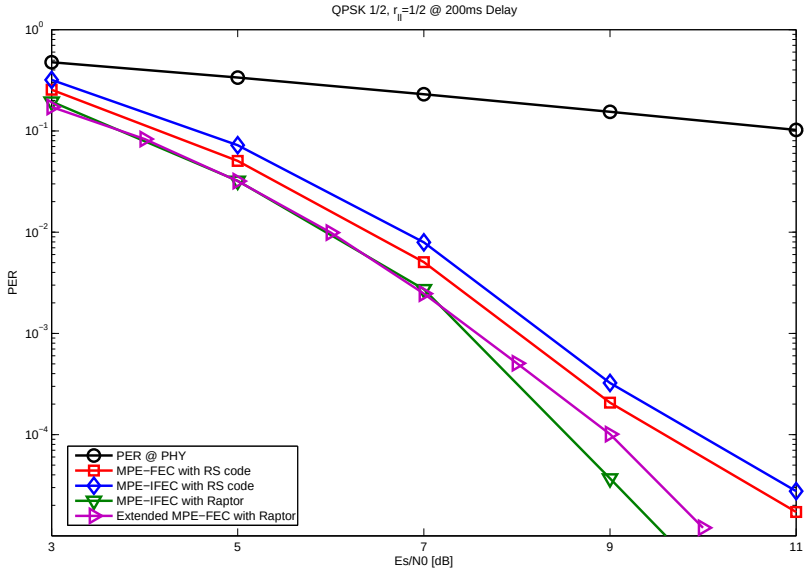

Fig. D.12: Performance of different LL-FEC schemes with $v_{\text{train}} = 100\text{km/h}$).

results than the any MPE-IFEC.

It can be concluded that the codes analyzed here can be used for both purposes, to protect against LOS+PA scenarios as well as Rayleigh environments. Especially by the use of the extended MPE-FEC with Raptor codes as finally specified in DVB-RCS+M consistently shows superior results than with other link layer FEC for railway scenarios.

D.7 Conclusions

A thorough performance analysis of the LL-FEC codes and frameworks available in the DVB family for the application to DVB-S2 in railway scenarios has been presented. It has been shown that LL-FEC completely removes the effect of PAs for the speeds of interest for the two typical railway scenarios analyzed. Both theoretical and simulation analysis reveal that LL-FEC can overcome the fade in the railway scenario by selecting appropriate FEC codes. In particular, we have proved that the analyzed DVB codes and frameworks are more suitable for the LOS+PA scenario than for the Rayleigh scenario, which needs a relatively high E_s/N_o to achieve a good performance. This is due to the important fact that the Rayleigh channel is not an erasure channel. Specifically, the use of the extended MPE-FEC with Raptor codes as finally specified in DVB-RCS+M consistently shows superior results than the other analysed FEC options. Further, two possible novel cross-layer architectures have been proposed for DVB-S2 unicast transmission that allows adaptive QoS provision for Internet services. The architectures allow the migration from traditional packet encapsulation based on MPEG2-TS to new schemes such as the Generic Stream.

Bibliography

[1] ETSI EN 302 304 v1.1.1, Digital Video Broadcasting (DVB): Transmission System for Handheld Terminals (DVB-H), Nov. 2004.

[2] ETSI TS 102 585 v1.1.1, Digital Video Broadcasting (DVB): System Specifications for Satellite services to Handheld devices (SH) below 3 GHz, July, 2007.

[3] A. Shokrollahi, "Raptor Codes," *IEEE Trans. on Inform. Theory.*, vol. 52, no. 6, pp. 2551 - 2567, Jun. 2006.

[4] 3GPP TS26.346, "Multimedia Broadcast/Multicast Service (MBMS): Protocols and Codecs (release 8)," Sep. 2008.

[5] DVB BlueBook A054r4.1, Digital Video Broadcasting (DVB): Interaction channel for satellite distribution systems (draft EN 301 790 V1.5.1 - DVB-RCS+M), Jan. 2009.

[6] ETSI EN 300 421 v1.1.2, Digital Video Broadcasting (DVB): Framing structure, channel coding and modulation for 11/12 GHz satellite services, Aug. 1997.

[7] ETSI EN 302 307 v1.1.1, Digital Video Broadcasting (DVB): Second generation framing structure, channel coding and modulation system for Broadcasting, Interactive Services, News Gathering and other broadband satellite applications, June 2004.

[8] ITU-T Recommendation G.1010. End-user multimedia QoS categories.

[9] E. Lutz, M. Werner, and A. Jahn, *Satellite Systems for Personal and Broadband Communications*. Springer, New York, NY, USA, 2000.

[10] A. D. Panagopoulos, P. D. M. Arapoglou, and P. G. Cottis, "Satellite Communications at Ku, Ka, and V Bands: Propagation Impairments and Mitigation Techniques," *IEEE Commun. Surveys and Tutorials*, vol. 6, no. 3, pp. 2 - 14, Third Quarter, 2004.

[11] E. Kubista, F. P. Fontan, M. A. V. Castro, S. Buonomo, B. R. Arbesser-Rastburg, and J. P. V. Polares Baptista, "Ka Band Propagation Measurements and Statistics for Land Mobile Satellite Applications," *IEEE Trans. on Veh. Technol.*, vol. 49, no. 3, pp. 973 - 983, May 2000.

[12] A. Benarroch and L. Mercader, "Signal Statistics Obtained form a LMSS Experiment in Europe with the MARECS Satellite," *IEEE Trans. on Commun.*, vol. 42, no. 2 - 4, pp. 1264 - 1269, Feb.¨CApr. 1994.

[13] S. Scalise, R. Mura, and V. Mignone, "Air Interfaces for Satellite based Digital TV Broadcasting in the Railway Environment," *IEEE Trans. on Broadcast*, vol. 52, no. 2, pp. 158 - 166, Jun. 2006.

[14] S. Cioni, A. Vanelli-Coralli, C. P. Niebla, S. Scalise, G. S. Granados, and M. A. Vázquez Castro, "Antenna Diversity and GSE-based packet level FEC for DVB-S2 systems in Railway scenarios", in *Proc. 25th AIAA International Communications Satellite Systems Conference*, Seoul, South Korea, Apr. 2007.

[15] F. Pérez-Fontán, M. A. Vázquez Castro, C. E. Cabado, J. P. Garcia, and E. Kubista, "Statistical Modeling of the LMS Channel," *IEEE Trans. on Publication*, vol. 50, no. 6, pp. 1549 - 1567, Nov. 2001

[16] F. Pérez-Fontán, J. P. Gonzalez, M. J. S. Ferreiro, M. A. Vázquez Castro, S. Buonomo, and J. P. Baptista, "Complex envelope threestate Markov model based simulator for the narrow-band LMS channel", in *Proc. Int. Journal on Satellite Commun.*, vol. 15, no. 1, pp. 1 - 15, Dec. 1998.

[17] Jakes WC (ed.). *Microwave Mobile Communications*. Wiley: New York, 1974.

[18] ETSI TS 102 472 v1.2.1, IP Datacast over DVB-H: Content Delivery Protocols (CDP), June 2006.

[19] M. Luby, "LT Codes," *Forty-third Annual IEEE Symposium on Foundations of Computer Science*, Vancouver, BC, Canada, pp. 16 - 19, Nov. 2002.

[20] ETSI EN 301 192 v1.4.1, Digital Video Broadcasting (DVB): DVB Specification for Data Broadcasting, Nov. 2004.

[21] P. Marco, F. Rosario, C. Giovanni, and E. V. C. Alessandro, "On The Application of MPE-FEC to Mobile DVB-S2: Performance Evaluation in Deep Fading Conditions," *International Workshop on Satellite and Space Communications*, Salzburg, Austria, pp. 223 - 227, Sep. 2007.

[22] DVB Bluebook DVB A131, MPE-IFEC, Nov. 2008.

[23] ETSI TS 102 606 v1.1.1, Digital Video Broadcasting (DVB): Generic Stream Encapsulation (GSE) Protocol, Oct. 2007.

[24] J. Lei, G. S. Granados, and M. A. Váquez Castro, "MPE/ULE-FEC vs GSE-FEC Efficiency Comparison of IP Datagram Transmission over DVB-S2," in *Proc. 25th AIAA Int. Commun. Satellite Systems Conf.*, Seoul, South Korea, Apr. 2007.

[25] A. Mayer, F. Vieira, J. Lei, B. Collini-Nocker, and M. A. Váquez Castro, "Analytical and Experimental IP Encapsulation Efficiency Comparison of GSE, MPE, and ULE over DVB-S2," in *Proc. Int. Workshop on Satellite and Space Commun.*, Salzburg, Austria, pp. 114 - 118, Sep. 2007.

[26] F. Vieira, M. A. Váquez Castro, and J. Lei, “Datacast Transmission Architecture for DVB-S2 Systems in Railway Scenarios,” in *Proc. 10th Int. Workshop on Signal Process. for Space Commun.,* Rhode Island, Greece, Oct. 2008.

[27] M. A. Váquez Castro and G. S. Granados, “Cross-Layer Packet Scheduler Design of a Multibeam Broadband Satellite System with Adaptive Coding and Modulation,” *IEEE Trans. on Wireless Commun.*, vol. 6, no. 1, pp. 248 - 258, Jan. 2007.

Paper E

MPE/ULE-FEC vs GSE-FEC Efficiency Comparison of IP Datagram Transmission over DVB-S2

J. Lei, G. Seco Granados, and M. A. Vázquez Castro

25th AIAA International Communication Satellite Systems Conference, (ICSSC 2007) Seoul, Korea, 10-13 April, 2007.

Abstract

In this paper, the transport efficiency of Multi Protocol Encapsulation (MPE), Unidirectional Lightweight Encapsulation (ULE) and Generic Stream Encapsulation (GSE) for typical IP packet sizes is compared. Moreover, the aggregated efficiency when applying packet-level forward error correction (PL-FEC) with MPE, ULE and GSE is also analyzed. MPE-FEC is the mechanism used by DVB-H whereas GSE-FEC is our proposed modification to be used in DVB-S2. A layered efficiency calculation model is presented in order to simplify the computation. The performance of GSE-FEC is also analyzed when adopted by the IP traffic and DiffServ Classes with different modulations and coding rates (ModCods). Theoretical analysis and simulation revealed that GSE-FEC is more efficient than MPE-FEC and ULE-FEC for DVB-S2 networks.

E.1 Introduction

DVB-S2 is the second-generation DVB specification for broadband satellite applications [1], developed after the ccess of the first generation specifications of DVB-S (shown in [2]) for broadcasting and DVB-DSNG in [3]) for satellite news gathering and contribution services, benefiting from the technological achievements of the last decade. It has been designed for:

- Broadcast Services for standard definition TV and High-Definition TV (HDTV).
- Interactive Services including Internet Access for consumer applications.
- Professional Applications, such as Digital Television (DTV) contribution and News Gathering, TV distribution to terrestrial Very High Frequency/UltraHigh Frequency (VHF/UHF) transmitters, Data Content distribution and Internet Trunking.

The DVB-S2 standard has been specified around three key concepts: best transmission performance, total flexibility and reasonable receiver complexity. It is a specification for next-generation digital satellite transmission emerging from technical ad-hoc DVB working groups. It should progressively complement DVB-S aiming at offering new services and improving capacity dramatically.

The encapsulation of DVB-S2, unlike DVB-S, allows for several input stream formats. In addition to MPEG transport streams (TS), generic streams (GS) are encompassed by the standard. The DVB-S2 standard introduces generic stream transport method not only for providing digital TV services, but also as technology for building IP networks and dedicated data streaming.

Multi Protocol Encapsulation (MPE) is widely used in current DVB-S systems for encapsulating Internet Protocol (IP) datagrams over MPEG-TS, which is based on the Digital Storage Media Command and Control (DSM-CC) [4]. MPEG-TS is used in almost all contemporary digital broadcasting systems, including the DVB and the standards of Advanced Television Systems Committee (ATSC) family as the format of baseband data, organized in a statistically multiplexed sequence of fixed-size, 188-byte TS Packets. Initially intended to convey MPEG-2 encoded audio and video streams, the MPEG-2 TS was eventually used also for the transport of IP traffic, with the adaptation method introduced in [5] and named as Multi Protocol Encapsulation. The adoption of MPE accented the role of DTV platforms as access networks for IP-based broadband data and multimedia services [6]. Broadcasters have the potential to use a part of the capacity of the broadcast channel to include unicast or multicast IP traffic along with the audiovisual streams [4]. What is more, state-of-the-art broadcasting technologies, such as DVB-H or DVB-S2 are IP-oriented and actually expected to carry exclusively IP data rather than MPEG-2 content.

This tendency towards the convergence of the worlds of digital broadcasting and IP-based telecommunications has initiated research efforts towards a more efficient and flexible encapsulation protocol [7]. The IP-over-DVB (IPDVB) working group of IETF has proposed an improvement of MPE, namely the Unidirectional Lightweight Encapsulation (ULE, formerly Ultra Light Encapsulation) [8–10]. In comparison to MPE, ULE offers simplicity, improved efficiency, native IPv6/MPLS (Multi Protocol Label Switching) support and greater flexibility via optional Extension Headers. ULE has been adopted by IETF as a "Request for Comments" (RFC) document.

Anther alternative protocol is Generic Stream Encapsulation (GSE), which is designed for the transmission of IPv4 datagrams and other network protocol packets directly over the DVB-S2 Generic Stream [1]. The protocol specifies an encapsulation format and fragmentation over DVB-S2 baseband frames (BBFrames), the size of which is variable ranging from 384B to 7274B. The encapsulation part of GSE relies in some fundamental design choices of ULE. GSE uses the same Type Field as ULE that allows it to carry additional header information to assist in network/Receiver processing, but specifies a generic fragmentation method, a different base encapsulation format and another processing method because of the substantially different underlying link-layer.

Forward Error Correction (FEC) will be likely introduced in applications where signal reception shows high Packet Loss Ratio (PLR). Such high PLR may be caused for example by the repeated presence of obstacles, such as the power arches in the railway. With the FEC about 25% of TS or GS data will be allocated to parity overhead, because 64 columns of FEC frame (255 columns) are used to pad RS data. The protocol of MPE-FEC is introduced in [5] and [11]. The issues of MPE efficiency have been studied by some papers from different angles. In [12], the authors compared two different schemes (padding and packing) of stuffing at the end of TS packet. The transport efficiency of MPE and ULE has been analyzed in [8; 9] and [13] over MPEG-2/DVB networks. In [10], a network simulation model is built to compare the performance of MPE and ULE. The layered model of DVB-S2 has been studied in [14].

In this paper, the efficiency of MPE, ULE and GSE is compared for typical IP packet sizes. Moreover, we also analyze the aggregated efficiency when applying packet-level forward error correction (PL-FEC) at MPE, ULE and GSE. The efficiency of DiffServ is also analyzed using GSE-FEC over DVB-S2 network. The intention of this paper is to compare the transport efficiency of MPE-FEC, ULE-FEC and GSE-FEC for IP transmission and to present the characteristics of GSE-FEC used in IP traffic and DiffServ classes over DVB-S2 networks. The rest of this paper is organized as follows. Section E.2 analyses the encapsulation procedure for each protocol and outlines the benefits of GSE for DVB-S2. Section E.3 presents a layered efficiency calculation model to compute the encapsulation efficiency for each protocol. Section E.4 defines the simulation parameters and compares the results of encapsulation efficiency for each protocol over DVB-S2 networks. Section E.5 concludes the paper.

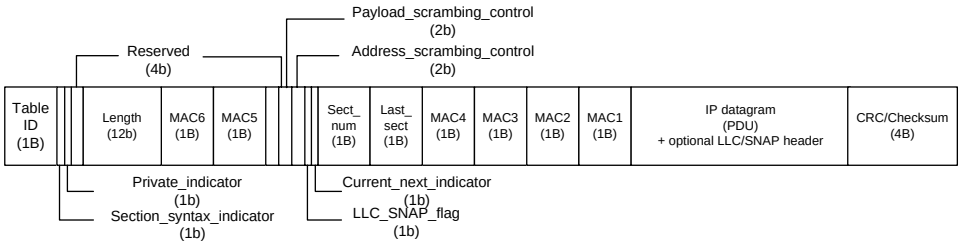

Fig. E.1: Structure of the MPE SNDU section.

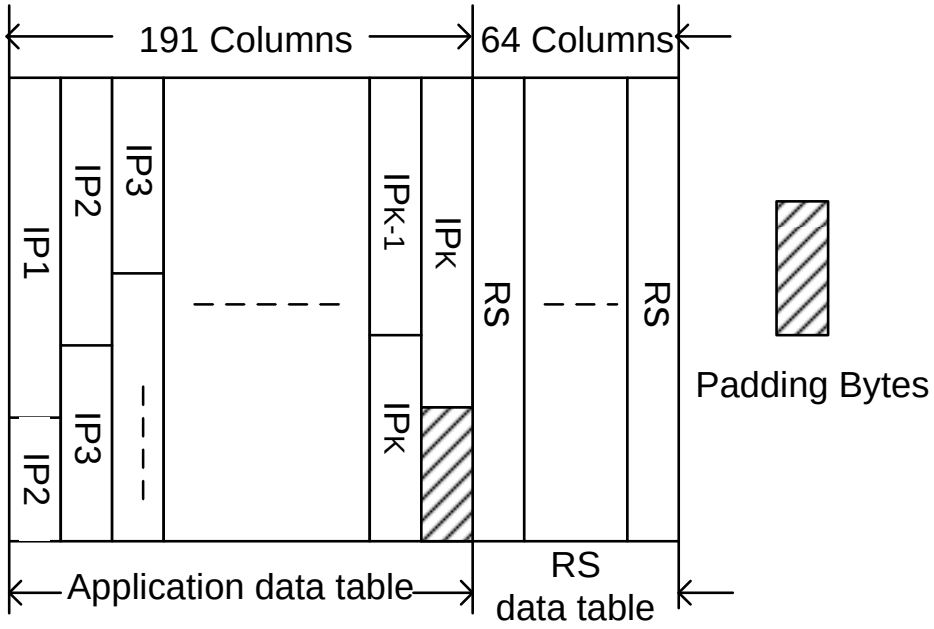

Fig. E.2: The structure of the MPE-FEC frame.

E.2 Encapsulation Protocol Overview

E.2.1 Multi Protocol Encapsulation

MPE has already been world-widely adopted in both IP/MPEG-2 Gateways and decapsulators/receivers, as being the only IP-to-MPEG-2 encapsulation protocol for almost a decade. Using MPE, each IP packet arriving at an MPEG Encapsulation Gateway has an MPE header attached to form a network layer packet named Protocol Data Unit (PDU). The entire PDU is then fragmented to form a series of MPEG-2 TS Packets. Since IP packets are of variable size, it is reasonable to expect most IP packets will be placed in a series of TS packets. A one-bit Payload Unit Start Indicator (PUSI) in the TS packet header and one-byte PTR after the TS header indicate a specific TS packet carries the start of a new TS Packet payload.

The basic MPE header format carries a MAC destination address, but no payload type field. This leads to the assumption in most current Receiver driver software that

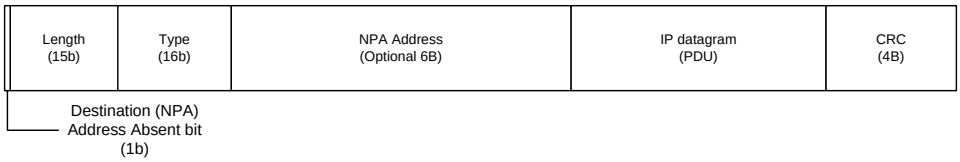

Fig. E.3: Structure of the ULE SNDU section.

the payload is IPv4. If the payload is other IPv4, such as IPv6 packet, a type field is required to de-multiplex the received packets. In MPE, this requires the inclusion of the optional Logical Link Control/Sub-Network Access Point (LLC/SNAP) header (4 bytes).

In most cases, the end of an IP packet does not precisely align to the end of a TS packet payload, one or more bytes will typically be free and may be unused (Padding) or used to carry a subsequent packet (Packing). Encapsulators and the corresponding receivers may use either mechanism, but must choose the same one. TS packet padding is the default mechanism within MPE.

As shown in Fig. E.1, the structure of MPE Subnetwork Data Unit (SNDU) section, the main drawback of MPE is the inclusion of several MPEG specific fields in the section header, which in fact can as well be omitted. Moreover, the declaration of the receiver MAC address, which is not always necessary, since the TS is itself a sub-network layer and the traffic is already divided in logical channels, is mandatory in MPE, adding an overhead of 6 more bytes. Another issue is the absence of the declaration of type of data contained in the SNDU. MPE offers the option of either having a pure IP payload (no discrimination between v4 and v6), or carrying the data with an LLC/SNAP header. Thus, there is no uniform representation of the type of the encapsulated data, as it exists e.g. in Ethernet framing with the Type field.

MPE-FEC is the mechanism used by DVB-H [11], which is introduced in order to support reception in situations of high PLR on the MPE section level. The use of MPE-FEC is not mandatory and is defined separately for each elementary stream in the TS. For each elementary stream it is possible to choose whether or not MPE-FEC is used, and if it is used, to choose the trade-off between FEC overhead and RF performance. The MPE-FEC Frame is arranged as a matrix with 255 columns and a flexible number of rows. The number of rows is specified at header and the value is variable. Fig. E.2 shows the structure of the MPE-FEC frame.

E.2.2 Unidirectional Lightweight Encapsulation

ULE is an alternative encapsulation method to MPE, providing simplicity, efficiency and configurability. It was designed with the aim of making the encapsulation process as lightweight as possible without sacrificing flexibility. It follows the approach of “data piping” i.e. directly mapping the PDU into the TS payload, adding only a small header. ULE header contains just a Length field which declares the length of the SNDU, and a Type field which has the same functionality with that of Ethernet i.e.

it declares the type of the payload. Thanks to the Type field, ULE provides native support for state-of-the-art network protocols, such as IPv6 and MPLS. Depending on the value of this field, the PDU can be an IPv4 datagram, IPv6 datagram, MPLS and so on.

The ULE header can also include a 6-byte destination address corresponding to the receiver's Network Point of Attachment (NPA). The NPA address (which can correspond to the receiver's MAC) is used to uniquely identify a receiver in the MPEG-2 transmission network and is mandatory only in the case that the PDU is to be processed by a receiver-router, which will further forward it to its final destination. If this is not the case and the data is directly received by the destination terminal, this field can be omitted and filtering can be performed at IP level.

If there is additional SNDU-level signaling which cannot be carried in the existing header fields, ULE provides the option of adding one or more Extension Headers after the standard header and before the PDU, carrying the data which are needed. Finally, a CRC-32 tail is appended (as in MPE) to ensure proper reception and synchronization. Figure E.3 shows the structure of the ULE SNDU section. The framing has become as lightweight as possible (comparing with Fig. E.1), retaining only the necessary fields for proper de-encapsulation and forwarding of the IP datagram. After framing, the ULE SNDU is mapped to the payload of MPEG-2 TS packets. In the case that the SNDU length is not an integer multiple of the TS payload and the stuffing techniques of Padding or Packing can be employed.

Figure E.3 shows the structure of the ULE SNDU section. Comparing with MPE, it is sufficient to demonstrate the simplicity introduced by lightweight header. By reducing the framing fields only to the necessary ones, ULE saves bandwidth and processing time at the encapsulator.

E.2.3 Generic Stream Encapsulation

Anther alternative lightweight encapsulation protocol to MPE is GSE, which is designed specially for DVB-S2 networks and allows TS Packets to be sent as GSE SNDU sections.

GSE protocol allows for direct encapsulation of IP and other network-layer packets over DVB-S2 physical layer frames. The encapsulation and fragmentation of IP datagrams for transport over DVB-S2 Generic Streams have been defined in [12]. Firstly, the PDUs are encapsulated in SNDUs by adding the SNDU header and optional checksum bytes. The structure of PDU and SNDU are illustrated in Fig. E.4. Then the SNDU sections are encapsulated in one or more GS units. Each GS unit is made of GS header and Data Field. The size of GS header ranges from 2B to 5B depending on the PDU fragmented or not. The length of GS Date Field is variable ranging from 1B to 4kB, because the size of IP packets and the number of GS units in each SNDU section are both variable. Figure E.4 also shows the encapsulation of SNDUs and the structure of GS units.

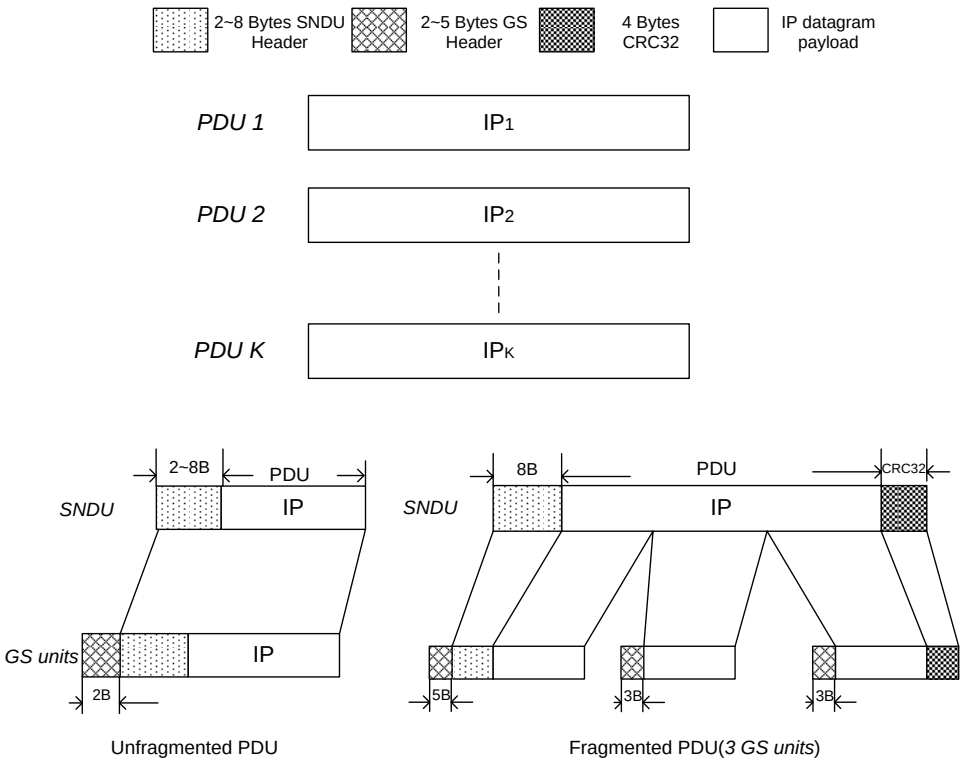

Fig. E.4: The structure of PDU, SNDU and GS units.

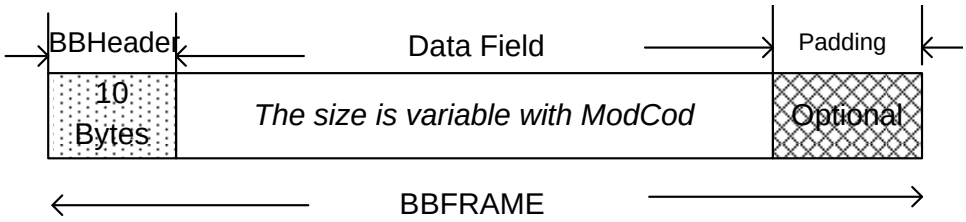

Fig. E.5: The structure of BBFrame.

The size of SNDU header ranges from 2B to 8B because the part of Label (3B or 6B) is optional and Protocol field (2B) is mandatory. CRC32 (4B) will be attached at the end of the last GS unit if SNDU section is encapsulated in several GS units as shown in Fig. E.4.

The SNDU is transmitted over a DVB-S2 link by placing it either in a single GS which is sent in one BBFrame, or if required, a PDU may be fragmented into several GS units, which are sent in one or a series of BBFrames. The size of BBFrames varies from 384 bytes to 7274 bytes. Adaptive Coding and Modulation (ACM) allows for changing ModCods on-the-fly and in accordance with the link quality perceived at the receivers. Consequently the receiver will be able to demodulate and decode only those BBFrames whose ModCods matches the perceived link quality. The DVB-S2 standard permits an encapsulator to transmit different network layer packets destined to a specific receiver into BBFrames with different ModCods, and feedback from the receiver

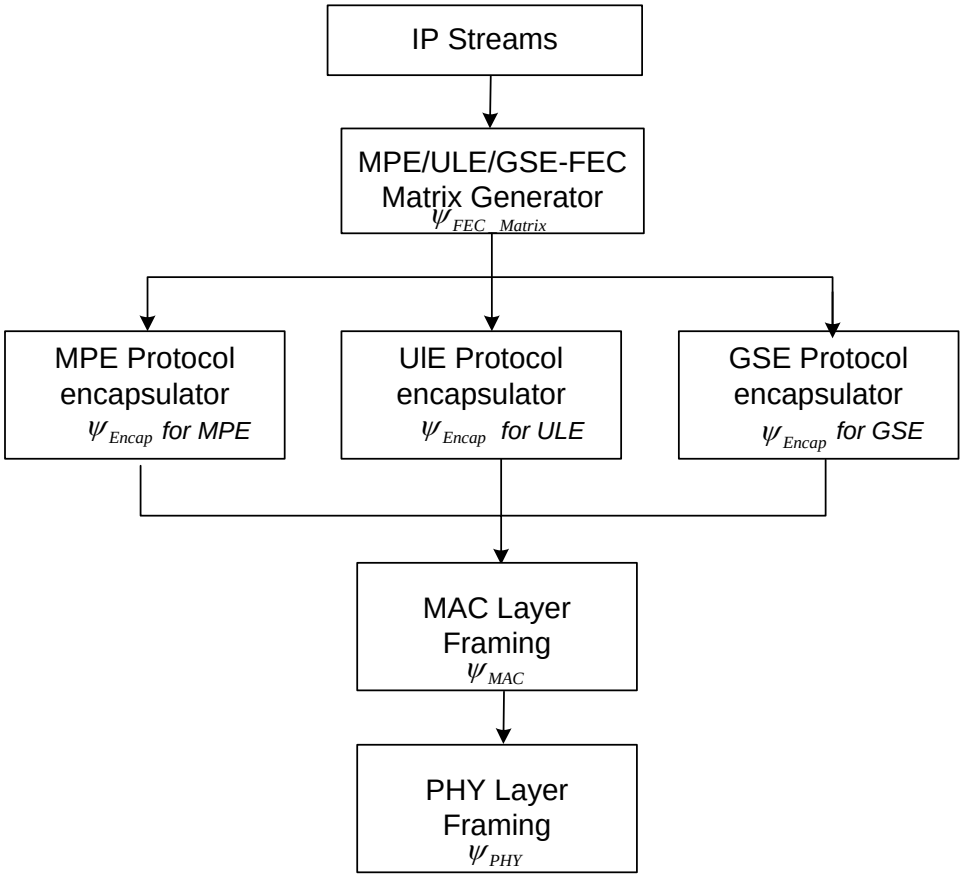

Fig. E.6: The flow chat of the encapsulation efficiency.

about its link quality may trigger ModCods changes at any time. The 10B header of a BBFrame carries the length of the Datafield, but it is different to the 4B header of a TS packet, does neither include the PUSI nor a Transport Error Indicator (TEI), GS units will resemble its own Start and End Indicator for reassembly of encapsulated units instead. The structure of BBFrames is shown in Fig. E.5.

GSE-FEC is a modification of MPE-FEC mechanism to use in DVB-S2. The PL-FEC is applied in DVB-S2 using the same logic as in DVB-H, that is to say, it is applied on the IP datagrams. The GSE-FEC matrix is constructed with IP datagrams in the left-hand side (191 columns) and parity byte (RS data) on the right-hand side (64 columns without puncturing) as Fig. E.2 shows. Thus about 25% of GS data will be allocated to parity overhead.

E.3 Definition of the Encapsulation Efficiency

In order to estimate the packet level encapsulation efficiency for transporting IP packets over DVB-S2 networks, a layered simulation model is presented in Fig. E.6. Tra-

Table E.I: The number of slots and Physical Layer efficiency with different Modulation type

η_{MOD}	$S(\eta_{MOD})$	$\psi_{PHY}(\eta_{MOD})$
2(QPSK)	360	99.72%
3(8PSK)	240	99.59%
4(16APSK)	180	99.45%
5(32APSK)	144	99.31%

ditionally, the encapsulation efficiency is defined using Eq. (E.1).

$$\psi = \frac{L_{PL}}{L_{TM}}, \tag{E.1}$$

where L_{PL} and L_{TM} are payload bits and total transmitted bits after encapsulation respectively.

Considering the layered conception shown in Fig. E.6, the total efficiency of DVB-S2 can be expressed using Eq. (E.2).

$$\begin{aligned}&\psi_{TOT}(L_{IP}, \eta_{punct}, \eta_{Cod}, \eta_{Mod}) = \\ &\psi_{FEC-Matrix}(L_{IP}, \eta_{punct})\psi_{Encap}(L_{IP})\psi_{MAC}(L_{IP}, \eta_{Cod})\psi_{PHY}(\eta_{Mod}),\end{aligned} \tag{E.2}$$

where the total efficiency is composed of four parts: $\psi_{FEC-Matrix}$, ψ_{Encap}, ψ_{MAC} and ψ_{PHY}, which are the FEC matrix framing efficiency, encapsulation efficiency for MPE, ULE or GSE, MAC layer framing efficiency and PHY layer efficiency respectively. And L_{IP} is the packet size of IP datagram. η_{punct}, η_{Cod} and η_{Mod} are the puncturing column efficiency, coding rate, and modulation spectral efficiency.

Regarding the effect of the statistical distribution of the IP packet size for different Quality of Service (QoS), the efficiency of Eq. (E.2) can be rewritten as follows:

$$\bar{\psi}_{TOT}(\eta_{punct}, \eta_{Cod}, \eta_{Mod}) = \sum_{L_{IP}} \psi_{TOT}(L_{IP}, \eta_{punct}, \eta_{Cod}, \eta_{Mod}) p(L_{IP}). \tag{E.3}$$

Each part of the total efficiency can be expressed using the following equations.

$$\psi_{FEC-Matrix}(L_{IP}, \eta_{punct}) = \frac{L_{PL-Matrix}(L_{IP})}{L_{PL-Matrix}(L_{IP}) + L_{RS}(\eta_{punct}) + L_{Matrix-padding}}, \tag{E.4}$$

$$\psi_{Encap}(L_{IP}) = \frac{L_{PL-Encap}(L_{IP})}{L_{PL-Encap}(L_{IP}) + L_{H-Encap} + L_{CRC}}, \tag{E.5}$$

$$\psi_{MAC}(L_{IP},\eta_{Cod}) = \frac{L_{PL-BBFrame}(L_{IP},\eta_{Cod})}{L_{PL-BBFrame}(L_{IP},\eta_{Cod}) + L_{H-BBFrame} + L_{CRC} + L_{BBFrame-padding}}, \tag{E.6}$$

$$\psi_{PHY}(\eta_{Mod}) = \frac{90S(\eta_{Mod})}{90(S(\eta_{Mod})+1) + 36\text{int}\left\{\frac{S(\eta_{Mod})-1}{16}\right\}}, \tag{E.7}$$

where L_{RS} and L_{CRC} are the size of RS data and CRC data. $L_{H-Encap}$ is size of the SNDU header and MPE, ULE or GSE header. $L_{H-BBFrame}$ is the size of BBFrame header. $L_{PL-Matrix}$ and $L_{PL-BBFrame}$ are the size of the FEC Matrix payload and BBFrame payload. The packets of the MAC layer are presented as BBFrames in DVB-S2. The PHY layer efficiency of DVB-S2 depends on the modulation scheme. The packets of the Physical layer are a stream of FLFrames. The FLFrame is composed of an FLHeader and an integer number $S(\eta_{Mod})$ of slots, each slot contain 90 symbols. And pilot blocks (optional) insert every 16 slots to help receiver synchronization, and each pilot block is composed of 36 pilot symbols. Table E.I presents the PHYFraming efficiency with normal FECFRAME (64800 bits) for different Modulation type [14]. The efficiency is very close to 100%. Therefore, the total efficiency of DVB-S2 network can be approximated without considering the spectral efficiency of Modulation. Therefore, Eq. (E.2) and (E.3) can be approximated as Eq. (E.8) and (E.9).

$$\psi_{TOT}(L_{IP},\eta_{punct},\eta_{Cod}) \approx \psi_{FEC-Matrix}(L_{IP},\eta_{punct})\psi_{Encap}(L_{IP})\psi_{MAC}(L_{IP},\eta_{Cod}), \tag{E.8}$$

$$\bar{\psi}_{TOT}(\eta_{punct},\eta_{Cod}) \approx \sum_{L_{IP}} \psi_{TOT}(L_{IP},\eta_{punct},\eta_{Cod})p(L_{IP}). \tag{E.9}$$

The FEC matrix framing efficiency $\psi_{FEC-Matrix}$ will be 75% without using padding columns and puncturing RS columns, which is affected by the size of IP datagram and puncturing column efficiency. $\psi_{FEC-Matrix}$ can be improved by introduce the conception of puncturing RS columns or appropriate size of IP packet. But puncturing columns will deteriorate the performance of the receiver because of the less FEC bytes attached. Therefore, it should balance the performance and efficiency here.

ψ_{Encap} is calculated when IP datagrams are encapsulated as PDU, SNDU and then fragmented as TS packets for MPE and ULE or GS units for GSE. For MPE and ULE, ψ_{Encap} is affected by the size of SNDU header and IP packets, also affected by the type of stuffing schematic (padding or packing) used at the end of each TS packet. The larger size of IP packet the better, because each IP datagram is encapsulated as one SNDU. For GSE, anther factor affects ψ_{Encap} is the number of GS units encapsulating each SNDU. The more GS units the worse because of much more overhead introduced

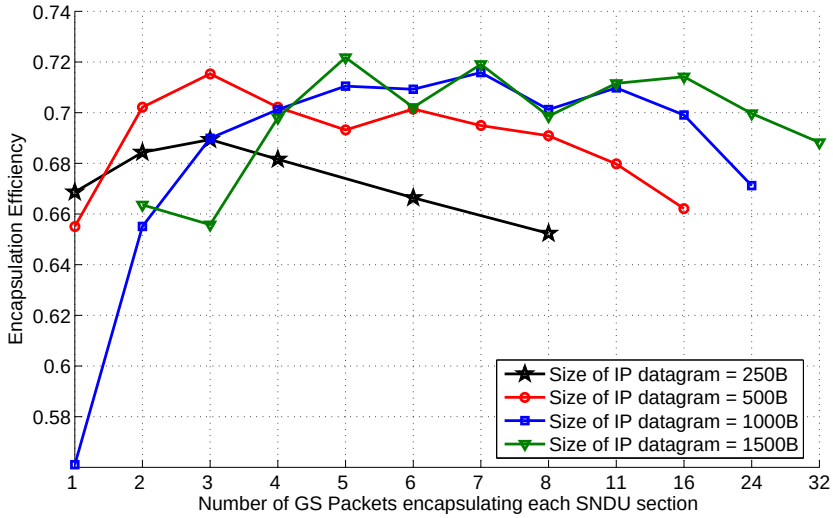

Fig. E.7: The Efficiency of GSE-FEC over BBFraming with different number of GS units.

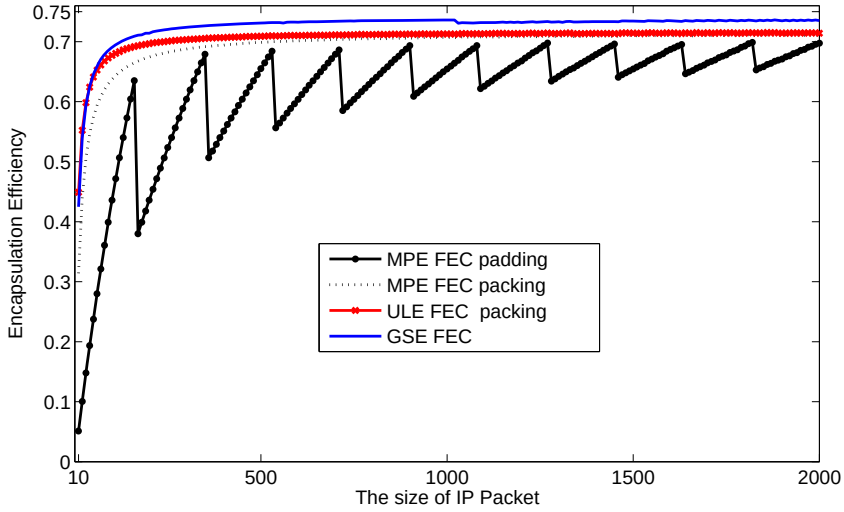

Fig. E.8: The Efficiency of GSE-FEC, ULE-FEC and MPE-FEC ($\psi_{TOT}(L_{IP}, \eta_{punct} = 0, \eta_{Cod} = 3/4)$).

by the GS header.

ψ_{MAC} is affected by the Coding rate and statistical distribution of the IP packets.

E.4 Simulation Description

In this paper, the simulation is done in MATLAB. The efficiency of MPE, ULE and GSE with FEC is computed over DVB-S2 using the model presented in Section E.3.

Table E.II: Packet size definitions for DiffServ classes

DiffServ-Class	Class Name	Packet Size
EF	Premium	60 Byte
AF Class 1 (AF1)	Gold	40 Byte
AF Class 2 (AF2)	Silver	552 Byte
AF Class 3 (AF3)	Bronze	576 Byte
BE	Best-Effort	1500 Byte

The size of IP datagram ranges from 10B to 2000B when comparing the efficiency of these three encapsulation protocols. And the typical IP packet sizes (shown in Table E.II) for DiffServ Classes are also simulated. Two different types of stuffing schematic, padding and puncturing, are simulated and compared for MPE and ULE protocol. The number of rows of the FEC matrix is 1024 (Byte), which makes the total FEC frame 2M bits.

Figure E.7 presents the efficiency of GSE-FEC with different number of GS units fragmented by the SNDU section. The efficiency first increases and then drops for any size of IP datagram. Because the padding is dominant when the number of GS unit is small and the overhead of total GS header is dominant when the number of GS unit is large. So an optimal number of GS unit exist when fragmenting each SNDU section. The efficiency of MPE-FEC, ULE-FEC and GSE-FEC is shown in Fig. E.8. It's clear that the result of all the types is below 75% because of the FEC framing, and padding mode is worse than packing. The efficiency fluctuates with packet size, is the same for these three protocols. The zigzag efficiency for padding mode results from the fixed size of TS packet (188B) and the efficiency will be maximized when the SNDU fits exactly into an integer number of TS packets.

The conception of puncturing RS columns is conducted in Fig. E.9 and Fig. E.10 in order to decrease overhead introduced by the RS data. It's clear that puncturing will increase efficiency because the punctured RS columns are not transmitted. A decreased level appears at Fig. E.8 and Fig. E.9 when the size of IP datagram is larger than 1024B due to the number of the column is fixed at 1024 and the efficiency will be maximized when the size of IP datagram is exactly 1024B.

$$\psi_{TOT}(L_{IP}, \eta_{punct}) \approx \psi_{FEC-Matrix}(L_{IP}, \eta_{punct})\psi_{Encap}(L_{IP})\psi_{MAC}(L_{IP}), \tag{E.10}$$

$$\bar{\psi}_{TOT}(\eta_{punct}) \approx \sum_{L_{IP}} \psi_{TOT}(L_{IP}, \eta_{punct})p(L_{IP}). \tag{E.11}$$

Figure E.10 shows the average efficiency of IP traffic with different Coding Rates. And the efficiency is computed using the Eq. 9 with GSE-FEC encapsulation. The probability distribution of IP packet size of IP traffic is shown in Fig. E.11, which is

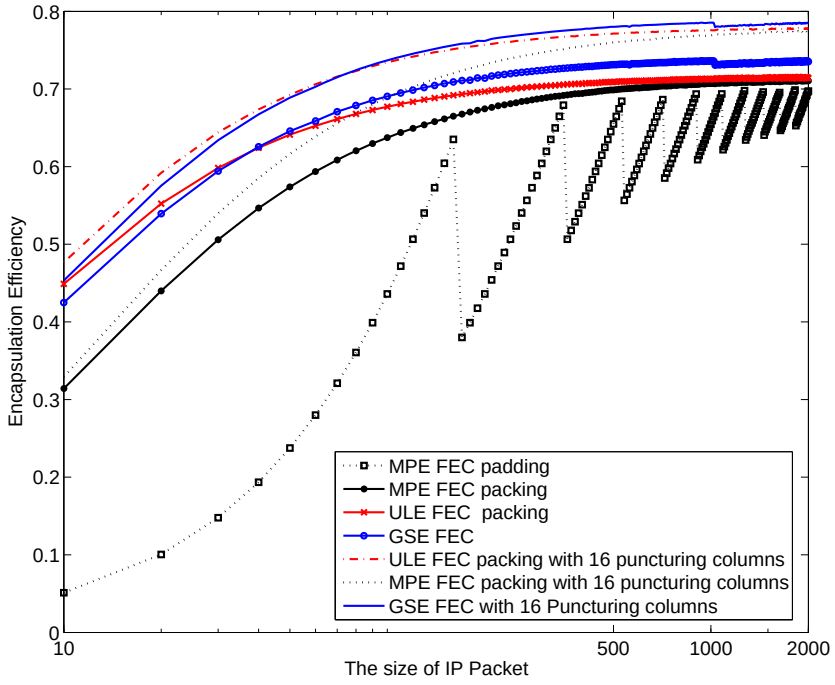

Fig. E.9: The efficiency of GSE-FEC, ULE-FEC and MPE-FEC with and without puncturing RS columns ($\psi_{TOT}(L_{IP}, \eta_{punct} = 0 or 16, \eta_{Cod} = 3/4)$).

referred in [15]. The efficiency increases with the increasing of coding rate, which can be explained that the higher coding rate the larger size of Data Field for the BBFrame (shown in Fig. E.5). Therefore, the overhead will decrease because of more payload datagram encapsulated in each BBFrame. However, the influence of the coding rate is less than IP packet size and puncturing efficiency. The efficiency increases only 0.7% when Coding Rates change from 1/4 to 9/10. Therefore, the total efficiency in Eq. (E.8) and (E.9) can be simplified as Eq. (E.10) and (E.11) without considering Coding Rates.

Table E.II is the typical packet size for DiffServ classes [16], the efficiency varies from the DiffServ classes, such as Assured Forwarding (AF), Expedited Forwarding (EF) and Best Effort (BE). Table E.III is the efficiency of GSE-FEC with different Mod-Cods for DiffServ classes. The results show that BE has the best efficiency because the efficiency is proportional with the packet size as Fig. E.8 and Fig. E.9 shows. And the efficiency for all DiffServ Classes can be improved with puncturing columns.

E.5 Conclusion

In this paper, PL-FEC is applied at three different encapsulation protocols MPE, ULE and GSE. A layered efficiency calculation model is presented in order to compute the transport efficiency of MPE-FEC ULE-FEC and GSE-FEC over DVB-S2 networks.

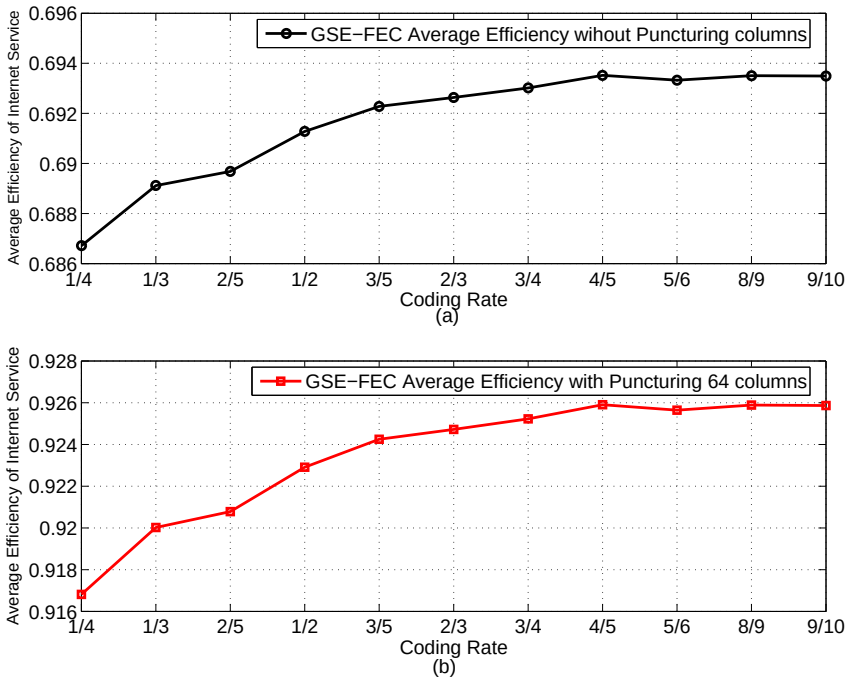

Fig. E.10: The average efficiency of internet service with different coding rate using GSE-FEC ((a)$\bar{\psi}_{TOT}(\eta_{punct}=0,\eta_{Cod})$; (b)$\bar{\psi}_{TOT}(\eta_{punct}=64,\eta_{Cod})$).

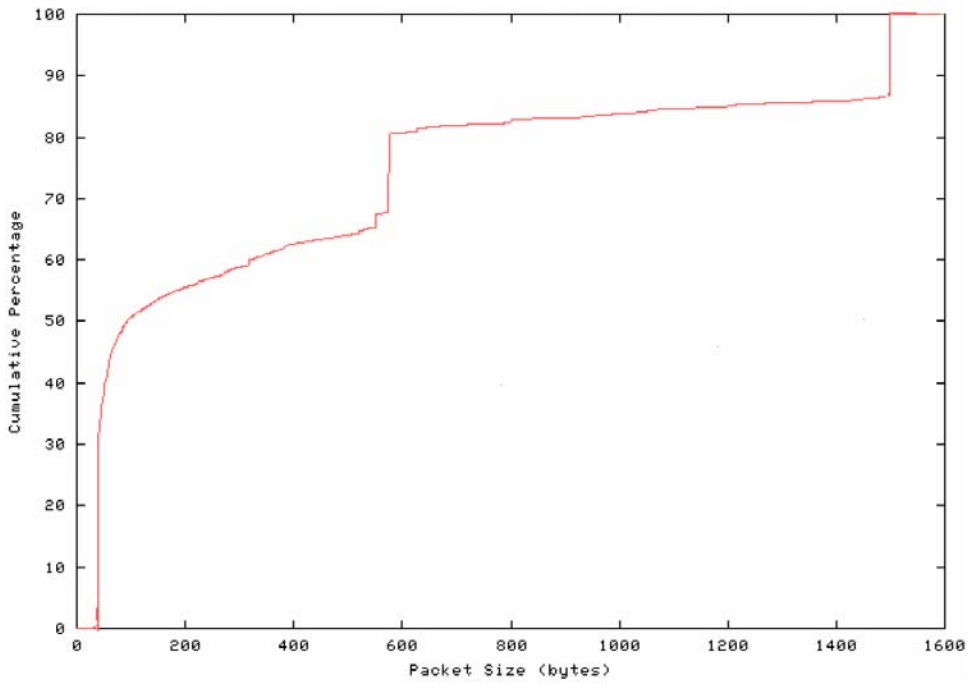

Fig. E.11: The cumulative distribution of packet sizes of IP traffic.

The performance of GSE-FEC is also analyzed when adopted by the IP traffic and

Table E.III: The efficiency of DiffServ classes with different ModCod using GSE-FEC encapsulation ($\psi_{TOT}(L_{IP}, \eta_{punct} = 0 \text{ or } 64, \eta_{Cod})$)

	MODCOD		DiffServ Classes				
	Modulation	Coding Rate	EF	AF1	AF2	AF3	BE
Without Puncturing Columns	QPSK	1/4	0.6500	0.6194	0.7251	0.7254	0.7273
	8PSK	3/5	0.6580	0.6225	0.7299	0.7302	0.7321
	16APSK	3/4	0.6575	0.6234	0.7298	0.7300	0.7320
	32APSK	8/9	0.6573	0.6224	0.7292	0.7294	0.7314
Puncturing 64 Columns	QPSK	1/4	0.8678	0.8269	0.9681	0.9685	0.9710
	8PSK	3/5	0.8785	0.8311	0.9745	0.9749	0.9774
	16APSK	3/4	0.8778	0.8323	0.9743	0.9746	0.9773
	32APSK	8/9	0.8775	0.8310	0.9735	0.9738	0.9765

DiffServ Classes with different ModCods. The results show that the total efficiency of DVB-S2 network has a low relation with ModCods and can be approximated as a function only with the distribution of IP packet size and puncturing efficiency. The theoretical analysis and comparison of the simulation results revealed that GSE-FEC is more efficient than MPE-FEC and ULE-FEC for DVB-S2 networks. The efficiency of GSE-FEC can be also improved by puncturing RS columns. The results show that the efficiency is improved about 5% with puncturing 16 RS columns and 25% with puncturing 64 RS columns. But the number of punctured RS columns should be designed precisely because it will deteriorate the performance of the receive systems.

Bibliography

[1] ETSI TR 102 376 v1.1.1, Digital Video Broadcasting: User guidelines for the second generation system for Broadcasting Interactive Services, News Gathering and other broadband satellite applications(DVB-S2), Feb. 2005.

[2] ETSI EN 300 421, Digital Video Broadcasting: Framing structure, channel coding and modulation for 11/12 GHz satellite services (DVB-S).

[3] ETSI EN 301 210, Digital Video Broadcasting: Framing structure, channel coding and modulation for Digital Satellite News Gathering (DSNG) and other contribution applications by satellite (DVB-DSNG).

[4] Generic Coding of Moving Pictures and Associated Audio Information (MPEG-2) Part 1: Systems, ISO/IEC 13818-1, Second edition, Dec. 2000.

[5] ETSI EN 301 192 v1.4.1, Digital Video Broadcasting(DVB); DVB specification for data broadcasting, Nov. 2004.

[6] D. Kouis and D. Loukatos et al., "On the Effectiveness of DVB-T for the Support of IP-based Services in Heterogeneous Wireless Networks," *Computer Networks*, vol. 48, no. 1, pp. 57 - 73, May 2005.

[7] DVB-UMTS Ad Hoc Group, The Convergence of Broadcast and Telecomms Platforms Report No 1, Mar. 2001.

[8] G. Xilouris, G. Gardikis, H. Koumaras, and A. Kourtis, "Unidirectional Lightweight Encapsulation: Performance Evaluation an Dapplication Perspectives," *IEEE Trans. on Broadcasting*, vol. 52, no. 3, pp. 374 - 380, Sep. 2006.

[9] T. C. Hong, W. Chee, and R. Budiarto, "A Comparison of IP Datagrams Transmission using MPE and ULE over Mpeg-2/DVB Networks," in *Proc. Fifth Int. Conf. on Inf., Commun. and Signal Process.*, pp. 1173 - 1177, Dec. 2005.

[10] T. C. Hong, W. Chee, and R. Budiarto, "Simulation and Desigh of IP over DVB using Multi-Protocol Encapsulation and Ultra Lightweight Encapsulation," in *Proc. National Computer Science Postgraduate Colloquium*, Penang, Malaysia, Jun. 2005.

[11] ETSI TR 102 377 V1.2.1, Digital Video Broadcasting: DVB-H Implementation Guidelines, Nov. 2005.

[12] Technical Note GBS 05311, DVB TM-GBS, "Procedure for Comparative Evaluation of IP/DVB-S2 Encapsulation Protocol over Generic Streams."

[13] G. Fairhurst and A. Matthews, "A comparison of IP transmission using MPE and a new lightweight encapsulation," in *Proc. IEE Seminar on IP Over Satellite - The next Generation: MPLS, VPN and DRM Delivered Services*, pp. 106 - 120, 2003.

[14] M. A. Vázquez-Castro, A. Cardoso, R. Rinaldo, "Encapsulation and Framing Efficiency of DVB-S2 Satellite Systems," in *Proc. IEEE 59th Veh. Technol. Conf.,-Spring*, vol. 5, pp. 2896 - 2900, May 2004.

[15] S. McCreary, "Packet Length Distribution" [online database], URL: $http://www.caida.org/analysis/AIX/plen_hist/index.xml$.

[16] "40-Gig Router Test Results" [online database], URL: $http://www.lightreading.com/page_number = 1\&table_number = 4$.

Paper F

Application of Link Layer FEC to DVB-S2 for Railway Scenarios

J. Lei, T. Stockhammer, M. A. Vázquez Castro, and F. Vieira

10th International Workshop on Signal Processing for Space Communications (SPSC 2008), Rhodes Island, Greece, 6 - 8 Oct. 2008.

Abstract

In this paper, we analyze the performance improvement of the Second Generation Digital Video Broadcasting via Satellite (DVB-S2) when applying Forward Error Correction (FEC). DVB-S2 was designed for fixed terminals and thus we apply FEC at the Link Layer (LL) level in order to achieve reliable reception in mobile environment. Specifically, we focus on the railway scenario and analyze the performance and compatibility of the different LL-FEC schemes already available in the DVB family of standards: Multiple Protocol Encapsulation-FEC (MPE-FEC), MPE-FEC Sliding Encoding and MPE Inter-Burst FEC (MPE-IFEC). These are analyzed and compared when adopting Reed-Solomon (RS) or Raptor FEC Codes. A simulation framework for LL-FEC over DVB-S2 systems is presented and an optimization of FEC code parameters is proposed. Two typical railway scenarios have been analyzed: Line-of-Sight together with the effect of Power Archers (LOS+PA) and non-Line of Sight (nLOS). Theoretical analysis and simulation revealed that LL-FEC can overcome the fade in the railway scenarios in case appropriate FEC codes parameters are used.

F.1 Introduction

Increased interactivity is a general trend for telecommunication services today. Satellite communications can be a “natural” solution for extending the interactive services for point-to-point multimedia applications, by taking advantage of satellites’ capability to efficiently distribute information over very large geographical areas and given the large available bandwidth in the Ku/Ka band. Particularly in Europe, due to the success of digital video broadcasting via satellite (DVB-S) [1], an important technical foundation has been laid for the evolution of satellite communications into this new market by using the second generation of DVB-S [2], commonly referred to as DVB-S2, as well as the Return Channel via Satellite (DVB-RCS) [3] standards.

In general, the mobile terminals will have to cope with stringent frequency regulations (especially in Ku band), Doppler effects, frequent handovers and impairments in the synchronization acquisition and maintenance. Furthermore, the railway scenario is affected by shadowing and fast fading due to mobility, as well as deep and frequent fades. This mainly results from the presence of metallic obstacles along electrified lines and long blockages, for example, due to the presence of tunnels and large train stations. In this paper, Link Layer Forward Error Correction (LL-FEC) will be introduced as fading countermeasure of to compensate the impact of the railway scenarios, in particular shadowing, fast fading and power arches (PA).

Specifically, we analyze various LL-FEC frameworks, namely Multiple Protocol Encapsulation-Forward Error Correction (MPE-FEC), MPE-FEC with Sliding Encoding (SE) and MPE Inter-Burst FEC (MPE-IFEC). Moreover, different codes, namely Reed-Solomon (RS) codes and Raptor codes [4] (also specified in 3GPP [5], DVB and IETF) are applied within the different LL-FEC frameworks. The remainder of this paper is organized as follows. Section F.2 introduces the requirements for extending DVB-S2 to railway scenarios and discusses the modeling of the railway channel. Section F.3 identifies the FEC codes for the available link-layer frame-works in the family of DVB standards. SectionF.4 presents our proposed evaluation and simulation framework of MPE-FEC and MPE-IFEC and also discusses how to optimize the parameters of different FEC schemes. Section F.5 provides selected simulation results before concluding the paper in section F.6.

F.2 DVB-S2 to Railway Scenarios Environment - Transmission Conditions and Service Requirements

F.2.1 Typical Service Requirements

Services being considered in typical satellite-to-railway scenarios are heterogeneous and range from low bit-rate, delay critical Voice over Internet Protocol (VoIP) services to high bit-rate, but usually less delay-sensitive applications such as file downloads or video streaming services. Typically, less delay-sensitive applications can be supported more easily and more efficiently, as by time diversity means, especially FEC interleaving, spreading over a larger time is feasible and there-fore less code rate is required to overcome signal variations. To manage the variety of service with different service requirements, typically a reduced set of service categories is defined. Each category gets assigned maximum delay, loss and bit rate requirements. Generally, services of individual or even multiple users are bundled such that LL-FEC solutions require to support bit-rates up to a full DVB-S2 channel of 30 Mbit/s. Additional extensions require the support of even higher bitrates in range of several 100 MBit/s. Residual packet loss rates require to be quite low, in the range of 10^{-4} or even lower. For the purpose of the evaluation of LL-FEC solutions, a maximum delay of 200ms has been considered as most relevant for the purpose of evaluating the performance. However, specific solutions shall be flexible to support a variety of service requirements, for example delays up to 10 seconds may have to be supported.

F.2.2 Satellite-to-Railway Transmission Environment

The satellite-to-railway environment appears to differ substantially with respect to the scenarios normally considered when modeling the Land-Mobile Satellite Channels (LMSC) [6]. LMSC models generally exclude railway tunnels and do not consider the frequent presence of metallic obstacles. Power arches (Fig. F.1, uppermost), posts with horizontal brackets (Fig. F.1, lowermost), which may be often grouped together, and catenaries, i.e., that is, electrical cables are frequent to obstacles to LOS reception. Results of direct measurements performed along the Italian railway aiming to characterize these peculiar obstacles are reported in [7]. In summary, the attenuation introduced by the catenaries (less than 2 dB) and by posts with brackets (2-3 dB) is relatively low and can be compensated by an adequate link margin. However, the attenuation introduced by the power arches increases to values much as high as 10 dB and beyond, depending on the geometry, the antenna radiation pattern and the carrier frequency. Therefore, advanced fading countermeasures are needed to compensate such attenuation phenomena.

In this paper, reception conditions for Line-of Sight in combination with the effect of Power Arches (LOS+PA) and non Line-of-Sight (nLOS) are modeled taking into account railway environment specifics. LOS reception conditions are modeled as typical Rice distribution and nLOS conditions are modeled as typical Rayleigh distribution.

Fig. F.1: Examples of specific obstacles in the railway scenarios.

F.3 Available FEC Codes and Link Layer Frameworks in the DVB Family of Standards

To compensate signal outages, the application of erasure-based FEC codes extending the time diversity is a well-known method. Generally, the larger the time-diversity, the higher the efficiency of the system, as signal outages can be averaged out more easily. Reed-Solomon (RS) codes had commonly been used if only small dimension block codes are required. RS codes are applied in the first generation of DVB family of standards, e.g. in DVB-C, DVB-S or DVB-H. Raptor Codes have been invented lately and introduced into standards: In contrast to RS codes they provide more flexibility, large code dimensions, and lower decoding complexity. Raptor codes have therefore been adopted in latest DVB standards, e.g. within DVB-H for file delivery or DVB-IPTV. Therefore, RS codes and Raptor codes have been chosen for performance evaluation for the LL-FEC in the railway scenarios in this pa-per. Different frameworks to generate repair data from original data streams and to add the repair data to the original streams have been investigated.

F.3.1 MPE-FEC Framework of DVB-H

LL-FEC has been adopted in DVB-H at the data link layer (MPE Layer) referred to as MPE-FEC. At the time when DVB-H was specified, only RS codes were available, and therefore, the MPE-FEC is based on RS codes. For MPE-FEC the repair data is generated based on an Application Data Table (ADT) with size of at most 190 kByte, such that for 200ms latency data rates of at most 7.8 Mbit/s can support, and for 10 seconds delay, only up to 156 kbit/s are supported.

F.3.2 MPE-IFEC Framework of DVB-SH

During the DVB-SH standardization activities, it was recognized that for satellite-to-handheld services, the MPE-FEC is not sufficient. Therefore, it was decided to specify a multi-burst link layer FEC framework referred to as Inter-Burst FEC (IFEC) [8]. The MPE-IFEC was introduced to support reception in situations of long erasures at the MPE section level spanning several consecutive time-slice bursts due to the characteristics of the LMSC. Obstacles may hinder direct satellite reception and induce losses of several successive bursts. Slid-ing Encoding had been proposed initially to enable multi-burst protection based on RS codes [9], but with the availability of more powerful and low-complexity Raptor erasure codes, the MPE-IFEC has been generalized.

Therefore, the MPE-IFEC is specified as a generic frame-work that presents enough flexibility for a variety of applications. For a usage in DVB-SH, its parameters are restricted to some specific values via the “framework mapping”. Two of such “mappings” are presented in this paper. One is based on MPE-FEC Reed Solomon code [10]. The other mapping is based on Raptor code as specified in the Content Delivery Protocols (CDP) specification of IP Datacast over DVB-H [11]. For more details on Raptor codes please refer to [4] and the specification in 3GPP, DVB and IETF.

The MPE-IFEC is defined by the parameters encoding period EP, which reflects the ADT size in compared to the burst size, data burst spread B, i.e. over how many multiple of EP bursts an ADT is spread, FEC spread S, i.e., over how many multiples of EP bursts the FEC is spread, the sending delay D, i.e. how long the sending of data is delayed at sender in units of time-slice bursts, the code rate r_{phy} as well as code being used, namely Raptor or RS codes. Note that whereas Raptor codes allow very flexible parameters, for RS codes due to restricted code parameters only $EP = 1$ can be used.

F.3.3 Extended MPE-FEC

Despite its flexibility, the MPE-IFEC is still designed for the purpose of multicasting live video over time-slice bursts. The FEC is designed for the purpose to minimize tune-in de-lays, but not to minimize end-to-end delay, which is essential for bidirectional data delivery services. Furthermore, There-fore an extension of MPE-FEC

Table F.I: Supported code rates (in greeen if below 2/9, in yellow if between 2/9 and 1) for different bitrates and latency in ms for RS codes (MPE-FEC) and Raptor codes (extended MPE-FEC)

RS Code	Latency in ms													
Bitrate in kbit/s	10	20	40	80	160	320	640	1280	2560	5120	10240	20480	40960	81920
32	0.02	0.02	0.02	0.02	0.02	0.03	0.04	0.07	0.14	0.24	0.38	na	na	na
64	0.02	0.02	0.02	0.02	0.03	0.04	0.07	0.14	0.24	0.38	na	na	na	na
128	0.02	0.02	0.02	0.03	0.04	0.07	0.14	0.24	0.38	na	na	na	na	na
256	0.02	0.02	0.03	0.04	0.07	0.14	0.24	0.38	na	na	na	na	na	na
512	0.02	0.03	0.04	0.07	0.14	0.24	0.38	na	na	na	na	na	na	na
1024	0.03	0.04	0.07	0.14	0.24	0.38	na	na	na	na	na	na	na	na
2048	0.04	0.07	0.14	0.24	0.38	na	na	na	na	na	na	na	na	na
4096	0.07	0.14	0.24	0.38	na	na	na	na	na	na	na	na	na	na
8192	0.14	0.24	0.38	na	na	na	na	na	na	na	na	na	na	na
16384	0.24	0.38	na	na	na	na	na	na	na	na	na	na	na	na
32768	0.38	na	na	na	na	na	na	na	na	na	na	na	na	na
65536	na	na	na	na	na	na	na	na	na	na	na	na	na	na
131072	na	na	na	na	na	na	na	na	na	na	na	na	na	na
262144	na	na	na	na	na	na	na	na	na	na	na	na	na	na
524288	na	na	na	na	na	na	na	na	na	na	na	na	na	na
1048576	na	na	na	na	na	na	na	na	na	na	na	na	na	na

Raptor Code	Latency in ms													
Bitrate in kbit/s	10	20	40	80	160	320	640	1280	2560	5120	10240	20480	40960	81920
32	0.00	0.00	0.00	0.00	0.00	0.00	0.00	0.00	0.00	0.00	0.00	0.00	0.00	0.00
64	0.00	0.00	0.00	0.00	0.00	0.00	0.00	0.00	0.00	0.00	0.00	0.00	0.00	0.00
128	0.00	0.00	0.00	0.00	0.00	0.00	0.00	0.00	0.00	0.00	0.00	0.00	0.00	0.00
256	0.00	0.00	0.00	0.00	0.00	0.00	0.00	0.00	0.00	0.00	0.00	0.00	0.00	0.01
512	0.00	0.00	0.00	0.00	0.00	0.00	0.00	0.00	0.00	0.00	0.00	0.00	0.01	0.02
1024	0.00	0.00	0.00	0.00	0.00	0.00	0.00	0.00	0.00	0.00	0.00	0.01	0.02	0.04
2048	0.00	0.00	0.00	0.00	0.00	0.00	0.00	0.00	0.00	0.00	0.01	0.02	0.04	0.08
4096	0.00	0.00	0.00	0.00	0.00	0.00	0.00	0.00	0.00	0.01	0.02	0.04	0.08	na
8192	0.00	0.00	0.00	0.00	0.00	0.00	0.00	0.00	0.01	0.02	0.04	0.08	na	na
16384	0.00	0.00	0.00	0.00	0.00	0.00	0.00	0.01	0.02	0.04	0.08	na	na	na
32768	0.00	0.00	0.00	0.00	0.00	0.00	0.01	0.02	0.04	0.08	na	na	na	na
65536	0.00	0.00	0.00	0.00	0.00	0.01	0.02	0.04	0.08	na	na	na	na	na
131072	0.00	0.00	0.00	0.00	0.01	0.02	0.04	0.08	na	na	na	na	na	na
262144	0.00	0.00	0.00	0.01	0.02	0.04	0.08	na	na	na	na	na	na	na
524288	0.00	0.00	0.01	0.02	0.04	0.08	na	na	na	na	na	na	na	na
1048576	0.00	0.01	0.02	0.04	0.08	na	na	na	na	na	na	na	na	na

towards larger ADT sizes is most suitable for DVB-S2 railway scenarios. Such extensions require larger dimensions for the block code and are therefore most suitable provided by Raptor codes.

Table F.I shows the supported code rates for different bitrates and latencies for RS codes (MPE-FEC) and Raptor codes (extended MPE-FEC). Note that the value provides the lowest code rate, any higher code rates are also supported at this la-tency/bit-rate combination. The extended MPE-FEC supports higher bit-rates as well as latencies in much larger dimensions and is therefore significantly more suitable for the considered scenarios.

F.4 Simulation Framework and Optimization of Codes Parameters

F.4.1 Simulation Framework of the LL-FEC

A LL-FEC simulation platform has been developed in order to quickly assess the performance of different parameter configurations without repeating the time-consuming

physical layer simulations. The simulator as shown in Fig. F.2 includes options to:

- Apply different transmission characteristics, such as models for fading at different velocities, outages dues to obstacles such as power arches, and different C/N or E_s/N_0. Modify the modulations and coding (MODCOD) schemes of the DVB-S2 link.
- Apply the different FEC schemes as discussed in section F.3 with different parameter settings for the LL-FEC and different codes.
- Adapt to Quality of Service (QoS) requirements such as different delays and loss rates and optimize the transmission parameters towards these requirements.
- Assess different criteria such as Maximum Tolerant Burst Length (MTBL) and Packet Error Rate (PER).

Given that this performance assessment entails many layers, in particular, from the physical to the network layers of the protocol stack, a modular approach has been considered. The Physical-Layer module, which generates the time series of Channel Dumps, interfaces with the Link Layer simulator. The rightmost module in Fig. F.2 is the simulator framework of MPE-FEC: It takes a stream of IP packets as input and applies MPE-FEC encoding technique as described in [10], generating an MPEG-2 Transport Stream (TS) by encapsulating MPE sections and MPE-FEC sections. At this point, the output of the physical-layer simulator is used to mark the MPEG-2 TS packets as correctly received or being erroneous. Next, the MPE-FEC decoding process is applied by reconstructing columns of the FEC matrix applying the correction capabilities of the RS code. Finally, the sequence of IP packets affected by the unreliable columns (an IP packet is considered wrong if any part of it falls inside an unreliable column which cannot be corrected) is obtained and the PER at IP level is computed.

The input of the MPE-IFEC simulation platform is the same as MPE-FEC. Only the decoding process is different, shown in the leftmost of Fig. F.2. For MPE-IFEC, the marked MPEG-2 TS packets are first mapped into the MPE Sections or MPE-IFEC Sections and subsequently to the Decoding Matrix (ADT + iFDT). Then, decoding each of the Decoding Matrix at each Encoding Period with RS code or Raptor Code eliminates the unreliable columns of the Decoding matrix.

By making use of MPEG-2 TS loss patterns the LL-FEC simulator is useful to quickly assess the performance of differ-ent parameter configurations without repeating the tedious physical layer simulations.

F.4.2 Parameters Optimization of the LL-FEC

The introduced LL-FEC frameworks allow a significant variability in terms of parameter settings: Table F.II summarizes the description of some main parameters, for

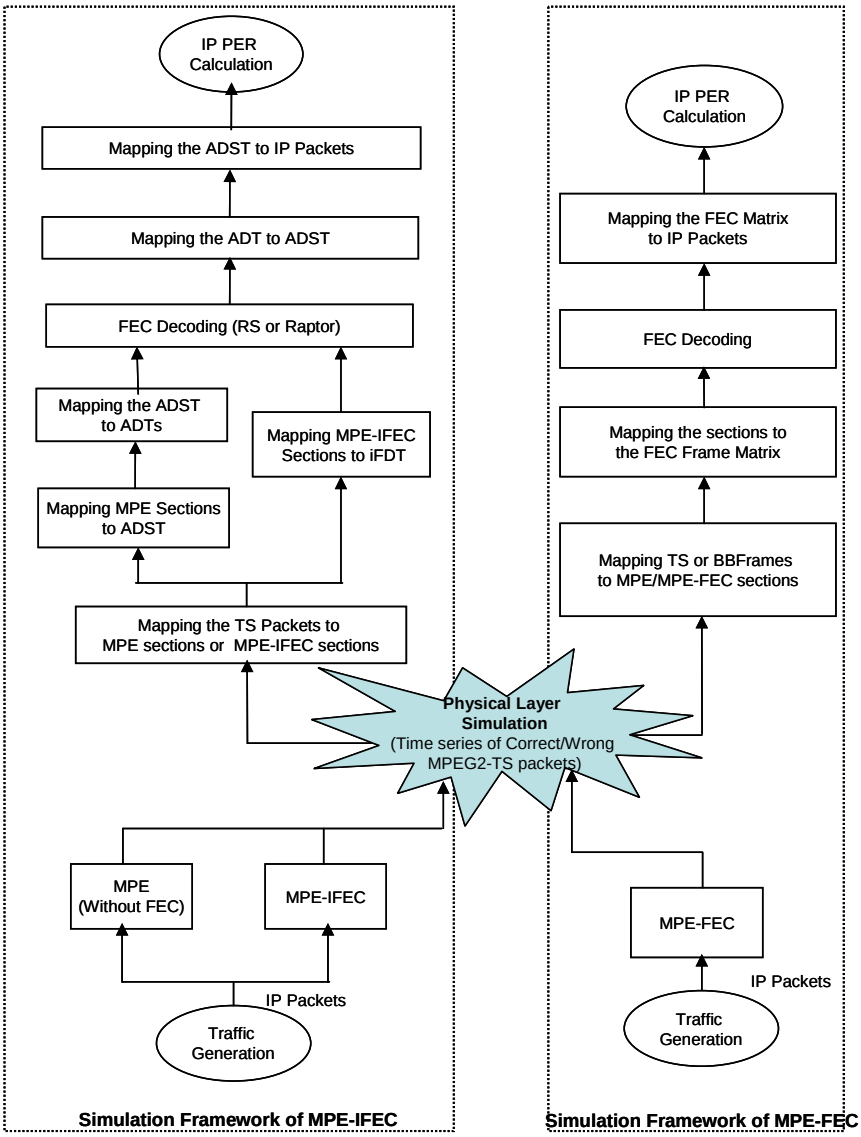

Fig. F.2: The simulation framework of MPE -FEC and MPE-IFEC.

details on other parameters such D, EP, G, B, S, R and T we refer to the MPE-IFEC specification [8].

Then, the amount of data (bits) that can be protected with target delay τ can be computed as:

$$S_{\text{protect}} = \tau B_s M r_{\text{phy}} r_{\text{ll}}, \tag{F.1}$$

and the size of ADT (for MPE-FEC) or ADST (for MPE-IFEC) in the time slice burst can be derived as:

$$S_{\text{ADT}} = S_{\text{protect}} r_{\text{ll}}. \tag{F.2}$$

Table F.II: System and Simulation Parameters

Parameters	Description
B_s	Symbol rate
S_{IP}	Size of IP packet
τ	Target delay
M	Size of signal constellation (QPSK $M = 2$, 16QAM $M = 4$)
r_{phy}	The PHY layer coding rate
S_{protect}	Amount of data bit to be protected during the target delay
S_{burst}	Amount of data bit in each time slice burst
S_{adt}	Size of the ADT
N_{burst}	Number of bursts protected during the target delay
r_{ll}	Link layer coding rate
v_{train}	vehicle velocity
N_{rows}	Number of rows of MPE-FEC frame
l_{PA}	The duration/length of power arches
d_{PA}	The distance between power arches

Thus, the number of time slice bursts that can be protected within target delay τ is given as

$$N_{\text{burst}} = \lfloor \frac{S_{\text{protect}}}{S_{\text{ADT}}} \rfloor = \lfloor \tau v_{\text{burst}} \rfloor, \tag{F.3}$$

where $v_{\text{burst}} = B_s M r_{\text{phy}} / S_{\text{burst}}$ is the rate at which bursts are transmitted. The amount of data in each time slice burst S_{burst} cannot exceed 2 Mbit for the MPE-FEC framework with RS codes due to the address field being only 18 bit [10].

F.4.2.1 Parameters Optimization of the MPE-FEC

For an RS referred to as $RS(n, k)$, where n denotes the number of columns of the FEC frame matrix, k the number of columns of the ADT and N_{rows} the number of rows of the typical MPE-FEC frame used in DVB-H. Optimal values of n, k and N_{rows} can be calculated with the following formulas for a given desired protection:

$$k = \lfloor \frac{S_{\text{protect}}}{8 N_{\text{rows}}} \rfloor. \tag{F.4}$$

The available number of FEC matrix rows in the standard [10] is $N_{\text{rows}} \in \{256, 512, 768, 1024\}$.

Then, for a given n the link layer code rate can be computed as:

$$r_{\text{ll}} = \frac{k}{n}. \tag{F.5}$$

We will extend N_{rows} to be larger (e.g. 2048 or 4096) in order to be tolerant to long burst errors in the mobile scenario.

F.4.2.2 Parameters Optimization for MPE-FEC SE

For MPE-FEC Sliding Encoding, with the availability of the size of the burst, S_{burst}, n can be computed as

$$n = \lfloor \frac{S_{\text{burst}}}{8N_{\text{rows}}} \rfloor, \tag{F.6}$$

where N_{rows} is defined as for the MPE-FEC. Then k can be calculated from (F.5). The size of the sliding windows SW yields:

$$SW = \lfloor \frac{S_{\text{protect}}}{8kN_{\text{rows}}} \rfloor. \tag{F.7}$$

F.4.2.3 Parameters Optimization of MPE-IFEC with RS Code

For the MPE-IFEC with RS code $RS(n,k)$, $D = 0$, $EP = 1$ and $G = 1$ are assumed in order to simplify. Then

$$T = \frac{N_{\text{rows}}}{G} \text{ with } N_{\text{rows}} \in \{256, 512, 768, 1024\}, \tag{F.8}$$

n can be calculated from (F.6) and then k can be derived from the (F.5) with known n.

The parameters B and S can be calculated from (F.9) as

$$\begin{cases} B + S = \frac{N_{\text{burst}}}{EP} = N_{\text{burst}}, \\ S = \lceil (1 - r_{\text{ll}})(B + S) \rceil = \lceil (1 - r_{\text{ll}}) N_{\text{burst}} \rceil, \\ B = (B + S) - \lceil (1 - r_{\text{ll}})(B + S) \rceil = N_{\text{burst}} - \lceil (1 - r_{\text{ll}}) N_{\text{burst}} \rceil. \end{cases} \tag{F.9}$$

F.4.2.4 Parameters Optimization of MPE-IFEC with Raptor Code

Let us present Raptor codes as $Raptor(n,k,T)$ with n and k the code parameters and with the symbol size T. For the MPE-IFEC with Raptor code, $D = 0$ and $G = 1$ is

selected for minimum delay and lowest decoding complexity. Then T corresponds to the row size and can also be calculated from (F.8).

Furthermore, n can be derived as

$$n = \left\lfloor \frac{S_{\text{burst}}}{8N_{\text{rows}}} \right\rfloor EP, \tag{F.10}$$

where EP is an integer. k can be derived from the (F.5) with known n. Then B and S can be calculated from (F.11) as:

$$\begin{cases} B + S = \frac{N_{\text{burst}}}{EP}, \\ S = \lceil (1 - r_{\text{ll}})(B + S) \rceil, \\ B = (B + S) - \lceil (1 - r_{\text{ll}})(B + S) \rceil. \end{cases} \tag{F.11}$$

F.4.2.5 Parameters Optimization of the Extended MPE-FEC with Raptor Code

For an $RS(n, k)$-based MPE-FEC applied in DVB-RCS, the optimization of parameters n and k is the same as presented in Section F.4.2.1. For a $Raptor(n, k, T)$, the code parameters may be $4 \leq k \leq 8192$, $k \leq n \leq 65536$ and T any power-of-two integer that divides N_{rows}. Preferably k is chosen at least as great as 1000 to keep the inefficiency of the Raptor code to below 0.2%. Therefore, for a given amount of data bit to be protected, S_{protect}, k should be selected as the smallest value larger than 1000 such that $kT \geq S_{\text{protect}}$ and T any power-of-two integer that divides N_{rows} such that $N_{\text{rows}} = GT$. Then, for a given LL code rate r_{ll}, n is selected as k/r_{ll}. Furthermore N_{rows} may be selected appropriately to ensure $k \geq 1000$. However, obviously values $k < 1000$ can also be selected without harming the performance significantly.

F.5 Simulation Results Analyses

Table F.III shows the parameter settings for the conducted simulations. The parameters for MPE-FEC, MPE-IFEC and extended MPE-FEC can be derived based on the guidelines in the Section F.4.

F.5.1 LOS+PA

Before presenting the simulation results, we compute the theoretical values of MTBL following the approach presented in Section F.4. The theoretical MTBL can be calculated as

$$l_{\text{PA}}\left(N_{\text{BB-p}}\right) = \frac{N_{\text{BB-p}} v_{\text{phy}}}{v_{\text{BB}}}, \tag{F.12}$$

Table F.III: The parameters setting for LOS+PA scenario

Parameters	Description
B_s	27.5 M baud/s
S_{IP}	1500 bytes
τ	200 ms
M	2
r_{phy}	1/2
S_{burst}	512 K bytes
S_{adt}	256 K bytes
N_{burst}	10
r_{ll}	1/2
v_{train}	100 km/h

where $v_{\text{BB}} = B_s M r_{\text{phy}}/S_{\text{BBFrame}}$ is the rate at which BB-Frames are transmitted and the $N_{\text{BB-p}}$ is the number of BB-Frames protected by the target delay τ, (e.g. 200 ms in this paper) with various LL-FEC schemes.

The appropriate number of BB-Frames included in one protection period can be computed as

$$N_{\text{ideal-BB-p}} = \left\lfloor \frac{\tau v_{\text{TS}} (1 - r_{\text{ll}})}{N_{\text{TS-BB}}} \right\rfloor, \tag{F.13}$$

where $v_{\text{TS}} = B_s M r_{\text{phy}}/S_{\text{TS}}$ is the rate at which TS Packets are transmitted (here S_{TS} =188 bytes) and $N_{\text{TS-BB}} = [(S_{\text{BBFrame}} - 10 \times 8)/(8 S_{\text{TS}})]$ is the number of TS packets encapsulated in one BBFrame. The actual number of BB-Frames that can be protected for the different LL-FEC schemes can be computed as:

$$N_{\text{BB-p}} = \left\lfloor \frac{(n-k) N_{\text{rows}} SW}{184 N_{\text{TS-BB}}} \right\rfloor. \tag{F.14}$$

We obtain theoretical ideal values of MTBL of 2.86m for QPSK 1/2. However, Table F.IV shows the theoretical MTBL of various LL-FEC schemes showing a slight degradation with respect to the ideal.

Typical length of PAs in Europe are in the range of 0.5 to 3m [6; 7] and therefore the theoretical results already show that the FEC codes shown in Table F.IV can overcome the effect of the PAs for high speeds. This is an acceptable result since the time of the train is at speeds below 100 km/h is almost negligible.

Figure F.3 shows the results of the MPE-FEC sliding encod-ing with different values of SW. The system parameters for this simulation are:

Table F.IV: The MTBL of LOS+PA scenario

LL-FEC scheme	MODCOD	FEC codes	MTBL	
			30 km/h	100 km/h
MPE-FEC	QPSK 1/2	RS(128,64), N_{rows} =4096	0.65m	2.18m
MPE-IFEC	QPSK 1/2	RS(128,64), N_{rows} =512 EP =1, $B = S$ =5 or Raptor(640,320),N_{rows} =512 EP =5, $B = S$ =1	0.82m	2.73m
MPE-FEC Sliding Encoding	QPSK 1/2	RS(128,64), N_{rows} =4096 SW =10	0.82m	2.73m
Extend MPE-FEC	QPSK 1/2	Raptor(2560, 1280, 256) N_{rows} =1024,G =4	0.82m	2.73m

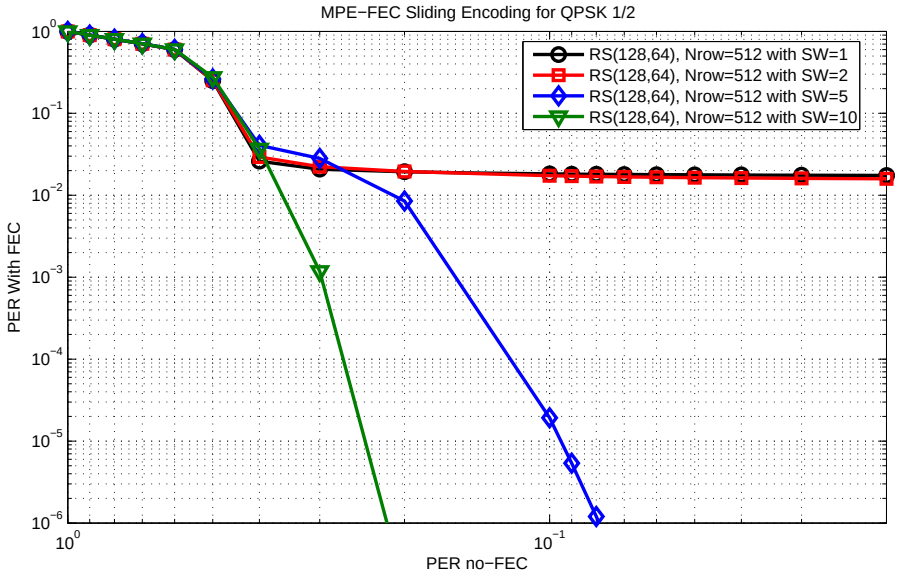

Fig. F.3: Performance of MPE-FEC sliding encoding with different SW.

- l_{PA} =1m and d_{PA} =49m.
- v =100km/h and B_s=27.5 Mbaud.

The results show that the MPE-FEC sliding encoding can not overcome the effect of PA with $SW \leq 2$ for and there will be an error floor around 10^{-2}. The error floor disappears when $SW \geq 5$.

We can conclude that MPE-FEC completely removes the effect of PAs for high

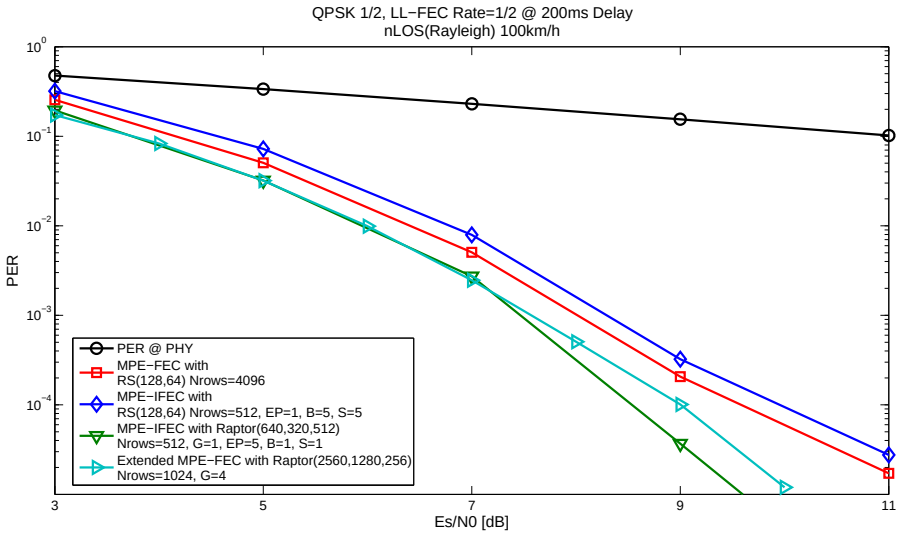

Fig. F.4: Performance of different LL-FEC schemes with $v = 100$km/h.

speeds only, due to the fact that the tar-get protection delay is limited due to the restrictions in the standard. On the other hand, MPE with sliding encoding can also completely remove the effect of PAs while there is no limitation on the target delay that can be protected. The opti-mal window for the selected system parameters is 10 for a target delay of 200 ms and QPSK 1/2.

F.5.2 Non Line-Of-Sight Reception

The system parameters of nLOS Scenario are the same as in the LOS+PA Scenario except for the channel model. The time series of channel dumps were generated from the Rayleigh Channel, which corresponds to the nLOS channel model.

Figure F.4 shows the performance of PER over the E_s/N_0 for different link layer schemes with v =100km/h, compared to the performance without link layer FEC. Note that for MPE-FEC and extended MPE-FEC with RS codes, the transmission parameters did not allow suitable parameter settings (shown in Table F.I). But here we increase the size column up to 4096 Bytes for RS codes in order to compare the performance under the same target delay assumption.

Generally, a residual packet loss rate of about 10^{-4} (or even lower) needs to be achieved for data services. The uncoded performance is completely unsatisfying. With the use of LL-FEC, the target performance can be achieved. The MPE-IFEC may solve the problem and the performance of Raptor-based MPE-IFEC outperforms RS by about 1.5 dB, because the error correction capability of Raptor coders is better than RS coders. And the extended MPE-FEC with Raptor codes outperforms MPE-FEC with RS by about 0.5dB. This is due to the fact that the extended MPE-FEC does not have any restrictions in terms of time-slice bursts. For lower speeds at around 30km/h as well as for larger delays the extended MPE-FEC shows consistently better

results than the any MPE-IFEC.

It can be concluded that the codes analyzed here are more can be used for both purposed, to protect against LOS+PA scenarios as well as Rayleigh environments. Especially by the use of the MPE-IFEC and extended MPE-FEC with Raptor codes as finally specified in DVB-RCS+M consistently superior results than with other link layer FEC for railway scenarios. The optimized parameter selections for the combination of LOS+PA and nLOS are further study.

F.6 Conclusion

The application of LL-FEC based on RS and Raptor codes is discussed and analyzed in this paper. Theoretical analysis and simulation revealed that LL-FEC can overcome the fade in the railway scenarios by adjusting the FEC Codes parameters and the extended MPE-FEC with Raptor Codes is the best scheme to counteract the railway fade.

In particular, we have shown that MPE-FEC completely removes the effect of PAs for high speeds only, due to the fact that the target protection delay is limited in the current version of the standard. On the other hand, we have shown that MPE-FEC with sliding encoding can also completely remove the effect of PAs while in this case there is no limitation on the target delay that can be protected. Moreover we have obtained the optimal windows for the selected system parameters (10 for a target delay of 200ms for QPSK 1/2).

Acknowledgment

The authors want to express their gratitude to the University of Bologna (UoB) for their providing of the physical layer time series of the nLOS scenario, so allowed us to achieve the results presented in this paper. Also the collaboration with the experts in the DVB TM-RCS group, led by Dr. Harald Skinnemon, was a great pleasure and significantly inspired this work.

Bibliography

[1] ETSI EN 302 304 v1.1.1, Digital Video Broadcasting (DVB): Transmission System for Handheld Terminals (DVB-H), Nov. 2004.

[2] ETSI EN 302 307 v1.1.1, Digital Video Broadcasting (DVB): Second generation framing structure, channel coding and modulation system for Broadcasting, Interactive Services, News Gathering and other broadband satellite applications, June 2004.

[3] ETSI EN 301 790 v1.4.1, Digital Video Broadcasting (DVB): Interaction channel for satellite distribution systems.

[4] A. Shokrollahi, "Raptor Codes," *IEEE Trans. on Inform. Theory.*, vol. 52, no. 6, pp. 2551 - 2567, Jun. 2006.

[5] 3GPP TS26.346, "Multimedia Broadcast/Multicast Service (MBMS): Protocols and Codecs (release 8)," Sep. 2008.

[6] E. Lutz, M. Werner, and A. Jahn, *Satellite Systems for Personal and Broadband Communications*. Springer, New York, NY, USA, 2000.

[7] S. Scalise, R. Mura, and V. Mignone, "Air Interfaces for Satellite based Digital TV Broadcasting in the Railway Environment," *IEEE Trans. on Broadcast,* vol. 52, no. 2, pp. 158 - 166, Jun. 2006.

[8] DVB document TM-3880, "MPE IFEC Specification," Alcatel-Lucent, UDCast, Digital Fountain, Sep. 2007.

[9] P. Marco, F. Rosario, C. Giovanni, and E. V. C. Alessandro, "On The Application of MPE-FEC to Mobile DVB-S2: Performance Evaluation in Deep Fading Conditions," in *Proc. Int. Workshop on Satellite and Space Commun.*, Salzburg, Austria, pp. 223 - 227, Sep. 2007.

[10] ETSI EN 301 192 v1.4.1, Digital Video Broadcasting (DVB): DVB Specification for Data Broadcasting, Nov. 2004.

[11] ETSI TS 102 472 v1.2.1, IP Datacast over DVB-H: Content Delivery Protocols (CDP), Jun. 2006.